RELIABILITY-BASED DESIGN OF OFFSHORE STRUCTURES FOR OIL AND GAS APPLICATIONS

By

© **Aghatise Okoro**

A thesis submitted to the School of Graduate Studies

In partial fulfillment of the requirements for the degree of

Doctor of Philosophy

Faculty of Engineering and Applied Science

Memorial University of Newfoundland

February 2023

St. John's Newfoundland, Canada

Dedication

This work is dedicated to God Almighty, who walked with me every step of this journey. To my father, Late Benjamin Okoro, who knew this day would come, my mother, Elizabeth Okoro, my wife, Beauty Okoro, and my children Ebere Theophilia Okoro, Cleodora Okoro, and Nathan Okoro.

ABSTRACT

Offshore structures are complex in their structural and functional form and operate in a harsh and uncertain environment with complex interactions between ocean variables. Consequently, the ocean environment presents a high risk to these structures hence the need to develop an efficient and reliable design. Therefore, the need for a design that effectively: captures complex ocean parameter interactions, reduces the computational burden in structural response determination, quantifies the structure's ability to bounce back when faced with disruptive events, and minimizes cost under uncertainty at the desired safety levels of the asset is critical. A robust offshore structural design under uncertainty is essential for the safety of life, asset, and the environment during oil and gas exploration and production activities. This thesis presents improved methods for the effective reliability-based design of offshore structures. First, a framework is developed to capture the dependency of multivariate environmental ocean variables using vine copula and its impact on the reliability assessment of offshore structural systems. The model was tested using a cantilever beam and applied to an offshore jacket structure. The comparative results from the jacket structure and cantilever problem reveals that failure probability considering dependence between ocean variables is closer to the reference value than when variables are independent or modeled with a Gaussian copula. The outcome shows the importance of capturing nonlinearity and tail dependence between ocean variables in reliability evaluation. Secondly, the effectiveness of a hybrid metamodel, which is a combination of two commonly and independently used methods, Kriging and Polynomial Chaos Expansions (PCE), is investigated for offshore structural response determination and reliability studies. The hybrid metamodel herein, called (APCKKm-MCS) is constructed from an adaptive process with multiple enrichment of Experimental Design (ED). The hybrid approach was tested on simple non-linear functions, a truss bar, and an offshore deepwater

Steel Catenary Riser (SCR). The study's outcome revealed that APCKKm-MCS produced a high predictive response capacity, reduced model evaluation, and shorter computing time during reliability evaluation than the single enrichment case (APCK-MCS) and the adaptive ordinary Kriging case (AK-MCS) considered. In addition, a novel framework is developed for the resilience quantification of offshore structures in terms of their time-varying reliability, adaptability, and maintainability. The developed framework was demonstrated using an internally corroded pipeline segment subject to disruptive events of leak, burst, and rupture. The framework captured the resilience index of the natural gas pipeline for its design life, and its sensitivity analysis revealed the influence of the pipe wall thickness and corrosion depth growth rate on the resilience of the pipeline. The framework provides a quantitative approach to determine the resilience of offshore structures and ascertain their critical influencing parameters for effective decision-making. Finally, a methodology for optimal structural design under uncertainty considering the dependency of environmental variables with the implementation of a hybrid metamodel in the inner loop of a nested optimization problem is presented and demonstrated on a steel column function and a segmented SCR. The study showed different decision outcomes for various vine tree configurations in the dependence modeling for the steel column function noting the importance of choosing the appropriate variable order in the vine tree for optimal design under uncertainty. Also, the research reveals the suitability of adaptive PCK for the inner loop reliability phase for a double-loop structural optimization due to its high predictive capacity and observed relatively low cross-validation error. The method shows the importance of effective dependence modeling of environmental ocean variables in structural cost minimization and selecting optimal structural design variables under uncertainty. From the research outcomes, considering multivariate dependence between ocean variables using vine copula and utilizing multiple enrichment hybrid

metamodels in response evaluation for reliability and optimal design assessment of offshore structures could better predict their failure probability and enhance a safer structural design. In addition, the resilience quantification framework developed provides a vital decision-making tool for offshore structural systems' design and integrity management. The research into high dimensional dependence modeling of offshore structures using vine copula, comparative study of sampling strategies required for the hybrid (Kriging and PCE) metamodel construction, dependence-based structural resilience quantification, and multiobjective dependence-based structural optimization under uncertainty are among areas proposed for future investigation.

ACKNOWLEDGEMENT

I am most grateful to the Almighty God, the infinite fountain of everlasting wisdom, for the protection, direction, health, knowledge, and mercies granted throughout my research.

I want to express my profound gratitude to my supervisor Dr. Faisal Khan for his mentorship, love, patience, guidance, and financial support and who made my quest for a doctoral degree possible. To my co-supervisor, Dr. Salim Ahmed, thank you for the mentorship, guidance, and valuable contributions to my research. A special thanks to my supervisory committee comprising Drs. Faisal Khan, Salim Ahmed, Sunday Adedigba, and Yahui Zhang, your professional input and mentorship during various phases of my studies guided me and helped shape my thought process and the research in general.

Also, I appreciate the financial support provided by the Canada Research Chair Tier 1 Program in Offshore Safety and Risk Engineering.

I want to thank Dr. Rosemary Norman, Dr. Eshan Mesbahi, Dr. Bruno Sudret, Dr. Emeka Amalu, Dr. John Akpobi, and Dr. Maliki Moustapha for their support, mentorship, and encouragement during my PhD studies. A special thanks to the Centre for Risk, Integrity and Safety Engineering (CRISE) members for the numerous research and academic engagement, which was a motivation throughout my studies.

I thank the owners of Structural Analysis and Computer Systems (SACS) and Flexcom software - Bentley Inc and Wood Group Plc, respectively, for the software support required for numerical analysis as part of my research.

To my mum (Elizabeth Okoro), thank you for the constant prayers, care, and support. To my brother and sister, Nana Okoro and Sandra Okoro, I want to thank you for your concern and love. To my amiable wife, Beauty Okoro, and lovely kids Ebere, Cleodora, and Nathan, words cannot express how thankful I am to see you all on this journey with me. The sacrifice, support, advice, love, and encouragement are beyond imagination.

TABLE OF CONTENTS

ABSTRACT iii

ACKNOWLEDGEMENT vi

LIST OF TABLES xiv

LIST OF FIGURES xvii

NOMENCLATURE xx

Chapter 1 1

Introduction 1

1.1. Background and Motivation 1

1.2. Objectives 5

1.3. Scope and limitations 9

1.4. Organization of the thesis 9

1.5. Co-authorship Statement 12

References 13

Chapter 2 15

Literature Review 15

2.1. Dependence-based modeling in offshore structure reliability assessment 15

2.2. Metamodels for complex offshore structures 17

2.3. Resilience in the marine and offshore industry 19

2.4. Optimization of ocean structure under uncertainty 21

2.5. Knowledge Gaps and Research Tools 23

References 25

Chapter 3 40

Reliability Assessment of Marine Structures considering Multidimensional Dependency of the variables 40

Preface 40

Abstract 40

3.1. Introduction 41

3.2. Preliminaries on Copulas and Structural Reliability 46

3.2.1 Structural Reliability 46

3.2.2 Copula Functions 48

3.2.3 Dependence measures 51

3.3. Framework for Reliability Assessment using Vine Copulas 51

3.3.1 Implementation procedure 52

3.3.2. Application example: Cantilever Beam Structure 53

3.4. Application of Framework to an Offshore Structure 62

3.4.1. Statistical parameters and probability distribution 63

3.4.2. Dependence modeling using D-vine Copula 65

3.4.3. Metamodel and reliability assessment of the structure 68

3.4.4. Discussion on dependence modeling results 70

3.5. Conclusions 72

Acknowledgment 73

Appendix 3A 73

References 79

Chapter 4 86

An Active Learning Polynomial Chaos Kriging Metamodel for Reliability Assessment of Marine Structures 86

Preface 86

Abstract 86

4.1. Introduction 87

4.2. Preliminaries on the hybrid metamodel 91

4.2.1. Metamodels 91

4.2.2. Active Learning Function and ED Enrichment 95

4.2.3. Structural Reliability 97

4.3. Methodology for metamodel development 99

4.3.1. Procedural Steps 99

4.3.2. Illustrative examples using benchmark functions 102

4.4. Application of the Proposed Metamodel to Marine Structures 108

4.4.1. Ten-Bar Truss Structure 108

4.4.2. SCR application of hybrid metamodel 111

4.4.3. Discussion of results 121
4.5. Conclusions 123
Acknowledgment 125
Appendix 4A 125
References 130
Chapter 5 139
A methodology for time-varying resilience quantification of an offshore natural gas pipeline . 139
Preface 139
Abstract 139
5.1. Introduction 140
5.2. Preliminaries of resilience quantification 146
5.2.1. Engineering Resilience 146
5.2.2. Structural Resilience Metric 147
5.2.3. Time-Dependent Structural Reliability Analysis 152
5.2.4. Random Process Discretization 154
5.3. The Methodology for Resilience Quantification 155
5.3.1. Steps for structural resilience quantification 155
5.4. Application of the framework to a natural gas pipeline 160
5.4.1. Background (Offshore Pipeline Resilience) 160
5.4.2. Case Study: Internally Corroded Natural Gas Pipeline Segment 160

5.4.3. Discussion of results 176
5.5. Conclusions 177
Acknowledgment 178
Appendix 5A 179
References 180
Chapter 6 191
Reliability-Based Design Optimization of Complex Offshore Structure 191
Preface 191
Abstract 191
6.1. Introduction 192
6.2. RBDO Formulation and Preliminaries 196
6.2.1. RBDO problem formulation 196
6.2.2. Copula Functions (D-vine Copula) 198
6.2.3. Metamodel construction and reliability for RBDO 201
6.2.4. RBDO Outer Loop Optimization 204
6.3. The Methodology (RBDO with dependence) 205
6.4. Application of the RBDO with dependence 211
6.4.1. Steel Column Function [modified from(Eldred et al., 2008)] 211
6.4.2. Practical Application: Segmented SCR Optimization 221
6.5. Discussion 234

6.6. Conclusions 236

Acknowledgment 238

Appendix 6A 239

References 241

Chapter 7 255

Contributions, Conclusions and Recommendations for Future Research 255

7.1. Novelty and Contributions 255

7.2. Conclusions 256

7.2.1. A Multivariate Dependence Modeling Approach for Offshore Structures 257

7.2.2. A Hybrid Metamodel for Reliability Assessment of Offshore Structures 257

7.2.3. Structural Resilience Quantification for Offshore Structures 257

7.2.4. Dependence-based Structural Optimization under Uncertainty 258

7.3. Future Research Activities 258

LIST OF TABLES

Table 3.1. Statistical information of random variables for the cantilever beam. 54

Table 3.2. Dependence measures for the cantilever beam. 54

Table 3.3. Independence test statistics for the cantilever beam. 56

Table 3.4. Parameter and Rotation (θ, θ_R) of selected copula function. 56

Table 3.5. Cantilever beam reliability assessment. 59

Table 3.6. Statistical information of random variables (C-CORE, 2017). 63

Table 3.7. Selection of EVD for ocean variables. 64

Table 3.8. Dependence measures between variables of Jacket Structure (C-CORE, 2017). 65

Table 3.9. Independence test for variables of the jacket structure. 66

Table 3.10. Copula selection for the jacket structure using the MLE approach. 66

Table 3.11. Optimal copula for variables of the jacket structure. 67

Table 3.12. Offshore jacket structure failure probability for different load directions. 70

Table 3A.1. Selected bivariate copula functions. 73

Table 3A.2. PCK metamodel validation error at approach angle to jacket structure. 76

Table 4.1. Reliability analysis summary (Ten-dimensional nonlinear function) 104

Table 4.2. Statistical parameters for the infinite slope model (Phoon,2008). 106

Table 4.3. Reliability analysis summary (infinite slope function). 107

Table 4.4. Parameters of truss bar input variables [modified from (Liu & Xie, 2020)]. 109

Table 4.5. Reliability analysis summary (ten-bar truss system). 110

Table 4.6. SCR and FPSO parameters. 112

Table 4.7. Statistical summary of environmental variables (C-CORE,2017) 113

Table 4.8. Dependence parameters using D-vine copula. 115

Table 4.9. SCR system reliability analysis summary. 118

Table 4A.1. Classical Orthogonal Polynomials (Xiu & Em Karniadakis, 2003). 126

Table 4A.2. Minimum AIC values for variables Hs , Tz and Vc. 126

Table 4A.3. Bivariate Copula Functions. 128

Table A4.4. Target failure probability (DNV,2001). 130

Table 5.1. Definition of the concept of resilience in different sectors. 141

Table 5.2. Parameters of the offshore natural gas pipeline [modified from:(Pandey, 1998)] 162

Table 5.3. Initial defect length and depth dimensions of the natural gas pipeline segment. 164

Table 5.4. Corrosion Parameters for natural gas pipeline [modified from (Kale et al., 2004)].. 165

Table 5.5. Corrosion depth growth rate statistical information. 166

Table 5.6. Offshore natural gas pipeline repair and maintainability data. 173

Table 5.7. Performance ratio of the natural gas pipeline (recovery and loss). 173

Table 6.1. Statistical summary of the steel column function variables [modified from(Eldred et al., 2008)]. 212

Table 6.2. Non-parametric relationship of steel column loads. 213

Table 6.3. D-vine copula parameters and rotations for steel column loads. 215

Table 6.4. RBDO outcome considering steel column loads dependency. 217

Table 6.5. DDO outcome for steel column function. 218

Table 6.6. Segmented SCR parameters and FPSO dimensions. 221

Table 6.7. Statistical summary of environmental variables (operating condition) (C-CORE, 2017). 222

Table 6.8. Flemish Pass Ocean Current profile at 1200m water depth (C-CORE,2017). 223

Table 6.9. Copula Selection (operating load case). 223

Table 6.10. Statistical parameters of the segmented SCR design variables 224

Table 6.11. RBDO optimal weight and design variables for segmented SCR. 231

Table 6A.1. Expression for selected copula functions (Elliptical and Archimedean). 239

Table 6A.2. Tail dependence expression for selected copulas 239

Table 6A.3. Minimum AIC values for variables Hs , Tz and Vc..... 240

Table 6A.4. Target failure probability (DNV,2001)..... 240

Table 6A.5. Metamodel error for the segmented SCR 240

LIST OF FIGURES

Figure 1.1. Offshore Structure Reliability-Based Design. Objectives 8

Figure 1.2. Organization of doctoral thesis and related publications. 11

Figure.3.1. Framework for reliability analysis using vine copula. 53

Figure 3.2. Cantilever beam structure. 54

Figure 3.3. D-vine structure for cantilever beam variables. 55

Figure.3.4. Scatter plot for cantilever beam variables. 57

Figure 3.5. Cantilever convergence plot (a) considering dependency (D-vine) (b) Using IS. 59

Figure 3.6. Copula parameter sensitivity plot for the cantilever beam. 61

Figure 3.7. Model of jacket structure in SACS Version 13.0 (Bentley, 2018). 62

Figure 3.8. Offshore jacket structure D-vine configuration for ocean variables. 65

Figure 3.9. Scatter plots for H, Vs and Vm variables for jacket structure. 67

Figure 3.10. Contribution of variables to jacket structure reliability assessment. 69

Figure 3A.1. Fitting extreme value distribution to H (m) data. 75

Figure 3A.2. Fitting extreme value distribution to Vs(m/s) data. 75

Figure 3A.3. Fitting extreme value distribution to Vm(m/s) data. 76

Figure 3A.4. Convergence plots for various environmental load angles on a jacket structure. .. 78

Figure 4.1. Flowchart for reliability assessment using APCKKm-MCS. 101

Figure 4.2. Average computational time (Ten-dimensional function). 104

Figure 4.3. Infinite soil slope problem. 106

Figure 4.4. Average CPU time (Infinite slope model). 107

Figure 4.5. Ten-Bar Truss System. 108

Figure 4.6. Load response FEA for the ten-bar truss. 110

Figure 4.7. Reliability plot for ten-bar truss system. 111

Figure 4.8. SCR configuration and dimensions. 112

Figure 4.9. Dependence of SCR variables using D-vine copula. 114

Figure 4.10. SCR tension and stress profile (a) effective tension profile (b) stress profile. 116

Figure 4.11. SCR reliability and convergence plot. 118

Figure 4.12. SCR tension and stress LSF responses. 120

Figure 4A.1. Probability distribution fit for ocean variables Hs , Tz and Vc. 127

Figure 5.1. Resilience performance curve showing transition phase. 148

Figure 5.2. Resilience Quantification Flowchart 159

Figure 5.3. Histogram of corrosion depth growth rate ($dg(t)\ mm/year$) 166

Figure 5.4. EOLE random process discretization eigenvalues for Pp(t). 168

Figure 5.5. Pipeline reliability index for the leak, burst, and rupture failure condition. 170

Figure 5.6. Pipeline Importance Sampling $CoV_{P_{fc}}{}^{IS}$ plot ($N_{IS} = 10^6$). 171

Figure 5.7. Resilience index ($\eta(t)$) for the offshore natural gas pipeline. 174

Figure 5.8. Pipeline resilience sensitivity plot of the using Borgonovo Index. 175

Figure 6.1. Double-loop RBDO flowchart considering variable dependency. 210

Figure 6.2. D-vine copula configuration for steel column function loads. 213

Figure 6.3. Steel column function scatter plots of bivariate copulas. 216

Figure 6.4. DDO iteration steps for steel column function. 219

Figure 6.5. Convergence plot for D-vine structure (a) $Z1$-$Z2$-$Z3$ (b) $Z2$-$Z1$-$Z3$ (c) $Z2$-$Z3$-$Z1$.

..... 220

Figure 6.6. Copula scatter plot for SCR environmental data. 224

Figure 6.7. Segmented SCR FEA model using Flexcom (Wood,2019). 227

Figure 6.8. Response plot of segmented SCR at hang angle (16.5^o). 229

Figure 6.9. Response validation plots using adaptive PCK for SCR at hang angle (18.5^o). 230

Figure 6.10. SCR optimization plots at different hang angles. 234

NOMENCLATURE

Acronyms

AIC	Akaike Information Criteria
ANN	Artificial Neural Network
API	American Petroleum Institute
ASME	American Society for Mechanical Engineers
BN	Bayesian Network
BSF	Base Shear Force
CBN	Copula Bayesian Network
CDF	Cumulative Density Function
CoV	Coefficient of Variation
CPU	Central Processing Unit
C-vine	Canonical Vine
DBN	Dynamic Bayesian Network
DDO	Deterministic Design Optimization
DNV	Det Norske Veritas
D-vine	Drawable Vine
ED	Experimental Design
EFF	Expected Feasibility Function

EGO Efficient Global Optimization

EOLE Expansion Optimal Linear Estimation

EVD Extreme Value Distribution

FEA Finite Element Analysis

FORM First Order Reliability Method

FPSO Floating Production Storage Offloading

GA Genetic Algorithm

IS Importance Sampling

KKT Karush-Kuhn-Tuker

LARS Least Angle Regression Selection

LHS Latin Hypercube Sampling

LIF Least Important Function

LNG Liquified Natural Gas

LSF Limit State Function

MCS Monte Carlo Simulation

MLE Maximum Likelihood Estimation

MOP Maximum Operating Pressure

MPP Most Probable Point

OLE Orthogonal Series Expansion

PCE Polynomial Chaos Expansion

PCK Polynomial Chaos Kriging

PDF Probability Density Function

PSO Particle Swarm Optimization

RBDO Reliability-Based Design Optimization

RBF Radial Basis Function

SACS Structural Analysis Computer Software

SCR Steel Catenary Riser

SLA Single Loop Approach

SLS Serviceability Limit State

SMYS Specified Minimum Yield Strength

SORA Sequential Optimization and Reliability Assessment

SORM Second-Order Reliability Method

SQP Sequential Quadratic Programming

SVR Support Vector Regression

SwRI Southwest Research Institute

TDP Touch Down Point

TLP Tension Leg Platform

ULS Ultimate Limit State

VIV Vortex-Induced Vibration

Variables, Parameters, and Functions

$C_{(.)}$	Copula density
V_s , V_c	Current velocity at mean sea level
V_m	Current velocity at mudline
$\emptyset_i(t)$	Eigenvector of the covariance matrix
$\bar{H}(t)$	Expectation for Gaussian random process
$M_f(t)$	Folias factor
g(.), G(.)	Limit state function
$L(\theta)$	Logarithm likelihood function
M (t_g)	Maintainability function
t_g	Maintainability repair goal
N_{IS}	Number of important sampling samples
N_{itr}	Number of iterations
N_{mc}	Number of Monte Carlo samples
N_{mod}	Number of model evaluations
d_i	Observation rank difference
q_e	Performance loss ratio at disrupted state
q_{avg}	Performance (average) loss ratio

q_r	Performance recovery ratio
P_f,$P_{fc}(.)$	Probability of failure
Z_i, X_i	Random variables
H,H_s	Significant wave height
$m_j(.)$	Soft constraint for reliability-based optimization
$\hat{P}_{fh}$	Target probability of failure
R (0, t)	Time-varying reliability
$\widehat{H}(t,0)$	Truncated series of Gaussian random process
N_{xx}	Truncation terms for the random process
T_Z	Zero crossing period

Greek Letters

β_{HL}, β_h	Reliability index
$\hat{\beta}_h$	Target reliability index
δ_{B_i}	Borgonovo sensitivity index
$\in_{LOO}, \varepsilon_{LOO}$	Leave one out cross-validation error
$\eta(t)$	Resilience index
θ, θ_c	Copula Parameter
θ_R	Copula Rotation
λ_i	Eigenvalue of the covariance matrix

λ_L	Lower tail dependence
λ_U	Upper tail dependence
$\mu_{\hat{g}}, \mu_{\hat{Y}}$	Predicted mean
v, v^s	Degree of freedom parameter
$\xi_i(\theta)$	Independent standard normal variables
ρ_p	Pearson correlation coefficient
ρ_{rho}	Spearman's rho
$\sigma_{\hat{g}}^2, \sigma^2{}_{\hat{Y}}$	Variance
τ_k	Kendall's tau
$\boldsymbol{\phi}$	Standard normal distribution
$\Psi(.)$	Orthogonal polynomial basis
ψ_r	System recovery

Chapter 1

Introduction

1.1. Background and Motivation

Offshore oil and gas support structures are critical infrastructures that operate in the harsh and uncertain ocean environment and help in the exploration and production of essential mineral resources (oil and gas). These facilities include fixed structures (Jacket structures, Gravity Based structures), floating structures (drillships, semi-submersible, Spars, Tension Leg Platforms (TLP)), flexible structures (marine risers, umbilical, TLP tendons), pipelines, support vessels, and Floating Production Storage and Offloading units (FPSO) (Casciati & Roberts,1996). The imposed loads and complex loading combinations, including environmental loads such as wind, wave, current, seismic, and ice, can induce failure in the structure, thereby affecting lives, assets, and the environment (Faltinsen,1990). Some notable offshore accidents due to structural failure which lead to loss of lives include semi-submersible (Alexander Kielland, Ocean Ranger), drillship (Seacrest, Glomar Java Sea), Jack-up rig (Bohai 2), and platform (Mumbai High North) (Dhillon,2010). These disasters could be traced to the impact of environmental load on the structure, presenting the need to focus on structural safety for the life cycle of marine assets and considering the many forms of uncertainty (Li et al., 2016) associated with the structural system's demand (load) and capacity (strength). The satisfactory performance of offshore assets over their design life is essential, and the assurance of performance in probabilistic terms considering known criteria of the offshore structure, describes its reliability (Haldar & Mahadevan, 2000). Also, considering the given performance criteria, a relationship is developed between the demand and capacity of a structure and its response [Limit State Function (LSF)]. A state beyond the limit state surface

where the functional requirement of the system is not satisfied is considered a failure domain. Shittu et al.(2020) describe four limit states considered in the reliability assessment of offshore structures (serviceability, ultimate, fatigue, and accidental) limit states.

Typically, environmental load variables exhibit complex dependency (American Petroleum Institute (API), 2020; DNVGL,2020); this needs to be accounted for and their impact monitored when evaluating the reliability of offshore structures to ensure confidence in the outcome of the assessment. For simplicity in the structural reliability evaluation of offshore structures, most research considers independence between environmental variables or a linear dependence based on Pearson correlation and Nataf transformation (Schober et al., 2018; Lebrun & Dutfoy, 2009). Consequently, this creates concern about the accuracy of the environmental load acting on the structure, thus reducing the confidence in the reliability outcome for the performance criteria considered. Copulas provide a flexible and marginal independent approach to model dependency between two or more variables (Nelsen,2006). They have wide applications in finance and actuarial science and are gradually becoming an integral concept for dependence modeling for engineering systems. Also, a vital copula characteristic is that it captures linear dependence, nonlinearity, and tail dependence between variables (Joe,2014). The inability to capture these complex dependencies among the various ocean variables can significantly affect the reliability evaluation outcome. In addition, it can be a point of concern for the safety of offshore assets over their design life. Although limited studies exist in the literature where copulas have been used for dependence modeling of environmental load for offshore structures, most of the existing studies have focused on bivariate analysis (Zhang et al., 2018). A consideration of multivariate analysis using copula for effective modeling of dependence of ocean variables is desired to ensure confidence in the outcome from reliability assessment.

Offshore support structures are complex in their form and operate in an uncertain environment which further creates more complexities. An explicit LSF function (those with a close form function of input variables) is typically unavailable to describe the relationship between the input variables and the structure's response. Consequently, numerical computational methods such as Finite Element Analysis (FEA) present a viable alternative for specific response determination of these structures given the corresponding input variables and allowable response required for a given limit state condition (Haldar & Mahadevan, 2000). However, the numerical analysis approach can be computationally expensive and time-consuming for large and complex structures to determine the response required for reliability evaluation. Metamodels provide a cheap and approximate alternative in response determination and reduce the computational burden of the FEA approach. Various types of metamodels have been applied in engineering, including but not limited to Polynomial Regression, Support Vector Regression (SVR), Low-Rank Tensor Approximation, PCE, Radial Basis Function (RBF), and Kriging (Bucher & Most, 2008). The metamodel is essential in the practical reliability assessment of offshore structures.

From the literature, ordinary Kriging and PCE are methods widely applied in metamodel construction for offshore structures compared to other methods. However, given the complexity of offshore structural systems, an ensemble or a combination of such metamodels (Goel et al., 2007) and strategies to reduce the computational burden of construction by sampling around the limit state surface are required to produce a robust model that improves the accuracy of response structure approximation.

The paper by C.S Holling (Holling,1973), which focused on the resilience of ecological systems, set the foundation for resilience research. Consequently, resilience has been an essential topic of discussion and research in many disciplines, including ecology, built environment, supply chain

management, engineering, nuclear, and process systems. Various metrics and resilience assessment methods have been described based on the discipline. In the context of engineering resilience, Yodo et al.(2017) presented a connection between reliability and system recovery in describing the resilience of an engineering system. Similarly, offshore structures are faced with disruptive events during their operational life. Their ability to withstand these events and recover by restoring the system's functionality(resilience) is critical for the overall safety of the asset, lives, and the environment. Although the concept of resilience is widespread in other disciplines and sectors, very few research activities have focused on the resilience of offshore structures and the ability to quantify it for single or multiple disruptive states. Also, with the nature of the ocean environment and the natural or man-made disruptive events that are likely to occur and cause a threat to structural safety during operation, developing a framework for structural resilience quantification of offshore oil and gas support assets is critical.

The trade-off between structural safety and cost is integral to designing complex structural systems operating in an uncertain environment like the ocean. The need for an economical design that considers the structure's uncertainties related to material, geometry, manufacturing, and loading is essential. The trade-off between these competing factors (safety and cost) creates an optimization problem required for design decisions. Consequently, the Reliability-Based Design Optimization (RBDO) of offshore support structural systems results in an improved design performance under uncertainty, considering target reliability values and stated constraints. The RBDO approach leads to structural weight reduction and cost savings. In terms of offshore structures, evaluating uncertainty in ocean variables, material, and other existing load and resistance makes a reliability-based approach more feasible to ensure a proper trade-off between cost and structural safety.

To ensure confidence in the optimal results obtained and associated design variables, the need to consider the dependence between environmental load and utilize a metamodel with a better prediction capability in the inner loop of the RBDO process is of utmost importance.

With the quest for oil and gas exploration and production moving into deepwaters which is harsh and uncertain, offshore assets' safety is critical, and a robust reliability-based design is necessary. The poor dependence modeling (using Pearson correlation), simplicity in handling the interaction of ocean variables required for offshore structural load determination during reliability assessment, and non-consideration of dependency in optimal structural design evaluations are primary reasons for this study. In addition, the accuracy obtained from the response evaluation of offshore structures (mainly large and complex) is needed to improve further using a metamodel that reduces the computational cost and time and reflects the system's response from numerical analysis. Finally, with less emphasis in the literature on an important area related to offshore structures' adaptive and restorative capacity when faced with disruptive events during their operational life, this research takes a step further to develop a framework for offshore structural resilience quantification.

1.2. Objectives

Offshore structures are complex and faced with uncertainty and numerous challenges in the operational environment. Consequently, a robust and safe design of these structures is crucial. This study attempts to answer the following research questions for reliability-based offshore structural design.

i. How can multivariate dependency be captured for environmental ocean variables that induce load on offshore structures?

ii. What is the impact of dependence modeling on offshore structural safety?

iii. Will a combination of high-performance metamodels improve computational accuracy and time in the response determination for complex offshore structures?

iv. How can a performance-based resilience quantification framework for offshore structures be developed?

v. What impact will the consideration of multivariate dependency of environmental variables have in the optimization of complex ocean structures under uncertainty?

Although various aspects of consideration exist in the reliability-based design of structures, based on the presented research questions in this section, this research focuses on the following objectives:

i. To develop a framework to capture dependence between multivariate ocean variables using vine copula.

ii. To examine the significance and effect of dependence through a vine copula-based reliability assessment of offshore structures.

iii. To investigate the impact of a combination of metamodels (Kriging and PCE) considering their unique properties in the reliability evaluation of offshore structures.

iv. Develop a framework that considers reliability, adaptability, and maintainability in quantifying the resilience of oil and gas support structures faced with multiple disruptive events.

v. To develop a double-loop framework for structural cost minimization of offshore structures under uncertainty that considers the dependency between the environmental variables using vine copula.

Considering these areas outlined in the objectives provides an opportunity to develop an improved reliability-based design process and ensure safety for complex offshore structural systems. The aspects described in the objectives of this study are clearly shown in Figure 1.1.

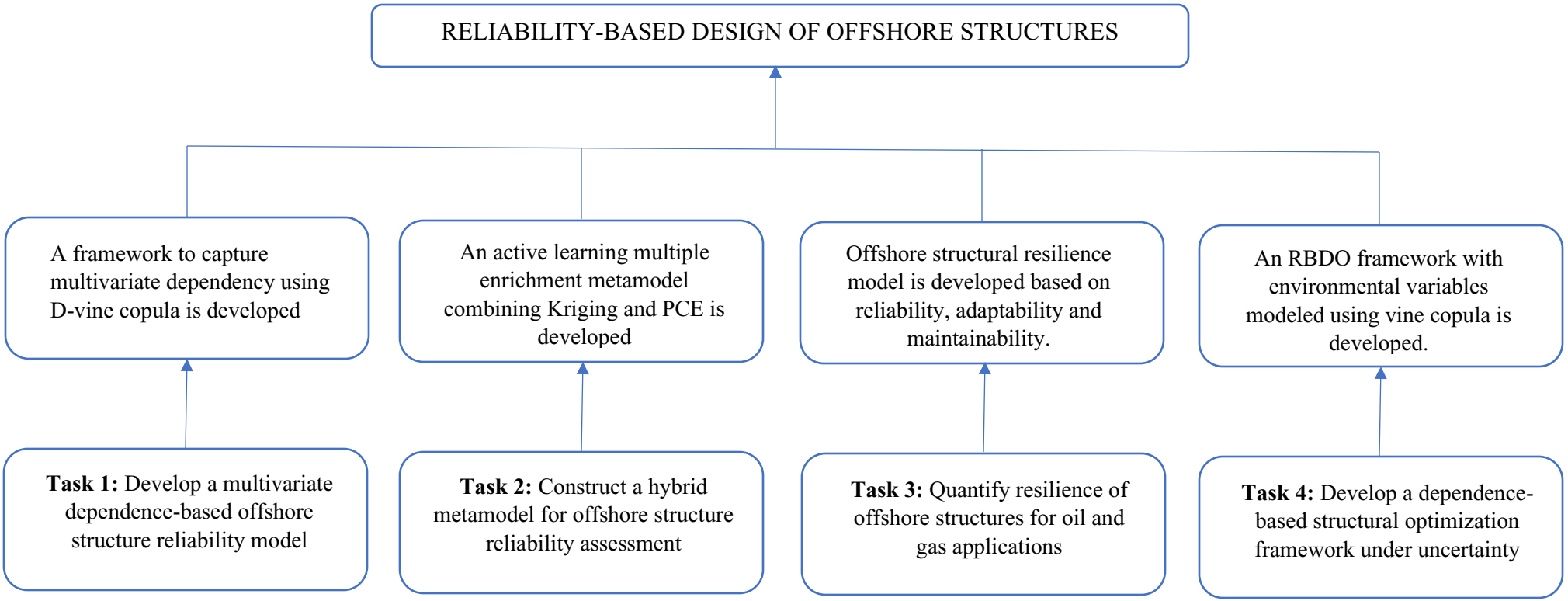

Figure 1.1. Offshore Structure Reliability-Based Design.

1.3. Scope and limitations

The study focuses on offshore structures which support oil and gas exploration and production activities. The research questions initially highlighted guide the scope of this research. For the reliability and resilience assessment activities presented in this study, the limit state approach has been utilized with a focus on Ultimate Limit State (ULS) and Serviceability Limit State (SLS) conditions. This study does not consider the structures' accidental and fatigue limit states. In terms of environmental load on the offshore system, this research has focused on wind, wave, and current conditions due to data availability. Although many copula types exist in the literature for dependence modeling purposes, the analysis in this study has been limited to commonly used copula (Gaussian, Student t, Gumbel, Clayton, and Frank). In addition, the demonstration examples have been focused on an offshore jacket, pipeline, and riser structure due to the limited numerical computational tools available to the author during this study for response determination.

1.4. Organization of the thesis

The manuscript format is adopted for this thesis, which comprises seven chapters. The research outcomes are presented in four chapters in this work and have been submitted to peer-reviewed journals (three have been accepted, and the fourth is under review). In this thesis, Chapters 1, 2, and 7 are the introduction, literature review, and conclusion. Also, Chapters 3 to 6 are chapters developed based on papers submitted to peer- review journals. Figure 1.2 shows the organization of the doctoral thesis. A summary of the contents for the rest of this thesis is presented as follows:

Chapter 2 presents a comprehensive literature review of previous studies relevant to this work and related to offshore structure dependence modeling, metamodel application, resilience modeling, and RBDO. In addition, identified knowledge gaps are outlined.

Chapter 3 presents a methodology for multivariate dependence modeling of environmental ocean variables for reliability assessment of offshore structures using a vine copula (D-vine). The demonstration of the approach was on an offshore jacket structure considering environmental load from the harsh ocean environment. This chapter is published in *Ocean Engineering 2021; 230:109021*.

Chapter 4 proposes a hybrid metamodel that combines Kriging and PCE for structural reliability assessment of complex offshore structures. The hybrid approach is applied to a series of examples, including an oil and gas SCR. This chapter is published in *Ocean Engineering 2021; 235:109399*.

Chapter 5 presents a framework to quantify the resilience of offshore structures utilizing time-varying reliability, adaptability, and maintainability. The framework is applied to an internally corroded offshore pipeline segment. This chapter is published in the *Journal of Pipeline Science and Engineering 2022;100054.*

Chapter 6 investigates the effect of environmental variables' dependence on the optimal design of offshore structures under uncertainty. This approach is demonstrated on a segmented SCR operating in deepwater. This chapter is under peer review in *Reliability Engineering and System Safety Journal.*

Chapter 7 presents the contributions and conclusions drawn from the thesis. In addition, recommendations for future studies are presented.

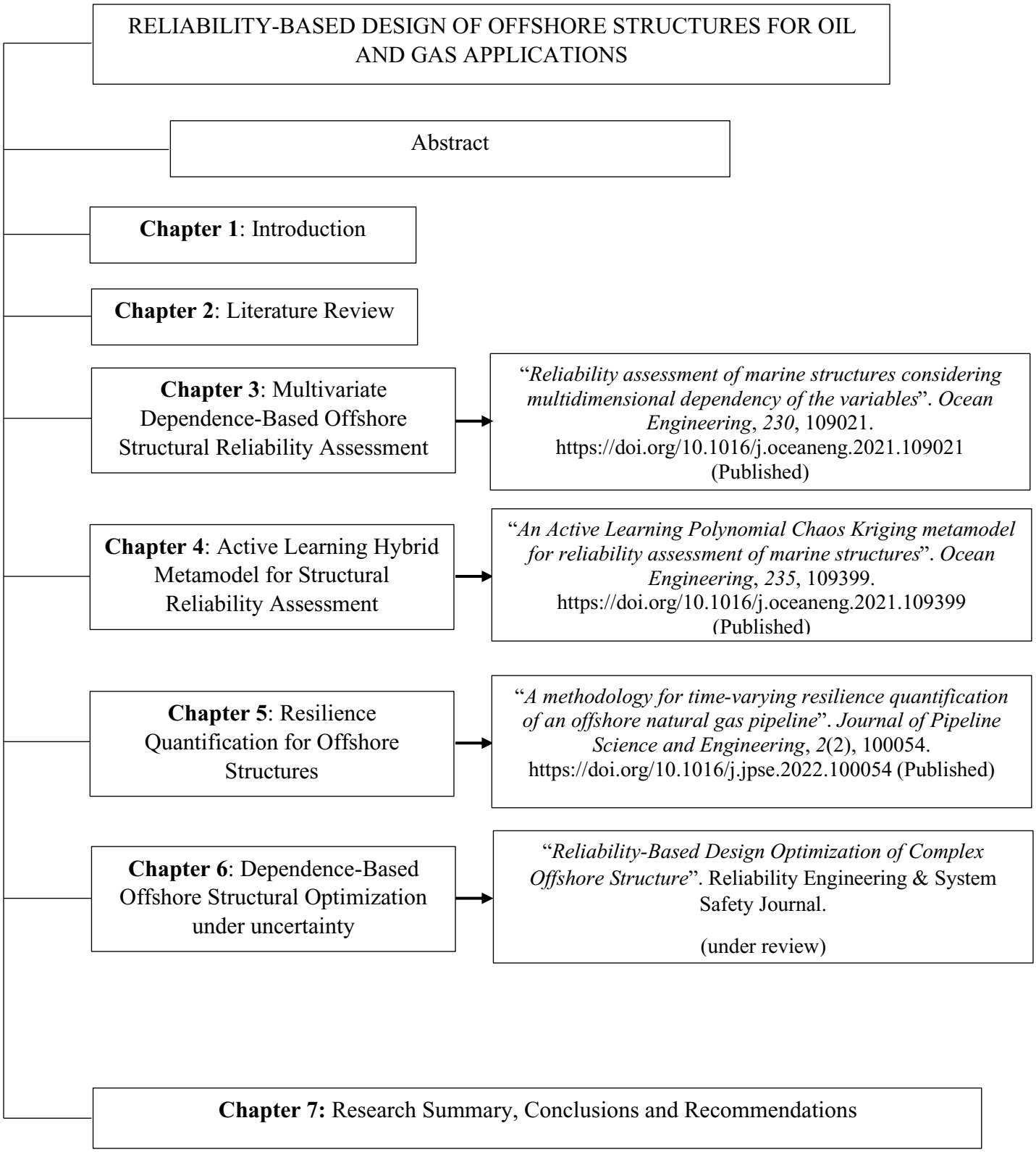

Figure 1.2. Organization of doctoral thesis and related publications.

1.5. Co-authorship Statement

This thesis is the sole authorship of the doctoral candidate (Aghatise Okoro) under the guidance of a supervisory committee. Members of the supervisory committee are Drs Faisal Khan, Salim Ahmed, Yahui Zhang, and Sunday Adedigba. My contribution and that of the supervisory committee members to the research and thesis are outlined below.

Aghatise Okoro: Concept formulation, methodology development, model testing and validation, software analysis, writing the original draft of the manuscript, reviewing and revising the manuscript in response to feedback from co-authors and reviewers from a journal.

Faisal Khan: Supervision, research guidance, concept formulation and improvement, review of methodology, manuscripts review and reorganization, review of thesis.

Salim Ahmed: Supervision, research guidance, review of methodology, manuscripts review and reorganization, review of thesis.

Yahui Zhang: Guidance in doctoral research activities and review of thesis.

Sunday Adedigba: Guidance in doctoral research activities and review of thesis.

References

American Petroleum Institute (API). (2020). *Recommended practice for planning, designing, and constructing fixed offshore platform – working stress design. API RP 2A WSD.*

Bucher, C., & Most, T. (2008). A comparison of approximate response functions in structural reliability analysis. *Probabilistic Engineering Mechanics*, *23*(2–3), 154–163. https://doi.org/10.1016/j.probengmech.2007.12.022

Casciati, F., & Roberts, B. (1996). *Mathematical Models for Structural Reliability Analysis* (Nicola Bellomo (ed.)). CRC Press. Boca Raton.

Dhillon, B. S. (2010). *Mine Safety: A modern approach* (H. Pham (ed.); Springer S). Springer London.

DNVGL. (2020). *Environmental conditions and environmental load recommended practice DNV-RP-C205*.

Faltinsen, O. M. (1990). *Sea Loads on Ships and Offshore Structures*. Cambridge University Press.

Goel, T., Haftka, R. T., Shyy, W., & Queipo, N. V. (2007). Ensemble of surrogates. *Structural and Multidisciplinary Optimization*, *33*, 199–216. https://doi.org/10.1007/s00158-006-0051-9

Haldar, A., & Mahadevan, S. (2000). *Reliability assessment using stochastic finite element analysis.* Wiley.

Holling, C. S. (1973). Resilience and stability of ecological systems. *Annual Review of Ecology and Systematics*, *4*, 1–23.

Joe, H. (2014). Dependence modeling with copulas. In *Dependence Modeling with Copulas* (First). Chapman & Hall /CRC. https://doi.org/10.1201/b17116

Lebrun, R., & Dutfoy, A. (2009). A generalization of the Nataf transformation to distributions with elliptical copula. *Probabilistic Engineering Mechanics*, *24*(2), 172–178. https://doi.org/10.1016/j.probengmech.2008.05.001

Li, G., Lu, Z., Li, L., & Ren, B. (2016). Aleatory and epistemic uncertainties analysis based on non-probabilistic reliability and its kriging solution. *Applied Mathematical Modelling*, *40*(9–10), 5703–5716. https://doi.org/10.1016/j.apm.2016.01.017

Nelsen, R. B. (2006). *An Introduction to Copulas: Lecture Note in Statistics*. Springer US. https://doi.org/https://doi.org/10.1007/0-387-28678-0_1

Schober, P., Boer, C., & Schwarte, L. A. (2018). Correlation Coefficients: Appropriate Use and Interpretation. *Anesthesia & Analgesia*, *126*(5), 1763–1768. https://doi.org/10.1213/ANE.0000000000002864

Shittu, A. A., Kolios, A., & Mehmanparast, A. (2020). A systematic review of structural reliability methods for deformation and fatigue analysis of offshore jacket structures. *Metals*, *11*(1), 1–37. https://doi.org/10.3390/met11010050

Yodo, N., Wang, P., & Zhou, Z. (2017). Predictive Resilience Analysis of Complex Systems Using Dynamic Bayesian Networks. *IEEE Transactions on Reliability*, *66*(3).

Zhang, Y., Kim, C., Beer, M., Dai, H., & Guedes, C. (2018). Modeling multivariate ocean data using asymmetric copulas. *Coastal Engineering*, *135*, 91–111. https://doi.org/10.1016/j.coastaleng.2018.01.008

Chapter 2

Literature Review

2.1. Dependence-based modeling in offshore structure reliability assessment

To appropriately determine the reliability of offshore structures, consideration of dependency between the environmental variables is essential. Most research on the reliability of complex ocean support structures for oil and gas operations assumes independence between variables for simplicity of analysis. An investigation of the non-negligible effect of this relationship between variables is essential for the efficient reliability-based design of these structures. Consequently, studies considering Pearson correlation between variables and copula functions for bivariate dependence analysis have been seen in the literature. Several studies have utilized the Pearson correlation coefficient to determine the dependence between pairs of ocean variables comprising wind, wave, and current and their overall impact on load determination on marine structures (Dong et al., 2008; Nizamani et al., 2017). A study into the effect of spatial Pearson correlation of ocean wave parameters along a ship's route on its vertical bending moment also shows the importance of considering correlation in ship operations (Mikulić et al., 2021). The dependency between wave height and period is captured using a Gaussian copula (Huang & Dong, 2021), which does not consider nonlinearity and tail dependence between variables but can capture the linear relationship.

The use of bivariate copulas to model dependence between pairs of ocean variables has been a significant focus in the literature. The modeling approach using copulas allows the consideration of nonlinearity and tail dependence between variables. Studies into the dependence between wave height and other ocean parameters such as zero-crossing period (Vanem, 2016), storm surge (Li et al., 2021; Chen et al.,2019), steepness (Antão & Guedes Soares, 2014), and extreme sea level

(Mazas & Hamm, 2017) has been considered in the literature. In the case of a tropical cyclone, the dependency between wind speed and wave height was modeled using a Gumbel copula (Sheng & Hong, 2020). Also, asymmetric and truncated copula approach for bivariate ocean data dependency cases have been considered (Zhang et al., 2018; Ma & Zhang, 2022; Zhang et al., 2015).

In the reliability assessment of offshore structures, the research into considering the bivariate dependency of the environmental load has been presented in the literature. In the case of a semi-submersible platform, consideration of dependence between wave parameters (Zhao & Dong, 2021), wind-wave variables of the structural elements of the semi-submersible (Fu & Khan,2020), and dependency on station keeping capability of a semi-submersible for short and long-term extreme loads (Zhao et al., 2020) are areas where copulas have been used to capture dependency. Tao et al.(2013) modeled the dependence between the extreme wave height and wind speed in determining the base shear stress on a jacket structure at different return periods using the Gaussian and Frank Copula.

In addition, Ramadhani et al.(2021) presented a comparative study of the influence of symmetric and asymmetric copula in the dependence modeling of ocean variables (wind speed and wave height) and its effect on the reliability assessment of offshore structures.

For most of the cases in the literature where dependence is considered in the reliability assessment of complex offshore structures, studies have been limited to bivariate environmental load. Consequently, multivariate consideration is necessary to capture the dependence properties of three or more input variables, and the need to investigate the impact of copula parameter choice in the overall reliability assessment process is necessary.

2.2. Metamodels for complex offshore structures

In dealing with large and complex ocean systems, a cheap and accurate model is essential to replace the computationally intensive FEA approach required for structural response determination. Metamodel approaches such as Polynomial regression, Artificial Neural Network (ANN), Kriging, RBF, and SVR relieve the computational burden of numerical methods (Cheng et al., 2020). Kriging and PCE have broad applications to complex multivariate ocean structural systems. The PCE is non-intrusive with model response described by the sum of orthogonal polynomial basis defined by the distribution type of the input variables (Lüthen et al., 2021). The application of the PCE metamodel approach spans various aspects of marine research activities, such as maritime evacuation safety (Xie et al., 2020), determination of frequency response for marine shafting systems (Zhang et al., 2021), determination of the crosstalk's statistical characteristics for a naval ship's wiring harness (Chi et al., 2017) and ship performance research (Xia et al., 2021). In addition, is the implementation of PCE in the uncertainty quantification for ship hull optimization (Scholcz, 2019). For offshore and subsea analysis, the PCE approach is employed in the displacement response determination at the top of a marine riser considering its dynamic response and fluid-structure interaction (Ni et al., 2019), the prediction of the uplift capacity and reliability of plate anchor in clay soil (Charlton & Rouainia, 2016; Charlton & Rouainia, 2019) and in the prediction of surge motion for moored offshore structure (Lim et al., 2021). Other areas PCE metamodel have been applied include the uncertainty propagation and reliability of chlorine-induced corrosion on reinforced concrete offshore structures (Bastidas-Arteaga et al., 2020) and Vortex-Induced Vibration (VIV) prediction of top tension risers (Lim et al., 2017). For metamodel type sensitivity analysis, PCE has played an essential role in the

determination of the influence of the input variable on the structural response parameter (Wei et al., 2019; Radhakrishnan et al., 2021).

Kriging is an interpolation metamodel type and treats the interest function as a Gaussian process realization (Cheng et al., 2020); it comprises a trend and Gaussian process term. Although originating from geostatistics, the concept has been applied in modeling oil and gas support structures. The superior performance of Kriging metamodel over the polynomial regression approach in reliability analysis is demonstrated using a fatigue growth rate assessment of the weld toe of a welded joint plate and the ultimate strength analysis of a stiffened plate for marine applications (Dong et al., 2020; Gaspar et al., 2017). Shi et al.(2015) used a combination of Kriging and the First Order Reliability Method (FORM) for metamodel construction and reliability assessment of the stiffened plate for a ship. A Kriging model was developed for the structural risk assessment of a jacket platform considering serviceability and strength limit state (Vazirizade & Haldar, 2021). For the reliability assessment of the mooring line strength of semi-submersible and floating structures, the model describing the mooring line's extreme tension is constructed using ordinary Kriging (Xu et al., 2020; Gumley et al., 2016). The active learning technique further improves the computation efficiency of constructed Kriging metamodel by starting with a small initial Experimental Design (ED) of input variables and enriching the ED with sample points in the vicinity of the limit state surface. The concept of Kriging construction using the active learning approach has been applied in developing metamodel for complex marine hull structures (Gaspar et al., 2017), reliability assessment of ships (intact and damaged), subsea pipelines, and even in reliability code calibration from target reliability values (Teixeira & Soares, 2018).

The response from constructed metamodels is only an approximate representation of the real-world scenario for structural systems, which include offshore structures. Consequently, with the need for

appropriate structural safety evaluation under uncertainty, the quest for continuous improvement of metamodel accuracy is essential. Kriging and PCE metamodels have vast engineering applications; research into the effect on offshore structural response determination (computational accuracy and efficiency) and reliability from combining their unique properties are essential.

2.3. Resilience in the marine and offshore industry

Structures operating in the offshore environment are faced with natural and man-made hazards; the ability of these structures to absorb, adapt, and recover in the face of disruptive events is critical. Considering the structure's pre and post events activities from a performance perspective in its design and operational phase is vital to enhance structural lifecycle safety, reduce risk, and ensure effective offshore asset management.

The concept of resilience has received research interest in specific sectors of the marine and offshore industry, such as marine operations, marine transport, ship power, and port operations. In maritime operations, the concept of the Bayesian Network (BN) has been used for resilience assessment to investigate potential hydrocarbon release during an FPSO and a marine Liquified Natural Gas (LNG) loading operation (Hu et al., 2021; Sarwar et al., 2018). Other research activities involving resilience assessment include ship bunkering (Vairo et al., 2020), offshore helicopter operations (Gomes et al., 2009), and marine fleet design for more resilient operations (Pettersen & Asbjørnslett, 2016).

The concept of resilience has seen significant application in marine transport. Some areas of application include cyber resilience during vessel navigation (Nissov et al., 2021), the dynamic resilience assessment of arctic shipping (Liu et al., 2022), and crew resilience and coping strategies following a ship accident in a polar climate (Ivar Kruke, 2021). In addition, the risk-based

resilience approach (Wan et al., 2019) and methodologies for resilience management for the port and vessel route operations (Dui et al., 2021) are additional research focus areas in the literature.

The resilience assessment of port activities and networks typically affects the supply chain and vessel transportation. Xu et al.(2019) investigated the resilience of the chain handling system in a container port. Also, the resilience determination of seaport structures due to seismic effect with its improvement strategies (Hur et al., 2019) and an investigation into port operations and scenario-based methods for resilience due to the impact of disruptive events (Al-Mutairi et al., 2022; Verschuur et al., 2020; Liu & Chen, 2021) are areas of focus in maritime and port activities.

In the aspect of shipboard power resilience, Billah Kushal & Illindala (2020) developed a data-driven framework to determine the best performance predictors of the shipboard power plant during a contingency to reduce the power recovery time and ensure its availability. Furthermore, a resilience control mechanism is developed for a shipboard direct current power system (Li et al., 2018).

Finally, considering the complexity of offshore support structures and the environment in which they operate, very few attempts and methodologies have been developed to quantify the resilience of these structures. Ramadhani et al.(2022) developed a method for the resilience assessment of offshore structures considering ice load. Also, an approach to quantify the resilience of subsea pipelines using the Dynamic Bayesian Network (DBN) and Markov Process has been considered (Bao-ping et al.,2020; Yazdi et al., 2022).

While various metrics and methods to quantify resilience exist and more are constantly being developed in multiple fields, few attempts have been made to quantify the resilience of offshore structures from a performance standpoint. Resilience is a system concept with safety as the

emerging property; thus, the need for appropriate resilience design for critical offshore and marine structural systems. Developing a performance-based resilience framework in terms of the structural system's reliability, recoverability, and maintainability considering multiple disruptive events, is vital.

2.4. Optimization of ocean structure under uncertainty

From the literature, the optimal design of some offshore oil and gas support structures fails to consider the uncertainty arising from the operating environment, loading conditions, and manufacturing tolerances. Examples of these cases include floating structural systems such as semi-submersible hull optimization (Tian et al., 2021) and the hull and tendon optimal design of a TLP (Du Kim & Jang, 2016; Nordgren, 1989; Vannucci, 1996). In addition, the weight and volume optimization of offshore jacket structures (Motlagh et al., 2021; Burak & Mengshoel, 2021; Ni & Ge, 2019) and the optimal design of the spud can, gearbox, and hull shape of a Jack-up platform (Yu et al., 2022; Li et al., 2020; Yu et al., 2012; Tang et al., 2013) are more cases presented in the literature. Also are the optimal design of offshore mooring systems (Yu & Tan, 2010; Yan et al., 2018), flexible marine risers (Yang et al., 2018; Yuan et al., 2021), and cross-sectional layout optimization of marine umbilical (Yin et al., 2021; Yang et al., 2020). From the above literature, uncertainty quantification and propagation were not considered in the designs presented which are integral for a realistic evaluation of optimal design decisions for offshore oil and gas support structures.

On the other hand, some research activities in optimizing offshore structural systems have considered the effect of uncertainty and the use of metamodels. Yong et al.(2011) applied a moving least square approach to minimize the weight of an FPSO riser support using classical RBDO methods considering different constraints such as the operating, extreme, damage, and installation

conditions. Another case is the weight optimization of an SCR using the ordinary Kriging metamodel (Yang & Zheng, 2011). Furthermore, the stack-up of a marine drilling riser is optimized using an RBF metamodel (Yang et al., 2018). RBDO has also been applied to a subsea control cable (umbilical) to minimize its mass per unit length using a Particle Swarm Optimization (PSO) technique (Yan et al., 2017). In addition, the RBDO approach has been applied to different types of marine structures, such as adaptive composites rotors (Young et al., 2010), Cranes (Li et al., 2021), and pipeline insulation for subsea production systems (Hong et al., 2020). The effect of the choice of a metamodel for optimization was demonstrated in the fatigue RBDO study of a bending stiffener for an umbilical by a comparative analysis of the response surface method, RBF, and Kriging approach with the Kriging method providing better performance (Yang & Wang, 2012).

RBDO has been applied in optimizing structural components of a ship with constraints related to sizing, materials type, shape, topology, and the structural system in general (Akpan et al., 2015; Ayyub et al., 2015). The various aspects include the minimization of a ship's stiffened panel weight subject to constraints related to buckling (plate and longitudinal stiffened panel), collapse, and stiffener torsion (Leheta & Mansour, 1997). The application of the Sequential Optimization and Reliability Assessment (SORA) framework to optimize plates and beams elements of a multipurpose ship using the Kriging and PSO approach (Hu & Wang, 2016) and fatigue optimization of the stiffened panel of ship considering stochastic loads (Garbatov & Huang, 2020) are other areas of focus in marine vessel components optimization.

Furthermore, structural optimization under uncertainty has been applied to offshore structures. The offshore tower optimization considers critical stress, buckling, and natural frequency probabilistic constraints under extreme loading conditions (Karadeniz et al., 2009; Togan et al., 2010). The

structural optimization of an oil and gas production platform (Ang et al., 2021), minimizing the weight of a fixed-type offshore platform (Kim et al., 2021), and the column and braces of a jack-up platform (Datta et al., 2019). Regarding oil well production and intervention structures, the RBDO approach is implemented to minimize a casing tubular cross-sectional area (da Silveira & Lima Junior, 2019).

The ocean environment is harsh and uncertain, and the safety of lives, assets, and its operating surrounding are critical. The concept of considering uncertainty and a cost-safety trade-off for offshore structures has relatively limited application compared to other types of systems. Also, from the literature, there is little knowledge on the impact of considering variables dependency in RBDO analysis of offshore structures. Consequently, further research into dependency modeling, uncertainty consideration, and a metamodel ensemble or hybrid is essential in an efficient trade-off for the optimal design of oil and gas support structures.

2.5. Knowledge Gaps and Research Tools

A comprehensive study of the existing literature on the reliability-based design of offshore structures for oil and gas applications reveals the following gap requiring further research.

i. Limited research activities in the reliability assessment of ocean structures consider the possible nonlinearity and tail dependence of the environmental input variables.
ii. Current research involving input variables for reliability studies of offshore structures at best considers bivariate dependence of ocean variables. The existing literature does not account for the multivariate dependency of variables in reliability assessment.

iii. Although significant advancements have been made in using Kriging and PCE for constructing metamodels to reduce the computational burden of complex offshore structures, an investigation into the impact of a combination of these methods (hybrid) has not been significantly explored.

iv. Although the concept of resilience has been widely studied in various disciplines and even in oil and gas process operations, there are still limited research activities in the resilience quantification of offshore structures (structural resilience).

v. From the literature and to the extent reviewed by the author, no known studies consider the multivariate dependency of environmental variables in optimizing offshore structures under uncertainty and a hybrid metamodel construction in a nested RBDO problem.

In this thesis, journal articles obtained from related scientific databases are used to ascertain the state of knowledge and determine possible gaps for research purposes. The engineering and simulation analysis uses an i7-7500U computer with a Central Processing Unit (CPU) of 2.90GHz and an 8GB memory. The codes and algorithms for uncertainty quantification, metamodel construction, resilience analysis, stochastic discretization, and optimization were implemented using MATLAB. The open-source package R-Studio and Microsoft office excel were used for statistical and probabilistic analysis. For numerical simulation, modeling and FEA were implemented using SACS (Version 13.0) and Flexcom software (Version 8.10.4) for fixed and floating structures. The environmental ocean data utilized for offshore applications are mainly obtained from reports of site-specific data for offshore Newfoundland and Labrador (Grand Banks and Flemish Pass). Also, the language for writing this thesis was made as clear and concise as possible for easy communication of thoughts and ideas.

References

Akpan, U. O., Ayyub, B. M., Asce, F., Koko, T. S., & Rushton, P. A. (2015). Development of Reliability-Based Damage-Tolerant Optimal Design of Ship Structures. *ASCE-ASME J. Risk Uncertainty Eng. Sys*, *1*(4). https://doi.org/10.1061/AJRUA6.0000836

Al-Mutairi, A., AlKheder, S., Alzwayid, S., Talib, D., Heji, M. B., & Lambert, J. H. (2022). Scenario-based preferences modeling to investigate port initiatives resilience. *Technological Forecasting and Social Change, 176,*121498. https://doi.org/10.1016/j.techfore.2022.121498

Ang, A. H., Leon, D. De, & Fan, W. (2021). Optimal reliability-based design of complex structural systems.*Structural Safety*, 90,102048. https://doi.org/10.1016/j.strusafe.2020.102048

Antão, E. M., & Guedes Soares, C. (2014). Approximation of bivariate probability density of individual wave steepness and height with copulas. *Coastal Engineering*, *89*, 45–52. https://doi.org/10.1016/j.coastaleng.2014.03.009

Ayyub, B. M., Asce, F., Akpan, U. O., Koko, T. S., & Dunbar, T. (2015). Reliability-Based Optimal Design of Steel Box Structures. I : Theory. *ASCE-ASME J. Risk Uncertainty Eng. Syst*, *1*(3). https://doi.org/10.1061/AJRUA6.0000829

Bao-ping, C. A. I., Yan-ping, Z., Xiao-bing, Y., Chun-tan, G. A. O., Yong-hong, L. I. U., Guo-ming, C., Zeng-kai, L. I. U., & Ren-jie, J. I. (2020). A Dynamic-Bayesian-Networks-Based Resilience Assessment Approach of Structure Systems : Subsea Oil and Gas Pipelines as A Case Study. *China Ocean Engineering*, *34*(5), 597–607.

Bastidas-Arteaga, E., El Soueidy, C. P., Amiri, O., & Nguyen, P. T. (2020). Polynomial chaos expansion for lifetime assessment and sensitivity analysis of reinforced concrete structures subjected to chloride ingress and climate change. *Structural Concrete*, *21*(4), 1396–1407. https://doi.org/10.1002/suco.201900398

Billah Kushal, T. R., & Illindala, M. S. (2020). Correlation-based feature selection for resilience analysis of MVDC shipboard power system. *International Journal of Electrical Power and Energy Systems*, *117*, 105742. https://doi.org/10.1016/j.ijepes.2019.105742

Burak, J., & Mengshoel, O. J. (2021). A multi-objective genetic algorithm for jacket optimization. *GECCO 2021 Companion - Proceedings of the 2021 Genetic and Evolutionary Computation Conference Companion*, 1549–1556. https://doi.org/10.1145/3449726.3463150

Charlton, T., & Rouainia, M. (2016). The uplift capacity of horizontal plate anchors in spatially variable clay using sparse polynomial chaos expansions. *ECCOMAS Congress 2016 - Proceedings of the 7th European Congress on Computational Methods in Applied Sciences and Engineering*, *4*, 8769–8777. https://doi.org/10.7712/100016.2448.7622

Charlton, T. S., & Rouainia, M. (2019). Uncertainty quantification of offshore anchoring systems in spatially variable soil using sparse polynomial chaos expansions. *International Journal for Numerical Methods in Engineering*, *120*(6), 748–767. https://doi.org/10.1002/nme.6155

Chen, Y., Li, J., Pan, S., Gan, M., Pan, Y., Xie, D., & Clee, S. (2019). Joint probability analysis of extreme wave heights and surges along China's coasts. *Ocean Engineering*, *177*, 97–107. https://doi.org/10.1016/j.oceaneng.2018.12.010

Cheng, K., Lu, Z., Ling, C., & Zhou, S. (2020). Surrogate-assisted global sensitivity analysis: an overview. *Structural and Multidisciplinary Optimization*, *61*(3), 1187–1213. https://doi.org/10.1007/s00158-019-02413-5

Chi, Y., Li, B., Yang, X., Wang, T., Yang, K., & Gao, Y. (2017). Research on the statistical characteristics of crosstalk in naval ships wiring harness based on polynomial chaos expansion method. *Polish Maritime Research*, *24*, 205–214. https://doi.org/10.1515/pomr-2017-0084

da Silveira, G. ., & Lima Junior, E. . (2019). RBDO as a decision-making tool in the tubular design against collapse. *XL Ibero-Latin-American Congress on Computational Methods in Engineering, ABMEC*.

Datta, G., Bhattacharjya, S., & Chakraborty, S. (2019). Adaptive Metamodel-Based Efficient Robust Design Optimization of Offshore Structure Under Wave Loading. In A. Rama Mohan Rao & K. Ramanjaneyulu (Eds.), *Recent Advances in Structural Engineering, Volume 1* (pp. 465–476). Springer Singapore.

Dong, S., Liu, W., & Xu, P. (2008). Combination criteria of joint extreme significant wave height and wind speed in weizhoudao offshore area. *Proceedings of the International Conference on Offshore Mechanics and Arctic Engineering - OMAE*, *2*, 241–246. https://doi.org/10.1115/OMAE2008-57219

Dong, Y., Teixeira, A. P., & Guedes Soares, C. (2020). Application of adaptive surrogate models in time-variant fatigue reliability assessment of welded joints with surface cracks. *Reliability Engineering and System Safety*, *195*, 106730. https://doi.org/10.1016/j.ress.2019.106730

Du Kim, J., & Jang, B. S. (2016). Application of multi-objective optimization for TLP considering hull-form and tendon system. *Ocean Engineering*, *116*, 142–156. https://doi.org/10.1016/j.oceaneng.2016.02.033

Dui, H., Zheng, X., & Wu, S. (2021). Resilience analysis of maritime transportation systems based on importance measures. *Reliability Engineering and System Safety*, *209*, 107461. https://doi.org/10.1016/j.ress.2021.107461

Fu, J., & Khan, F. (2020). Monitoring and modeling of environmental load considering dependence and its impact on the failure probability. *Ocean Engineering*, *199*, 107008. https://doi.org/10.1016/j.oceaneng.2020.107008

Garbatov, Y., & Huang, Y. C. (2020). Multiobjective Reliability-Based Design of Ship Structures Subjected to Fatigue Damage and Compressive Collapse. *Journal of Ocean Mechanics and Arctic Engineering*, *142*. https://doi.org/10.1115/1.4046378

Gaspar, B., Teixeira, A. P., & Guedes Soares, C. (2017). Adaptive surrogate model with active refinement combining Kriging and a trust region method. *Reliability Engineering and System Safety*, *165*, 277–291. https://doi.org/10.1016/j.ress.2017.03.035

Gomes, J. O., Woods, D. D., Carvalho, P. V. R., Huber, G. J., & Borges, M. R. S. (2009). Resilience and brittleness in the offshore helicopter transportation system: The identification of constraints and sacrifice decisions in pilots' work. *Reliability Engineering and System Safety*, *94*(2), 311–319. https://doi.org/10.1016/j.ress.2008.03.026

Gumley, J. M., Henry, M. J., & Potts, A. E. (2016). A novel method for predicting the motion of moored floating bodies. *Proceedings of the ASME 2016 35th International Conference on Ocean, Offshore and Arctic Engineering*.

Hong, C., Wang, Y., Yang, J., Estefen, S. F., & Igor, M. (2020). Optimization of Pipe Insulation Volume for a Subsea Production System. *Transactions of ASME*, *142*. https://doi.org/10.1115/1.4046001

Hu, J., Khan, F., & Zhang, L. (2021). Dynamic resilience assessment of the Marine LNG offloading system. *Reliability Engineering and System Safety*, *208*, 107368. https://doi.org/10.1016/j.ress.2020.107368

Hu, X., & Wang, D. (2016). Reliability-based Design Optimization of Ship Structure Using Sequential Optimization and Reliability. *Proceedings of the Twenty-Sixth International Ocean and Polar Engineering Conference*, 949–954.

Huang, W., & Dong, S. (2021). Joint distribution of significant wave height and zero-up-crossing wave period using mixture copula method. *Ocean Engineering*, *219*, 108305. https://doi.org/10.1016/j.oceaneng.2020.108305

Hur, J., Shafieezadeh, A., & Chen, Z. (2019). An Integrated Assessment of Seismic Hazard Vulnerability and Resilience of Seaports. In P. Jain & W. S. Stahlmann (Eds.), *ASCE : Ports Engineering 15th Triennial International Conference* (pp. 11–22).

Ivar Kruke, B. (2021). Survival through coping strategies for resilience following a ship accident in polar waters. *Safety Science*, *135*. https://doi.org/10.1016/j.ssci.2020.105105

Karadeniz, H., Togan, V., & Vrouwenvelder, T. (2009). An integrated reliability-based design optimization of offshore towers. *Reliability Engineering and System Safety*, *94*, 1510–1516. https://doi.org/10.1016/j.ress.2009.02.008

Kim, H.-S., Kim, H.-S., Park, B., & Lee, K. (2021). Reliability-Based Design Optimization of 130m Class Fixed-Type Offshore Platform. *Journal of Computational Structural Engineering Institute of Korea*, *34*(5), 263–270.

Leheta, H. W., & Mansour, A. E. (1997). Reliability-based Method for Optimal Structural Design of Stiffened Panels Xp. *Marine Structures*, *10*, 323–352.

Li, J., Bai, L., Gao, W., Shi, N., Wang, N., Ye, M., & Gu, H. (2021). Reliability-based design optimization for the lattice boom of crawler crane. *Structures*, *29*, 1111–1118. https://doi.org/10.1016/j.istruc.2020.12.024

Li, J., Liu, F., Chen, Y., Shao, C., Wang, G., Hou, Y., & Mei, S. (2018). Resilience control of DC shipboard power systems. *IEEE Transactions on Power Systems*, *33*(6), 6675–6685. https://doi.org/10.1109/TPWRS.2018.2844161

Li, S., Song, C., Zhu, C., Song, H., & Du, X. (2020). Optimization of teeth distribution for promote gearbox used in jack-up offshore platforms using improved genetic algorithm. *Journal of Advanced Mechanical Design, Systems and Manufacturing*, *14*(6), 1–16. https://doi.org/10.1299/JAMDSM.2020JAMDSM0086

Lim, H., Manuel, L., Min Low, Y., & Srinil, N. (2017). Uncertainty quantification of riser fatgue damage due to VIV using a distributed wake oscillator model. *Proceedings of the ASME 2017 36th International Conference on Ocean, Offshore and Arctic Engineering*.

Lim, H. U., Manuel, L., & Min Low, Y. (2021). On Efficient Surrogate Model Development for the Prediction of the Long-Term Extreme Response of a Moored Floating Structure. *Journal of Offshore Mechanics and Arctic Engineering*, *143*(1), 1–9. https://doi.org/10.1115/1.4047545

Liu, X., & Chen, Z. (2021). An Integrated Risk and Resilience Assessment of Sea Ice Disasters on Port Operation. *Risk Analysis*, *41*(9), 1579–1599. https://doi.org/10.1111/risa.13660

Liu, Y., Ma, X., Qiao, W., & Han, B. (2022). A Methodology to Model the Evolution of System Resilience for Arctic Shipping from the Perspective of Complexity. *SSRN Electronic Journal*. https://doi.org/10.2139/ssrn.4046078

Lüthen, N., Marelli, S., & Sudret, B. (2021). Sparse polynomial chaos expansions: Literature survey and benchmark. *SIAM-ASA Journal on Uncertainty Quantification*, *9*(2), 593–649. https://doi.org/10.1137/20M1315774

Ma, P., & Zhang, Y. (2022). Modeling asymmetrically dependent multivariate ocean data using truncated copulas. *Ocean Engineering*, *244*, 110226. https://doi.org/10.1016/j.oceaneng.2021.110226

Mazas, F., & Hamm, L. (2017). An event-based approach for extreme joint probabilities of waves and sea levels. *Coastal Engineering*, *122*, 44–59. https://doi.org/10.1016/j.coastaleng.2017.02.003

Mikulić, A., Katalinić, M., Ćorak, M., & Parunov, J. (2021). The effect of spatial correlation of sea states on extreme wave loads of ships. *Ships and Offshore Structures*, *16*(S1), 22–32. https://doi.org/10.1080/17445302.2021.1884817

Motlagh, A. A., Shabakhty, N., & Kaveh, A. (2021). Design optimization of jacket offshore platform considering fatigue damage using Genetic Algorithm. *Ocean Engineering*, *227*, 108869. https://doi.org/10.1016/j.oceaneng.2021.108869

Ni, L., & Ge, Y. (2019). Structural Optimization of Jacket Platform Based on Genetic Algorithm. *IOP Conference Series: Earth and Environmental Science*, *242*(3). https://doi.org/10.1088/1755-1315/242/3/032048

Ni, P., Li, J., Hao, H., Xia, Y., & Du, X. (2019). Stochastic dynamic analysis of marine risers considering fluid-structure interaction and system uncertainties. *Engineering Structures*, *198*. https://doi.org/10.1016/j.engstruct.2019.109507

Nissov, M. C., Dagdilelis, D., Galeazzi, R., & Blanke, M. (2021). Analysing Cyber-resiliency of a Marine Navigation System using Behavioural Relations. *2021 European Control Conference, ECC 2021*, 1385–1392. https://doi.org/10.23919/ECC54610.2021.9654972

Nizamani, Z., Woan Yih, L., Wahab, M. M. A., & Mustaffa, Z. (2017). Determination of Correlation for Extreme Metocean Variables. *MATEC Web of Conferences*, *103*. https://doi.org/10.1051/matecconf/201710304013

Nordgren, R. P. (1989). The Design of Tension Leg Platforms by a Constrained Optimization Method. *Journal of Offshore Mechanics and Arctic Engineering*, *111*(3), 194–202. https://doi.org/10.1115/1.3257147

Pettersen, S. S., & Asbjørnslett, B. E. (2016). A design methodology for resilience in fleets for service operations. *PRADS 2016 - Proceedings of the 13th International Symposium on PRActical Design of Ships and Other Floating Structures*.

Radhakrishnan, G., Han, X., Sævik, S., Gao, Z., & Johan Leira, B. (2021). System uncertainty effects on the wave frequency response of floating vessels based on Polynomial Chaos Expansion. *Proceedings of the ASME 2021 40th International Conference on Ocean, Offshore and Arctic Engineering*.

Ramadhani, A., Khan, F., Colbourne, B., Ahmed, S., & Taleb-Berrouane, M. (2021). Environmental load estimation for offshore structures considering parametric dependencies. *Safety in Extreme Environments*, *3*(2), 75–101. https://doi.org/10.1007/s42797-021-00028-y

Ramadhani, A., Khan, F., Colbourne, B., Ahmed, S., & Taleb-Berrouane, M. (2022). Resilience assessment of offshore structures subjected to ice load considering complex dependencies. *Reliability Engineering and System Safety*, *222*, 108421. https://doi.org/10.1016/j.ress.2022.108421

Sarwar, A., Khan, F., Abimbola, M., & James, L. (2018). Resilience Analysis of a Remote Offshore Oil and Gas Facility for a Potential Hydrocarbon Release. *Risk Analysis*, *38*(8), 1601–1617. https://doi.org/10.1111/risa.12974

Scholcz, T. P. (2019). Data driven uncertainty quantification for computational fluid dynamics based ship design. *8th International Conference on Computational Methods in Marine Engineering, MARINE 2019*, 309–320.

Sheng, C., & Hong, H. P. (2020). On the joint tropical cyclone wind and wave hazard. *Structural Safety*, *84*, 101917. https://doi.org/10.1016/j.strusafe.2019.101917

Shi, X., Palos Teixeira, Â., Zhang, J., & Guedes Soares, C. (2015). Kriging response surface reliability analysis of a ship-stiffened plate with initial imperfections. *Structure and Infrastructure Engineering*, *11*(11), 1450–1465. https://doi.org/10.1080/15732479.2014.976575

Tang, W., Tang, Z., Xia, T., & Zhang, J. (2013). Optimum structural design of the hull on jack-up platform. *Advanced Materials Research*, *631–632*, 936–941. https://doi.org/10.4028/www.scientific.net/AMR.631-632.936

Tao, S., Dong, S., & Xu, Y. (2013). Design Parameter Estimation of Wave Height and Wind Speed with Bivariate Copulas. *Proceedings of the ASME 2013 32nd International Conference on Ocean, Offshore and Arctic Engineering*.

Teixeira, A. P., & Soares, C. G. (2018). Adaptive methods for reliability analysis of marine structures. *Proceedings of the International Conference on Offshore Mechanics and Arctic Engineering - OMAE*, *11B*, 1–10. https://doi.org/10.1115/OMAE2018-77311

Tian, X., Sun, X., Liu, G., Xie, Y., Chen, Y., & Wang, H. (2021). Multi-objective optimization of the hull form for the semi-submersible medical platform. *Ocean Engineering*, *230*, 109038. https://doi.org/10.1016/j.oceaneng.2021.109038

Togan, V., Karadeniz, H., & Daloglu, A. . T. (2010). An integrated framework including distinct algorithms for optimization of offshore towers under uncertainties. *Reliability Engineering and System Safety*, *95*, 847–858. https://doi.org/10.1016/j.ress.2010.03.009

Vairo, T., Gualeni, P., Fabiano, B., & Benvenuto, A. C. (2020). Resilience assessment of bunkering operations for A LNG fuelled ship. In P. Baraldi, F. Di Maio, & E. Zio (Eds.), *30th European Safety and Reliability Conference, ESREL 2020 and 15th Probabilistic Safety Assessment and Management Conference, PSAM 2020* (pp. 3693–3701). https://doi.org/10.3850/978-981-14-8593-0

Vanem, E. (2016). Copula-Based Bivariate Modelling of Significant Wave Height and Wave Period and the Effects of Climate Change on the Joint Distribution. *Proceedings of the ASME 2016 35th International Conference on Ocean, Offshore and Arctic Engineering*.

Vannucci, P. (1996). Simplified optimal design of a tension leg platform (TLP). *Structural Optimization*, *12*(4), 265–268. https://doi.org/10.1007/BF01197367

Vazirizade, S. M., & Haldar, A. (2021). A Novel Risk Evaluation Procedure Using a Kriging-Based Surrogate Modeling for Offshore Structures. *KSCE Journal of Civil Engineering*, *25*(7), 2603–2612. https://doi.org/10.1007/s12205-021-1411-0

Verschuur, J., Koks, E. E., & Hall, J. W. (2020). Port disruptions due to natural disasters: Insights into port and logistics resilience. *Transportation Research Part D: Transport and Environment*, *85*, 102393. https://doi.org/10.1016/j.trd.2020.102393

Wan, C., Yang, Z., Yan, X., Zhang, D., Blanco-Davis, E., & Ren, J. (2019). Risk-Based Resilience Analysis of Maritime Container Transport Network. In E. Bear,Michael and Zio (Ed.), *Proceedings of the 29th European Safety and Reliability Conference* (pp. 3667–3674). https://doi.org/10.3850/978-981-11-2724-3

Wei, X., Chang, H., Feng, B., & Liu, Z. (2019). Sensitivity analysis based on polynomial chaos expansions and its application in ship uncertainty-based design optimization. *Mathematical Problems in Engineering*, *2019*. https://doi.org/10.1155/2019/7498526

Xia, L., Zou, Z. J., Wang, Z. H., Zou, L., & Gao, H. (2021). Surrogate model based uncertainty quantification of CFD simulations of the viscous flow around a ship advancing in shallow water. *Ocean Engineering*, *234*, 109206. https://doi.org/10.1016/j.oceaneng.2021.109206

Xie, Q., Li, S., Ma, C., Wang, J., Liu, J., & Wang, Y. (2020). Uncertainty analysis of passenger evacuation time for ships' safe return to port in fires using polynomial chaos expansion with Gauss quadrature. *Applied Ocean Research*, *101*, 102190. https://doi.org/10.1016/j.apor.2020.102190

Xu, B., Li, J., Yang, Y., Wu, H., & Postolache, O. (2019). Model and Resilience Analysis for Handling Chain Systems in Container Ports. *Complexity*, 1–12. https://doi.org/10.1155/2019/9812651

Xu, S., Teixeira, A. P., & Soares, C. G. (2020). Conditional reliability analysis of a semi-submersible mooring line with random hydrodynamic coefficients. *Journal of Offshore Mechanics and Arctic Engineering*, *142*(1). https://doi.org/10.1115/1.4044653

Yan, J., Qiao, D., & Ou, J. (2018). Optimal design and hydrodynamic response analysis of deep water mooring system with submerged buoys. *Ships and Offshore Structures*, *13*(5), 476–487. https://doi.org/10.1080/17445302.2018.1426282

Yan, J., Yang, Z., Zhao, P., Lu, Q., Wu, W., & Yue, Q. (2017). Reliability Optimization Design of the Steel Tube Umbilical. *Proceedings of the ASME 2017 36th International Conference on Ocean, Offshore and Arctic Engineering OMAE2017*.

Yang, H., Glasgow, G., Low, Y. M., Francis, P., & Adaikalaraj, B. (2018). Multi-objective design optimization of drilling riser operability envelope for ultra-deep water. *Proceedings of the ASME 2018 37th International Conference on Ocean, Offshore and Arctic Engineering OMAE2018*.

Yang, H., & Wang, A. (2012). Fatigue Reliability Based Design Optimization of Bending Stiffener. *Journal of Ship Research*, *56*(2), 120–128.

Yang, H., & Zheng, W. (2011). Metamodel approach for reliability-based design optimization of a steel catenary riser. *Journal of Marine Science and Technology*, *16*(2), 202–213. https://doi.org/10.1007/s00773-011-0121-6

Yang, Z., Yan, J., Sævik, S., Zhen, L., Ye, N., Chen, J., & Yue, Q. (2018). Multi-objective optimization design of flexible risers based on Bi-scale response surface models. *Proceedings of the International Conference on Offshore Mechanics and Arctic Engineering - OMAE*, *5*. https://doi.org/10.1115/OMAE2018-77947

Yang, Z., Yin, X., Shi, D., Yan, J., Wang, L., Lu, Q., & Yue, Q. (2020). Optimization design of the cross-section of the umbilical based on the pseudo mechanical mechanism. *Proceedings of the International Conference on Offshore Mechanics and Arctic Engineering - OMAE*, *4*, 3–8. https://doi.org/10.1115/OMAE2020-19234

Yazdi, M., Khan, F., Abbassi, R., & Quddus, N. (2022). Resilience assessment of a subsea pipeline using dynamic Bayesian network. *Journal of Pipeline Science and Engineering*, *2*(2), 100053. https://doi.org/10.1016/j.jpse.2022.100053

Yin, X., Yang, Z., Shi, D., Yan, J., Wang, L., Lu, Q., & Tian, G. (2021). The optimization design of the cross-sectional layout of an umbilical based on the hybrid genetic algorithm. *Proceedings of the International Conference on Offshore Mechanics and Arctic Engineering - OMAE*, *4*, 1–7. https://doi.org/10.1115/OMAE2021-63384

Yong, C., Lee, J., & Mo, J. (2011). Reliability-based design optimization of an FPSO riser support using moving least squares response surface metamodels. *Ocean Engineering*, *38*(2–3), 304–318. https://doi.org/10.1016/j.oceaneng.2010.11.001

Young, Y. L., Baker, J. W., & Motley, M. R. (2010). Reliability-based design and optimization of adaptive marine structures. *Composite Structures*, *92*(2), 244–253. https://doi.org/10.1016/j.compstruct.2009.07.024

Yu, H., Sun, Z., He, L., & Yang, L. (2022). Research on Optimal Design of Spudcan Structures to Ease Spudcan-Footprint Interactions in Clay and Comparative Analyses with Different Measures. *Polish Maritime Research*, *29*(1), 43–56. https://doi.org/10.2478/pomr-2022-0005

Yu, L., & Tan, J. (2010). Optimal design methodology for multi-component mooring systems in deep water. *Proceedings of the International Conference on Offshore Mechanics and Arctic Engineering - OMAE*, *4*, 91–97. https://doi.org/10.1115/OMAE2010-20190

Yu, Y., Lin, Y., & Ji, Z. (2012). A Parametric Structure Optimization Method for the Jack-Up Platform. *Proceedings of the ASME 2012 31st International Conference on Ocean, Offshore and Arctic Engineeering*, 1–6.

Yuan, J., Hou, Y., & Tan, Z. (2021). Optimization of frequency domain fatigue analysis for unbonded flexible risers. *Proceedings of the International Conference on Offshore Mechanics and Arctic Engineering - OMAE*, *4*, 1–7. https://doi.org/10.1115/OMAE2021-62886

Zhang, Y., Beer, M., & Quek, S. T. (2015). Long-term performance assessment and design of offshore structures. *Computers and Structures*, *154*, 101–115. https://doi.org/10.1016/j.compstruc.2015.02.029

Zhang, Y., Kim, C., Beer, M., Dai, H., & Guedes, C. (2018). Modeling multivariate ocean data using asymmetric copulas. *Coastal Engineering*, *135*, 91–111. https://doi.org/10.1016/j.coastaleng.2018.01.008

Zhang, Z., Ma, X., Yu, H., & Hua, H. (2021). Stochastic dynamics and sensitivity analysis of a multistage marine shafting system with uncertainties. *Ocean Engineering*, *219*, 108388. https://doi.org/10.1016/j.oceaneng.2020.108388

Zhao, Y., & Dong, S. (2021). Design loads and reliability assessment of marine structures considering statistical models of metocean data. *Ocean Engineering*, *241*, 110099. https://doi.org/10.1016/j.oceaneng.2021.110099

Zhao, Y., Dong, S., Yang, Z., & Manuel, L. (2020). Estimating design loads for floating structures using environmental contours. *Proceedings of the International Conference on Offshore Mechanics and Arctic Engineering - OMAE*, *6*B-*2020*, 1–7.

Chapter 3

Reliability Assessment of Marine Structures considering Multidimensional Dependency of the variables

Preface

A version of this chapter has been published in ***Ocean Engineering 2021; 230:109021.*** *I am the primary author that produced this work, along with Co-authors Faisal Khan and Salim Ahmed. I thoroughly reviewed the relevant literature and developed the concept and methodology of multivariate dependence modeling of offshore structures for reliability assessment using vine copula. I prepared the original manuscript, carried out formal analysis and software implementation, reviewed and revised the manuscript following the co-authors' feedback and peer review from the journal. Co-author Faisal Khan assisted in the concept development and methodology refinement, supervision, funding for the work, reviewing, and editing of the manuscript. Co-author Salim Ahmed assisted in concept development and methodology, research supervision, reviewing, and manuscript editing.*

Abstract

For an improved estimation of marine structural reliability, a consideration of random variable dependency is essential. With a limited study on dependence modeling of marine structures, this study proposes a framework for the reliability assessment of ocean structural systems with multidimensional variables. This framework captures possible nonlinearity and tail dependence in the variables using vine copula. The proposed method develops a graphical structure of random variables consisting of nodes, edges, and trees using the D-vine approach. This study demonstrates the developed framework on a jacket support structure subjected to the extreme environmental

load conditions at Jeanne D' Arc basin on Canada's east coast. The structure's reliability is evaluated with optimally selected copulas in the D-vine trees and associated marginal distributions. A comparison between the reliability result using the D-vine copula method, Gaussian coupling assumption, and statistical independence between variables proved its superiority in modeling variable dependence of complex marine systems. The probability of failure (P_f) using the D-vine copula was closer to the reference Importance Sampling (IS) results than other methods.

Keywords: Structural Reliability; vine copula; probability of failure (P_f); Limit State Function (LSF)

3.1. Introduction

Structural reliability methods such as the response surface approach, FORM, and Second-Order Reliability Method (SORM) involve the determination of the reliability index (β_{HL}) in the standard normal space and, consequently, the probability of failure (P_f) of a structure with the common assumption that the random input variables are independent. Practically, there exists dependency among variables, which may affect the reliability estimation of the structural system.

From the literature on the variable dependency of marine structures, Nataf and Rosenblatt's transformation are essential methods for dealing with the challenges of dependence between input variables (Melchers & Beck, 2018). Rare consideration is given to Rosenblatt transformation since it requires the determination of the joint Probability Density Function (PDF) of the variables for analysis, which is difficult to obtain. Also, Nataf transformation has been widely used in dealing with correlated non-normal variables. Der Kiureghian & Liu (1986) developed an empirical derivation of Pearson's correlation coefficient (ρ_p)for the conversion of correlated non-normal variables to standard normal variables. Li et al. (2012) applied Nataf transformation in the

reliability analysis of complex correlated variables. Ditlevsen (2002) used the Nataf transformation for dynamic analysis of correlated wind and wave effects on offshore structures. Chang et al. (1995) combined Nataf transformation and Monte Carlo Simulation (MCS) to analyze complex systems. Lebrun & Dutfoy (2009) research revealed that Nataf transformation results were the same as using a Gaussian copula. Although Nataf transformation can convert correlated non-normal variables to independent standard normal variables for reliability analysis, its major limitation is the inability to capture tail dependence between variables.

Recently, bivariate copula functions have gained useful application in dependency and reliability studies. Goda (2010) studied the relationship between peak and residual displacement in the reliability of structures subject to seismic loads. Also, in a risk-based design, Shao et al. (2019) developed a data-driven approach for risk assessment of concrete dams using copula functions. In the field of uncertainty quantification, Uzielli & Mayne (2012) research focused on load-displacement uncertainty in soil geotechnics for shallow footing structures using copula functions. Lu & Zhu (2018) applied the copula concept and the moment matching principles in structural system reliability analysis. Tang et al. (2013a) studied the effect of bivariate copula on systems' reliability in parallel. Liu & Fan (2016) applied a mixed copula to analyze a series-parallel system's structure. Another research area considers copulas' effect in the sensitivity analysis of a structural system with truncated variables (Xiao et al., 2017). Tang et al. (2013b) developed a framework for dependence analysis of structures using bivariate copulas.

The ocean environment is complex. The need to study the interaction effect among ocean parameters such as wave, wind, current, and geotechnical conditions is critical for a realistic description of marine structural design and operations. In recent times, research has considered the dependence modeling of ocean variables. Antão & Guedes Soares (2014) developed a model

considering the dependence of wave steepness and wave height in the ocean environment. Zhang et al.(2018) modeled the significant wave height dependency with average wave period and wind speed using asymmetric copulas. Michele et al. (2007) considered the dependence modeling of storm conditions (significant wave height, duration, direction, and interarrival time) using copulas. Masina et al.(2015) studied the dependence between sea levels and waves using copulas. Gupta & Bhaskaran (2017) studied the interdependency between ocean parameters (wind and waves) in the Indian Ocean basin for about two decades. The correlation between sea-state loads on fixed offshore structures has been successfully studied using Archimedean copulas (Zhai et al.,2017). Yang & Zhang (2013) studied the joint probability distribution of wave load and wind speed at Bohai Bay using Clayton and Gumbel copulas. Montes-Iturrizega & Heredia-Zavoni (2016) modeled offshore mooring lines' wave height and peak period dependence using copula.

From the preceding literature, it is evident that more research has focused on using copula functions for component or system reliability assessment with mainly bivariate input variables.

Regarding the determination of dependency for more than two input random variables (multidimensional), Bedford & Cooke (2002) introduced the concept of vine copula to decompose the joint PDF into a cascade of bivariate copulas and the marginal distribution of the variables. Furthermore, considering traditional copulas' central problem of flexibility in handling higher dimensional variables, the vine copula offers simplicity in its application and flexibility in combining different bivariate copulas for dependence modeling. This set of copulas can capture complex dependency amongst input variables compared with traditional multivariate copulas.

Although its early application has been in financial mathematics, the vine copula has recently gained useful engineering applications. Vine copulas can deal with dependency and capture

nonlinearity and tail dependence between variables. More specifically, modeling variables using the vine copula has been an area of research interest in geotechnics, hydrology, and power systems engineering.

In geotechnics, the research focus has mainly been on soil properties. Wang & Li (2019) studied the dependence of soil properties modeled by the random field method using a vine copula-based approach. Tang et al.(2020) applied the concept of vine copulas in soil slope reliability assessment considering various soil properties such as friction angle, soil cohesion, and unit weight of the soil. Lü et al.(2020) investigated the dependency of structured clay's multiple soil parameters using the vine copula method. Wang & Li (2017) research demonstrates the importance of copulas in stability reliability studies of tunnel excavation using a stochastic surrogate model through a comparative study.

In hydrology, Wang et al.(2018) developed a framework to study monthly river flow in the dry season using vine copula. Jiang et al.(2019) modeled the dependence for multivariate hydrological designs with vine copula. Tu Pham et al.(2018) applied a vine copula-based approach to generate the evapotranspiration, precipitation, and temperature time series required for discharge in a rainfall model. Also, Tosunoglu et al. (2020) applied the vine copula concept to model the dependence between flood characteristics: peak, volume, and discharge.

In the field of power-based systems, Qiu et al.(2019) have applied the concept of vine copula in modeling the dependence of the output of multiple wind power generation systems. Khuntia et al.(2019) focused on the spatial relationship between wind power plants and electrical load using a vine copula.

Integrating copulas with BN has seen applications in mechanical and process systems. Sun et al. (2021) utilized the Copula Bayesian Network concept (CBN) in the reliability assessment of a mechanical gantry system, given its components' prior probability. Hashemi et al. (2016) applied the idea of CBN in process facility safety analysis. Similarly, Guo et al.(2019) used the CBN concept to model safety accidents. Fundamentally, CBN has a conditional independence assumption in its dependence structure, which may not be a preferred option for dependence modeling in structural reliability analysis.

Conversely, vine copula considers conditional dependence among its dependence structure variables, making it a useful tool for practical structural reliability problems. The CBN approach is effective in dealing with high-dimensional variables. However, it does not pose a significant advantage since one primary concern in structural reliability is the *curse of dimensionality*, where the computational cost of structural reliability analysis grows exponentially with an increased number of input variables (Hurtado,2004). Consequently, the primary focus is on reducing the variable dimension as much as possible, considering the most critical variables affecting the quantity of interest. This approach allows for improved computational efficiency in reliability analysis given the LSF.

The existing literature shows that dependence modeling and reliability assessment of marine structures have focused on Pearson correlation; copulas for the bivariate structural system or variables have been assumed statistically independent for simplicity of analysis. Consequently, using correlation only captures linear dependence (at best) between variables. Marine structures are subject to extreme ocean conditions where tail dependency and nonlinearity between the variables might be critical. For such systems, the results obtained using the correlation method (Pearson) may present some bias and inaccuracy in modeling the association between its

environmental variables. From the literature, copula utilization in marine structural reliability is limited to two variables at a time.

With the apparent advantage of vine copula for dependence modeling of multivariate systems and with limited attention to its use in modeling dependency of marine structures, this study

1. Proposes a framework through a flexible approach (vine copula) to model variable dependence for complex marine structural systems.
2. Evaluates the effect of considering nonlinearity and tail dependence of variables captured by the vine copula approach on the reliability assessment of marine structures under given limit state conditions.

The organization of the remaining part of this work is as follows: Section 3.2 briefly introduces the preliminaries on copula functions; Section 3.3 outlines the methodology of the proposed vine copula framework with an illustrative example; Section 3.4 considers the application of the framework to an offshore structure; Section 3.5 gives a summary of the entire work.

3.2. Preliminaries on Copulas and Structural Reliability

This section gives a general overview of the structural reliability concept, copula functions, and measures of dependence between variables.

3.2.1 Structural Reliability

The LSF divides the standard normal plane for random variables into the safe and failure region in reliability analysis. If the LSF is given by $G(X) = 0$, where X represents the random variables of the function, then the failure region is the domain of $G(X) < 0$, and the safe area is the domain

of $G(X) > 0$. The P_f of a structure over the failure domain can be represented by the expression in Eq. (3.1).

$$P_f = \int \dots \int_{G(X)<0} f(x_1, x_{2,} x_3 \dots . x_n) dx_1 dx_2 dx_3 \dots dx_n \quad (3.1)$$

Where $f(x_1, x_{2,} x_3 \dots . x_n)$ is the joint PDF of n-random variables $X_1, X_2, \mathrm{X}_3 \dots . . X_{\mathrm{n}}$.

The difficulty in determining the joint PDF has led to approximate methods like FORM and SORM to obtain the standard normal plane design point and, consequently, the system's reliability. Simulation-type methods such as MCS, Importance Sampling (IS), and Subset Simulation are other commonly used methods for evaluating the P_f; these methods use large simulation cycles and provide greater accuracy but are computationally expensive and cumbersome (Melchers & Beck, 2018).

This work utilizes the approximate method (SORM) and simulation techniques in the structural reliability evaluation of the LSF. The IS approach (Eq. (3.2)), which relies on the convergence speed of FORM and the robustness of MCS, is used as a benchmark for the results obtained.

$$P_f = \frac{1}{N} \sum_{i=1}^{N} I_g(x_i) \frac{f_x(x_i)}{f_I(x_i)} \quad (3.2)$$

For Eq. (3.2), N is the number of simulations, I_g an indicator function, $f_I(x_i)$ is the sampling density function and x_i are realizations of random variables for the i^{th} simulation.

In reliability assessment, copulas are an important linking function between marginal distributions to enhance the estimation of the P_f of a system.

3.2.2 Copula Functions

Copulas are multivariate probability distributions with uniform marginals, allowing dependence modeling under uncertainty, and are useful and flexible linking tools for random input variables. The 1959 Sklar's theorem serves as a foundation for the concept of copulas; it explains the decomposition of multivariate distribution into univariate marginals and copulas, which allows for the expression of dependency between variables (Nelsen, 2006).

Eqs. (3.3) to (3.5). show important expressions of Sklar's theorem.

$$F(x_1 \ldots . x_n) = C\left(F_1(x_1) \ldots \ldots F_n(x_n)\right) \tag{3.3}$$

$$f(x_1, x_2, \ldots . x_n) = c\left(F_1(x_1), F_2(x_2) \ldots \ldots F_n(x_n)\right) \prod_{i=1}^{n} f_i(x_i) \tag{3.4}$$

$$P(X_1 \leq x_1, X_2 \leq x_2 \ldots \ldots X_n \leq x_n) = P\left(X_1 \leq F_1^{-1}(u_1), \ldots \ldots . X_1 \leq F_n^{-1}(u_n)\right) \tag{3.5}$$

Where C is the unique copula distribution function, which is the dependence structure, $F_i(x_i)$ is the continuous marginal distribution function for the i^{th} variable with an n-dimension random vector. F (.) is the joint distribution function with x_i realization of the random variable X_i. The effect of copula creates simplicity in analyzing the joint PDF $[f(x_1, x_2, \ldots . x_n)]$ where c is the copula density function and u_i the uniform marginal of the copula. From Sklar's theorem, it becomes possible to create an approximate joint PDF from copulas and marginals of random variables.

Among the commonly used copula functions are the elliptical copulas (Gaussian, Student t copula) and the Archimedean copulas (Clayton, Frank, Gumbel); Table 3A.1 of Appendix 3A shows various copulas and their properties. This study will limit optimal copula selection to those mentioned in this section.

The vine copula is a simple and efficient way of dealing with conditional dependence between variables, nonlinear correlation, and tail dependence. It comprises a graphical object of nodes and edges with connected trees; it uses bivariate copulas to construct an approximate joint PDF for multivariate distributions. Vine copulas have wide applications in the financial, insurance, genetics, and health sectors; it is an evolving area in various engineering sectors for determining dependency between system variables (Chang et al., 2019). Among the class of vine copulas used for linking marginals and dealing with the variables are the D-vine and the Canonical Vine (C-vine), with the PDF relating its n-dimensional variables as shown in Eqs. (3.6) and (3.7), respectively (Aas et al., 2009).

$$f(x_1 \ldots . x_n)$$

$$= \prod_{k=1}^{n} f(x_k) \prod_{j=1}^{n-1} \prod_{i=1}^{n-j} c_{i,i+j|i+1\ldots i+j-1} \left\{F\left(x_i \middle| x_{i+1} \ldots \ldots, x_{i+j-1}\right), F\left(x_{i+j} \middle| x_{i+1} \ldots \ldots, x_{i+j-1}\right)\right\} \qquad (3.6)$$

$$f(x_1 \ldots . x_n)$$

$$= \prod_{k=1}^{n} f(x_k) \prod_{j=1}^{n-1} \prod_{i=1}^{n-j} c_{j,j+i|1\ldots j-1} \left\{F\left(x_j \middle| x_1 \ldots \ldots, x_{j-1}\right), F\left(x_{j+i} \middle| x_1 \ldots \ldots, x_{j-1}\right)\right\} \qquad (3.7)$$

In Eqs. (3.6) and (3.7), j represents the trees of the D-vine and C-vine, respectively. Also, i means the edges within each tree of the vine copula.

When a leading variable drives interaction between the data set, a C-vine copula is adopted

(Aas et al., 2009). In the absence of such variables, the D-vine Copula provides a more direct approach to modeling dependency between variables. This study adopts the D-vine approach since the problems presented have no leading variable governing random variables' interaction.

A statistical independence test is essential in ascertaining a relationship (linear or nonlinear) between random variables, especially in the first tree of a D-vine structure. The non-parametric Kendall's test which is simple to implement, interpret, and depends on the empirical Kendall's tau (τ_k) is applied in this study to test for independence between variables before copula type determination.

Eq. (3.8) shows an expression for Kendall's test statistic where N' represents the number of variable observations, and T is the test statistic value. A null hypothesis of independence is accepted when $T < 1.96$ at a 5% significance level (Genest & Favre, 2007).

$$T = \sqrt{\frac{9N'(N'-1)}{2(2N'+5)}}\,|\tau_k| \tag{3.8}$$

For copula selection, this study adopts the Maximum Likelihood Estimation (MLE) approach in copula parameter (θ) determination and the Akaike Information Criterion (AIC) in the optimal selection of copulas for the D-vine structure. The AIC value captures the information loss in determining θ while fitting various copula in the vine tree. A minimum value of AIC indicates less information loss. The selection of the most suitable copula model for the vine depends on the copula with the minimum AIC value (Zhai et al.,2017).

The AIC creates a trade-off between the goodness of fit of the copula and its simplicity. The expression for the logarithm-likelihood function, AIC, and determination of θ, are shown in Eqs. (3.9) to (3.11), respectively.

$$InL(\theta) = \prod_{i=1}^{n} c(u_1 \dots u_n; \theta) = \sum_{i=1}^{n} Inc(u_1 \dots u_n; \theta) \tag{3.9}$$

$$AIC = -2InL(\theta) + 2K \tag{3.10}$$

$$\frac{\partial InL(\theta)}{\partial \theta} = 0 \qquad (3.11)$$

L(θ) represents the logarithm likelihood function,$(u_1 \dots u_n)\epsilon[0,1]$ standard uniform, *K* is the number of model parameters.

The system's structural reliability is determined from the estimated joint PDF obtained from corresponding copulas and their marginals.

3.2.3 Dependence measures

Dependence measures are essential in modeling copulas. In the reliability study, ρ_p is the most common measure of dependence due to its simplicity in implementation; this is not without its shortcomings of capturing only linear relationships between variables. Also, ρ_p is with the assumption of normality and homoscedasticity between the variables.

Other measures of dependence are Spearman's correlation (ρ_{rho}) which considers the correlation of ranks and τ_k which represents the likelihood of concordance over discordance of data. These other dependence measures are non-parametric and independent of the marginal distribution (Joe, 2014). The mathematical expression describing these measures is shown in (Eqs. (3A.1) to (3A.3), Appendix 3A).

3.3. Framework for Reliability Assessment using Vine Copulas

This section describes a five-step approach for the reliability assessment of marine structures considering dependency using vine copulas (D-vine).

3.3.1 Implementation procedure

Step 1: With the data for random variables and their associated marginal distributions, the dependence measures between variables is determined using the non-parametric τ_k, ρ_{rho} and ρ_{p} described in Section 3.2.3 and (Eq. (3A.3), Appendix 3A) of this study.

Step 2: Model the multivariate dependence between the random variables using the D-vine copula approach described in (Eq. (3.6), Section 3.2.2). The D-vine structure shows the dependency (conditional and unconditional) between variables in graphical form. The order of the random variables in the first tree of the D-vine structure is determined based on experience or combinatorics (using τ_k obtained in Step 1 and determining the minimum 1-$|\tau_k|$ path).

Step 3: Using the τ_k obtained in Step 1, a test of statistical independence between random variables is carried out using (Eq. (3.8)) described in Section 3.2.2 of this study. The independence test helps reduce the complexity of the vine modeling by identifying edges in the vine tree where no dependence relationship exists (especially for high-dimensional cases); this also enhances the order of the D-vine first tree, presented in Step 2.

Step 4: Select the optimal copula from known elliptical and Archimedean copulas for conditional and unconditional variables in the D-vine trees described in Section 3.2.2 for the edges of the D-vine tree structure developed. The MLE approach and minimum AIC for optimal copula selection, copula parameter determination (θ), and tail dependence evaluation (where necessary) are described in Eqs. (3.9) to (3.11) and (Table 3A.1, Appendix 3A) of this study.

Step 5: From Step 4, the estimate of the joint PDF for the variables is determined for the given copula and marginals of the random variables considered. From the realization of the D-vine structure developed in Step 4, the methods described in Section 3.2.1 is employed in the reliability

analysis of the structural system to obtain the P_f. The reliability implementation is done in UQLab, an uncertainty quantification tool in MATLAB (Marelli & Sudret, 2014).

Figure 3.1 shows the procedure described for reliability assessment considering dependency between variables using a D-vine copula.

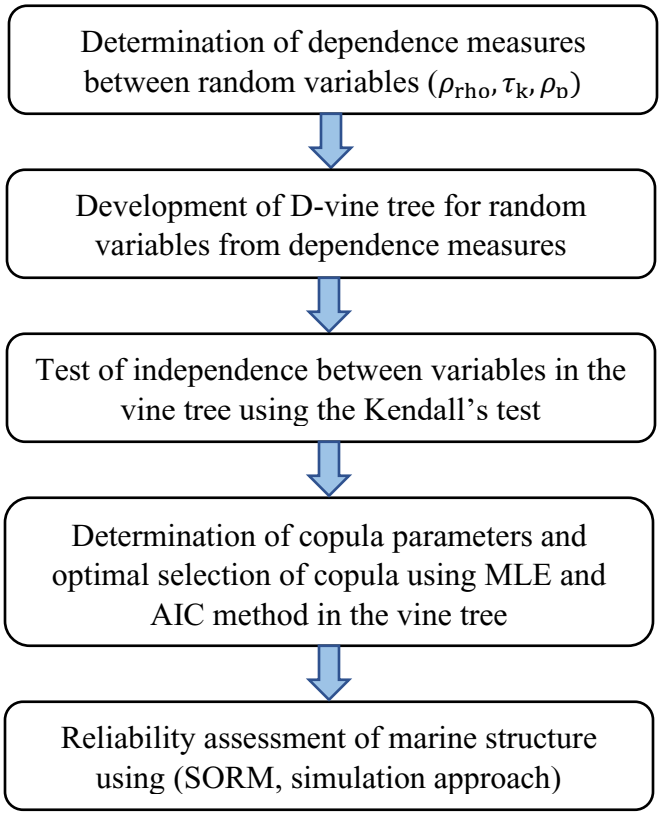

Figure.3.1. Framework for reliability analysis using vine copula.

3.3.2. Application example: Cantilever Beam Structure

A cantilever beam example that models part of a drilling module clarifies the framework described in Section 3.3.1.

Eq. (3.12) shows the LSF of a cantilever beam (Figure 3.2) where X_1, X_2 represent the resisting moment capacity of the section. P_1 and P_2 represents the applied load at the cantilever mid-span

and derrick end, respectively. Also, the length of the cantilever is denoted by L_2 which is 3m in dimension. X_1,X_2,$P_1$and $P_2$are assumed as random variables with parameters shown in Table 3.1.

$$g\,(X_1, X_2, P_1, P_2) = X_1X_2 - P_1L_1 - P_2L_2 \tag{3.12}$$

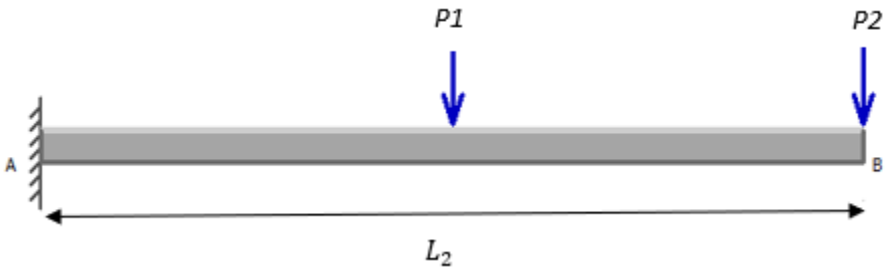

Figure 3.2. Cantilever beam structure.

Table 3.1. Statistical information of random variables for the cantilever beam.

Variables	Mean	Standard Deviation	Distribution Type
$X_1(\mathrm{kN/m^2})$	$25\mathrm{x}10^4$	$25\mathrm{x}10^3$	Lognormal
$X_2(\mathrm{m^3})$	$2.2\mathrm{x}10^{-3}$	$1.1\mathrm{x}10^{-4}$	Lognormal
$P_1(\mathrm{kN})$	100	10	Weibull
$P_2(\mathrm{kN})$	100	10	Weibull

Step1: Determination of dependence measures

The dependence measures (ρ_{p}, ρ_{rho}, and τ_{k}) of the cantilever beam's random variables obtained from 300 samples of random variables are shown in Table 3.2.

Table 3.2. Dependence measures for the cantilever beam.

Variables	ρ_{p}	ρ_{rho}	τ_{k}
X_1, X_2	-0.848	-0.876	-0.844
X_1, P_1	0.779	0.803	0.618

X_1, P_2	-0.051	0.031	0.019
X_2, P_1	-0.854	- 0.860	-0.728
X_2, P_2	-0.072	-0.121	-0.093
P_1, P_2	0.418	0.457	0.311

Step 2: vine structure construction for the random variables

A D-vine structure [P_2-P_1-X_2-X_1] as shown in Figure 3.3 is developed for the random variables P_2, P_1, X_2 and X_1 for this problem. The architecture consists of nodes and edges, with Tree 1 containing all four random variables of the problem.

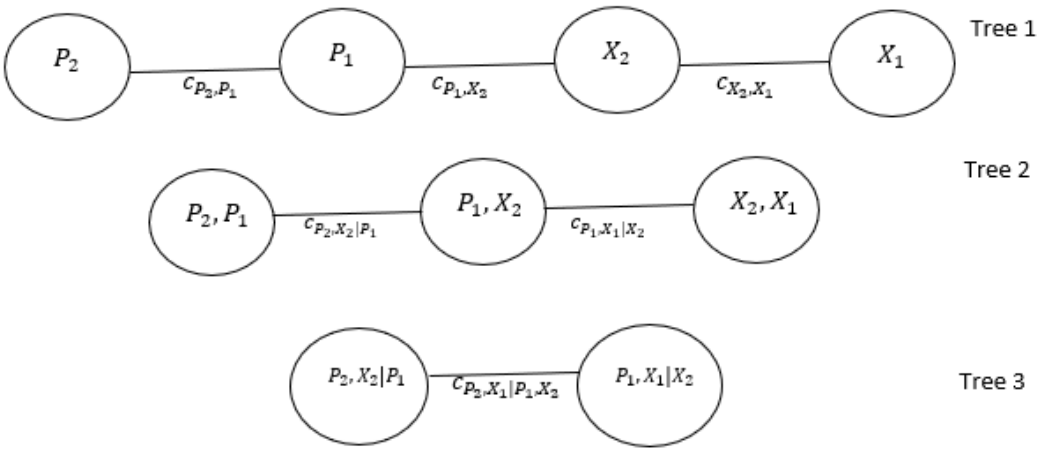

Figure 3.3. D-vine structure for cantilever beam variables.

Step 3: Test for independence

A test for independence of variables in Tree 1 of the D-vine structure shown in Figure 3.3 is determined using Kendall's test as obtained in Eq. (3.8). From the results (Table 3.3), since T > 1.96, the null hypothesis of independence between variables is rejected at a 5% confidence level.

Table 3.3. Independence test statistics for the cantilever beam.

Variables	T (Statistic)
P_2, P_1	8.04
P_1, X_2	18.53
X_2, X_1	23.01

Consequent to Kendall's test outcome, independence between variables are not considered in the analysis of Tree 1 of the D-vine structure.

Step 4: Optimal copula selection between random variables

An optimal copula choice between the random variables is made from known elliptical and Archimedean copulas. This work limits selection to the six (6) commonly used copulas; Independent, Gaussian, Student t, Clayton, Gumbel, and Frank Copulas. Furthermore, the minimum AIC is used as a criterion for optimal copula selection among the random variables and determination of θ. Table 3.4 shows the selected copula types in the D-vine trees based on the AIC.

Table 3.4. Parameter and Rotation (θ, θ_R) of selected copula function.

Tree	Copula Density	Selected Copula	θ_R	θ
1	c_{P_2,P_1}	Frank	270	-3.09
1	c_{P_1,X_2}	Clayton	270	5.40
1	c_{X_2,X_1}	Gumbel	90	9.34
2	c_{P_2,X_2P_1}	Clayton	0	2.66
2	$c_{P_1,X_1\|X_2}$	Clayton	90	4.60
3	$c_{P_2,X_1\|P_1,X_2}$	Independent	0	0

The copula rotation (θ_R) and θ for the selected copula, as shown in Table 3.4, are essential for the drilling cantilever beam's reliability assessment. For the beam's random variables, Figure.3.4 shows the scatter plot (the visual relationship between realizations of random variables). Figure 3.4 shows evidence of nonlinearity and tail dependence between the cantilever beam's random variables, which obviously cannot be captured using Pearson correlation.

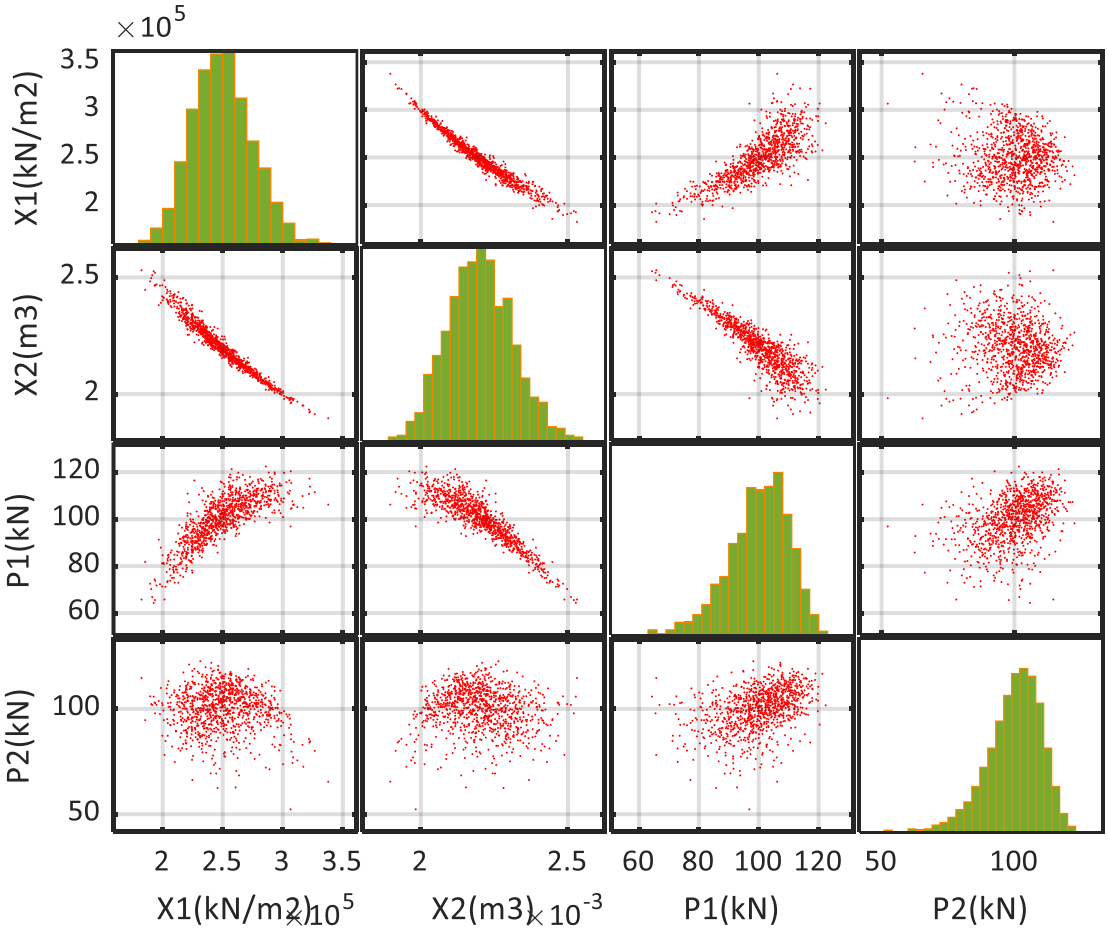

. **Figure.3.4.** Scatter plot for cantilever beam variables.

Step 5: Reliability Analysis

Reliability analysis is evaluated using SORM to determine the P_f of the structure while considering the effect of dependency using selected copulas and LSF of the cantilever beam. The results are benchmarked with results from $N = 10^5$ simulation cycle using IS (Figure 3.5). From Figure 3.5a, the reliability plot using the approximate SORM approach shows a convergence outcome (whose equivalent failure probability is close to the reference IS (Figure 3.5b) for the cantilever beam.

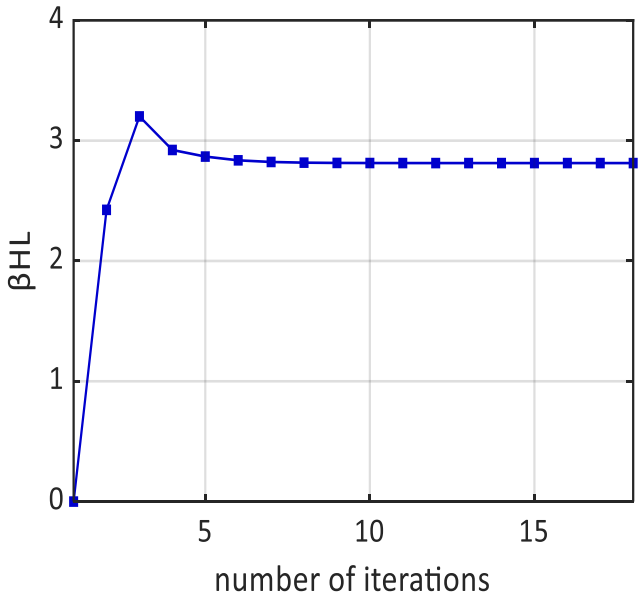

(a)

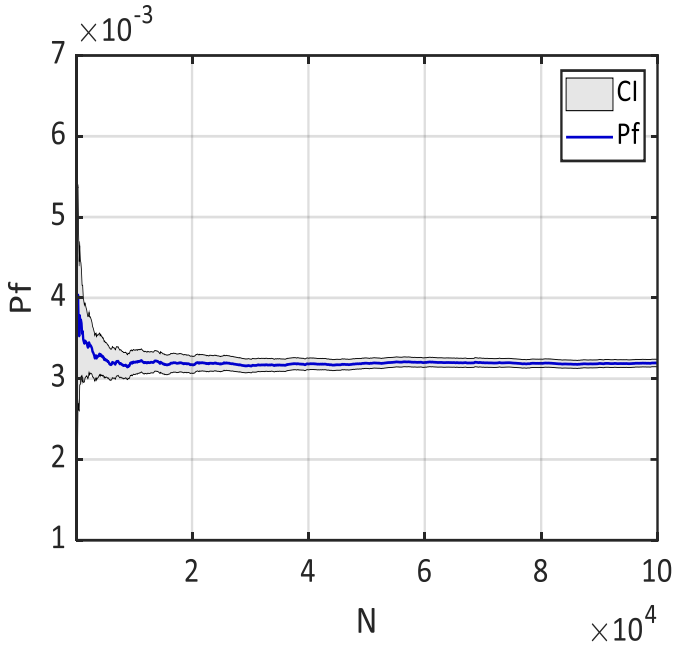

(b)

Figure 3.5. Cantilever convergence plot (a) considering dependency (D-vine) (b) Using IS.

To check the result's efficiency from D-vine coupled random variables, a comparative reliability analysis is carried out between statistically independent, Gaussian coupled, and D-vine coupled cantilever variables. The comparison evaluates the accuracy of reliability results compared with benchmark values obtained from IS, as shown in Table 3.5.

Table 3.5. Cantilever beam reliability assessment.

Assumed Variable Relationship	P_f (10^{-3})	β_{HL}
Statistically Independent	78.35	1.42
Gaussian Copula (correlation)	10.35	2.31
D-vine Copula	2.90	2.76
IS (reference)	3.09	2.74

Also, Figure 3.6 shows the effect of a change in θ on P_f for selected copulas in the first tree of the D-vine structure. The sensitivity plot for the Gumbel and Clayton copula (Figure 3.5 a,b) revealed a sharp drop in P_f with an increase in θ. However, the Frank copula (Figure 3.5 c) only showed a slight change in P_f with θ. Consequently, this spotlights the significance of appropriate determination of the value of θ as it could have a significant impact on the evaluation of P_f.

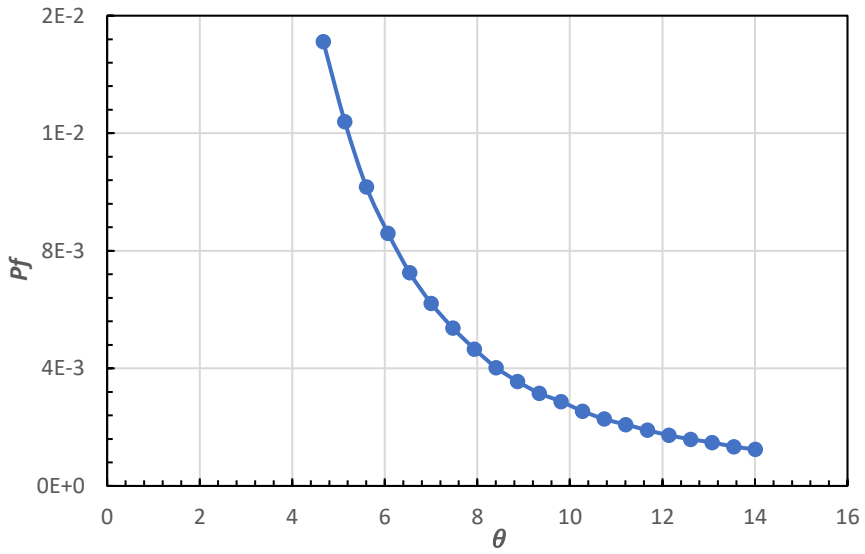

(a) c_{X_2,X_1} (Gumbel,90^o)

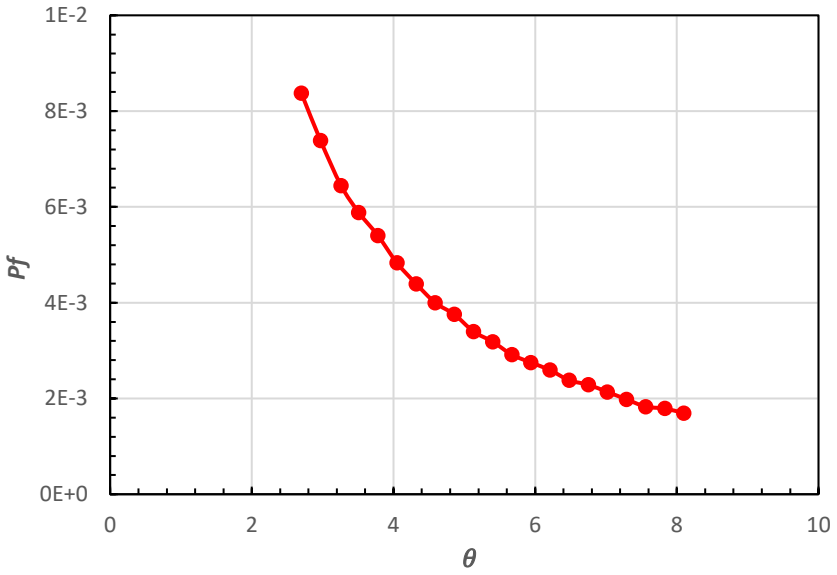

(b) c_{P_1,X_2} (Clayton, 270^o)

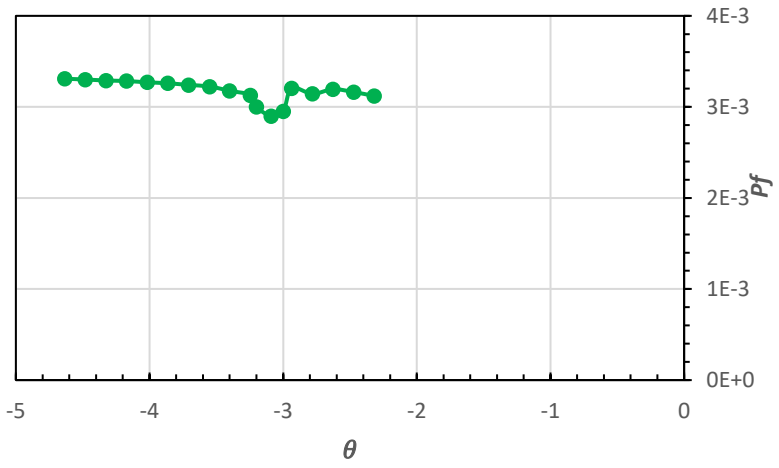

(c) c_{P_2,P_1} (Frank,270^o)

Figure 3.6. Copula parameter sensitivity plot for the cantilever beam.

3.4. Application of Framework to an Offshore Structure

In this section, the framework discussed in Section 3.3 is demonstrated on a proposed 97m jacket support structure with four legs; the structure is subjected to extreme sea state conditions at the Jeanne D'Arc basin on Canada's east coast. This basin is a significant source for oil and gas exploration in Canada and is located offshore Newfoundland and Labrador. Jacket structures are tubular steel structures (Figure 3.7) that can support drilling and production operations in shallow and intermediate water depths.

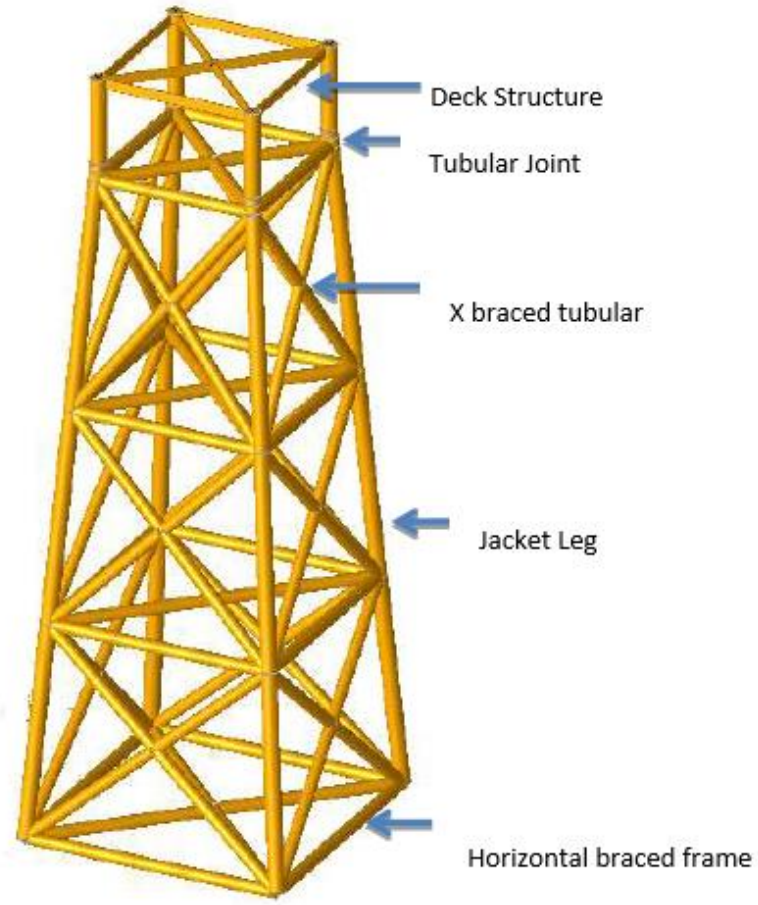

Figure 3.7. Model of jacket structure in SACS Version 13.0 (Bentley, 2018).

3.4.1. Statistical parameters and probability distribution

The random variables considered for the structure include wave effects [significant wave height (H)], current at mean sea level (V_s) and current at the mudline(V_m). With a significant part of the jacket support structure submerged in water, the wind speed on the structure for a 100-year return period is considered deterministic, with an average magnitude and direction of $32.7\text{m/s}, \text{SW } 235^{O}$. The wind is assumed to approach the jacket approximately 10m above the mean sea level. The structure's response required to develop the LSF under extreme load conditions is the Base Shear force (BSF).

The jacket support structure (Figure 3.7) is modeled (including soil-structure interaction), and structural response is obtained under ULS conditions using Structural Analysis Computer Software (SACS) to model jackets and tubular structures. The structure is assumed to be located at a water depth of 90m in the basin for modeling purposes. Information on prevailing and extreme environmental conditions in the offshore basin is obtained from site-specific met-ocean data and reports (C-CORE, 2017). Table 3.6 provides the statistical overview of ocean variables for extreme load events (100yr return period) related to ocean waves (H) and current (V_s, V_m) obtained from the C-CORE report for the Grand Banks region offshore Newfoundland.

Table 3.6. Statistical information of random variables (C-CORE, 2017).

Variables	Mean (100-year return period)	Coefficient of Variation (CoV)	Unit
H	15.5	0.1	m
V_s	2.07	0.1	m/s
V_m	0.77	0.1	m/s

Also, the observation data of random variables (H, V_s, V_m) obtained from the block maxima approach are fitted to Extreme Value Distribution (EVD) using the MLE (minimum AIC) method; this is to determine the appropriate EVD to fit the random variables related to environmental load on the jacket support structure, as shown in Table 3.7. This study assumes sea state data of a given random variable as independent and identically distributed and limits the selection to commonly used EVD for ocean data (Weibull and Gumbel).

Table 3.7. Selection of EVD for ocean variables.

Variables	EVD	MLE (AIC)
H (m)	Weibull	115.72
	Gumbel	129.89
V_s (m/s)	Weibull	-10.98
	Gumbel	-7.313
V_m (m/s)	Weibull	-76.90
	Gumbel	-54.49

The AIC values in Table 3.7 helps in the choice of the possible EVD for each ocean variable that affects the offshore structure. The EVD corresponding to the minimum AIC is chosen for the variables related to wave and current for analysis. As shown in Table 3.7, P-P and Q-Q plots of Appendix 3A (Figure 3A.1, 3A.2, and 3A.3), the random variables fit the Weibull distribution. This is used in the reliability assessment of the jacket support structure.

3.4.2. Dependence modeling using D-vine Copula

For the support structure, the dependence measure between random variables H, V_s and V_m as shown in Table 3.8, is obtained from the analysis of met-ocean data obtained in the C-CORE report. The ρ_p and ρ_{rho} (Table 3.8) provide similar results of correlation between variables, and the non-parametric τ_k presents the strength of dependence between the ocean variables (such as the strong positive dependence observed between V_s and V_m).

Table 3.8. Dependence measures between variables of Jacket Structure (C-CORE, 2017).

Variables	ρ_p	ρ_{rho}	τ_k
H and V_s	-0.7159	-0.7740	-0.6
V_s and V_m	0.8901	0.9337	0.7931
H and V_m	-0.7007	-0.7958	-0.6046

Considering the dependency between the variables (H, V_s, V_m), a D-vine structure of order [H-V_s-V_m] is developed, as shown in Figure 3.8.

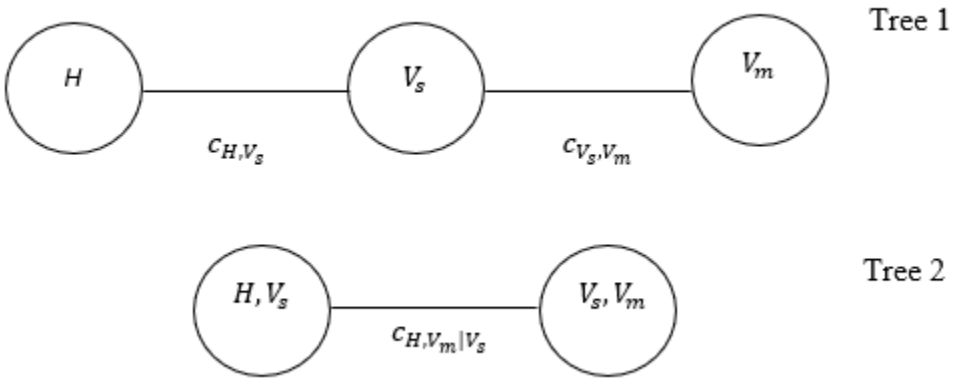

Figure 3.8. Offshore jacket structure D-vine configuration for ocean variables.

Kendall's test (Eq. (3.8)) helps ascertain the possibility of independence in the D-vine tree. Table 3.9 shows the independence test statistic between ocean variables for the jacket structure using Kendall's test. Since the value of $(T > 1.96)$ is observed in Table 3.9, the study rejects the null hypothesis of independence between ocean variables at a 5% confidence, as described in Eq.(3.8).

Table 3.9. Independence test for variables of the jacket structure.

Variables	T (Statistic)
H, V_s	4.657
V_s, V_m	6.155
H,V_m	4.692

The optimal selection of copulas is made from the elliptical (Gaussian, Student t) and Archimedean (Clayton, Gumbel, Frank) copula families using the MLE approach (Table 3.10 and Table 3.11).

Table 3.10. Copula selection for the jacket structure using the MLE approach.

Copula Type	AIC c_{H,V_s}	AIC c_{V_s,V_m}	AIC $c_{H,V_m\|V_s}$
Independent	-	-	0
Gaussian	-28.62	-58.25	0.67
Student t	-26.90	-57.31	2.94
Clayton	-31.43	-55.39	1.52
Gumbel	-31.52	-61.10	1.82
Frank	-24.98	-56.10	0.87

Table 3.11. Optimal copula for variables of the jacket structure.

Copula	Optimal Copula Type	θ_R(Deg)	θ
c_{H,V_s}	Gumbel	270	2.50
c_{V_s,V_m}	Gumbel	180	4.83
$c_{H,V_m\|V_s}$	Independent	0	0

The result from copula selection (Table 3.11) using the MLE method is essential in characterizing the dependency between variables for the jacket reliability assessment.

The scatter plots of the random variables (H,V_s,V_m) is shown in Figure 3.9. The plot in Figure 3.9 suggests evidence of nonlinearity and upper tail dependence between ocean variables captured by the Gumbel copula.

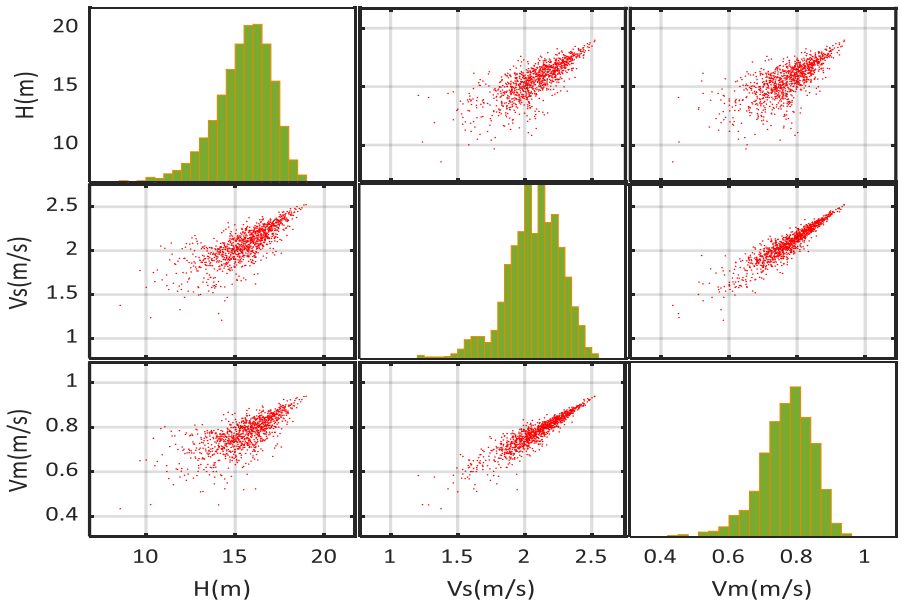

Figure 3.9. Scatter plots for H, V_s and V_m variables for jacket structure.

3.4.3. Metamodel and reliability assessment of the structure

The LSF of most complex marine structures is implicit in form. To reduce the computational burden due to large runs using the Finite Element Method for reliability assessment, a metamodel describing the jacket ULS condition is developed using ED points and corresponding responses. The ED is constructed using the Latin Hypercube Sampling (LHS) infill sampling technique, and 150 sampling points are obtained from met-ocean statistical summary data, as shown in Table 3.6. BSF responses of the jacket for the sampling points are determined using SACS at different environmental load angles.

The Polynomial Chaos Kriging (PCK) technique is used to develop a metamodel for reliability analysis. PCK (Eq. (3.13)) combines the advantages of the PCE and Kriging metamodel, as it captures both the global behavior and local variability of the model.

$$M^{PCK}(x) = \sum_{\alpha \varepsilon A} y_\alpha \varphi_\alpha(x) + \sigma^2 z(x, \omega) \quad (3.13)$$

$M^{PCK}(x)$ is the approximated PCK response, σ^2 is the variance of the Gaussian process, $z(x, \omega)$ represents the stationary Gaussian process, and $\varphi_\alpha(x)$ represents the orthonormal polynomial with the corresponding coefficient y_α.

The PCK model substitutes the trend function of Kriging with orthonormal polynomials (Schobi et al., 2015). With sampling points, copula functions, and responses, the PCK approach is used to develop the metamodel required for reliability analysis. The metamodel is validated with 50 environmental load data and their corresponding BSF responses, which showed minimal deviation from the actual structural responses (see Table 3A.2, Appendix 3A). In this case, $g(H, V_s, V_m) \approx M^{PCK}(x)$ represents the LSF of the jacket structure.

Next, the jacket's reliability is determined from the constructed metamodel at various environmental load angles. For reliability analysis, this study focuses on the ULS condition, with its violation resulting in an eventual collapse of the jacket structure. Also, it considers the dependency between environmental variables affecting the jacket support structure using a D-vine copula. Current and wave loads are assumed to approach the jacket from the same direction and at a step of 45^o. The metamodel is constructed at various approach angles to the structure, considering dependency.

Appendix 3A (Figure 3A.4) shows the convergence plot at various approach angles of the jacket structure's environmental load.

The contribution of the variables (Figure 3.10) to the reliability assessment using the D-vine copula is also determined to ascertain the essential and leading variables that affect the structure's reliability.

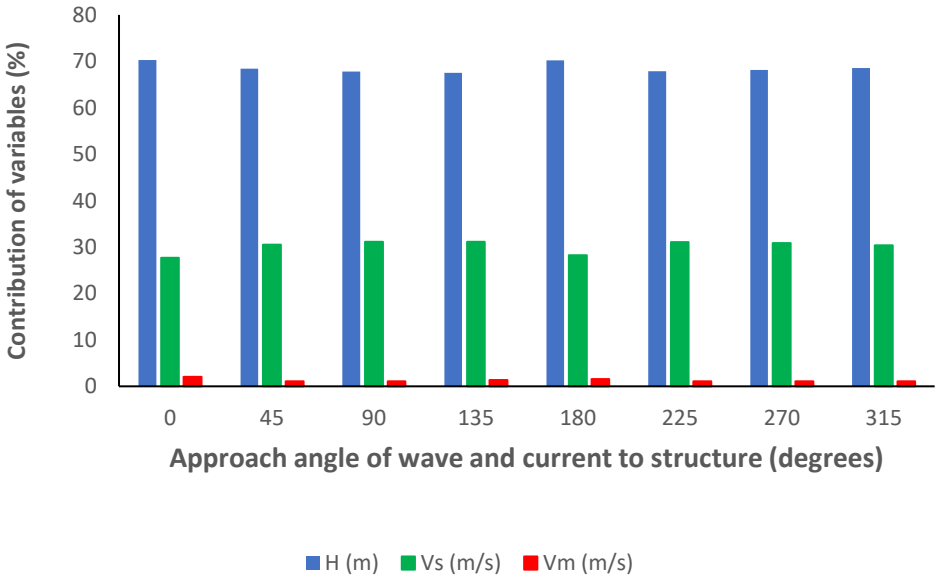

Figure 3.10. Contribution of variables to jacket structure reliability assessment.

The IS simulation approach (10^5 simulation cycles) is utilized as a reference to compare results obtained from reliability assessment using D-vine Copula, Gaussian Copula, and statistically independent variables, as shown in Table 3.12. This comparison further emphasizes the effectiveness of the D-vine copula approach in obtaining an improved estimate of the P_f for the structure.

Table 3.12. Offshore jacket structure failure probability for different load directions.

Load Direction	Statistically Independent	Gaussian Copula	D-vine Copula	Reference
	$\mathbf{10^{-11}}$	$\mathbf{10^{-10}}$	$\mathbf{10^{-5}}$	$\mathbf{10^{-5}}$
$0/360^o$	104.47	149.52	5.99	6.08
45^o	47.28	86.06	4.66	6.36
90^o	3.32	13.80	4.14	5.98
135^o	6.55	22.12	4.05	6.44
180^o	4.02	11.05	4.68	6.02
225^o	6.16	20.19	7.06	6.81
270^o	3.31	13.97	4.66	5.91
315^o	50.75	88.10	5.90	6.57

3.4.4. Discussion on dependence modeling results

From the cantilever beam example in Section 3.3 and the case study presented in this section, it is evident that the introduction of D-vine copula to model dependency between random variables provides a better approximation of the P_f for complex marine structures compared to Gaussian Copula or when variables are assumed statistically independent. In the case of the cantilever beam, P_f result for the D-vine copula approach was found to be relatively closer to the IS benchmark

result (P_f deviation $1.9\text{x}10^{-4}$) as shown in Table 3.5. Similarly, P_f results for all approach angles of the environmental loads to the jacket support structure (Table 3.12) show the comparative superiority of D-vine copulas in the reliability assessment to the benchmark values. D-vine copula provides robustness in its ability to capture nonlinearity and tail dependence between variables, as seen in the selection of Clayton and Gumbel copulas in the presented example and case study. The D-vine Copula overcomes the Gaussian Copula's limitation, which uses correlation values and can only capture linear dependence between variables.

Although vine copulas are flexible for dependence modeling, the results from the copula sensitivity plot for Tree 1 of the cantilever beam (Figure 3.6) reveal that the Clayton and Gumbel copulas are highly sensitive to a change in copula parameters. In contrast, the Frank copula is the least susceptible to parameter change. The results suggest the need for optimal copula selection and accurate determination of copula parameters during dependence modeling of structures to obtain reliable results with a higher confidence level. In this study, the optimal copula choice is made considering the copula type with the lowest AIC value between random variables, as illustrated in Table 3.10 for the jacket support structure.

From the reliability analysis results (Table 3.12) of the support structure using the D-vine copula (Gumbel and Independent), the highest P_f ($7.06\ x\ 10^{-5}$) is observed at an approach angle of 225^o of wave and current to the jacket structure. Consequently, this value indicates how the structure meets target reliability values and gives insight into the critical environmental load direction required in the site-specific structural reliability design and reassessment under ULS conditions.

As shown in Figure 3.10, the random variable *H(m)* provides approximately 70% of the contribution to the LSF and is the most significant variable in the reliability assessment of the

jacket structure, with the most negligible contribution from $V_m(m/s)$ in all directions. The contribution of random variables to the LSF can help design engineers in variable screening and determining the essential variables during limit state design of marine structures.

Although a wide range of bivariate copulas exists, this study is limited to a few known copulas (Gaussian, Student t, Clayton, Gumbel, Independent, and Frank). However, this can be expanded to consider more copulas families to determine the best fit copula for modeling the dependency of marine structures under specific conditions. The selection of probability distribution for random variables is limited to the known extreme (Weibull and Gumbel) and continuous distributions. More distribution types can be considered, especially in a data-driven case, to ascertain the D-vine Copula's efficacy in the reliability study of marine structures. The case study (jacket) considered three-dimensional input random ocean variables due to limited data. The framework can be further investigated to determine its robustness with the availability of data for different ocean parameters, such as ice, earthquakes, and tidal effects.

3.5. Conclusions

This work develops a framework to model the dependency between variables of marine structures using a D-vine copula. The method overcomes the challenge of capturing the nonlinearity and tail dependence among variables that may affect its reliability evaluation and cannot be accounted for by the Pearson correlation.

The study applied the framework to an offshore structure, with results showing the efficiency of the D-vine copula in providing a more accurate estimate of the P_f compared to the Gaussian copula or when variables were assumed statistically independent. The bias in results using Gaussian

copula or statistically independent variables was evident in the jacket structure and cantilever beam problem presented in this work.

D-vine copula proved to be a powerful and flexible tool for modeling dependency between marine structural variables and ensuring an improved quality of reliability-based assessment.

The framework presented in this study can be applied to different marine structures with higher dimension variables, implicit LSF as well as low P_f under various limit state conditions.

With the limitation of this study to commonly used copulas, research into the use of other families of copulas can be investigated. An optimal selection among various copulas can improve the quality of dependence modeling for structural reliability assessment.

Acknowledgment

The authors thankfully acknowledge the financial support provided by the Natural Sciences and Engineering Research Council of Canada (NSERC) and the Canada Research Chair (Tier I) Program in Offshore Safety and Risk Engineering.

Appendix 3A

Table 3A.1. Selected bivariate copula functions.

Copula Type	Copula Function	Lower Tail Dependence (λ_L)	Upper Tail Dependence (λ_U)	Copula Parameter Range (θ)
Clayton	$(u_1{}^{-\theta} + u_2{}^{-\theta})^{-\frac{1}{\theta}}$	$2^{-\frac{1}{\theta}}$	0	(0,∞)
Gumbel	Exp {-[$(-\mathrm{In}u_1)^{\theta} + (-\mathrm{In}u_1)^{\theta}]^{\frac{1}{\theta}}$}	0	$2 - 2^{-\frac{1}{\theta}}$	(1,∞)

Frank	$-\frac{1}{\theta}\ln\left(1+\frac{(e^{-\theta u_1}-1)(e^{-\theta u_2}-1)}{(e^{-\theta}-1)}\right)$	0	0	$(-\infty,\infty)$
Gaussian	$\boldsymbol{\phi}\left(\Phi^{-1}(u_1), \Phi^{-1}(u_1)\middle\vert\theta\right)$	0	0	(-1,1)
Student t	$t_{\theta,v*}(t_v^{-1}(u_1), t_v^{-1}(u_1)\vert\theta)$	$t_{v+1}(-\sqrt{v+1})\sqrt{\frac{1-\theta}{1+\theta}}$	$2t_{v+1}(-\sqrt{(v+1)}\sqrt{\frac{1-\theta}{1+\theta}})$	(-1,1)

$v*$ is a parameter of the t copula.

Equations for Dependence Measures

$$\rho_p = \frac{\sum(x_i-\bar{x})(y_i-\bar{y})}{\sqrt{\sum(x_i-\bar{x})^2\sum(y_i-\bar{y})^2}} \qquad \text{3A. 1}$$

$$\rho_{rho} = 1-\frac{6\sum {d_i}^2}{n(n^2-1)} \qquad \text{3A. 2}$$

$$\tau_k = 4\int_{-1}^{1}\int_{-1}^{1} C(u_1,u_2\vert\theta)dC(u_1,u_2)-1 \qquad \text{3A. 3}$$

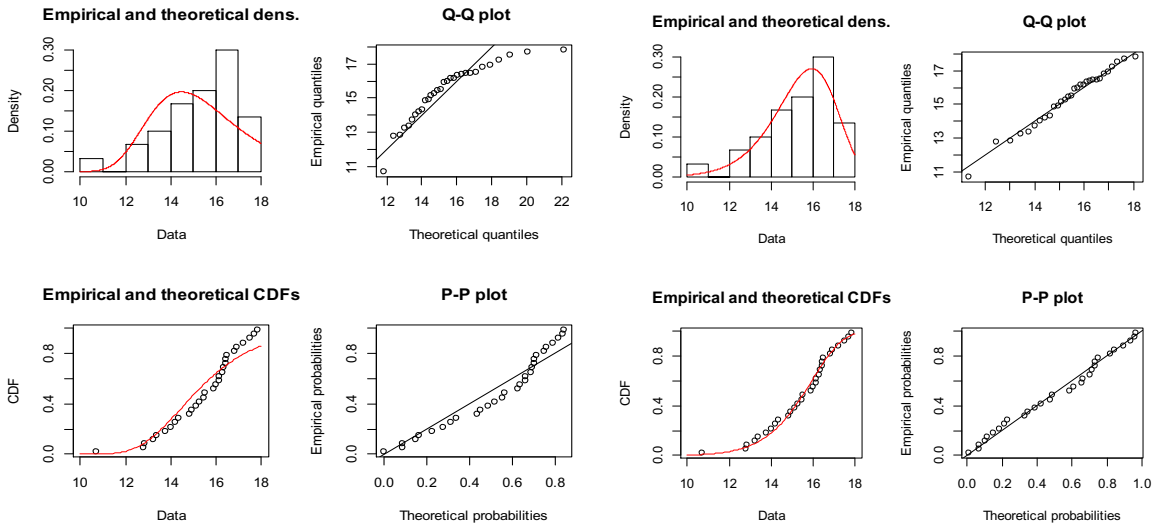

Gumbel Distribution Weibull Distribution

Figure 3A.1. Fitting extreme value distribution to H (m) data.

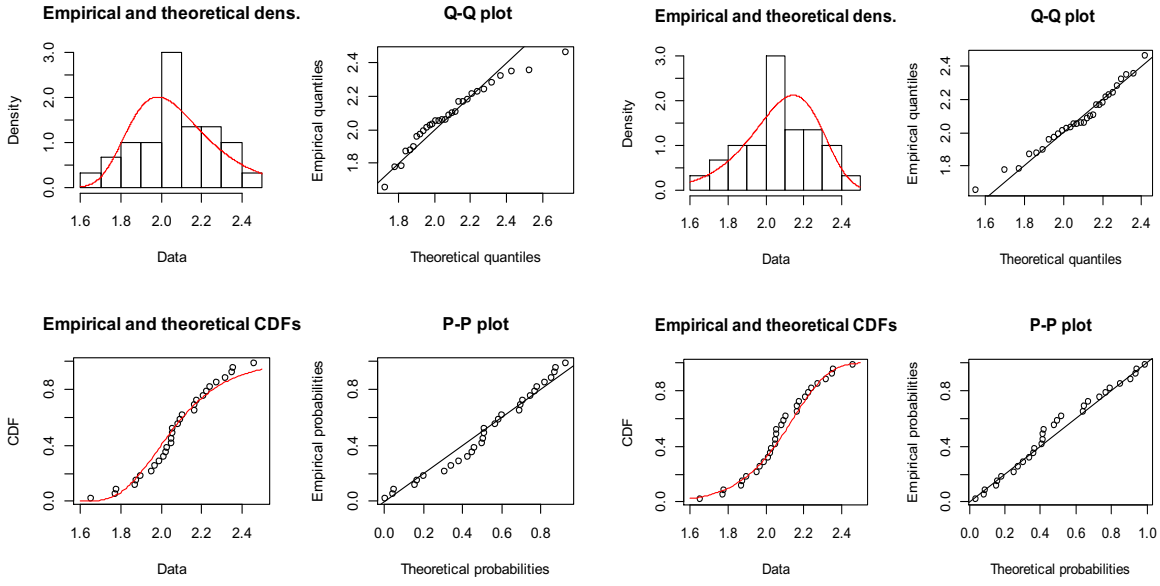

Gumbel Distribution Weibull Distribution

Figure 3A.2. Fitting extreme value distribution to V_s(m/s) data.

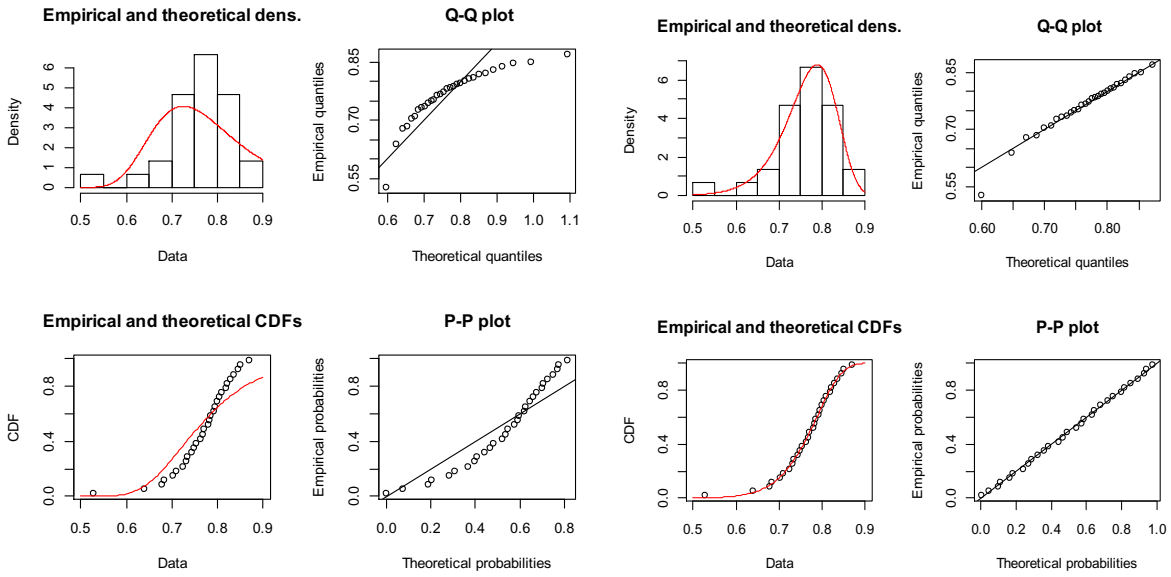

Gumbel Distribution Weibull Distribution

Figure 3A.3. Fitting extreme value distribution to V_m(m/s) data.

Table 3A.2. PCK metamodel validation error at approach angle to jacket structure.

Environmental load approach angle	PCK metamodel validation error (kN)
$0/360^o$	1.849×10^{-2}
45^o	2.006×10^{-2}
90^o	1.846×10^{-2}
135^o	1.751×10^{-2}
180^o	1.304×10^{-2}
225^o	1.664×10^{-2}
270^o	1.358×10^{-2}
315^o	1.987×10^{-2}

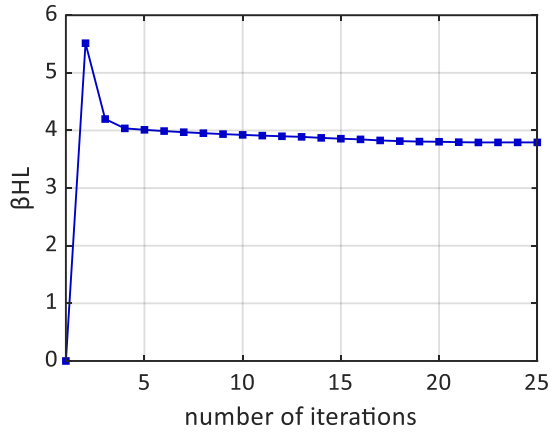

(a) $0^o/360^o$

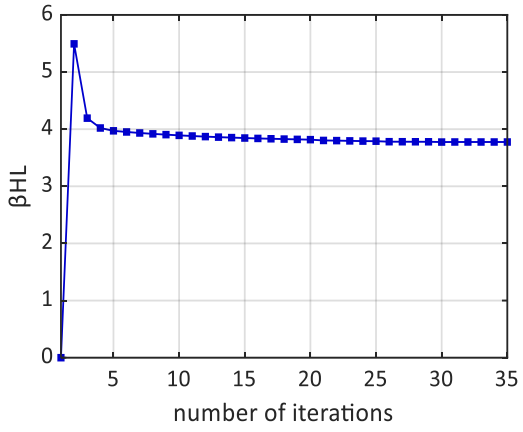

(b) 45^o

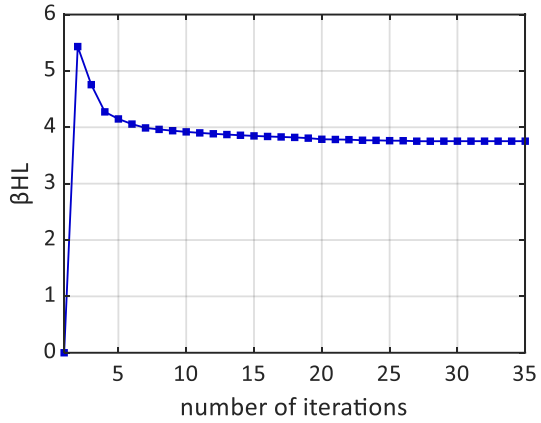

(c) 90^o

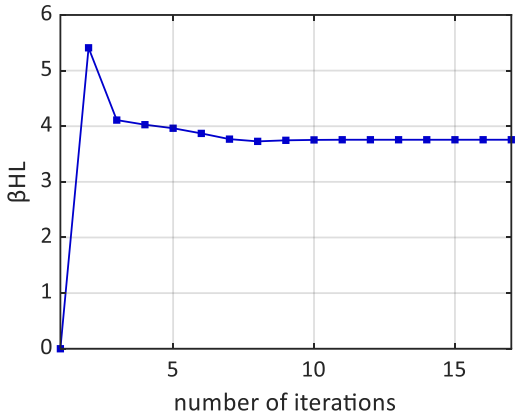

(d) 135^o

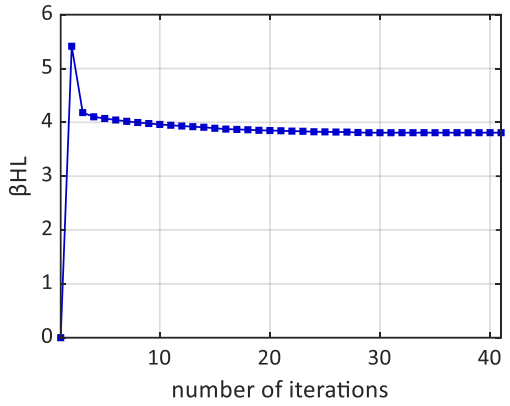

(e) 180^o

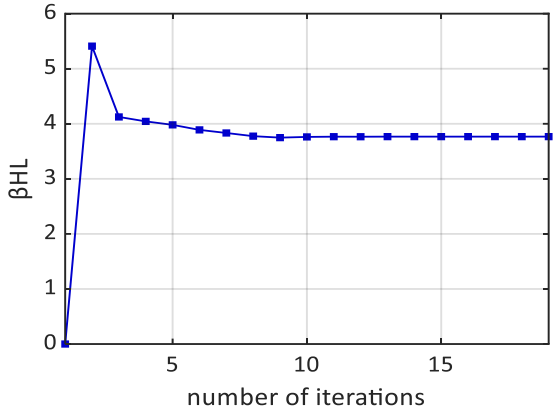

(f) 225^o

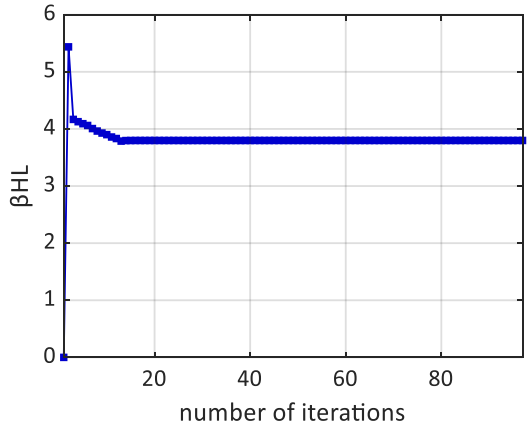

(g) 270^o

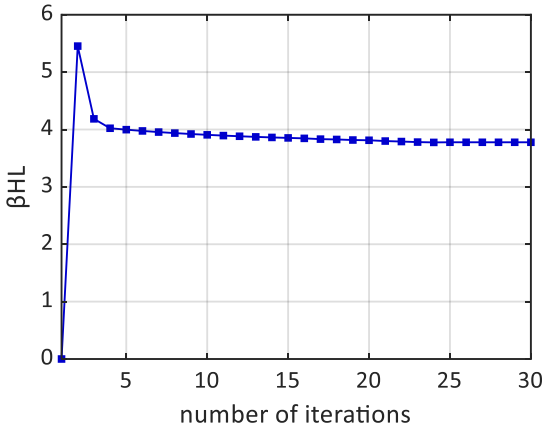

(h) 315^o

Figure 3A.4. Convergence plots for various environmental load angles on a jacket structure.

References

Aas, K., Czado, C., Frigessi, A., & Bakken, H. (2009). Pair-copula constructions of multiple dependence. *Insurance: Mathematics and Economics*, *44*(2), 182–198. https://doi.org/10.1016/j.insmatheco.2007.02.001

Antão, E. M., & Guedes Soares, C. (2014). Approximation of bivariate probability density of individual wave steepness and height with copulas. *Coastal Engineering*, *89*, 45–52. https://doi.org/10.1016/j.coastaleng.2014.03.009

Bedford, T., & Cooke, R. M. (2002). Vines – A new graphical model for dependent random variables. *Annals of Statistics*, *30*(4), 1031–1068. https://doi.org/10.1214/aos/1031689016

Bentley. (2018). SACS suite program. (Version 13.0). Exton, PA: Bentley Systems. Retrieved from www.bentley.com

Chang, B., Pan, S., & Joe, H. (2019). Vine copula structure learning via Monte Carlo tree search. *AISTATS 2019 - 22nd International Conference on Artificial Intelligence and Statistics*, *89*.

Chang, C. H., Tung, Y. K., & Yang, J. C. (1995). Monte Carlo simulation for correlated variables with marginal distributions. *Journal of Hydraulic Engineering*, *121*(7), 573. https://doi.org/10.1061/(ASCE)0733-9429(1995)121:7(573)

C-CORE. (2017). Offshore Newfoundland and Labrador Met Ocean Study: Detailed Analysis Basis Vol 1&2. St. John's.

Der Kiureghian, A., & Liu, P.L. (1986). Structural reliability under incomplete probability information. J Eng Mech ;112(1):85–104.

Ditlevsen, O. (2002). Stochastic model for joint wave and wind loads on offshore structures. *Structural Safety*, *24*(2–4), 139–163. https://doi.org/10.1016/S0167-4730(02)00022-X

Genest, C., & Favre, A. (2007). Everything You Always Wanted to Know about Copula Modeling but Were Afraid to Ask. *Journal of Hydrologic Engineering*, *12*, 347–368. https://doi.org/10.1061/(ASCE)1084-0699

Goda, K. (2010). Statistical modeling of joint probability distribution using copula: Application to peak and permanent displacement seismic demands. *Structural Safety*, *32*(2), 112–123. https://doi.org/10.1016/j.strusafe.2009.09.003

Guo, C., Khan, F., & Imtiaz, S. (2019). Copula-based Bayesian network model for process system risk assessment. *Process Safety and Environmental Protection*, *123*, 317–326. https://doi.org/10.1016/j.psep.2019.01.022

Gupta, N., & Bhaskaran, P. K. (2017). Inter-dependency of wave parameters and directional analysis of ocean wind-wave climate for the Indian Ocean. *International Journal of Climatology*, *37*(6), 3036–3043. https://doi.org/10.1002/joc.4898

Hashemi, S. J., Khan, F., & Ahmed, S. (2016). Multivariate probabilistic safety analysis of process facilities using the Copula Bayesian Network model. *Computers and Chemical Engineering*, *93*, 128–142. https://doi.org/10.1016/j.compchemeng.2016.06.011

Hurtado J.E. (2004) Dimension Reduction and Data Compression. In: Structural Reliability. Lecture Notes in Applied and Computational Mechanics, vol 17. Springer, Berlin, Heidelberg. https://doi.org/10.1007/978-3-540-40987-8_3

Jiang, C., Xiong, L., Yan, L., Dong, J., & Xu, C. Y. (2019). Multivariate hydrologic design methods under nonstationary conditions and application to engineering practice. *Hydrology and Earth System Sciences*, *23*(3), 1683–1704. https://doi.org/10.5194/hess-23-1683-2019

Joe, H. (2014). Dependence modeling with copulas. In *Dependence Modeling with Copulas*. Chapman & Hall /CRC. https://doi.org/10.1201/b17116

Khuntia, S. R., Rueda, J. L., & van der Meijden, M. A. M. M. (2019). A multivariate framework to study spatio-temporal dependency of electricity load and wind power. *Wind Energy*, *22*(12), 1825–1847. https://doi.org/10.1002/we.2407

Lebrun, R. & Dutfoy, A. (2009) *An innovating analysis of the Nataf transformation from the copula viewpoint*, Prob. Eng. Mech., 24, 312–320

Li, D. Q., Wu, S. B., Zhou, C. B., & Phoon, K. K. (2012). Performance of translation approach for modeling correlated non-normal variables. *Structural Safety*, *39*, 52–61. https://doi.org/10.1016/j.strusafe.2012.08.001

Liu, Y., & Fan, X. (2016). Time-Independent Reliability Analysis of Bridge System Based on Mixed Copula Models. *Mathematical Problems in Engineering*, *2016*.

Lu, H., & Zhu, Z. (2018). A method for estimating the reliability of structural systems with moment-matching and copula concept. *Mechanics Based Design of Structures and Machines*, *46*(2), 196–208. https://doi.org/10.1080/15397734.2017.1324312

Lü, T. J., Tang, X. S., Li, D. Q., & Qi, X. H. (2020). Modeling multivariate distribution of multiple soil parameters using vine copula model. *Computers and Geotechnics*, *118*, 103340. https://doi.org/10.1016/j.compgeo.2019.103340

Marelli, S. & Sudret, B. (2014). UQLab: A framework for uncertainty quantification in Matlab, Proc. 2nd Int. Conf. on Vulnerability, Risk Analysis and Management (ICVRAM2014), Liverpool, United Kingdom, 2554-2563.

Masina, M., Lamberti, A., & Archetti, R. (2015). Coastal flooding: A copula based approach for estimating the joint probability of water levels and waves. *Coastal Engineering*, *97*, 37–52. https://doi.org/10.1016/j.coastaleng.2014.12.010

Melchers, R., & Beck, A. T. (2018). Structural Reliability — Analysis and Prediction. In *Structural Safety* (Third). https://doi.org/10.1016/s0167-4730(01)00007-8

Michele, C. De, Salvadori, G., Passoni, G., & Vezzoli, R. (2007). A multivariate model of sea storms using copulas. *Coastal Engineering*, *54*, 734–751. https://doi.org/10.1016/j.coastaleng.2007.05.007

Montes-Iturrizega, R., & Heredia-Zavoni, E. (2016). Reliability analysis of mooring lines using copulas to model statistical dependence of environmental variables. *Physics Procedia*, *59*, 564–576. https://doi.org/10.1016/j.apor.2016.07.008

Nelsen, R. B. (2006). *An Introduction to Copulas: Lecture Note in Statistics*. Springer US. https://doi.org/https://doi.org/10.1007/0-387-28678-0_1

Qiu, Y., Li, Q., Pan, Y., Yang, H., & Chen, W. (2019). A scenario generation method based on the mixture vine copula and its application in the power system with wind/hydrogen production. *International Journal of Hydrogen Energy*, *4*, 5162–5170. https://doi.org/10.1016/j.ijhydene.2018.09.179

Schöbi, R., Sudret, B., & Wiart, J. (2015). Polynomial-chaos-based Kriging. *International Journal for Uncertainty Quantification*, *5*(2), 171–193. https://doi.org/10.1615/Int.J.UncertaintyQuantification.2015012467

Shao, C., Gu, C., Meng, Z., & Hu, Y. (2019). A Data-driven approach based on multivariate copulas for quantitative risk assessment of concrete dam. *Journal of Marine Science and Engineering*, *7*(10). https://doi.org/10.3390/jmse7100353

Sun, Y., Chen, K., Liu, C., Zhang, Q., & Qin, X. (2021). Research on reliability analytical method of complex system based on CBN model. *Journal of Mechanical Science and Technology*, *35*(1), 107–120. https://doi.org/10.1007/s12206-020-1210-4

Tang, X. S., Li, D. Q., Zhou, C. B., Phoon, K. K., & Zhang, L. M. (2013a). Impact of copulas for modeling bivariate distributions on system reliability. *Structural Safety*, *44*, 80–90. https://doi.org/10.1016/j.strusafe.2013.06.004

Tang, X. S., Li, D. Q., Zhou, C. B., & Zhang, L. M. (2013b). Bivariate distribution models using copulas for reliability analysis. *Proceedings of the Institution of Mechanical Engineers, Part O: Journal of Risk and Reliability*, *227*(5), 499–512. https://doi.org/10.1177/1748006X13481928

Tang, X. S., Wang, M. X., & Li, D. Q. (2020). Modeling multivariate cross-correlated geotechnical random fields using vine copulas for slope reliability analysis. *Computers and Geotechnics*, *127*, 103784. https://doi.org/10.1016/j.compgeo.2020.103784

Tosunoglu, F., Gürbüz, F., & Nuri, M. (2020). Multivariate modeling of flood characteristics using vine copulas. *Environmental Earth Sciences*, *79*. https://doi.org/10.1007/s12665-020-09199-6

Tu Pham, M., Vernieuwe, H., De Baets, B., & Verhoest, N. E. C. (2018). A coupled stochastic rainfall-evapotranspiration model for hydrological impact analysis. *Hydrology and Earth System Sciences*, *22*(2), 1263–1283. https://doi.org/10.5194/hess-22-1263-2018

Uzielli, M., & Mayne, P. W. (2012). Load-displacement uncertainty of vertically loaded shallow footings on sands and effects on probabilistic settlement estimation. *Georisk*, *6*(1), 50–69. https://doi.org/10.1080/17499518.2011.626333

Wang, F., & Li, H. (2017). Stochastic response surface method for reliability problems involving correlated multivariates with non-Gaussian dependence structure: Analysis under incomplete probability information. *Computers and Geotechnics*, *89*, 22–32. https://doi.org/10.1016/j.compgeo.2017.02.008

Wang, F., & Li, H. (2019). On the need for dependence characterization in random fields: Findings from cone penetration test (CPT) data. *Canadian Geotechnical Journal*, *56*(5), 710–719. https://doi.org/10.1139/cgj-2018-0164

Wang, W., Dong, Z., Zhu, F., Cao, Q., Chen, J., & Yu, X. (2018). A stochastic simulation model for monthly river flow in dry season. *Water (Switzerland)*, *10*(11). https://doi.org/10.3390/w10111654

Xiao, N., Duan, L., & Tang, Z. (2017). Surrogate-model-based reliability method for structural systems with dependent truncated random variables. *Journal of Risk and Reliability*, *231*(3), 265–274. https://doi.org/10.1177/1748006X17698065

Yang, X. C., & Zhang, Q. H. (2013). Joint probability distribution of winds and waves from wave simulation of 20 years (1989-2008) in Bohai Bay. *Water Science and Engineering*, *6*(3), 296–307. https://doi.org/10.3882/j.issn.1674-2370.2013.03.006

Zhai, J., Yin, Q., & Dong, S. (2017). Metocean design parameter estimation for fixed platform based on copula functions. *Journal of Ocean University of China*, *16*(4), 635–648. https://doi.org/10.1007/s11802-017-3327-3

Zhang, Y., Kim, C., Beer, M., Dai, H., & Guedes, C. (2018). Modeling multivariate ocean data using asymmetric copulas. *Coastal Engineering*, *135*, 91–111. https://doi.org/10.1016/j.coastaleng.2018.01.008

Chapter 4

An Active Learning Polynomial Chaos Kriging Metamodel for Reliability Assessment of Marine Structures

Preface

A version of this chapter has been published in the **Ocean Engineering 2021; 235:109399.** *I am the primary author that produced this work, along with Co-authors Faisal Khan and Salim Ahmed. I reviewed the relevant literature, developed the concept and methodology, prepared the original manuscript, software implementation, reviewed and revised the manuscript following the co-authors' feedback and peer review from the journal. Co-author Faisal Khan assisted in the concept development and methodology, research supervision, funding for the work, review, and editing of the manuscript. Co-author Salim Ahmed assisted in concept development and its methodology, validation, research supervision, reviewing, and manuscript editing.*

Abstract

Metamodel combined with simulation type reliability method is an effective way to determine the probability of failure (P_f) of complex structural systems and reduce the burden of computational models. However, some existing challenges in structural reliability analysis are minimizing the number of calls to the numerical model and reducing the computational time. Most research work considers adaptive methods based on ordinary Kriging with a single-point enrichment of the ED. This work presents an active learning reliability method using a hybrid metamodel with multiple-point enrichment of ED for structural reliability analysis. The hybrid method (APCKKm-MCS) takes advantage of the global prediction and local interpolation capability of Polynomial Chaos Expansion (PCE) and Kriging, respectively. The U learning function drives active learning in this approach, while K-means clustering is proposed for multiple-point enrichment purposes. Two

benchmark functions and two practical marine structural cases validate the performance and efficiency of the method. The results confirm that the APCKKm-MCS approach is efficient and reduces the computational time for reliability analysis of complex structures with nonlinearity, high dimension input random variables, or implicit function.

Keywords: Structural Reliability; Polynomial Chaos Kriging; Active learning function; Monte Carlo Simulation; Experimental Design

4.1. Introduction

Complex marine structures operating in the harsh and remote ocean environment require higher reliability to ensure the safety of life, asset, and the environment throughout their operational life. To ensure higher reliability, one would need efficient and robust reliability assessment models (Weinmeister et al., 2019). There have been efforts to develop and use metamodels for engineering structures and systems; this ranges from but is not limited to Polynomial Regression, ANN, SVR, PCE, and Kriging (Weinmeister et al., 2019). Ocean structures are complex in their physical and functional form, with mainly implicit or no closed-form LSF describing their various failure modes (Bai & Jin, 2016). For such structures, metamodel choice becomes crucial in the limit state design (Ultimate, Serviceability, Damage, and Fatigue). Among these metamodels, Kriging and PCE are non-intrusive and have gained wide application for reliability assessment in various engineering fields, including marine structures (Teixeira & Soares, 2018).

PCE is a well-established metamodel with wide application in mathematics and engineering; it started as a stochastic FEA concept in the 90s (Ghanem & Spanos, 1997). The method gained usefulness in reliability analysis as a metamodel in the 2000s (Sudret & Der Kiureghian, 2002). PCE is a spectra-based metamodeling approach that expresses the system response of finite variance in terms of the polynomial of its input variables. It comprises a series of multivariate

orthogonal polynomials and their corresponding coefficients. The PCE approach is relatively simple to construct; it provides an easy estimation of the global statistics of the system's response, which includes the statistical moment and distribution. PCE model allows for the computation of sensitivity analysis, and it is efficient for resampling purposes (Marelli &Sudret,2019).

Similarly, Kriging is an interpolation technique that originated in geostatistics. The system's response is assumed to follow a Gaussian process with a given covariance structure. The approach explores the correlation information of existing data samples to obtain the output for new input points. It captures the local variability of the response as a function of the neighboring data points. Kriging is flexible to a wide range of correlation functions, provides a strong interpolation capability among the data points, and can produce the mean prediction and associated variance for output response. Also, the statistical information from the output response can be utilized for model refinement through an adaptive process (Santner et al., 2003).

Various marine-related studies have applied the Kriging and PCE technique in prediction and reliability studies. Chi et al. (2017) demonstrated the Legendre PCE method's application in the statistical analysis of crosstalk in wire harnesses for naval ships. Ni et al. (2018) applied the concept of PCE in dynamic response analysis of marine risers. Zhang et al. (2021) studied the uncertainty propagation and sensitivity analysis of a marine vehicle's shafting system using the generalized PCE method. Bahmyari et al. (2017) research considered the effect of a combination of PCE and the Galerkin method for the bending analysis of deformable plates. Lim et al. (2018) utilized PCE in developing a long-term surge motion analysis for a moored offshore vessel. In another study, Nguyen et al.(2019) developed a PCE framework for extreme load analysis of a single-body wind energy converter. The reliability assessment of subsea anchors using the PCE approach also showed its application to subsea facilities (Charlton & Rouainia,2019). Hu et al.

(2019) investigated the performance of second and third-order PCE in hydrological modeling. The concept of developing a PCE metamodel has also gained practical application in marine concrete analysis. Bastidas-Arteaga et al. (2020) applied the PCE method in uncertainty propagation and sensitivity analysis of chloride-induced corrosion on marine concrete structures.

Furthermore, Kriging metamodels have found wide applications in marine science and technology; below are some research-related applications of Kriging in the reliability analysis of marine structures and maritime operations. Morató et al.(2019) applied Kriging for the reliability analysis of an offshore wind energy converter's monopile support structure. Teixeira et al. (2019) proposed an approach to reduce the computational effort in the fatigue stress analysis of an offshore wind tower using the Kriging method. Gaspar et al.(2014) studied Kriging's efficiency in developing metamodels for marine structures with its application to a stiffened plate; the study showed the superiority of Kriging over the polynomial regression method in structural reliability assessment. Chen et al. (2016) applied a combination of Kriging metamodels for flexible risers optimal design. Hill et al.(2016) developed a Kriging model for motion response monitoring of FPSO mooring lines. For a vessel-shaped fish farm mooring system, Kriging was applied for optimization purposes (Li et al., 2019). Shi et al. (2015) developed a metamodel using Kriging for reliability assessment of a marine vessel's bottom plate subject to environmental load. Kriging has also found applications in offshore semi-submersible reliability assessment (Xu et al.,2018). Brandt et al. (2017) demonstrated the application of Kriging in the fatigue assessment of an offshore wind turbine's jacket support structure. Wang et al.(2019) investigated the optimization of an autonomous underwater vehicle's appendage using Kriging. Abdalla et al.(2018) demonstrated the application of Kriging in studying the effect of chemicals on workers' exposure to new positions on a coastline. Bian et al.(2019) applied the concept of Kriging to monitor the marine environment

in coastal China. Zhang et al.(2018) used the interpolation ability of Kriging in determining the possibility of drilling sections of formations in oil and gas drilling operations.

The Kriging and PCE metamodels can capture local variability and global behavior of the output response, respectively, which is a significant strength of these models.

The PCK method combines these advantages of Kriging and PCE to produce a robust metamodel that can reduce the rigor involved with computational models (Schöbi et al., 2015). Recently, research has focused on combining metamodels for efficient reliability assessment, especially in aerospace-related research. Cheng & Lu (2020) study focused on developing a metamodel ensemble for reliability assessment. PCK metamodel has been applied in airfoil and aircraft engine nacelle analysis (Weinmeister et al., 2019). Also, Leifsson et al.(2020) utilized PCK metamodel in the yield estimation of multiband patch antennas.

Unlike the broad application of PCE and Kriging in various engineering design areas, the potential advantage of PCK has not been widely explored, especially in the reliability assessment of marine structures.

This study aims to achieve the following objectives

1. Develop an active learning PCK framework for marine structure reliability, combining PCE and ordinary Kriging advantages.
2. Implement a multiple sampling point ED enrichment of PCK metamodel by K-means clustering to reduce computational time during reliability analysis rather than a single point enrichment as commonly adopted in active learning studies.
3. To present a practical application of the developed framework for marine structural reliability assessment.

The proposed method is described in this work as an Active Learning PCK using K-means clustering (APCKKm-MCS).

The remainder of this work is organized as follows: Section 4.2 describes the preliminaries of active learning, metamodels, and reliability. Section 4.3 details the methodology with illustrative examples. Section 4.4 presents case studies applying the APCKKm-MCS approach in the reliability-based analysis of a truss system and an SCR under operating conditions. Section 4.5 concludes the study.

4.2. Preliminaries on the hybrid metamodel

4.2.1. Metamodels

With the burden from computational models for complex structures, metamodels provide an inexpensive way to approximate input and output relationships using cheap-to-evaluate analytical models. This section will establish the fundamentals of Kriging and PCE required in PCK construction.

4.2.1.1. Kriging

Kriging structure comprises a trend, and stochastic part, with the latter represented by a stationary Gaussian Process of zero mean and unit standard deviation. Eq. (4.1) is a typical representation of the Kriging model.

$$y \approx M^K(x) = \beta^T f(x) + \sigma_g^2 z(x) \tag{4.1}$$

$\beta^T f(x)$, σ_g^2 represents the mean value (trend function) and the variance of the Gaussian process, respectively. The notation $z(x)$; denotes the stationary Gaussian process, determined by the

autocorrelation function R. Also, the response approximation using Kriging metamodel is represented as $M^K(x)$.

The Kriging model parameters such as the coefficient of the trend function (β), process variance (σ_g^2) and the hyperparameters (θ_h) of the stationary Gaussian process are determined by the MLE approach as shown in Eqs. (4A.1) to (4A.4) of Appendix 4A.

For the stochastic term, kernel selection for the Kriging model is made from a range of autocorrelation functions such as linear, exponential, Gaussian, and Matérn. This study adopts the more generalized Matérn autocorrelation function (Santner et al.,2003) with shape parameter ν^s = 5/2, as shown in Eq. (4.2).

$$R(|x - x'|; l; \nu^s = {}^5/_2) = \prod_{i=1}^{M} \left(1 + \frac{\sqrt{5|x-x'|}}{l_i} + \frac{5|x_i - x_{i'}|^2}{3{l_i}^2}\right) \exp\left(\frac{-5|x_i - x_{i'}|}{l_i}\right) \quad (4.2)$$

From the expression, x , x'; are sample points, and l is the correlation length.

The Kriging unique predictor is based on available observation and response data. The predicted mean ($\mu_{\hat{Y}}$) at a given point gives the output shown in Eq. (4.3).

Finally, the predicted variance (Eqs. (4.4) and (4.5)) provides further information about the uncertainty of the mean.

$$\mu_{\hat{Y}}(x) = f(x)^T\beta + r(x)^T R^{-1}(y - F\beta) \quad (4.3)$$

$$\sigma^2{}_{\hat{Y}}(x) = \sigma^2[1 - r^T(x)R^{-1}r(x) + V^T(x)(F^T R^{-1}F)^{-1}V(x)] \quad (4.4)$$

Where $$V(x) = F^T R^{-1} r(x) - f(x) \quad (4.5)$$

$r(x)$ represents the cross-correlation vector between prediction point x and N sample points (Eq. (4.6)).

$$r(x) = [R_\theta(x, x^1), R_\theta(x, x^2), \dots \dots R_\theta(x, x^N)] \quad (4.6)$$

4.2.1.2. The orthogonal polynomial model (PCE)

PCE is a weighted sum of multivariate orthogonal polynomials and considers a finite output variance. Eq. (4.7) shows the structure of a PCE model.

$$y \approx M^{PCE} = \sum_{\alpha \in N^M} y_\alpha \Psi_\alpha(x) \quad (4.7)$$

$\Psi_\alpha(x)$ is the polynomial basis function of the multivariate polynomial and y_α; represents the coefficients of the function. The family of orthogonal polynomials satisfies an inner product requirement (Eq. (4A.5), Appendix 4A).

The multivariate polynomials are a tensor product of univariate polynomials, as shown in Eq. (4.8). These polynomials follow the orthogonality condition shown in Eq. (4.9).

$$\Psi_\alpha(X) = \prod_{i=1}^{M} \Psi_\alpha^{(i)}(X_i) \quad (4.8)$$

$$E\left(\Psi_\alpha \Psi_\beta\right) = \int_{D_x} \Psi_\alpha \Psi_\beta f_X(x) dx = \delta_{\alpha\beta} \quad (4.9)$$

There is a natural relationship between orthogonal polynomials and probability distribution. The Wiener-Askey scheme attributes specific orthogonal polynomials to a given probability distribution of the random variables (Xiu & Em Karniadakis, 2003). Table 4A.1 (Appendix 4A) shows the families of orthogonal polynomials and the associated distribution. For situations with no specific basis for the distribution type, an isoprobabilistic transformation to the desired distribution type in the conventional Askey scheme basis is considered (Lebrun & Dutfoy, 2009).

The PCE approach suffers from the curse of dimensionality, as shown in Eq. (4.10), where the number of required polynomials grows exponentially both in degree and dimension. The result increases the computational expense of the model. Consequently, there is a need for truncation of the terms of the polynomial.

$$P^O = \frac{(P + N_d)!}{P!\, N_d!} \tag{4.10}$$

P^O is the number of terms in the PCE, N_d represents the dimensionality of the random variable, and P is the maximum order of the basis polynomial. The truncation of the orthogonal polynomial infinite series is achieved using a sparse algorithm that disregards interactive terms and penalizes higher-order terms while selecting a P that minimizes the cross-validation error (Fajraoui et al., 2017). This approach increases the robustness of the method and prevents overfitting.

The Least Angle Regression Selection (LARS) provides an algorithm that allows for appropriate truncation, considering only the orthogonal basis's non-zero terms. This study adopts LARS for its successful application in obtaining the best sparse set (Blatman & Sudret, 2011). Eqs. (4.11) and (4.12) show the penalized least square with regularization (γ) and Leave-One-Out error ($\in_{LOO}$) which needs to be minimized to obtain the best sparse set of coefficients. $\in_{LOO}$ is a cross validation error which prevents the common overfitting problem peculiar to PCE (Lataniotis et al,2019).

$$y_\alpha = argmin \frac{1}{n} \sum_{i=1}^{n} (Y^T \Psi_\alpha(x^{(i)}) - M(x^{(i)}))^2 + \gamma \sum_{\alpha \in A} |y_\alpha| \tag{4.11}$$

$$\in_{LOO} = \frac{1}{n} \left[\frac{\sum_{i=1}^{n} \left(M(x_i) - M_{\hat{Y},(-i)}(x_i) \right)^2}{Var(y)} \right] \tag{4.12}$$

From Eqs. (4.11) and (4.12), n represents the number of sample points in the ED. $Var(y)$; denotes response data variance and $M_{\hat{Y},(-i)}(x_i)$; represents the model response with the exclusion of a data point from the ED.

4.2.1.3. The hybrid metamodel (PCK)

The hybrid model effectively combines Kriging and PCE's advantage, as highlighted in the introduction. To connect the metamodels, the sparse PCE term, shown in Eq. (4.7), is utilized as the trend function in Eq. (4.1). Consequently, a robust metamodel for the reliability assessment of marine structures is formed.

Eq. (4.13) shows a typical PCK expression with a polynomial trend term.

$$y \approx M^{PC-K}(x) = \sum_{\alpha=A} y_\alpha \Psi_\alpha(x) + \sigma_g^2 z(x) \tag{4.13}$$

In this approach, the sparse polynomial set obtained from the LARS algorithm is ranked based on its correlation with the residual obtained and introduced individually as a trend function in the Kriging model (Eq. (4.1)). In the process, the error is determined at each iterative step until the trend function contains all sparse set of polynomials initially defined. The iterative action which minimizes $\in_{LOO}$ is determined and used as the optimal PCK model. The calibrated model then serves as a metamodel for response determination. The least-square minimization approach has the obvious advantage of using an arbitrary number of input points to determine the coefficients if they represent the random input variables.

4.2.2. Active Learning Function and ED Enrichment

In recent times, the enrichment of ED in metamodel construction has become an attractive means to reduce computational cost. The enrichment concept reduces the performance function's

computational evaluation and improves the metamodel's efficiency and accuracy. It selects the next best point in an iterative pattern from the candidate sample pool until the stopping criteria are met. Current research focuses on developing active learning functions, although these are mainly variants of the existing learning functions.

The Efficient Global Optimization (EGO) method for computational cost reduction pioneered the concept of active learning (Jones et al.,1998). Other active learning methods have developed after the EGO approach. The Expected Feasibility Function (EFF) (Bichon et al.,2008) and the U function (Echard et al., 2011) selects points from the candidate population with consideration of sample points close to the limit state surface and with considerable uncertainty of the prediction. Lv et al. (2015) proposed the H function, which considers sample points with significant prediction error and information entropy close to the limit state surface. Also, Sun et al. (2017) proposed the Least Important Function (LIF), which considers the improvement of P_f of the Kriging model with enrichment of the ED. Although, there exist several active learning functions, they are rarely applied practically because of their difficulty in implementation. However, U function stands out in its simplicity in implementation and fast convergence. Consequently, it will be used for active learning in this study. More specifically, the U function selects from the candidate pool the sample with the maximum probability of misclassification. The U function is premised on the fact that the sign of the performance function affects the next point required for enrichment. The probability of misclassification (P_{mis}) is shown in Eq. (4.14).

$$P_{mis} = \Phi\left(\frac{-\left|\mu_{\hat{g}}(x)\right|}{\sigma_{\hat{g}}}\right) \tag{4.14}$$

Where $U(x) = \frac{|\mu_{\hat{g}}(x)|}{\sigma_{\hat{g}}}$

The sample point which minimizes $U(x)$ (Eq. (4.15)) has a high tendency to change the sign in the vicinity of the limit state surface and is considered the next new point in the ED. The smaller the U(x) value, the more prediction uncertain the sign is for the LSF. The stopping criterion of the U function is set as min U(x)≥2.

$$x_{new} = argmin\left(U(x)\right) \quad \text{for x} \in S_P \tag{4.15}$$

where S_P is the sample population

The initial development and application of active learning methods have focused on ordinary Kriging taking advantage of its interpolation and stochastic capabilities. Also, single-point enrichment has been the focus of the active learning methods developed.

The enrichment of ED is usually achieved by the next best point from the candidate pool, as described in Eq. (4.15). While most active learning approaches in the literature have enriched the ED with a single point, this work considers multiple enrichment using the weighted K-means clustering approach (Zaki & Meira, 2014). The clustering weight is determined by P_{mis} (Eq. (4.14)); the approach significantly reduces the number of iterations while still maintaining the quality of the metamodel and accuracy of the P_f.

4.2.3. Structural Reliability

The structural reliability approach determines the probability of structural failure given random input variables. $G(x)$ represents the LSF that characterizes the performance of the system. The limit state surface ($G(x) = 0$) divides the standard normal plane into safe ($G(x) > 0$) and failure regions ($G(x) < 0$). The integral of a joint PDF ($f_X(x)$) in the failure domain determines P_f (Eq.

(4.16)). X represents the random input vector where $X = [x_1, \ldots . x_n]^T$. For the joint PDF, obtaining a closed-form solution for this integral is challenging.

$$P_f = \int_{G(x)\leq 0} f_X(x)dx \qquad (4.16)$$

The gradient-based reliability approach (based on Taylor's expansion series) and the simulation type methods provide an alternative in the determination of the structural system P_f . Examples of this approach include the FORM and SORM (Zhao & Ono, 1999). However, the gradient-based method presents difficulty in dealing with nonlinear and complex LSF, system reliability problems, and multiple design points. The simulation methods include MCS and variance reduction methods like 'IS' (Ang et al.,1992), Line Sampling (Pradlwarter et al., 2007), and Subset Simulation (Au & Beck, 2001). The MCS method (Eq. (4.17)) is straightforward to implement, independent of the type of LSF and distribution of the input variables. MCS has gained useful applications in various engineering areas. From Eq. (4.17), N_{mcs} and $N_{G(x)\leq 0}$ represents the sampling size and samples in the failure domain or on the limit state surface respectively. Also, Eq. (4.18). shows the CoV which signifies the uncertainty in P_f from the MCS approach (Melchers & Beck, 2018).

$$P_f = \frac{N_{G(x)\leq 0}}{N_{mcs}} \qquad (4.17)$$

$$\text{CoV} = \sqrt{\frac{1-P_f}{P_f N_{mcs}}} \qquad (4.18)$$

The difficulty of MCS application in the reliability assessment of finite element models due to the computational burden during analysis has led to the concept of metamodels to simplify the reliability evaluation of complex engineering systems.

4.3. Methodology for metamodel development

This section describes the sequential steps for reliability assessment using the proposed APCKKm-MCS approach. For clarity, two benchmark functions further explain the framework.

4.3.1. Procedural Steps

Step 1: Obtain statistical parameters, probability distribution, and dependency information (where necessary) of random variables from observation data. This work determines the dependence between random variables using copula functions. Copulas are links between univariate marginals and significantly capture tail dependence and nonlinear relationships between random variables (Nelsen.,2006).

Step 2: With the PDF of the input distribution, generate candidate sample points using MCS (N_{mcs}). The sample points required for ED enrichment at each iterative step are drawn from the candidate pool.

Step 3: Initial sampling plan and points of data are determined. The study adopts a type of ED called LHS. The LHS approach is a space-filling method for generating sample points of random variables for metamodel construction (Forrester et al., 2008). The ED is dependent on the dimension of random input variables. For the initial ED, although there are no agreed methods to determine the number of samples required, one of the pioneering works on active learning, Echard et al. (2011), suggested a small initial ED for this purpose (about a dozen sample points). For systems with random input variables less than twelve (12), this study adopts an initial ED of at least 12 sample points. For random variables greater than 12, the initial ED utilized equals the number of random variables (where applicable).

Step 4: With a computational model or experiment, obtain structural responses for the quantity of interest using the initial ED obtained in Step 3.

Step 5: Train the proposed metamodel using initial ED (Step 3) and responses obtained in Step 4. Section 2 describes the construction process of the metamodel.

Step 6: Obtain candidate pool response with developed APCKKm-MCS metamodel. Consequently, evaluate the prediction sign required for candidate pool sample classification and the P_f.

Step 7: Develop weighted K-means clusters in the candidate pool. Using the U learning function, determine the *min U(x)* for K-means clusters.

Step 8: The *min U(x*) points that represent the potential enrichment points to the ED are checked against the stopping criteria (*U(x)*$\geq$*2).* If the possible enrichment points meet the stopping criteria, then MCS sufficiency is tested. Otherwise, update the ED in Step 5 with the best new sample points and their corresponding responses.

Step 9: Determine the candidate pool sufficiency. If the CoV is less than 5%, accept the P_f. Otherwise, the candidate sample pool is updated accordingly, and the process is repeated.

Figure 4.1 shows the procedure described above for reliability assessment using APCKKm-MCS.

This work uses code implementation for reliability analysis in MATLAB-based software Uqlab (Marelli & Sudret, 2014).

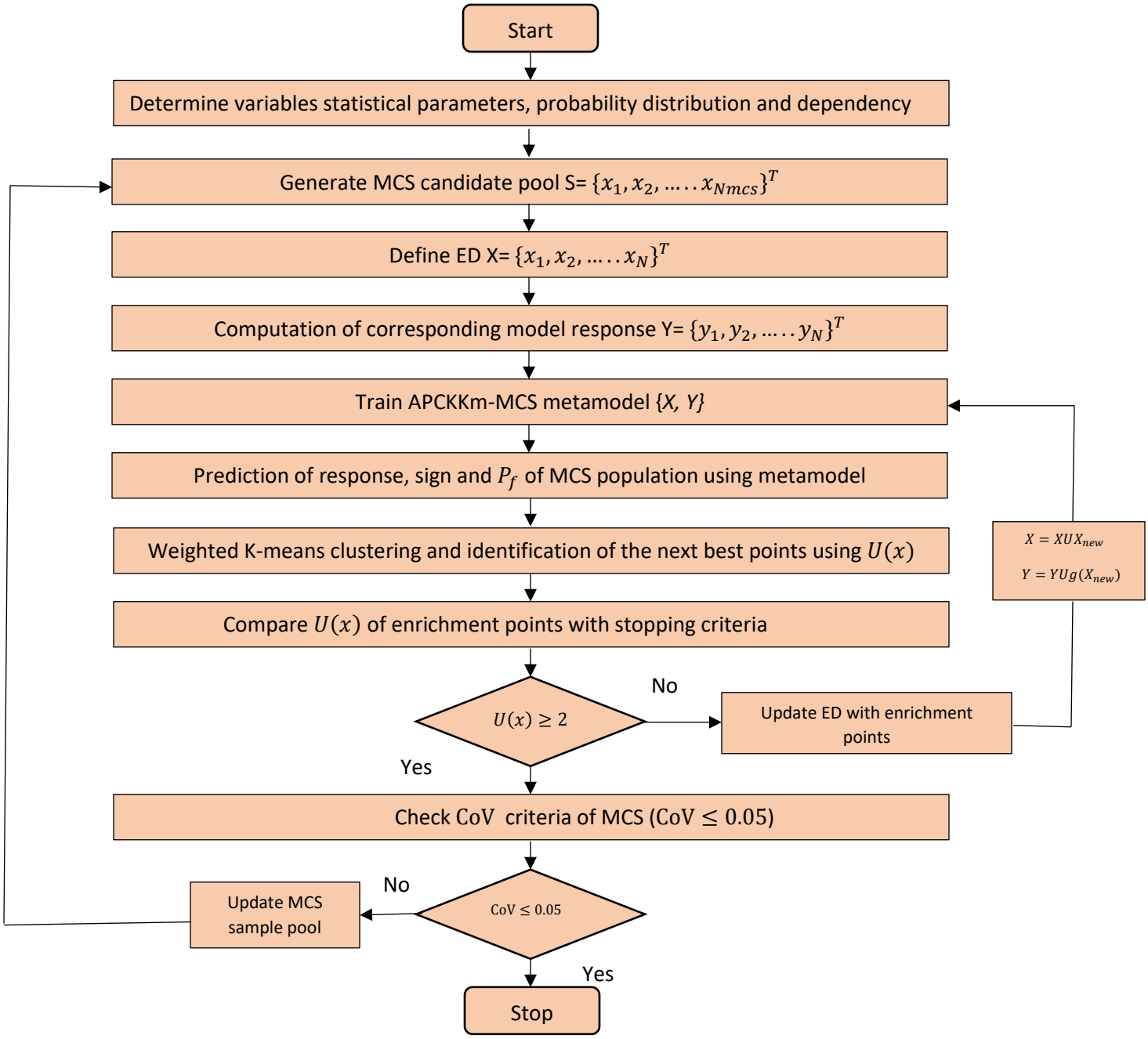

Figure 4.1. Flowchart for reliability assessment using APCKKm-MCS.

4.3.2. Illustrative examples using benchmark functions

This section explains the framework described in Section 4.3.1 using two benchmark functions. The reliability results from the proposed method are compared with active learning ordinary Kriging metamodel (AK-MCS) and active learning PCK with a single point enrichment approach (APCK-MCS).

4.3.2.1. Ten-dimensional nonlinear function

The Ten-dimensional function expressed in Eq. (4.19) is highly nonlinear and shows the relationship between independent random input variables (X) and the corresponding response $g(X)$.

$$g(X) = \left(\sum_{i=1}^{10} {X_i}^2\right) + 10X_1^2X_2^2 + \sum_{i=2}^{9} X_i^2\, X_{i+1}^2 - 16 \tag{4.19}$$

The steps detailed in Section 4.3.1 are applied to the function for metamodel development and reliability assessment.

Step 1: All variables of the Ten-dimensional function are assumed to be statistically independent and normally distributed $X_i \sim N\ (1,0.2) for\ i = 1,2 \ldots . 10$.

Step 2: The MCS candidate pool required for the enrichment of the ED comprises of $N_{mcs} = 10^6$ sample points for the input variables of known distribution.

Step 3: The initial ED comprises twelve (12) LHS sampling points for metamodel training.

Step 4: Determine the responses ($g(X)$) of the initial sampling points obtained in Step 3.

Step 5: Using the initial ED sampling points (Step 3) and the corresponding responses (Step 4), the proposed metamodel is constructed as described in Eqs. (4.1) to (4.13) of Section 2. The conventional Hermite orthogonal polynomial (Xiu & Em Karniadakis,2003) is selected as the polynomial basis in the metamodel construction with normally distributed variables.

Step 6: The signs for candidate sample points and reliability are determined using the developed metamodel.

Step 7: Points with the probability of misclassification are determined using the U learning function. This study considers three clusters (K=3) for the weighted K-means clustering.

Steps 8 & 9: Next best points from the clusters enrich the ED, and the iterative process continues as shown in Figure 4.1 until $U(x) \geq 2$ in the candidate pool. For reliability analysis, the stopping criterion is $\mathrm{CoV} \leq 0.05$.

The reliability results (Table 4.1) obtained with multiple enrichment (APCKKm-MCS) are compared with the single sample point enrichment case (APCK-MCS) and the conventional ordinary Kriging active learning (AK-MCS). Also, in Table 4.1 is the number of model evaluations (N_{mod}), which indicates the number of calls to the model, especially when dealing with implicit LSF. The number of iterations (N_{itr}) required in achieving the stopping condition, as shown in the framework (Figure. 4.1), is also detailed in Table 4.1.

Table 4.1. Reliability analysis summary (Ten-dimensional nonlinear function).

	APCKKm-MCS	APCK-MCS	AK-MCS	MCS (Reference)
P_f	8.528E-3	8.501E-3	8.242E-3	8.519E-3
N_{mod}	237	234	958	1E6
N_{itr}	75	222	946	-
ϵ_{LOO}	1.2116E-4	1.8593E-4	1.06E-2	
P_f deviation (%)	0.11	0.21	3.25	-
CoV	1.07E-2	1.08E-2	1.13E-2	

The average CPU time indicates the average time of convergence of a metamodeling approach. Simulation is implemented using an i7-7500U, 2.90GHz CPU with an 8GB memory computer. The average CPU time from 40 runs of the proposed method (APCKKm-MCS) is compared with APCK-MCS and AK-MCS using the same starting ED (Figure 4.2).

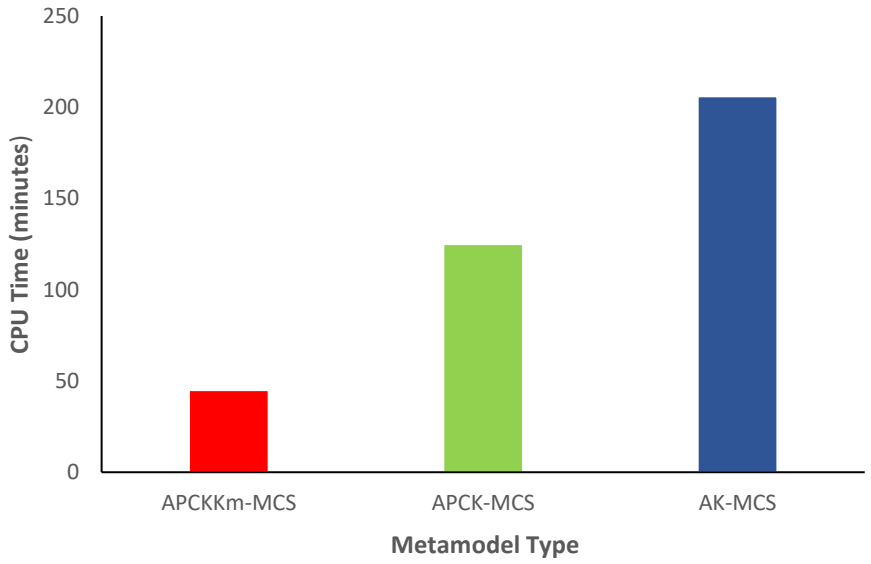

Figure 4.2. Average computational time (Ten-dimensional function).

4.3.2.2. Infinite Soil Slope Problem

This section applies the framework and procedure described in Section 4.3.2.1 to an infinite slope model (Figure 4.3), which characterizes soil slope stability subject to water infiltration (Phoon,2008). Eq. (4.20) shows the LSF for the infinite slope problem.

$$P = \frac{[\gamma(H-h)+h(\gamma_{sat}-\gamma_w)]cos\theta tan\emptyset}{[\gamma(H-h)+h\gamma_{sat}]sin\theta} - 1 \qquad (4.20)$$

The parameters γ (moist soil unit weight kNm^{-3}) and γ_{sat} (surface soil saturated unit weight kNm^{-3}); in Eq. (4.20) are obtained from Eqs. (4.21) to (4.23), respectively. The term γ_w is the unit weight of water ≈ 9.81 kNm^{-3} and $h(m)$ represents the groundwater table above bedrock.

$$\gamma = \gamma_w \frac{(G_s+0.2e)}{(1+e)} \qquad (4.21)$$

$$\gamma_{sat} = \gamma_w \frac{(G_s+e)}{(1+e)} \qquad (4.22)$$

$$U_h = \frac{h}{H} \qquad (4.23)$$

Six (6) random variables, as shown in Table 4.2, are considered for the infinite slope model.

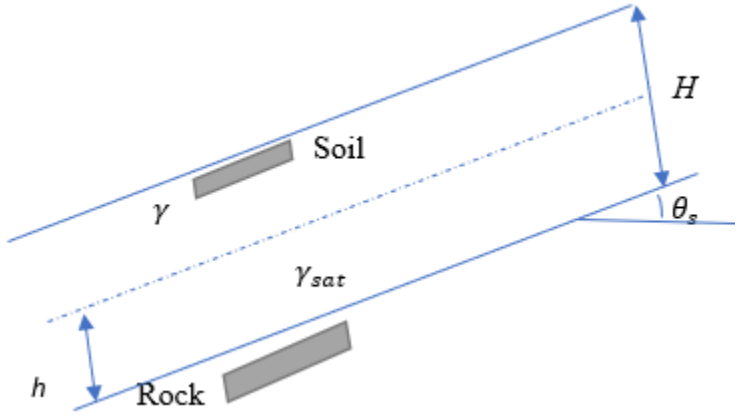

Figure 4.3. Infinite soil slope problem.

Table 4.2. Statistical parameters for the infinite slope model (Phoon,2008).

Variables	Symbols	Units	Distribution	Parameters	
Depth of soil above bedrock	H	m	Uniform	2.0	8.0
Relative height of water table	U_h	-	Uniform	0	1.0
Specific gravity of soil	G_s	-	Uniform	2.5	2.7
Void Ratio	e	-	Uniform	0.3	0.6
Slope Inclination	θ_s	radians	Lognormal	μ_{θ_s}:0.3491	σ_{θ_s}:0.0175
Effective stress frictional angle	$\emptyset$	radians	Lognormal	$\mu_{\emptyset}$:0.6109	$\sigma_{\emptyset}$:0.0489

The random variables are assumed statistically independent for simplicity of analysis. The candidate pool consists of 10^6 MCS sampling points. First, to train the APCKKm-MCS metamodel for the infinite slope problem, an initial ED containing 12 LHS sampling points and the corresponding responses are determined. Classical orthogonal polynomial related to the probability distribution of infinite slope random variables determines the polynomial basis (Eq. (4.8)). For the uniformly distributed random input variables, the Legendre polynomial is selected, and the Hermite orthogonal polynomial for other input random variables of the slope model. The LARS approach determines the appropriate polynomial truncation for the trend function, as detailed in Section 4.2. Multiple enrichment of ED for the infinite slope function is achieved using the K-means clustering approach (K=3). All stopping criteria and learning functions, as shown in Figure 4.1, are applied to the infinite slope model. The parameters of the metamodel are determined using the MLE approach (Eq. (4A.1) to (4A.4), Appendix 4A). Table 4.3 shows the results of the

reliability analysis using the proposed method. The results obtained from the reliability assessment are compared with other metamodel types of the same initial ED (Table 4.3).

Table 4.3. Reliability analysis summary (infinite slope function).

	APCKKm-MCS	APCK-MCS	AK-MCS	MCS (Reference)
P_f	5.771E-2	5.759E-2	5.641E-2	5.78E-2
N_{mod}	39	54	199	1E+6
N_{itr}	9	42	187	
ϵ_{LOO}	1.7813E-5	2.8758E-4	1.15E-2	
P_f deviation (%)	0.16	0.36	2.40	
CoV	3.70E-3	3.90E-3	4.20E-3	

Figure 4.4 shows the computational time (average) from 40 runs of the various metamodels using the same initial ED.

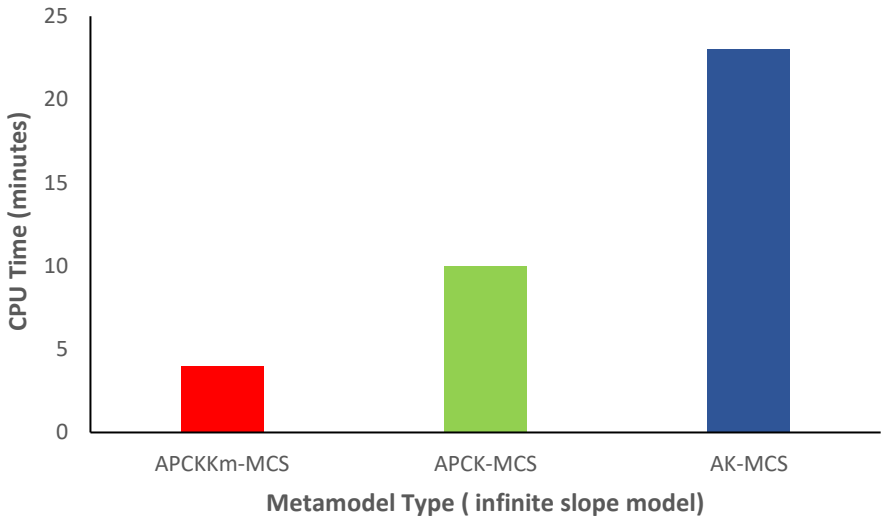

Figure 4.4. Average CPU time (Infinite slope model).

The illustrative examples show that the results obtained from the combination of PCE and Kriging (APCKKm-MCS, APCK-MCS) comparatively provide a better reliability approximation than the metamodel constructed by ordinary Kriging (AK-MCS).

4.4. Application of the Proposed Metamodel to Marine Structures

This section presents the practical engineering application of the framework described in Section 4.3 in the reliability-based design of marine structures. The proposed approach (APCKKm-MCS) is applied to a ten-bar truss structure and a marine riser (SCR).

4.4.1. Ten-Bar Truss Structure

The Truss system has practical application in various aspects of engineering. Some marine structural application includes offshore vessel guard rails, derrick structures, crane booms, jacket platforms, and truss-type jack-up leg structures.

This section considers a ten-bar truss system. The schematic diagram in Figure 4.5 shows the truss bar system.

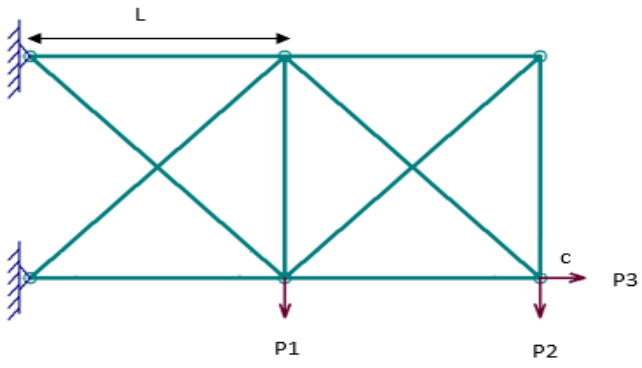

Figure 4.5. Ten-Bar Truss System.

Ten (10) random input variables are considered with statistical parameters shown in Table 4.4. The probabilistic parameters considered include the length of the bars (L), the sectional area of the truss bar (A), elastic modulus (E), and the applied point loads on the bar (P_i). The horizontal and vertical bars are assumed to be of equal length. All input variables are considered statistically independent.

Table 4.4. Parameters of truss bar input variables [modified from (Liu & Xie, 2020)].

Variables	Symbol	Unit	Distribution	Mean	CoV
Length of bar	L	m	Lognormal	1	0.05
Elastic Modulus (Horizontal)	E_H	GPa	Lognormal	100	0.05
Elastic Modulus (Vertical)	E_V	GPa	Lognormal	100	0.05
Elastic Modulus (Diagonal)	E_D	GPa	Lognormal	100	0.05
Sectional Area (Horizontal)	A_H	m^2	Gaussian	0.001	0.1
Sectional Area (Vertical)	A_V	m^2	Gaussian	0.001	0.1
Sectional Area (Diagonal)	A_D	m^2	Gaussian	0.001	0.1
Point Load	P_1	kN	Gaussian	80	0.05
Point Load	P_2	kN	Gaussian	10	0.05
Point Load	P_3	kN	Gaussian	10	0.05

The allowable vertical displacement of the ten-bar system at a given point 'c', as shown in Figure 4.5, is 0.005. Eq. (4.24) shows the implicit LSF of the truss system.

$$g(X) = 0.005 - |\Delta y| \tag{4.24}$$

The framework described in Section 4.3 is applied to the truss system. Concerning the initial ED for the truss, this paper utilizes 15 LHS points. The metamodel construction basis is the Hermite

orthogonal polynomial (with a nonlinear transformation of the lognormal distribution). The vertical displacement of the truss $|\Delta y|$; is obtained from FEA. A displacement representation of the ten-bar truss system due to applied load is shown in Figure 4.6.

The enrichment of the ED is from the candidate pool $N_{mcs}=10^6$, multiple point enrichment (K=3) is utilized from weighted K-means clusters in the pool. The determination of truss displacement for ED enrichment is achieved using the FEA approach.

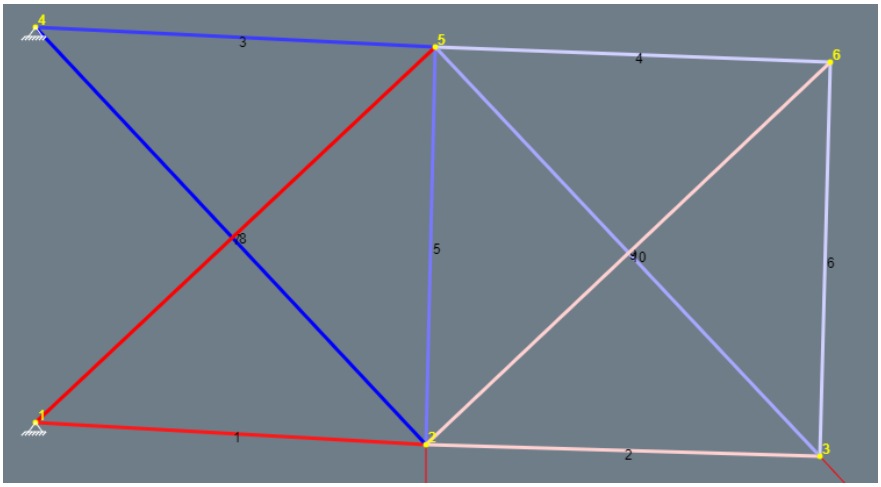

Figure 4.6. Load response FEA for the ten-bar truss.

Table 4.5 summarises the proposed method's results with the stopping criteria met.

Table 4.5. Reliability analysis summary (ten-bar truss system).

Method	P_f	N_{mod}	N_{itr}	CoV	ϵ_{LOO}	CPU Time (mins)
APCKKm-MCS	7.278E-4	39	8	0.036	1.06E-7	4
APCK-MCS	7.320E-4	39	24	0.037	5.58E-5	9
AK-MCS	6.814E-4	186	171	0.038	5.41E-3	54

Figure 4.7 shows the APCKKm-MCS reliability plot with iterative steps from the initial ED sample points while meeting the stopping criteria.

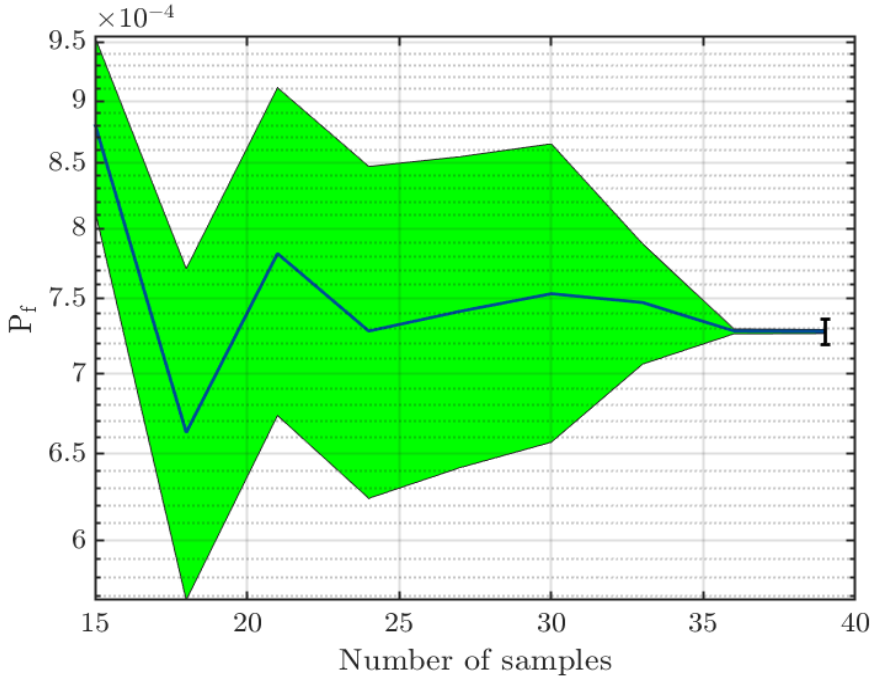

Figure 4.7. Reliability plot for ten-bar truss system.

4.4.2. SCR application of hybrid metamodel

As shown in Figure 4.8, SCR has practical application in various aspects of oil and gas activities, from product export to gas and water injection during petroleum production activities. TLP, Semi-Submersibles, Spars, and FPSO units are among the structures where SCR has been successfully applied (Bai & Bai,2005). This study considers the prevailing environmental conditions of the Flemish Pass basin. The basin has a huge potential for oil and gas exploration and is located about 400km offshore St John's, Newfoundland (Canada). Due to data availability, the study limits the environmental condition to the wave and current loads acting on the SCR during normal operating conditions.

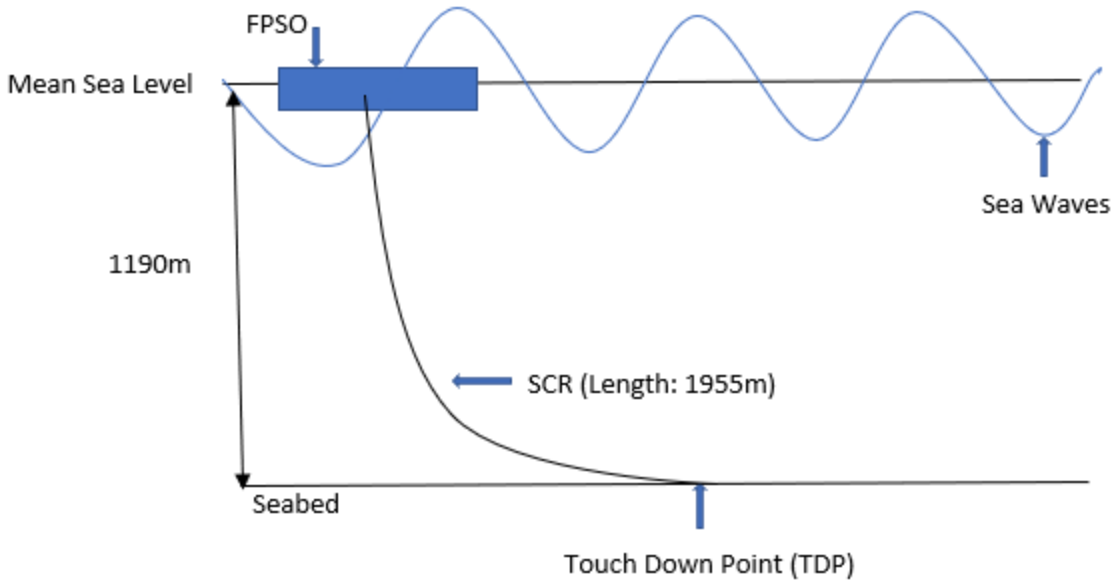

Figure 4.8. SCR configuration and dimensions.

Two essential points of the SCR are the Touch Down Point (TDP), as shown in Figure 4.8, where the SCR contacts the seabed while operating, and the SCR connection to the offshore vessel. The SCR is assumed free hanging from the flex joint and connected to an FPSO on its starboard side. The operating depth of the SCR in the basin is 1190m, and the internal transport fluid is crude oil. Table 4.6 provides more details of the SCR and FPSO for this study.

Table 4.6. SCR and FPSO parameters.

SCR and Vessel Parameters	Dimensions
Length	1955m
Diameter	0.22m
Hang-Off Angle	18.5^o
Mass of SCR	155.11kg/m
SCR Material	Steel X_{65} (API 5L), σ_y =450MPa
Internal Fluid	Medium Crude Oil (mass density: 950kg/m^3)

FPSO (Vessel)	Length: 400m, Height: 100m, Width:70m

4.4.2.1. Statistical parameters and probability distribution determination

The significant wave height (H_s), zero-crossing period (T_z) and mean surface current (V_c) represents the sea load random variables assumed to be acting on the SCR during operations in the Flemish Pass. The statistical summary of the annual environmental operating conditions, including the dominant wave and current directions (Table 4.7) for the Flemish Pass, is obtained from site-specific met ocean data (C-CORE, 2017).

The environmental data is fitted to continuous probability distributions to determine the best fit for the random variables. The MLE approach uses the minimum AIC to fit various data distributions (Table 4A.2 and Figure 4A.1, Appendix 4A). The distribution selection is based on the minimum AIC with Weibull distribution selected for H_s and V_c . For T_z , the lognormal distribution is selected, as shown in Table 4.7.

Table 4.7. Statistical summary of environmental variables (C-CORE,2017).

Variables	Distribution	Mean	CoV	Direction (Deg)
H_s (m)	Weibull	3.19	0.53	225^o
T_z (s)	Lognormal	10.21	0.18	225^o
V_c (m/s)	Weibull	0.284	0.56	180^o

4.4.2.2. SCR dependence modeling of variables

The dependence between random variables (H_s , T_z and V_c) is considered in this study and determined using a unique type of copula called the D-vine copula. The D-vine copula can handle dependence between variables by the process of decomposition (Aas et al.,2009). The vine is graphically oriented with the dependence relationships between SCR random variables in Tree 1 of the vine structure and conditional relationships in Tree 2 (Figure 4.9). For the vine structure, the non-parametric Kendall Tau (τ_k) values between the variables are essential in determining the architecture and dependence of the vine trees. Using Sklar's theorem and the minimum AIC approach (Nelsen.,2006), the copula's optimal selection is determined from bivariate copulas.

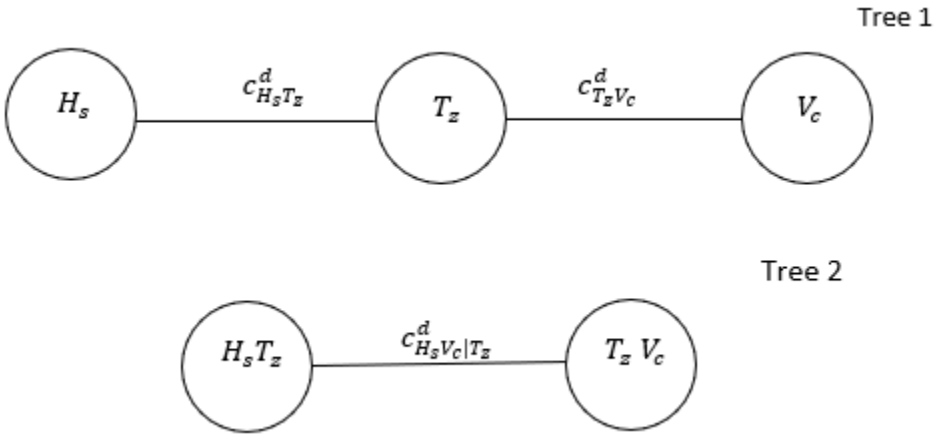

Figure 4.9. Dependence of SCR variables using D-vine copula.

The bivariate copulas considered for selection are the Gaussian, t, Clayton, Gumbel, Frank, and independent copulas (Table 4A.3, Appendix 4A). Table 4.8 shows the selected copulas based on minimum AIC values; it also shows the associated copula parameter (θ_c) and rotation (θ_R) of the vine structure using Eq. (4A.6) to (4A.8) of Appendix 4A.

Table 4.8. Dependence parameters using D-vine copula.

Tree	Copula density	Copula Type	τ_k	θ_c	θ_R (Deg)
1	$c^{d}_{H_s T_z}$	Clayton	0.0196	0.04	0
1	$c^{d}_{T_z V_c}$	Clayton	0.0240	0.05	270^o
2	$c^{d}_{H_s V_c \mid T_z}$	Independent	-	-	0

The Clayton and rotated Clayton (270^o) copulas are selected for modeling dependency between the SCR's random variables, as shown in Tree 1 of the D-vine structure (Table 4.8).

4.4.2.3. Initial ED and SCR responses

Following the determination of the optimal copulas for the SCR, the vectors of dependent random variables with continuous marginals are mapped (isoprobabilistic transform) onto independent random variables using the Rosenblatt transformations (Eqs. (4A.9) to (4A.11), Appendix 4A). Consequently, independent samples required for initial ED and metamodel construction are obtained. An initial ED, which comprises 20 LHS points of sea state data, is generated, with corresponding responses obtained through a time-domain dynamic strength analysis of the SCR using Flexcom (Wood,2019). The random sea wave characteristics are modeled using the Pierson-Moskowitz spectrum, widely used in wave analysis of structures operating in deepwater (Massel, 2018). For this demonstration, the seabed of the Flemish Pass is modeled as elastic and flat.

SCR responses considered include the maximum and minimum effective tension (T_{min}, T_{max}) and the maximum von Mises stress (S_{vms}) in operating condition.

From the SCR effective tension profile obtained for response analysis (Figure 4.10), T_{min} is observed within the seabed and touchdown zone (0-600m) of the SCR and T_{max} ; at the flex joint

region (1955m) for all ED point considered. Also, stress (S_{vms}) for the SCR is observed about the touchdown zone (400-600m).

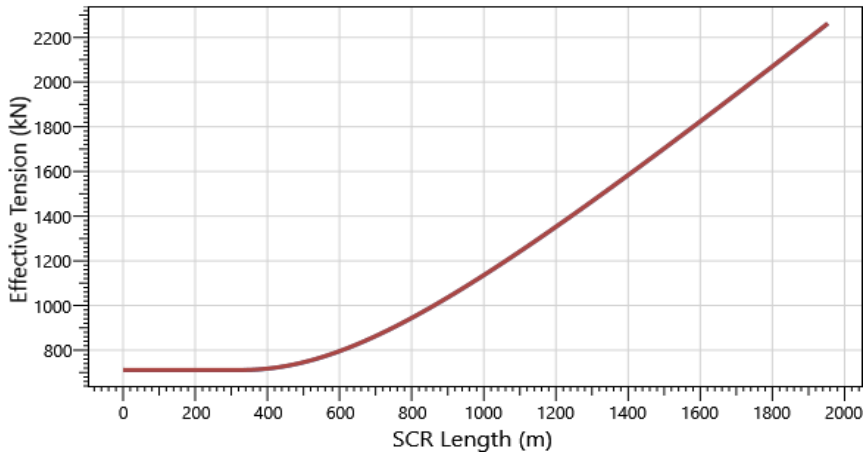

(a)

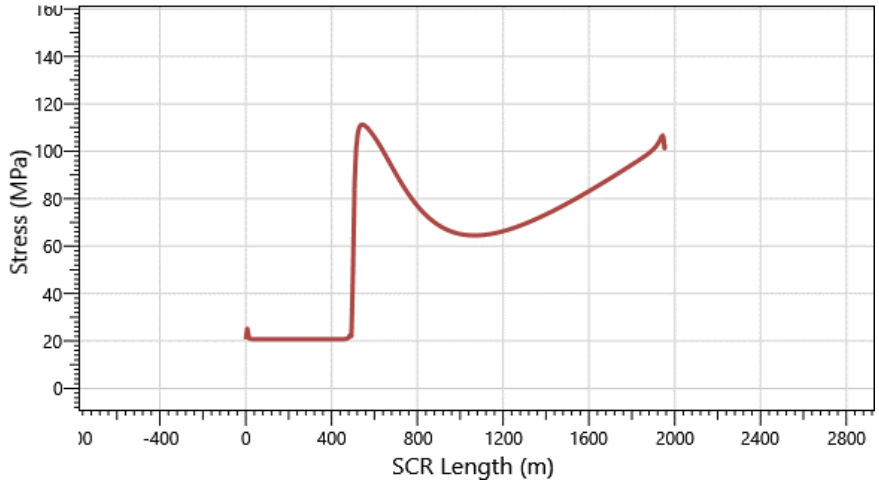

(b)

Figure 4.10. SCR tension and stress profile (a) effective tension profile (b) stress profile.

4.4.2.4. Enrichment of ED and reliability analysis

With the tension and stress responses obtained for the SCR and corresponding LHS points as detailed in Section 4.4.2.3, the APCKKm-MCS metamodel is constructed for the SCR system as described in Section 4.2 and further enriched from $N_{mcs} = 10^6$ candidate samples using the weighted K-means clustering approach (K=3). Based on the probability distribution of the random variables and an isoprobabilistic transformation, the classical Hermite orthogonal polynomial is used as the basis of the trend term.

$$g_1(H_s, T_z.V_c) = \mathrm{T_{min}} \qquad \mathrm{T_{min}} \geq 0 \tag{4.25}$$

$$g_2(H_s, T_z.V_c) = \mathrm{T_a} - \mathrm{T_{max}} \tag{4.26}$$

$$g_3(H_s, T_z.V_c) = S_a - S_{vms} \tag{4.27}$$

Eqs. (4.25) to (4.27) represents the implicit LSF of the SCR, considering effective tension and stress. The failure condition of the SCR is given by $g_i(H_s, T_z.V_c) \leq 0$ where i = 1,2,3. Failure occurs when any one of these conditions is satisfied. $\mathrm{T_{min}} \leq 0, T_{max}$ exceeds the allowable tension (T_a) or S_{vms} exceeds the allowable stress (S_a) at the given location. Consequently, this section formulates the SCR reliability assessment as a series problem. For demonstration, $\mathrm{T_a}$ for the given location is assumed to be 3500kN. Also, as described by the API standard, $\mathrm{S_a}$= $0.67\sigma_y$ for the SCR in operating conditions; with yield stress (σ_y) (API, 2013). The failure modes of the SCR are expressed as a series system (Eq. (4.28)).

$$P_{fs} = P[\cup_{i=1}^{n}\{g_i(H_s, T_z.V_c) \leq 0\}] \quad where\ n = 3 \tag{4.28}$$

$$g_{SCR}(H_s, T_z.V_c) = min\begin{Bmatrix} g_1(H_s, T_z.V_c) \\ g_2(H_s, T_z.V_c) \\ g_3(H_s, T_z.V_c) \end{Bmatrix} \tag{4.29}$$

Table 4.9 shows the enrichment of the system LSF (Eq. (4.29)) and the SCR reliability analysis results using the framework described in Section 4.2.

Table 4.9. SCR system reliability analysis summary.

Method	P_{fs}	N_{mod}	N_{itr}	CoV	ϵ_{LOO}	CPU Time (mins)
APCKKm-MCS	8.795E-2	89	23	0.0030	0.0105	12
APCK-MCS	8.771E-2	85	65	0.0032	0.0201	25
AK-MCS	8.567E-2	212	192	0.0035	0.4730	39

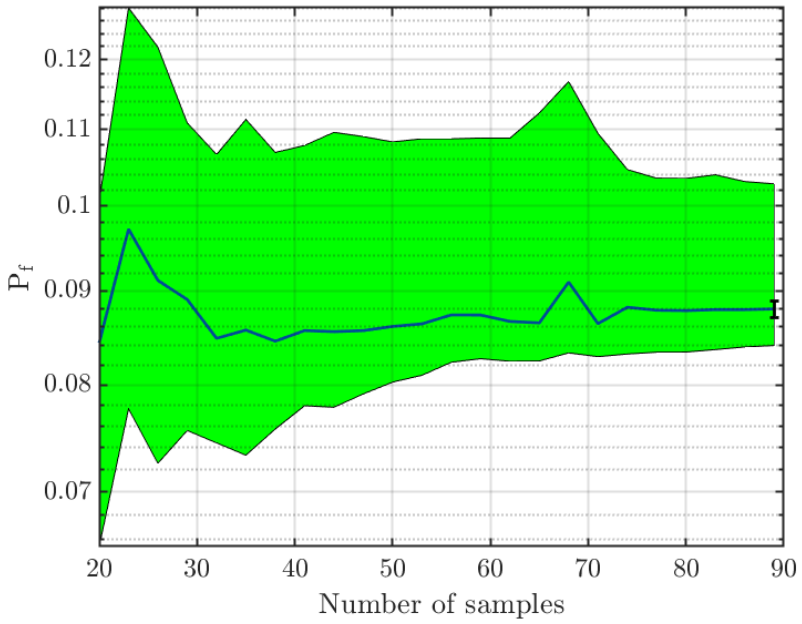

Figure 4.11. SCR reliability and convergence plot.

Figure 4.11 shows the convergence plot from the initial ED using the APCKKm-MCS approach for the SCR.

4.4.2.5. Predictive metamodel response for SCR

The predictive capacity of the constructed SCR metamodel is evaluated using fifteen (15) MCS sampling points. The results show that metamodel (APCKKm-MCS) response results are close to the FEA responses (effective tension and stress) from Flexcom.

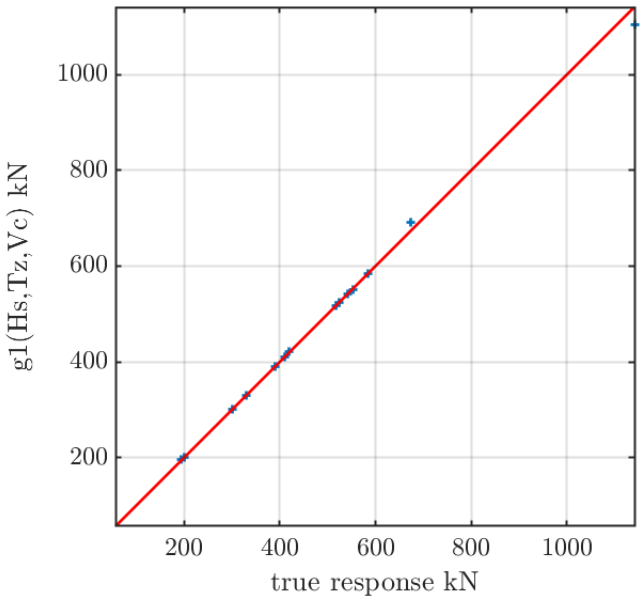

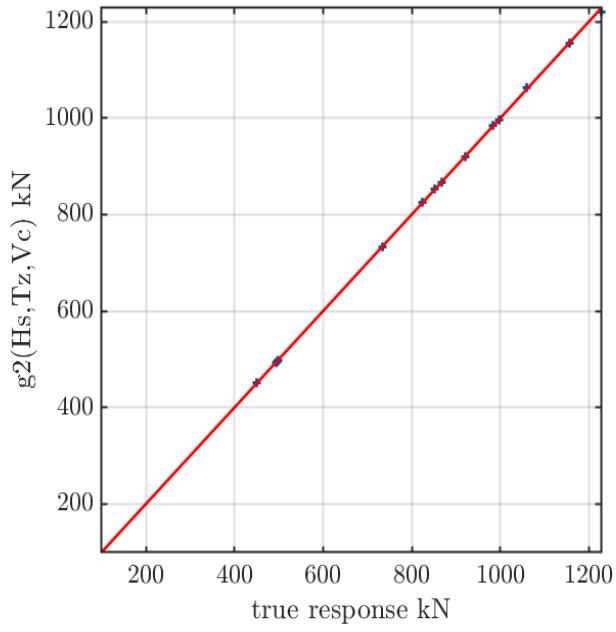

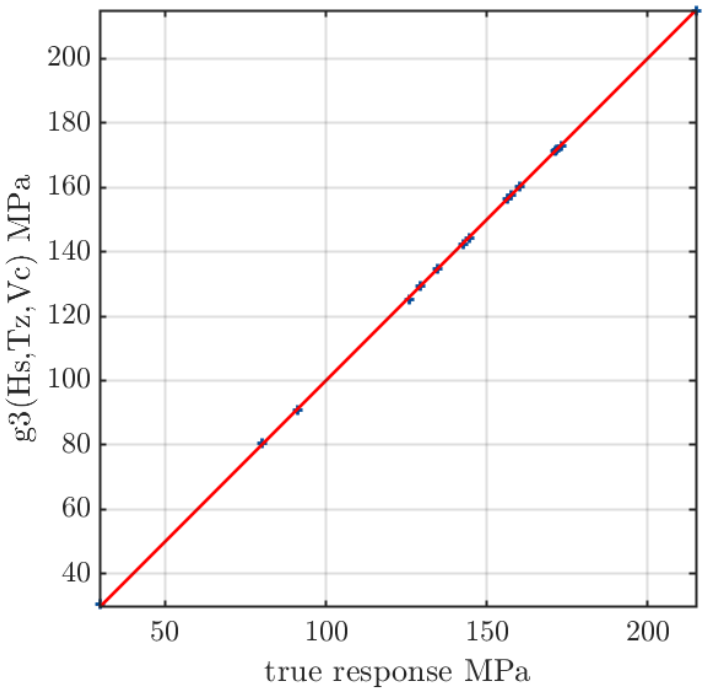

Figure 4.12. SCR tension and stress LSF responses.

The cluster of response points on a straight line (Figure 4.12) with a coefficient of determination (R^2) value of [$g_1(.)$=99.2% , $g_2(.)$=99.6% and $g_3(.)$=98.5%] proves the metamodel's effectiveness in predicting actual stress and tension on the SCR.

4.4.2.6. SCR safety compliance using the APCKKm-MCS model

For site-specific SCR safety design, reliability assessment results are compared with a target P_f . The target probability can be national, international, or facility owner's requirements. More specifically, the SCR reliability results in operating conditions using APCKKm-MCS metamodel (Table 4.9) is compared with the target (P_f) for serviceability conditions using the Det Norske

Veritas (DNV) requirement for dynamic risers (DNV,2001). Table 4A.4 (Appendix 4A) shows the SLS requirement by DNV.

From the DNV standard, the safety classes described in Table 4A.4 refer to the level of risk to humans and the environment arising from SCR failure. From the reliability results P_{fs}= 8.795E-2, as shown in Table 4.9 for the operating condition, the SCR can be classed under the normal safety class. From the code, the normal safety class considers injury to humans and the impact on the environment in the event of SCR failure.

4.4.3. Discussion of results

From the reliability assessment of the benchmark functions, it is evident that the deviation of the P_f from the MCS reference is relatively smaller for the hybrid metamodels compared to the conventional AK-MCS. With the APCKKm-MCS method, a deviation of 0.11% for the Ten-dimensional function (Table 4.1) and 0.16% for the infinite slope problem (Table 4.2) is observed. Conversely, the AK-MCS approach produces the highest deviation, with 3.25% for the Ten-dimensional function (Table 4.1) and 2.40% for the infinite slope problem (Table 4.2).

For the truss and SCR with implicit LSF, the comparative study of various metamodels (Table 4.5 and 4.9) reveals that the APCKKm-MCS approach provides the same accuracy level as the conventional AK-MCS and the APCK-MCS method.

The computational time reduces considerably using the proposed method compared to other metamodels described. For the benchmark functions, the average CPU time is 45mins and 4 mins for the Ten-dimensional function (Figure 4.2) and infinite slope problem (Figure 4.4), respectively. Also, time reduction is observed for the truss bar (Table 4.5) and the SCR (Table 4.9). The multiple enrichment using K-means clustering and rapid convergence from the combination of the Kriging

and PCE approach reduces the number of computational iterations (N_{itr}) during reliability assessment.

The APCKKm-MCS metamodel provides a high predictive capacity, given input data of random variables. From the SCR study, responses evaluated using this approach are close to those obtained from FEA, as evident in the alignment of plot points on a straight line for SCR tension and stress responses (Figure 4.12). Consequently, obtaining a computationally cheap and efficient method for response determination using the proposed framework.

The global error (ϵ_{LOO}) as determined by the cross-validation approach for the truss bar (ϵ_{LOO}=1.06E-7) as seen in Table 4.5 and the SCR (ϵ_{LOO}=1.05E-2) from Table 4.9 reveals a high quality of the constructed metamodel, making it suitable for response determination and reliability analysis of complex structures.

Regarding the DNV marine riser requirement (as detailed in Section 4.4.2.6), an upgrade in the SCR safety class to ensure improved reliability during normal operating conditions can be achieved by an RBDO scheme for its design parameters. This RBDO approach provides a trade-off between the design parameters requirements of the SCR and achieving a high safety class ($P_f = 10^{-2} - 10^{-3}$). According to the DNV requirement, a high safety class (Table A4.4, Appendix 4A) will imply a design to reduce the high risk of human injury and significant environmental pollution from system failure. The benefit of this is an improved SCR design with optimal parameters (length, diameter, material, thickness) while still achieving a high level of safety compliance requirement for the riser under serviceability conditions. Generally, the reliability results help evaluate marine structures' compliance with site-specific safety standards or regulations.

For demonstration purposes, this paper limits the multiple enrichment of ED to three clusters (K=3) only. Also, the SCR utilizes three random variables for reliability assessment due to the unavailability of data for other site-specific ocean parameters affecting the riser. Research into a robust metamodel construction for the SCR can be considered with data available for other ocean parameters. In this study, active learning is limited to the U learning function; other learning schemes for ED enrichment for the proposed metamodel can be explored in future research.

4.5. Conclusions

This study proposes an active learning hybrid metamodel framework (APCKKm-MCS) with multiple-point enrichment of ED for the reliability assessment of marine structures. The metamodel is constructed as a combination of PCE and Kriging models, considering their respective advantages and uniqueness. The learning and enrichment of ED are achieved using the U learning function and the K-means clustering approach, respectively. The framework is demonstrated on benchmark functions and practical marine structural problems (Truss Bars and SCR).

Comparing its performance with the commonly used active learning ordinary Kriging metamodel (AK-MCS) and a single point enrichment hybrid model (APCK-MCS), the study concludes as follows.

1. As demonstrated, the APCKKm-MCS approach handles a diverse range of reliability problems. It includes high dimensional functions, nonlinear functions, and marine structural problems with implicit LSF. The proposed method produces reliable results, allows fewer computational model evaluations, reduces the computational burden using FEA, and converges fast (minimal iterations) to the reference or actual P_f.

2. A more robust and highly efficient approach that combines state-of-the-art Kriging and PCE metamodeling methods that take advantage of their capabilities is achieved.
3. Taking a step ahead with the framework presented to consider multiple ED enrichment using the K-means clustering approach with MCS candidate sample points reduces the computational time for reliability analysis, as evident in the benchmark examples and marine structural problems.
4. APCKKm-MCS approach also showed a high predictive capacity with limited data (Figure 4.12), making it suitable for efficient response determination for marine structures.
5. The relatively low model error ϵ_{LOO}, evident in the truss bar and SCR cases, provides a high level of confidence for the model constructed using APCKKm-MCS.

The proposed framework (APCKKm-MCS) offers the possibility of applying a combination of metamodels with efficient reliability techniques such as variance reduction methods or subset simulation for reliability-based assessment of marine structures with small failure probability ($<10^{-5}$). Consequently, further research into the performance of multiple-enrichment active learning PCK using subset simulation methods or variance reduction techniques for the reliability of complex marine structures is necessary. Furthermore, its application to a marine riser (SCR) and truss system confirms the suitability of the methodology presented in this study for the reliability of different types of ocean structures.

Also, research into optimal cluster size determination for ED enrichment of high-dimensional structural problems is necessary. Finally, applying the proposed framework to the RBDO of marine systems will be essential.

Acknowledgment

The authors thankfully acknowledge the financial support provided by the Natural Sciences and Engineering Research Council of Canada (NSERC) through Discovery Grant and the Canada Research Chair (Tier I) Program in Offshore Safety and Risk Engineering.

Appendix 4A

Kriging Parameters MLE approach

$$\mathcal{L}(\beta, \sigma^2, \theta, y) = \frac{(detR)^{-\frac{1}{2}}}{(2\pi\sigma^2)^{\frac{N}{2}}} \exp\left[-\frac{1}{2\sigma^2}(y - F\beta)^T R^{-1}(y - F\beta)\right] \quad (4A.1)$$

$$\beta(\theta) = (F^T R^{-1} F)^{-1} F^T R^{-1} y \quad (4A.2)$$

$$\sigma_g^2(\theta) = \frac{1}{N}(y - F\beta)^T R^{-1}(y - F\beta) \quad (4A.3)$$

$$\hat{\theta}_{MLE} = arg \min_{\theta \epsilon D_\theta} \frac{1}{2}[Log(detR) + NLog(2\pi\sigma^2) + N] \quad (4A.4)$$

F and R represent the regression and correlation matrix, respectively

PCE Orthogonal Polynomials

$$< P_j^{(i)}, P_K^{(i)} > = \int_{D_i} {P_j}^{(i)}(x) {P_k}^{(i)}(x) f_{x_i}(x) dx = \delta_{jk} \quad (4A.5)$$

$$if\ j \neq k\ then\ \delta_{jk} = 0, if\ j = k\ then\ \delta_{jk} = 1$$

Where $P_j^{(i)}\ and\ P_k^{(i)}$ are candidate polynomials of the i^{th} variable. Also, $f_{x_i}(x)$ is the PDF of the i^{th} variable.

Table 4A.1. Classical Orthogonal Polynomials (Xiu & Em Karniadakis, 2003).

Distribution Type	Orthogonal Polynomial		Basis $\Psi_k(x)$
Uniform	Legendre	$P_k(x)$	$\frac{P_k(x)}{\sqrt{\frac{1}{2k+1}}}$
Gaussian	Hermite	$H_{e_k}(x)$	$\frac{H_{e_k}(x)}{\sqrt{k!}}$
Gamma	Laguerre	$L_k^a(x)$	$\frac{L_k^a(x)}{\sqrt{\frac{\Gamma(k+a+1)}{k!}}}$
Beta	Jacobi	$J_k^{a,b}(x)$	$\frac{J_k^{a,b}(x)}{I_{a,b,k}}$

Where $I_{a,b,k}^2 = \frac{2^{a+b+1}}{2k+a+b+1}\frac{\Gamma(k+a+1)\Gamma(k+b+1)}{\Gamma(k+a+b+1)\Gamma(k+1)}$

Table 4A.2. Minimum AIC values for variables H_s , T_z and V_c.

Probability Distribution	H_s(m)	T_z(s)	V_c(m/s)
	AIC	AIC	AIC
Gaussian	11300.08	11714.27	-2405.40
Lognormal	11495.82	11610.45	-2354.80
Exponential	12616.08	19386.39	-1569.61
Logistic	11330.69	11742.88	-2409.65
Weibull	10975.31	12013.79	-2855.03
Gamma	11063.35	11615.62	-2783.35

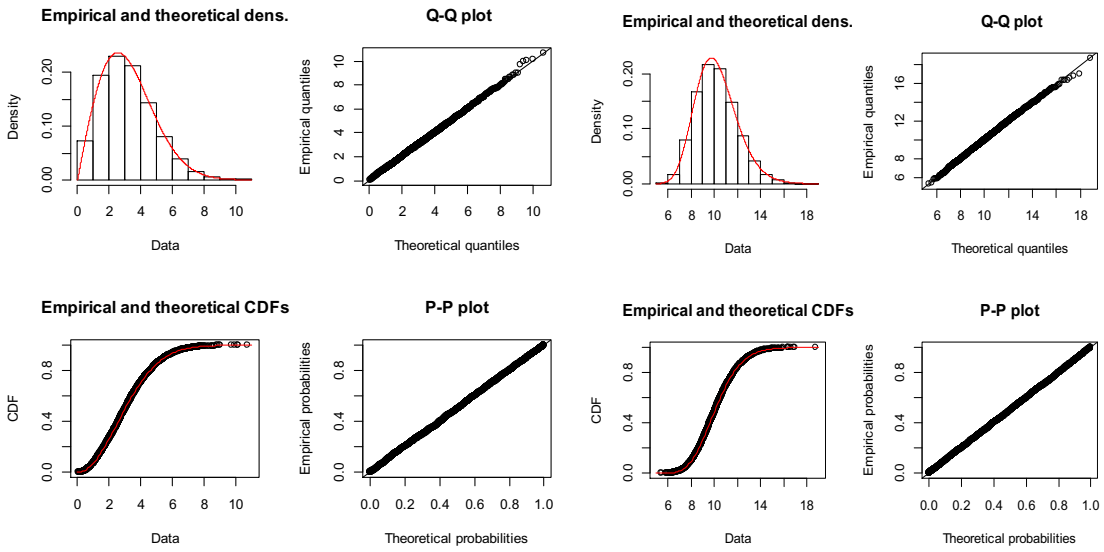

(a) Weibull fit H_s(m)

(b) Lognormal fit T_z (s)

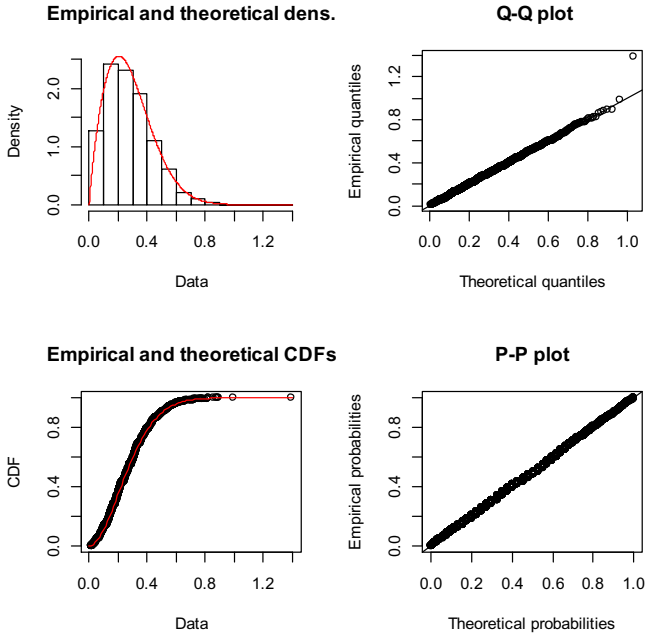

(c) Weibull fit V_c (m/s)

Figure 4A.1. Probability distribution fit for ocean variables H_s , T_z *and* V_c.

Vine Copula Expressions

$f(x_1 \ldots . x_n)$

$$= \prod_{k=1}^{n} f(x_k) \prod_{j=1}^{n-1} \prod_{i=1}^{n-j} c_{i,i+j|i+1\ldots i+j-1} \left\{F\left(x_i | x_{i+1} \ldots \ldots, x_{i+j-1}\right), F\left(x_{i+j} | x_{i+1} \ldots \ldots, x_{i+j-1}\right)\right\} \quad (4A.6)$$

$$InL(\theta_c) = \prod_{i=1}^{n} c(u_1 \ldots u_n; \theta_c) = \sum_{i=1}^{n} Inc(u_1 \ldots u_n; \theta_c) \quad (4A.7)$$

$$AIC = -2InL(\theta_c) + 2K \quad (4A.8)$$

In Eq. (4A.6), *j* represents the trees of the D-vine, and *i* represents the edges within each tree of the vine copula

$L(\theta_c)$ is the Loglikelihood function, K: the number of model parameters, $u_1 \ldots u_n \in [0,1]$, c represents the copula density function. *F(.)* represent the variable Cumulative Density Function (CDF) and $f(x_k)$*;* the variable PDF.

Table 4A.3. Bivariate Copula Functions.

Copula Type	Copula Function	Lower Tail Dependence (λ_L)	Upper Tail Dependence (λ_U)	Copula Parameter Range (θ_c)
Clayton	$(u_1^{-\theta_c} + u_2^{-\theta_c})^{-\frac{1}{\theta_c}}$	$2^{-\frac{1}{\theta_c}}$	0	(0,∞)
Gumbel	Exp {-$[(-Inu_1)^{\theta_c} + (-Inu_1)^{\theta_c}]^{\frac{1}{\theta_c}}$}	0	$2 - 2^{-\frac{1}{\theta_c}}$	(1,∞)
Frank	$-\frac{1}{\theta_c}\text{In}(1+\frac{(e^{-\theta_c u_1}-1)(e^{-\theta_c u_2}-1)}{(e^{-\theta_c}-1)})$	0	0	(−∞,∞)
Gaussian	$\boldsymbol{\phi}(\Phi^{-1}(u_1), \Phi^{-1}(u_1)\|\theta_c)$	0	0	(-1,1)

Student t	$t_{\theta_c,v*}(t_v^{-1}(u_1), t_v^{-1}(u_1)\|\theta_c)$	$t_{v+1}(-\sqrt{v+1})\sqrt{\frac{1-\theta_c}{1+\theta_c}}$	$2t_{v+1}(-\sqrt{(v+1)}\sqrt{\frac{1-\theta_c}{1+\theta_c}})$	(-1,1)

v $*$ is a parameter of the t copula.

Rosenblatt Transformation

X in the random vector $X = (X_1, \ldots \ldots X_n)$ with marginal distribution $F(x_i)$ and conditional distribution $F(x_i|x_1, x_{2\ldots\ldots\ldots,}x_{i-1})$. The Rosenblatt transform is given as $Z_i = T(X_i)$ (independent and uniformly distributed $[0,1]^n$) (Aas et al., 2009)

$$\left\{\begin{array}{c} T(X_1) = F(x_1) \\ T(X_2) = F(x_2|x_1) \\ T(X_3) = F(x_3|x_1, x_2) \\ . \\ . \\ T(X_n) = F\left(x_n|x_1, x_{2\ldots\ldots\ldots,}x_{n-1}\right) \end{array}\right\} \quad (4A.9)$$

$$X \to U{\sim}C_X\,,\; U \to Z{:}\; Z_i = C_{x_i|x_{1\ldots\ldots\ldots,}x_{i-1}}(u_i|u_{1\ldots\ldots\ldots,}u_{i-1}) \quad (4A.10)$$

Inverse Rosenblatt Transform

$$X_i = F^{-1}{}_{x_i|x_{1\ldots\ldots\ldots,}x_{i-1}}\left(u_i|u_{1,\ldots\ldots}u_{i-1}\right) = C^{-1}{}_{x_i|x_{1\ldots\ldots\ldots,}x_{i-1}}(u_i|u_{1\ldots\ldots\ldots,}u_{i-1}) \quad (4A.11)$$

Where $C_{x_i|x_{1\ldots\ldots\ldots,}x_{i-1}}(u_i|u_{1\ldots\ldots\ldots,}u_{i-1})$ is the conditional copula of X and $C^{-1}{}_{x_i|x_{1\ldots\ldots\ldots,}x_{i-1}}(u_i|u_{1\ldots\ldots\ldots,}u_{i-1})$ the conditional quantile function.

Table A4.4. Target failure probability (DNV,2001).

Limit State	Probability Basis	Safety Class		
		Low	Normal	High
Serviceability	Annual per riser	10^{-1}	10^{-1}-10^{-2}	10^{-2}-10^{-3}
Ultimate	Annual per riser	10^{-3}	10^{-4}	10^{-5}
Fatigue	Annual per riser	10^{-3}	10^{-4}	10^{-5}

References

Aas, K., Czado, C., Frigessi, A., & Bakken, H. (2009). Pair-copula constructions of multiple dependence. *Insurance: Mathematics and Economics*, *44*(2), 182–198. https://doi.org/10.1016/j.insmatheco.2007.02.001

Abdalla, N., Banerjee, S., Ramachandran, G., Stenzel, M., & Stewart, P. A. (2018). Coastline kriging: A Bayesian approach. *Annals of Work Exposures and Health*, *62*(7), 818–827. https://doi.org/10.1093/annweh/wxy058

Ang, G. L., Ang, A. H. -S., & Tang, W. H. (1992). Optimal Importance-Sampling Density Estimator. *Journal of Engineering Mechanics*, *118*(6), 1146–1163. https://doi.org/10.1061/(asce)0733-9399(1992)118:6(1146)

American Petroleum Institution [API]. (2013). "*Dynamic Risers for Floating Production Systems. API Standard 2RD*". Second Ed. API Publishing Services, Washington, DC

Au, S. K., & Beck, J. L. (2001). Estimation of small failure probabilities in high dimensions by subset simulation. *Probabilistic Engineering Mechanics*, *16*(4), 263–277. https://doi.org/10.1016/S0266-8920(01)00019-4

Bahmyari, E., Khedmati, M. R., & Soares, C. G. (2017). Stochastic analysis of moderately thick plates using the generalized polynomial chaos and element free Galerkin method. *Engineering Analysis with Boundary Elements*, *79*, 23–37. https://doi.org/10.1016/j.enganabound.2017.03.001

Bai, Y., & Bai, Q. (2005). Subsea Pipelines and Risers, Elsevier Ocean Engineering Book Series, Elsevier, Amsterdam. Doi:10.1016/B978-008044566-3/50042-7.

Bai, Y., & Jin, W. L. (2016). *Marine structural design* (Second). Elsevier Ltd.

Bastidas-Arteaga, E., El Soueidy, C. P., Amiri, O., & Nguyen, P. T. (2020). Polynomial chaos expansion for lifetime assessment and sensitivity analysis of reinforced concrete structures subjected to chloride ingress and climate change. *Structural Concrete*, *21*(4), 1396–1407. https://doi.org/10.1002/suco.201900398

Bian, X., Li, X., Qi, P., Chi, Z., Ye, R., Lu, S., & Cai, Y. (2019). Quantitative design and analysis of marine environmental monitoring networks in coastal waters of China. *Marine Pollution Bulletin*, *143*, 144–151. https://doi.org/10.1016/j.marpolbul.2019.04.052

Bichon, B. J., Eldred, M. S., Swiler, L. P., Mahadevan, S., & McFarland, J. M. (2008). Efficient global reliability analysis for nonlinear implicit performance functions. *AIAA Journal*, *46*(10), 2459–2468. https://doi.org/10.2514/1.34321

Blatman, G., & Sudret, B. (2011). Adaptive sparse polynomial chaos expansion based on least angle regression. *Journal of Computational Physics*, *230*(6), 2345–2367. https://doi.org/10.1016/j.jcp.2010.12.021

Brandt, S., Broggi, M., Hafele, J., Guillermo Gebhardt, C., Rolfes, R., & Beer, M. (2017). Meta-models for fatigue damage estimation of offshore wind turbines jacket substructures. *Procedia Engineering*, *199*, 1158–1163. https://doi.org/10.1016/j.proeng.2017.09.292

C-CORE. (2017). Offshore Newfoundland and Labrador Met Ocean Study: Detailed Analysis Basis Vol 1&2. St. John's.

Charlton, T. S., & Rouainia, M. (2019). Uncertainty quantification of offshore anchoring systems in spatially variable soil using sparse polynomial chaos expansions. *International Journal for Numerical Methods in Engineering*, *120*(6), 748–767. https://doi.org/10.1002/nme.6155

Chen, J., Yan, J., Yue, Q., & Tang, M. (2016). Flexible riser configuration design for extremely shallow water with surrogate-model- based optimization. *Journal of Offshore Mechanics and Arctic Engineering*, *138*(4), 1–7. https://doi.org/10.1115/1.4033491

Cheng, K., & Lu, Z. (2020). Structural reliability analysis based on ensemble learning of surrogate models. *Structural Safety*, *83*, 101905. https://doi.org/10.1016/j.strusafe.2019.101905

Chi, Y., Li, B., Yang, X., Wang, T., Yang, K., & Gao, Y. (2017). Research on the statistical characteristics of crosstalk in naval ships wiring harness based on polynomial chaos expansion method. *Polish Maritime Research*, *24*(s2), 205–214. https://doi.org/10.1515/pomr-2017-0084

DNV. (2001)."Offshore Standard DNV-OS-F201 dynamic risers". Det Norske Veritas.

Echard, B., Gayton, N., & Lemaire, M. (2011). AK-MCS: An active learning reliability method combining Kriging and Monte Carlo Simulation. *Structural Safety*, *33*(2), 145–154. https://doi.org/10.1016/j.strusafe.2011.01.002

Fajraoui, N., Marelli, S., & Sudret, B. (2017). On optimal experimental designs for Sparse Polynomial Chaos Expansions. *ArXiv*.

Forrester, A., Sobester, A., & Keane, A. (2008). *Engineering design via surrogate modelling: a practical guide.* Wiley.

Gaspar, B., Teixeira, A. P., & Soares, C. G. (2014). Assessment of the efficiency of Kriging surrogate models for structural reliability analysis. *Probabilistic Engineering Mechanics*, *37*, 24–34. https://doi.org/10.1016/j.probengmech.2014.03.011

Ghanem, R. G., & Spanos, P. D. (1997). Spectral techniques for stochastic finite elements. *Archives of Computational Methods in Engineering*, *4*(1), 63–100. https://doi.org/10.1007/BF02818931

Hill, N., Henry, M. J., & Potts, A. E. (2016). A Novel Method for Predicting the Motion of Moored Floating Bodies. *Proceedings of the ASME 2016 35th International Conference on Ocean, Offshore and Arctic Engineering OMAE2016, June 19-24, 2016, Busan, South Korea*, 1–9.

Hu, J., Chen, S., Behrangi, A., & Yuan, H. (2019). Parametric uncertainty assessment in hydrological modeling using the generalized polynomial chaos expansion. *Journal of Hydrology*, *57*, 124158. https://doi.org/10.1016/j.jhydrol.2019.124158

Jones, D. R., Schonlau, M., & Welch, W. J. (1998). Efficient Global Optimization of Expensive Black-Box Functions. *Journal of Global Optimization*, *13*, 455–492.

Lataniotis, C., Wicaksono, D., Marelli, S., & Sudret, B. (2019). *UQLab user manual – Kriging (Gaussian process modelling) Report # UQLab-V1.3-105.Chair of Risk, Safety and Uncertainty Quantification, ETH Zurich, Switzerland.*

Lebrun, R., & Dutfoy, A. (2009). A generalization of the Nataf transformation to distributions with elliptical copula. *Probabilistic Engineering Mechanics*, *24*(2), 172–178. https://doi.org/10.1016/j.probengmech.2008.05.001

Leifsson, L., Du, X., & Koziel, S. (2020). Efficient yield estimation of multiband patch antennas by polynomial chaos-based Kriging. *International Journal of Numerical Modelling: Electronic Networks, Devices and Fields*, *33*(6), 1–10. https://doi.org/10.1002/jnm.2722

Li, L., Jiang, Z., Ong, M. C., & Hu, W. (2019). Design optimization of mooring system: An application to a vessel-shaped offshore fish farm. *Engineering Structures*, *197*, 109363. https://doi.org/10.1016/j.engstruct.2019.109363

Lim, H. U., Manuel, L., & Low, Y. M. (2018). On efficient long-term extreme response estimation for a moored floating structure. *Proceedings of the International Conference on Offshore Mechanics and Arctic Engineering - OMAE*, *3*, 1–7. https://doi.org/10.1115/OMAE2018-78763

Liu, B., & Xie, L. (2020). An improved structural reliability analysis method based on local approximation and parallelization. *Mathematics*, *8*(2), 1–13. https://doi.org/10.3390/math8020209

Lv, Z., Lu, Z., & Wang, P. (2015). A new learning function for Kriging and its applications to solve reliability problems in engineering. *Computers and Mathematics with Applications*, *70*(5), 1182–1197. https://doi.org/10.1016/j.camwa.2015.07.004

Marelli, S., & Sudret, B. (2014). UQLab: A framework for uncertainty quantification in Matlab. *2nd Int. Conf. on Vulnerability, Risk Analysis and Management (ICVRAM2014)*.

Marelli, S., & Sudret, B. (2019). *UQLab user manual – Polynomial chaos expansions, Report # UQLab-V1.3-104, Chair of Risk, Safety and Uncertainty Quantification, ETH Zurich, Switzerland.*

Massel, S. R. (2018). *Ocean Surface Waves: Their Physics and Prediction. Advanced Series on Ocean Engineering* (P. L.-F. Liu (ed.); Third). World Scientific Publishing Co. Pte. Ltd.

Melchers, R., & Beck, A. T. (2018). Structural Reliability — Analysis and Prediction. In *Structural Safety* (Third). https://doi.org/10.1016/s0167-4730(01)00007-8

Morató, A., Sriramula, S., & Krishnan, N. (2019). Kriging models for aero-elastic simulations and reliability analysis of offshore wind turbine support structures. *Ships and Offshore Structures*, *14*(6), 545–558. https://doi.org/10.1080/17445302.2018.1522738

Nelsen, R. B. (2006). *An Introduction to Copulas: Lecture Note in Statistics*. Springer US. https://doi.org/https://doi.org/10.1007/0-387-28678-0_1

Nguyen, P. T. T., Manuel, L., & Coe, R. G. (2019). On the Development of an Efficient Surrogate Model for Predicting Long-Term Extreme Loads on a Wave Energy Converter. *Journal of Offshore Mechanics and Arctic Engineering*, *141*(6), 1–11. https://doi.org/10.1115/1.4042944

Ni, P., Li, J., Hao, H., & Xia, Y. (2018). Stochastic dynamic analysis of marine risers considering Gaussian system uncertainties. *Journal of Sound and Vibration*, *416*, 224–243. https://doi.org/10.1016/j.jsv.2017.11.049

Phoon, K-K. (2008). "Numerical recipes for reliability analysis – a primer," in *Reliability-based Design in Geotechnical Engineering: Computations and Applications*, K.-K Phoon, Ed. London: CRC Press, pp. 34–35.

Pradlwarter, H. J., Schuëller, G. I., Koutsourelakis, P. S., & Charmpis, D. C. (2007). Application of line sampling simulation method to reliability benchmark problems. *Structural Safety*, *29*(3), 208–221. https://doi.org/10.1016/j.strusafe.2006.07.009

Santner, T., Williams, B., & Notz, W. (2003). The design and analysis of computer experiments. Springer series in Statistics. Springer.

Schöbi, R., Sudret, B., & Wiart, J. (2015). Polynomial-chaos-based Kriging. *International Journal for Uncertainty Quantification*, *5*(2), 171–193. https://doi.org/10.1615/Int.J.UncertaintyQuantification.2015012467

Shi, X., Palos Teixeira, Â., Zhang, J., & Guedes Soares, C. (2015). Kriging response surface reliability analysis of a ship-stiffened plate with initial imperfections. *Structure and Infrastructure Engineering*, *11*(11), 1450–1465. https://doi.org/10.1080/15732479.2014.976575

Sudret, B., & Der Kiureghian, A. (2002). Comparison of finite element reliability methods. *Probabilistic Engineering Mechanics*, *17*(4), 337–348. https://doi.org/10.1016/S0266-8920(02)00031-0

Sun, Z., Wang, J., Li, R., & Tong, C. (2017). LIF: A new Kriging based learning function and its application to structural reliability analysis. *Reliability Engineering and System Safety*, *157*, 152–165. https://doi.org/10.1016/j.ress.2016.09.003

Teixeira, A. P., & Soares, C. G. (2018). Adaptive methods for reliability analysis of marine structures. *Proceedings of the International Conference on Offshore Mechanics and Arctic Engineering - OMAE*, *11B*, 1–10. https://doi.org/10.1115/OMAE2018-77311

Teixeira, R., Nogal, M., O'Connor, A., Nichols, J., & Dumas, A. (2019). Stress-cycle fatigue design with Kriging applied to offshore wind turbines. *International Journal of Fatigue*, *125*, 454–467. https://doi.org/10.1016/j.ijfatigue.2019.04.012

Wang, Y., Gao, T., Pang, Y., & Tang, Y. (2019). Investigation and optimization of appendage influence on the hydrodynamic performance of AUVs. *Journal of Marine Science and Technology (Japan)*, *24*(1), 297–305. https://doi.org/10.1007/s00773-018-0558-y

Weinmeister, J., Gao, X., & Roy, S. (2019). Analysis of a polynomial chaos-kriging metamodel for uncertainty quantification in aerodynamics. *AIAA Journal*, *57*(6), 2280–2296. https://doi.org/10.2514/1.J057527

Wood. (2019). Flexcom (Version 8.10.4) [Computer software]. Wood Group Kenny Ireland Limited, Technology Park, Parkmore, Galway, Ireland.

Xiu, D., & Em Karniadakis, G. (2003). The Wiener-Askey polynomial chaos for stochastic differential equations. *SIAM Journal on Scientific Computing*, *24*(2), 619–644. https://doi.org/10.1137/S1064827501387826

Xu, S., Guedes Soares, C., & Teixeira, A. P. (2018). Reliability Analysis of Short Term Mooring Tension of a Semisubmersible System. *Proceedings of the ASME 2018 37th International Conference on Ocean, Offshore and Arctic Engineering OMAE2018*.

Zaki, M. J. & Meira, W. J. (2014). Data Mining and Analysis: Fundamental Concepts and Algorithms. Cambridge University Press.

Zhang, Y., Duan, M., Kong, X., Sun, T., & Yang, F. (2018). Study of Drillability Evaluation in Deep Formations Using the Kriging Interpolation Method. *Chemistry and Technology of Fuels and Oils*, *54*(3), 382–385. https://doi.org/10.1007/s10553-018-0936-5

Zhang, Z., Ma, X., Yu, H., & Hua, H. (2021). Stochastic dynamics and sensitivity analysis of a multistage marine shafting system with uncertainties. *Ocean Engineering*, *219*, 108388. https://doi.org/10.1016/j.oceaneng.2020.108388

Zhao, Y. G., & Ono, T. (1999). A general procedure for first/second-order reliability method (FORM/SORM). *Structural Safety*, *21*(2), 95–112. https://doi.org/10.1016/S0167-4730(99)00008-9

Chapter 5

A methodology for time-varying resilience quantification of an offshore natural gas pipeline

Preface

A version of this chapter has been published in the ***Journal of Pipeline Science and Engineering 2022; 2:100054.*** *I am the primary author that produced this work, along with Co-authors Faisal Khan and Salim Ahmed. I reviewed the relevant literature and developed the concept of structural resilience quantification for offshore natural gas pipelines. I prepared the original manuscript, carried out formal analysis and software implementation, reviewed and revised the manuscript following the co-authors' feedback and peer review from the journal. Co-author Faisal Khan assisted in the concept development and methodology refinement, supervision, funding for the work, reviewing, and editing of the manuscript. Co-author Salim Ahmed assisted in concept development and methodology, research supervision, reviewing, and manuscript editing.*

Abstract

Many resilience definitions and metrics have been presented across various disciplines in recent times. However, from a design and operations perspective, a limited effort is focused on quantifying the resilience of oil and gas support structures. This study proposes a methodology for structural resilience quantification of an offshore hydrocarbon pipeline. Resilience is modeled as a function of the structure's time-dependent reliability, adaptability, and maintainability. The proposed model is demonstrated on an internally corroded offshore natural gas pipeline segment with multiple initial defects; and considers disruptive events arising from the leak, burst, and rupture failure modes. The resilience index and sensitivity analysis are evaluated for the offshore pipeline. The pipeline sensitivity analysis indicates the apparent effect of pipe wall thickness and

defect depth growth rate on resilience over its design life. The outcome of this study provides insight into the resilience quantification of structural systems considering multiple disruptive events. The proposed model is expected to serve as an essential tool for resilience evaluation during the design and operations of oil and gas structures.

Keywords: Resilience, Reliability, Adaptability, Maintainability, Stochastic Process

5.1. Introduction

The term resilience derives its origin from the Latin word "resilire" which means "to bounce back" (Hosseini et al.,2016). This meaning applies to the restoring ability of infrastructures, physical systems, communities, economy, and various aspects of life. From the preceding, the concept of resilience is multidisciplinary. The paper of C.S Holling on resilience and stability of ecological systems (Holling, 1973) sets a foundation for resilience research. Holling defined resilience as "a measure of the persistence of systems and their ability to absorb change and disturbance and maintain the same relationships between populations or state variables." Following this, resilience has evolved in diverse fields such as ecology, economics, geology, psychology, sociology, built environment, supply chain, and engineering. Consequently, resilience has different definitions as various disciplines, organizations and authorities define resilience in the context of their activities. Table 5.1 shows some definitions of resilience and its perception in multiple fields.

Table 5.1. Definition of the concept of resilience in different sectors.

Discipline	Definition
Social Resilience (Adger et al., 2018)	"ability of groups of communities to cope with external stresses and disturbances as a result of social, political, and environmental change."
Organizational Resilience (Denyer, 2017)	"the ability of an organization to anticipate, prepare for, respond to, and adapt to incremental changes and sudden disruptions in other to survive and prosper."
Economic Resilience (Rose & Liao, 2005)	"inherent ability and adaptive responses that enables firms and regions to avoid maximum potential losses."
Community Seismic Resilience (Bruneau et al.,2003)	"the ability of social units (e.g., organizations, communities) to mitigate hazards, contain the effects of disasters when they occur and carry out recovery activities in ways that minimize social disruption and reduce the impact of future earthquakes. "
Engineering Resilience I (National infrastructure and Advisory Council) (NIAC, 2009)	" the ability to predict, absorb, adapt, and quickly recover from a disruptive event such as natural disasters."
Engineering Resilience II (Yodo et al., 2017)	"a combination of passive and proactive survival rates; the former connected to system reliability and the latter on the recovery process after a disruptive event."
Structural Resilience (JCSS, 2008)	"a system's elastic ability to return to its original state after some perturbation."
System Resilience (Francis & Bekera,2014)	"the property of a system that provides the capacity to combat effectively (absorbing, adapting to, or rapid recovery."

Hosseini et al.(2016) provide additional information on the perception of resilience in different fields. Thus, from a broad perspective, resilience is the ability of a system to resist, mitigate and quickly recover from disruptive events. The bedrock of the concept of resilience is its dimensions (social, economic, organizational, and engineering) described in Table 5.1 and its system properties: robustness, rapidity, redundancy, and resourcefulness (Bruneau et al.,2003). Bruneau et al. (2003) clarify these system properties: robustness as the system's ability to withstand extreme events and still deliver service, rapidity as the system's recovery speed to a high functionality level. The terms robustness and rapidity describe the desired output of the system, otherwise called the "ends".

Furthermore, redundancy is the ability to substitute system components, and resourcefulness is the capacity for proper budgeting, material allocation, staffing, and logistics to achieve the desired system output. The properties (redundancy and resourcefulness) are called the "means," which describes the approach and inputs to achieve the desired system output.

Resilience is a significant metric in determining system performance when faced with disruptive events or situations. Some actions that may trigger disruptive events include natural disasters, environmental conditions, human-made accidents, and cyber attacks. Various metrics have been developed for resilience quantification for engineering and non-engineering disciplines (Hosseini et al., 2016; Yodo & Wang, 2017). A commonly discussed resilience metric designed for community resilience application is presented in this paper (Eq. (5A.1), Appendix 5A); some of these metrics might not find universal application since they were developed for specific sectors and disruptive conditions. Different systems have diverse failure modes and respond differently to several forms of disruptive events; hence, using a unique resilience quantification metric that effectively captures the required resilience input parameters, allows appropriate interpretation, and

provides confidence in its outcome is necessary.

The concept of resilience in the engineering domain is evolving; details of its definition in an engineering context can be seen in Table 5.1. The research activities in engineering resilience span infrastructure and built environment, transportation engineering, chemical process, energy, electrical, and port terminal operations.

In the last decade, a tremendous amount of research contribution to resilience has been seen in the infrastructure and built environment sector. This research includes the resilience of bridges (Stevens and Tuchscherer,2020), disruption to heating pipelines, gas, electrical, and water supply networks to buildings (Feofilovs & Romagnoli, 2017; Zhao et al.,2017; Cimellaro et al., 2013; Iannacone et al., 2022; Wu et al., 2021; Han et al., 2021), consideration of blast and seismic damages to buildings and infrastructures (Cimellaro et al.,2016; Quiel et al., 2016) and critical community-based infrastructures such as dams and power systems (Eldosouky et al.,2021).

Lately, the concept of resilience has evolved in the transportation sector (Minaie & Moon,2017; Kammouh et al.,2019; Zhou et al.,2019). In process engineering, Taleb-berrouane & Khan (2019) utilized stochastic Petri-nets for resilience quantification of process systems, focusing on the system's capacities (absorptive, adaptive, and recovery capacity). Also, Zinetullina & Yang (2020) quantified the resilience of a chemical process separator using the DBN technique. In addition, Zinetullina et al.(2021) applied a combination of DBN and functional resonance analysis in the resilience assessment of a chemical process comprising a two-phase separator and an acid gas sweetening unit. For oil and gas support structures resilience, Cai et al.(2020) developed an approach to quantify the resilience of a subsea pipeline using a combination of Markov Chain and DBN.

The concept of resilience has been a focal point regarding power and energy. Consequently, various resilience frameworks have been developed for energy systems. Some of these applications include wind energy devices (Feng et al.,2019), the Markov reward process for nuclear power plants subject to earthquake events (Zeng et al., 2021), and urban power distribution (Bie et al.,2017). Furthermore, contributions can be seen in offshore power systems using the Bayesian Network (Sarwar et al.,2018a), resilience quantification of electrical infrastructures (Toroghi & Thomas, 2020), Markov process for the electrical and control system of subsea blowout preventers (Cai et al., 2021) and availability-based DBN method for the resilience evaluation of network systems (Cai et al.,2018).

In port terminal operations research, the concept of resilience has gained practical application to characterize terminal activities at the ports (Pant et al., 2014). Similarly, research into seaport seismic resilience assessment has been conducted (Shafieezadeh & Ivey Burden, 2014). Hu et al.(2021) developed a framework for resilience assessment of LNG offloading operations under weather-related hazards.

The resilience approach across the engineering disciplines discussed in this section includes deterministic methods, expert knowledge (which is subjective), and the Markov state process (with implicit exponential distribution assumption). Also, rigorous mathematical techniques have been developed for network systems (community networks, transportation, process operations), raising questions about their ease of implementation and application in practice. Understanding how the structure can adapt and recover from disruptive events is essential for critical oil and gas support structures such as subsea pipelines operating in the uncertain ocean environment. Consequently, it is necessary to consider probabilistic techniques, limit state conditions, historical and expert

information, and a straightforward and efficient approach to quantifying resilience for an asset's operating life.

An essential part of resilience quantification is the recovery process. Recovery functions have been a common approach adopted to model recovery and eventually resilience. The commonly used functions range from linear (Sharma et al.,2018; Ayyub, 2015), power-law (Imani & Hajializadeh, 2020), and exponential (Reed et al., 2010; Todman et al., 2016). However, the difficulty in capturing all the required resilience metrics in a single expression, the choice of recovery function which adequately fits the circumstance considered, the inability to capture the performance loss, and the assumption that the post-recovery performance level is identical to the pre-disruption phase presents some challenges in the use of recovery function for resilience quantification (Cassottana et al., 2019). With the uncertainty involved in the phases of recovery after a disruptive event, the use of a probabilistic approach becomes an essential tool in resilience quantification.

The literature shows limited research on the resilience of oil and gas support structures (pipelines, offshore drilling structures, fixed platforms, and vessels).

From the above review and to fill the gaps identified, this study aims to:

1. Develop a probabilistic approach to quantify the resilience of an offshore natural gas pipeline.
2. Propose a maintainability-based method to characterize the recovery process for structural resilience assessment.

The organization of the remainder of this study is as follows: Section 5.2 describes the preliminaries of resilience quantification. Section 5.3 describes the framework for structural

resilience assessment. Section 5.4 presents a case study of the resilience quantification of an offshore natural gas pipeline segment. Finally, Section 5.5 concludes the study.

5.2. Preliminaries of resilience quantification

5.2.1. Engineering Resilience

The definition of engineering resilience (Youn et al.,2011; Yodo et al., 2017) is a foundation for modeling the resilience of an engineering system using passive and proactive survival rates. The passive survival rate describes the system's reliability, which is its ability to perform its intended function over a specified period (Choi et al.,2007). In this context, the focus of reliability is to maintain the performance and capacity of the system. Furthermore, the proactive survival rate describes the concept of system recoverability, which is restoring the system to a steady state after a disruptive event. Depending on the system restoration type, the steady state could typically be to the pre-disrupted state, slightly higher or lower. Also, Sarwar et al. (2018b) describe two essential components of a system's recoverability: adaptability and maintainability. The system's maintainability is a term that explains the probability at which a system is restored to a steady state in a given time following a disruptive event (Sarwar et al., 2018b). Also, system adaptability is the ability to continue operation in the face of unexpected events and conditions (Asadzadeh et al., 2020). The level of performance loss of a system following a disruptive event measures the degree of the system's adaptability.

Eq. (5.1) shows a mathematical description of the resilience of an engineering system.

$$\eta(t) \triangleq \mathrm{R}(0,\mathrm{t}) + \psi_r \qquad (5.1)$$

Where: t represents time, $\eta(t)$ represents the system resilience, $\mathrm{R}(0,\mathrm{t})$ is the time-dependent reliability from an initial start time 0 to a time t, and ψ_r the system recoverability. As described in

this section, ψ_r is a function of adaptability represented by A_d and maintainability denoted by $\mathrm{M}(t_g)$ (Eq. (5.2)). For maintainability, the term t_g describes the repair goal, which defines the target time set for the repair process.

$$\psi_r = \mathrm{f}\left(A_d, \mathrm{M}(t_g)\right) \tag{5.2}$$

The resilience value derived from Eq. (5.1). is expressed within the interval [0 1]. As $\eta(t)$ tends towards the upper bound, the structural system is highly resilient. Also, all elements describing $\eta(t)$ as shown in Eqs. (5.1) and (5.2) have no units (A_d , $\mathrm{M}(t_g)$, $\mathrm{R}(0,\mathrm{t})$) consequently $\eta(t)$ has no unit.

5.2.2. Structural Resilience Metric

This section details the structure's transition phase following a disruptive event and the derivation of the expression for structural resilience quantification described in Section 5.2.1. The transition phase describes the stages of the structural system's performance over time, from the pre-disruption phase (stable) through the disrupted to the recovery phase. Figure 5.1 presents a typical diagram showing performance change following disruptive events and the various resilience transition phases. The performance of a system can be related to its intended function, structural properties, production output, economic effects, and financial implications. The specific choice of performance measure is user-defined and focused on the intended aim of the resilience quantification process. The performance diagram (Figure 5.1) is an idealized plot and appears linear to clearly describe the resilience process and computational stages.

The timeline described in Figure 5.1 includes the structural system's time for initiation of disruption:t_e, time at the disrupted state:t_d and the time in its recovered state:t_r. For performance,

the performance pre-disruption is represented by P_o , performance at a disrupted state P_d which corresponds to the time t_d and performance at recovery P_r which corresponds to the time t_r.

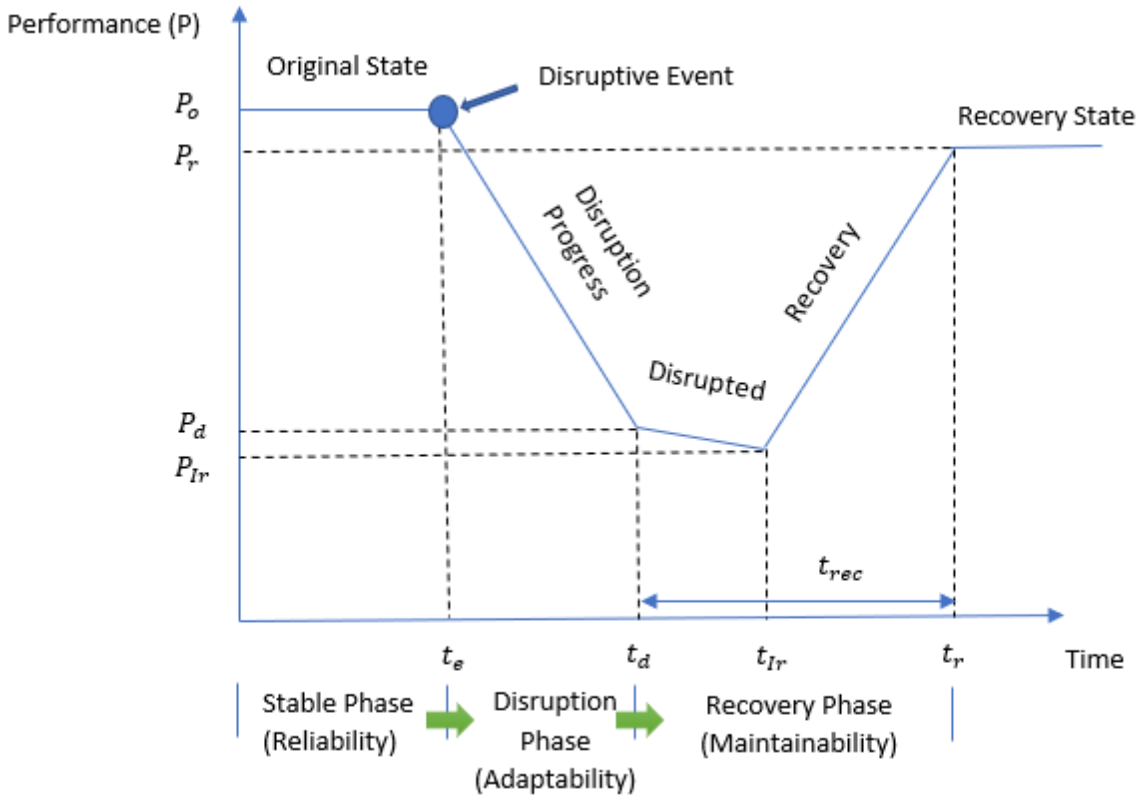

Figure 5.1. Resilience performance curve showing transition phase.

The symbol t_{Ir} and P_{Ir} (Figure 5.1) represents the time actual repair starts and the corresponding system performance at the beginning of repair, respectively. For most systems, recovery is not instantaneous and involves defect detection, careful planning, resource availability, and eventual repairs. Consequently, for a system in the disrupted state (t_d) and within the recovery phase, a further loss in performance is probable. In the recovery phase, all performance loss arising from delays in the repairs or during the repair process is accounted for by the average performance loss

represented by $\bar{P}$. The uncertainty in the determination of $\bar{P}$ is accounted for in the resilience analysis described in this study.

The mathematical formulation of the system's resilience is presented in Eqs. (5.3) to (5.12) and shows the key elements described in Eq. (5.1). First, the principle of total expectation is utilized to describe $\eta(t)$ as shown in Eq. (5.3) in terms of failure and non-failure events situations. In this formulation, failure events imply the disruptive event on the structural system, which is represented by S_f. Also, the symbol $\bar{S}_f$ describes a non-failure event which means no disruptive event on the system.

$$\eta(t) = \eta(t)|S_f . P_r(S_f) + \eta(t)|\bar{S}_f . P_r(\bar{S}_f) \tag{5.3}$$

From Eq. (5.3), $P_r(\bar{S}_f)$ describes the probability of a non-failure state which can be substituted by the time-dependent reliability of the system $\mathrm{R}(0,\mathrm{t})$. The expression $\eta(t)|\bar{S}_f$ in Eq. (5.3) describes the system's resilience given that no disruptive event occurs; since the bound of resilience is defined between [0 1] with a value of 1 denoting a highly resilient system, then $\eta(t)|\bar{S}_f = 1$. The term $P_r(S_f)$ (Eq. (5.3)) represents the probability of a system failure and can be expressed in terms of time-dependent reliability (Eq. (5.4)).

$$\eta(t) = \eta(t)|S_f . (1 - \mathrm{R}(0,\mathrm{t})) + \mathrm{R}(0,\mathrm{t}) \tag{5.4}$$

The term $\eta(t)|S_f$ (Eq. (5.4)) describes the resilience of a system given a disruptive event, and in describing the resilience of such a system, the recovery process is essential. The term related to resilience can be mathematically defined considering the concept of recovery, as shown in Eq. (5.5).

$$\eta(t)|S_f = P_r\left(Recovery|S_f\right).\left(\eta(t)|Recovery, S_f\right) \tag{5.5}$$

Barker et al. (2013) describes the concept of resilience (Eq. (5.6)) and relate the recovered performance of a structure at a given time with the performance loss following a disruptive event. This concept provides an approach to quantifying the resilience of a structural system and will be the foundation of this analysis.

$$\eta(t)|Recovery, S_f = \frac{Recovered\ Performance}{Performance\ Loss} \tag{5.6}$$

The recovered performance and performance loss are shown in Eq. (5.7) and Eq. (5.8)

$$Recovered\ Performance(t_r, t_d) = P_r - P_d - \bar{P}(t_r - t_d) \tag{5.7}$$

$$Performance\ Loss = P_o - P_d \tag{5.8}$$

Eq.(5.9) shows resilience in terms of performance during a disruptive event and recovery.

$$\eta(t)|Recovery, S_f = \frac{P_r - P_d - \bar{P}(t_r - t_d)}{P_o - P_d} \tag{5.9}$$

The resilience index can be expressed as a ratio of the system's initial performance before disruption, as shown in Eq. (5.10).

$$\eta(t)|Recovery, S_f = \frac{\frac{P_r}{P_o} - \frac{P_d}{P_o} - \frac{\bar{P}}{P_o}(t_r - t_d)}{1 - \frac{P_d}{P_o}} \tag{5.10}$$

The performance ratios derived from Eq. (5.10) are $\frac{P_r}{P_o} = q_r$, $\frac{P_d}{P_o} = q_e$ and $\frac{\bar{P}}{P_o} = q_{avg}$. The notation q_r, q_e and q_{avg} represents the performance recovery ratio, the performance loss ratio at the disrupted state, and the average performance loss ratio in the recovery phase. The value of q_e describes the system's adaptability (A_d) expressed in Eq. (5.2).

The time it takes the structure from its disrupted state to a final stable recovered state where necessary repairs have been completed is called the recovery time and is denoted by $t_{rec} = t_r - t_d$ Eq. (5.10).

The expression $P_r\left(Recovery|S_f\right)$ (Eq. (5.5)) describes the probability of recovery given a disruptive event. The probability of recovery will be determined in this paper using ($\mathrm{M}(t_g)$) shown in Eq. (5.2).

The substitution of Eqs. (5.10) and (5.5) into Eq. (5.4) provide an expression for the resilience of a structural component.

$$\eta(t) = \mathrm{M}(t_g).\frac{q_r - q_e - q_{avg}t_{rec}}{1 - q_e}.(1 - \mathrm{R}(0,\mathrm{t})) + \mathrm{R}(0,\mathrm{t}) \qquad (5.11)$$

The time-dependent reliability ($\mathrm{R}(0,\mathrm{t})$), the adaptability component (q_e) and maintainability ($\mathrm{M}(t_g)$) described in Eq. (5.1) are captured in Eq. (5.11). Also, the performance ratios related to the recovery process.

For multiple components or failure modes and mutually exclusive failure paths, Eq. (5.12) applies. A derivation of the expression in Eq. (5.12) is shown in the Appendix (Eq. (5A.2) to (5A.7), Appendix 5A).

$$\eta(t) = R_s(0,t) + \sum_{i=1}^{N_c}[(F_{pi}(0,t).\prod_{j=1}^{n^i}\mathrm{M}(t_g)^i(j) .(\frac{\sum_{j=1}^{n}(q_r^i(j) - q_e^i(j) - q_{avg}t_{rec}^i(j))}{n^i - \sum_{j=1}^{n^i}q_e^i(j)}) \qquad (5.12)$$

From Eq. (5.12), $N_c, F_{pi}(0,t), n^i$ represents the number of failure modes, the cumulative failure probability of a specific failure mode, and the number of defective components in a failure mode.

$R_s(0,t)$ describes the time-dependent system reliability.

5.2.3. Time-Dependent Structural Reliability Analysis

Following the degradation of structural elements with time and the stochastic load acting on them, time-dependent reliability methods have become a veritable approach to evaluating structural reliability. Time-dependent structural reliability is implemented using various techniques; this includes the outcrossing process (Hu & Du, 2013b), simulation method (Wang et al., 2014), metamodel approach (Hu & Mahadevan, 2016), and the extreme value approach (Hu & Du, 2013a). Also is the PHI2 technique, which combines the outcrossing method with FORM for time-dependent reliability analysis (Andrieu-Renaud et al., 2004). A straightforward approach with high accuracy to handle time-dependent reliability problems is using MCS. However, this approach becomes computationally expensive (requiring a large sample size), especially for small failure probability problems and LSF with no closed-form solution. This study adopts the variance reduction IS approach for time-varying reliability analysis. The IS approach samples around areas that contribute to the failure probability and combines the fast convergence using FORM and robustness from MCS (Wang et al., 2021).

Eqs. (5.13) to (5.18) present the expression for time-dependent reliability using the IS approach for obtaining the cumulative probability of failure ($P_{fc}(t_o, t_n)$) from a defined LSF $G(X, Y(t), t)$. The term $P_{fc}(t_o, t_n)$ describes the probability of occurrence of structural failure for a defined time domain (t_o, t_n) where t_o and t_n represents the initial and final time of the interval.

$$P_{fc}(t_o, t_n) = P_r[G(X, Y(t), t) \leq 0)], \exists\ t \in [t_o\ t_n] \tag{5.13}$$

$$P_{fc}{}^{IS}(t_0, t_e) \approx \frac{1}{N_{IS}} \sum_{n=1}^{N_{IS}} (I_k(x_{IS,n}, y(t)_{IS,n}) \frac{f_X(x_{IS,n}) f_{Y(t)}(y(t)_{IS,n})}{h(x_{IS,n}, y(t)_{IS,n})} \quad (5.14)$$

For Eq. (5.13), *X* is a vector of time-independent random variables, and *Y(t)* is a vector of a stochastic process of the LSF $G(X, Y(t), t)$. Eq. (5.14) represents the cumulative failure probability from the X and Y(t) PDF. For the IS approach, the sampling center shifts from origin to the Most Probable Point (MPP) using a sampling density function $h(x_{IS,n}, y(t)_{IS,n})$.

The failure indicator $I_k(x_{IS,n}, y(t)_{IS,n})$ (Eq. (5.14)) is given by

$$I_k(x_{IS,n}, y(t)_{IS,n}) = \begin{Bmatrix} 1 \; if \; \min\{(G(x, y(t), t) \leq 0\} for \; t_o \leq t \leq t_n \\ else \; 0 \end{Bmatrix} \quad (5.15)$$

Where $x_{IS,n}$ and $y(t)_{IS,n}$ are realizations from $f_X(x)$ and $f_{Y(t)}(y(t_o), \ldots . y(t_n))$ respectively for n =1…,.N_{IS} where N_{IS} is the number of sample points for the IS method. Also, $P_{fc}{}^{IS}(t_o, t_n)$ is the cumulative probability of failure using the IS approach for the given time-domain (Eq. (5.14)). The variance ($Var_{P_{fc}}{}^{IS}$) and Coefficient of Variation ($CoV_{P_{fc}}{}^{IS}$) from the IS approach are shown in Eqs. (5.16) and (5.17).

$$Var_{P_{fc}}{}^{IS} = \frac{1}{N_{IS}} \left[\frac{1}{N_{IS}} \sum_{n=1}^{N_{IS}} \left(I_k(x_{IS,n}, y(t)_{IS,n}), \frac{f_X(x_{IS,n}) f_{Y(t)}(y(t)_{IS,n})}{h(x_{IS,n}, y(t)_{IS,n})} \right)^2 - \left(P_{fc}{}^{IS}(t_0, t_e) \right)^2 \right] \quad (5.16)$$

$$CoV_{P_{fc}}{}^{IS} = \frac{\sqrt{Var_{P_{fc}}{}^{IS}}}{P_{fc}{}^{IS}(t_0, t_e)} \quad (5.17)$$

5.2.4. Random Process Discretization

In the case of the time-varying reliability analysis described in Section 5.2.3, quantities that vary randomly with time, which may be related to materials properties, degradation, or applied load, are treated as a random process. The random process exists in a continuous domain with infinite random variables, which presents the need to discretize and truncate the random process to ease computation. The discretization process allows the representation of a random process by random variables such that each random variable represents the random field at a specific time. A series expansion method is a common way of handling the discretization processes, such as the Karhunen-Loeve method (Ghanem & Spanos,1991), Orthogonal Series Expansion (OLE) approach (Zhang & Ellingwood,1994), and Expansion Optimal Linear Estimation (EOLE) method (Li & Der Kiureghian, 1993). Sudret and Der Kiureghian (2000) suggested the EOLE approach in dealing with exponential square autocorrelation functions since it produces better accuracy than earlier mentioned series expansion methods.

The EOLE approach is a spectral decomposition method proposed by Li and Der Kiureghian based on the optimal linear estimation theory. In the EOLE method, discretization is achieved by solving an eigenvalue problem. For EOLE, its shape function is described by the autocorrelation function of the random process.

Eqs. (5.18) to (5.20) describes the EOLE series decomposition for the random process.

$$C_{cov}(t_1, t_2) = \sum_{i=0}^{\infty} \lambda_i \, \emptyset_i(t_1)\emptyset_i(t_2) \tag{5.18}$$

$$H(t, \theta) = \bar{H}(t) + \sum_{i=1}^{\infty} \sqrt{\lambda_i}\, \xi_i(\theta)\emptyset_i(t) \tag{5.19}$$

By truncating the infinite series to N_{xx} terms the new EOLE series expression is shown in Eq. (5.20)

$$H(t,\theta) \approx \widehat{H}(t,\theta) = \bar{H}(t) + \sum_{i=1}^{N_{xx}} \sqrt{\lambda_i}\, \xi_i(\theta) \emptyset_i(t) \qquad (5.20)$$

For Eqs. (5.18) to (5.20), $C_{cov}(t_1, t_2)$ is the covariance matrix, λ_i and $\emptyset_i(t)$ describes the eigenvalues and eigenvectors of the covariance matrix. $\bar{H}(t)$ is the expectation of the Gaussian random process $H(t,\theta)$ with outcome θ. The approximate random process following the truncation of series terms is given by $\widehat{H}(t,\theta)$. This approach is applied for discretizing the stochastic input parameter of the natural gas pipeline.

5.3. The Methodology for Resilience Quantification

This section presents the proposed framework for structural resilience quantification using a seven-step approach, as outlined in Section 5.3.1. Also, Figure 5.2. shows the flowchart of the method described.

5.3.1. Steps for structural resilience quantification

The steps below are a chronological description of the stages of resilience quantification of an offshore natural gas pipeline using the process described in Section 5.2 of this study.

Step 1: *System identification, boundaries, hazards, and failure modes*

Identify the system required for resilience quantification, its boundaries, the likely disruptive events the system might encounter, and the possible failure modes from the disruptive events. This paper considers a natural gas pipeline segment operating in an offshore environment. Offshore pipelines face several hazards, such as extreme environmental loads (seismic loads), process deviation, internal and external corrosion, and dropped objects. This study will focus on system disruption from over-pressure conditions (process deviation), considering the remaining useful life

of an internally corroded natural gas pipeline segment with the leak, burst, and rupture conditions as the likely failure modes.

Step 2: *Define LSF of all failure modes incorporating possible degradation*

The LSF for the various failure modes, which describes the disruptive events of the structural system presented in Step 1, is determined. In cases where there exists an implicit LSF (no closed-form function of input variables), the construction of a metamodel is necessary to describe the performance of the structural system under a given limit state condition. Also, considering the degradation of the structure with time arising from corrosion is essential during the LSF construction.

Step 3: *Determine the probability distribution of random variables and discretize stochastic variables*

Determine if stochastic random variables for the parameters of the given failure modes identified in Step 1 exist. Consequently, a discretization process is utilized to determine the random variable's distribution information at each time step for stochastic random variables affecting the structure. This study adopts the EOLE method discussed in Section 5.2. Furthermore, the probability distribution for the associated parameters affecting the failure modes is determined.

Step 4: *Time-dependent reliability analysis of the LSF*

This step involves the evaluation of the reliability of the structure over time for the failure modes and LSF described in the previous steps outlined. For structural systems with multiple components, a possible approach to determine the failure paths for resilience assessment is by enumeration, which involves the identification of all possible combinations of success and failure of the system's components and the effect on the overall system. Consequently, the cumulative failure probability

is evaluated for series, parallel, or combined structural systems. This stage will utilize the variance reduction approach discussed in Section 5.2 for the offshore natural gas pipeline segment.

Step 5: *System Adaptability determination*

The ability of the structural system to adjust and operate in the disrupted state is determined by the performance loss ratio information (q_e) detailed in Section 5.2. For structures such as pipelines, this information can be obtained by numerical analysis such as Computational Fluid Dynamics during design analysis of failure scenarios (Reddy et al., 2016; Yousef et al., 2021) or from historical process data in operating cases obtained by flow sensors for similar failure situations considered. The method of performance information determination is also applicable to q_r and q_{avg}. It is essential to determine the performance parameters for the loss ratio determination. For pipelines, flow conditions (flow rate, output pressure, temperature), produced quantity, or production cost are possible performance parameters for loss ratio determination. The initial flow rate of natural gas in the pipeline before the disruptive event and at the disrupted state is required to determine the loss ratio (which has no unit) for the natural gas pipeline segment considered. The flow rate is typically measured in cubic meters per hour.

Step 6: *Recovery modeling from repair data*

System recovery is an essential part of structural resilience evaluation. As described in the earlier section, maintainability is proposed to characterize the recovery of structures. While system recovery has been represented in terms of recovery curve (Nocera et al., 2019) and specific recovery functions (Shang et al., 2022); this study proposes a model of recovery that relies on the probability of recovery within a specified time $\mathrm{M}(t_g)$. The repair goal denoted by t_g is the user-defined target time set for the recovery process, and it is integral in the concept of maintainability.

A decrease in the repair time (shorter completion time) relative to the set repair goal means an increase in the probability of recovery. In this step, the value $\mathrm{M}(t_g)$ is determined from historical recovery data of similar repair situations and sometimes from expert judgment when data is unavailable. In using available historical repair information, statistical analysis is utilized to determine the type of probability distribution that best fits and characterizes the repair data (repair distribution) to help develop a maintainability function that describes the probability of completing a recovery action at a specified time. Consequently, the recovery probability can be obtained from the defined function.

Step 7: *Structural Resilience Quantification and Sensitivity Analysis*

The structure's resilience is determined using outcomes from Steps (1-6) described in this section and the derived resilience expression in Section 5.2. The resilience index outcome is quantified with a bound between 0 and 1 and has no unit with a value close to 1, indicating a highly resilient structure. Also, the sensitivity of resilience parameters provides insight into how resilience changes with a change in input parameters. An acceptable target resilience level can be user-defined or determined by appropriate regulatory standards. Intuitively, a value close to 1 may be suitable for critical offshore structures. However, re-evaluating resilience parameters might be necessary where target values exist and the resilient index is below the set target. The sensitivity analysis outcome plays a vital role in the re-evaluation process.

.

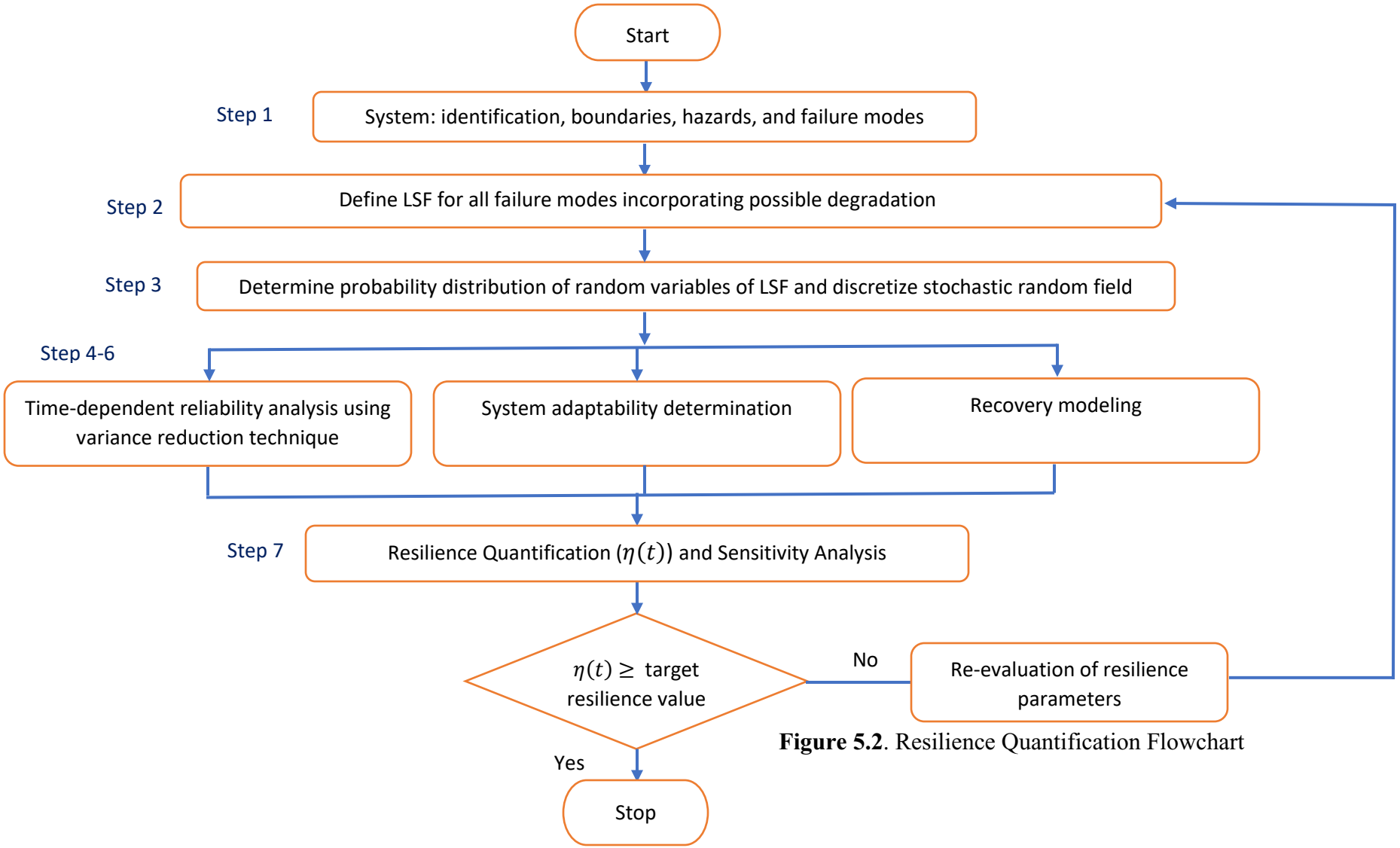

Figure 5.2. Resilience Quantification Flowchart

5.4. Application of the framework to a natural gas pipeline

This section presents the engineering application of the resilience quantification framework described in the previous section to an offshore natural gas pipeline segment.

5.4.1. Background (Offshore Pipeline Resilience)

Offshore pipelines are a vital transportation medium for oil and gas production activities; the safety of these facilities is critical during their operational life. Consequently, pipeline reliability and resilience assessment are essential during their design and operations to ensure a structure that can absorb, adapt, and restore performance when faced with disruptive events.

5.4.2. Case Study: Internally Corroded Natural Gas Pipeline Segment

5.4.2.1. Pipeline disruptive events and LSF

This case study is a hypothetical example that demonstrates the application of the resilience quantification framework to an offshore natural gas pipeline segment (API5L-X60, SCH 40) with multiple initial internal corrosion defects and a design life of 20 years. The disruptive events considered in this study are leak, burst, and rupture failure conditions and are represented by explicit LSF (closed-form function for input variables), as shown in Eqs. (5.21) to (5.23). In a situation where no explicit LSF exists, a metamodel is constructed to define the relationship between the system's random input and response variables.

Eqs. (5.21) to (5.23) show the LSF for the failure modes.

$$g_i^l(t) = t_w - d_i(t) \tag{5.21}$$

$$g_i^b(t) = P_b(t) - P_p(t) \tag{5.22}$$

$$g_i^r(t) = P_{rup}(t) - P_p(t) \tag{5.23}$$

$g_i^l(t)$, $g_i^b(t)$ and $g_i^r(t)$ represents the LSF for the leak, burst, and rupture, respectively $where\ i = 1,2 \ldots n_d$ (n_d is the number of defects)

The notation t_w represents the pipe wall thickness and $d_i(t)$ the corrosion defect depth. The natural gas flow pressure is represented by $P_p(t)$.

The expression for the burst pressure $P_b(t)$ and rupture pressure $P_{rup}(t)$ are presented in Eqs. (5.24) and (5.25) (Ossai et al., 2016). This study adopts the modified ASME B31G (ASME,2009) for the burst pressure condition with further details on $M_f(t)$ (Folias Factor) in the Appendix 5A (Eqs. (5A.8) and (5A.9)). In practice, modified ASME B31G has gained wide application for oil and gas pipeline burst pressure assessment and applied to low and moderate toughness pipes such as the X60 pipeline described in this study.

$$P_b(t) = \xi \frac{2t_w}{D}\left(\sigma_y + 69\right)\left[\frac{1 - 0.85\left(\frac{d_i(t)}{t_w}\right)}{1 - 0.85\left(\frac{d_i(t)}{t_w}\right)M_f(t)^{-1}}\right] \tag{5.24}$$

$$P_{rup}(t) = \frac{1.8\sigma_u t_w}{M_f(t)D} \tag{5.25}$$

The symbol ξ represents the model error for ASME burst pressure, σ_y : pipeline yield stress, σ_u: pipeline ultimate stress and D : outer pipe diameter: Table 5.2 presents further details on the pipeline parameters and statistical distribution.

Table 5.2. Parameters of the offshore natural gas pipeline [modified from:(Pandey, 1998)]

Parameter	Symbol	Unit	Mean	CoV (%)	Distribution
Pipe outer diameter	D	mm	457.2	3	Normal
Pipe wall thickness	t_w	mm	14.27	5	Lognormal
Yield Stress	σ_y	MPa	1.1SMYS	2.5	Normal
Ultimate Stress	σ_u	MPa	520	3.7	Lognormal
Fluid Pressure	$P_p(t)$	MPa	1.05MOP	2	Gaussian Process**
Defect growth rate (length)	$l_g(t)$	mm/yr	0.4	15	Gamma Process
Model error	ξ	-	1.026	25	Gumbel

** Gaussian process is defined by autocorrelation function $\exp\left(-(\Delta t/3)^2\right)$

The CoV describes the relative dispersion of the pipeline parameters about the mean. The Specified Minimum Yield Strength (SMYS) is 415MPa, and the Maximum Operating Pressure (MOP) is 9 MPa.

5.4.2.2. Pipeline Corrosion Rate Determination

This study considers an internally corroded offshore natural gas pipeline segment with initial defects. The effect of corrosion is time-dependent and a potential safety issue that could initiate disruption caused by a leak, burst, or rupture failure during operation and as the pipeline ages. The pipeline defect length $l_g(t)$ and depth $d_g(t)$growth rate considerably impacts its remaining strength. This study considers multiple initial internal corrosion defects (Table 5.3) with the corrosion growth rate (length and depth) modeled as a stochastic gamma process (Gong & Zhou, 2017). The stochastic gamma process is capable of modeling gradual deterioration, the process is easy to implement, increments are non-negative, and the scale parameter is time-dependent

(Noortwijk, 2009). Eq. (5.26) shows the expression for the gamma process for depth growth rate; a similar expression is utilized for the length growth rate.

$$F\left(d_g(t)\middle|at,b\right)=\frac{b^{at}{d_g}^{at-1}}{\Gamma(at)}\exp\left(-bd_g\right) \tag{5.26}$$

For the gamma process, *a* and *b* are the scale and shape parameters that are related to the year mean ($\frac{a}{b}$)and standard deviation ($\frac{a}{b^2}$) of the depth and length increment. Γ(.) represents the gamma function.

The expression below (Eqs. (5.27) and (5.28)) shows the natural gas pipeline defect length and depth growth rate model, respectively.

$$l_i(t)=l_{oi}+l_{gi}(t) \tag{5.27}$$

$$d_i(t)=d_{oi}+d_{gi}(t) \tag{5.28}$$

$$where\ i=1,2\ldots6\ (n_d=6)$$

This study considers six (6) non-interacting defects in the pipeline segment. The longitudinal and circumferential separation distance for adjacent defects is assumed to be greater than three times the pipe wall thickness ($3t_w$) (Bao & Zhou, 2021), and the defects are isolated such that developed stress and strain do not interact with an adjacent defect. Table 5.3 shows the offshore natural gas pipeline's initial defect dimensions (length and depth), which are assumed to follow a lognormal distribution.

Table 5.3. Initial defect length and depth dimensions of the natural gas pipeline segment.

i	Initial defect depth d_{oi} (mm)		Initial defect length l_{oi} (mm)	
	Mean	**CoV**	**Mean**	**CoV**
1	2.4	0.05	50	0.08
2	2.5	0.03	70	0.03
3	2.2	0.07	94	0.02
4	3.7	0.11	75	0.03
5	3.7	0.09	116	0.02
6	2.9	0.10	118	0.03

The statistical information of $l_g(t)$ is described in Table 5.2 of this section, and the method for the determination of the corrosion depth growth rate $d_g(t)$ is described in the next section using a semi-empirical model. The stochastic gamma process is utilized to determine $l_g(t)$ and $d_g(t)$ for the pipeline design life. A correlation coefficient of 0.7 is assumed between $l_g(t)$ and $d_g(t)$ for individual defects.

5.4.2.2.1. Determination of the Corrosion Rate (Depth)

Various semi-empirical corrosion models have been applied to corrosion rate determination in the oil and gas industry. Most of these models tend to focus on the influence of CO_2 on corrosion rate. These models include the popularly used de Waard, Norsok, Dream, Tulsa, Ohio, Cassandra, and Lipucor models (Nyborg, 2002). The corrosion effect of Hydrogen Sulphide (H_2S) is significant in natural gas pipelines, but the models earlier described cannot account for the influence of H_2S on the corrosion rate. The Southwest Research Institute (SwRI) model (Kale et al., 2004) is a linear

model which can account for not only the influence of Carbon-dioxide (CO_2) but also Oxygen (O_2) and H_2S. For $d_g(t)$ determination, the SwRI model is utilized in this study.

The SwRI semi-empirical model for the corroded natural gas pipeline in mm/year is expressed in Eq. (5.29).

$$d_g(t) = k \text{ x } C_1 \text{x } 0.0254 \text{ x } \big(8.7 + 9.86\text{x}10^{-3}(O_2) - 1.48\text{x}10^{-7}(O_2)^2 - 1.31(pH) + 4.93\text{x}10^{-2}(pCO_2)(pH_2S) - 4.82\text{x}10^{-5}(pCO_2)(O_2) - 2.37\text{x}10^{-3}(pH_2S)(O_2) - 1.11\text{x}10^{-3}(O_2)(pH)\big)\frac{mm}{year} \quad (5.29)$$

Table 5.4 shows the parameters that affect the natural gas pipeline with all parameters lognormally distributed. In Eq. (5.29), the partial pressure of CO_2 and H_2S is captured, k is the corrosion model error and C_I the inhibitor correction factor.

Table 5.4. Corrosion Parameters for natural gas pipeline [modified from (Kale et al., 2004)].

	$O_2(ppm)$	pH	$\%H_2S(mole)$	$\%CO_2(mole)$	k	C_I
Mean	7500	6.00	0.06	4.0	1.0	0.85
Standard Deviation	1800	0.06	0.005	0.08	0.5	0.26

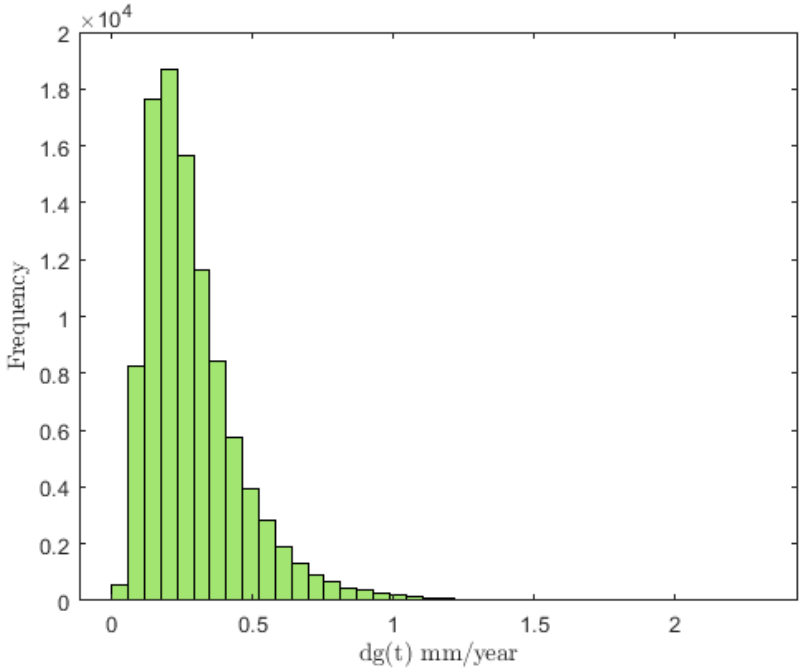

Figure 5.3. Histogram of corrosion depth growth rate ($d_g(t)\ mm/year$)**.**

Figure 5.3 shows the histogram for the corrosion rate using the SwRI model. In addition, Table 5.5 shows the statistical information on the corrosion rate of the natural gas pipeline using the semi-empirical model from Eq. (5.29).

Table 5.5. Corrosion depth growth rate statistical information.

	N^{cr}	Mean	CoV
$d_g(t)\ mm/year$	1E5	0.2919	0.61

The results presented in Table 5.5 show the essential statistical parameters of $d_g(t)$ for the natural gas pipeline, which is assumed to follow a stochastic gamma process. The number of MCS simulations in the determination of $d_g(t)$ is represented by N^{cr}.

5.4.2.3. Fluid pressure discretization

The internal fluid pressure $P_p(t)$ changes with time, and it is necessary to model this activity during the structural resilience assessment. The natural gas pressure $P_p(t)$ is modeled as a stationary Gaussian process with autocorrelation function $\exp(-(\Delta t/3)^2)$ (Sudret & Der Kiureghian, 2000). The stochastic random process for the fluid pressure is discretized into a random variable and for the pipeline's design life (20 years) using the EOLE approach discussed in Section 5.2. For the autocorrelation function presented in this study, its scaling parameter that describes the correlation between pressure values in the random field is three months. The discretization domain is 20 years (240 months), and the mean and CoV of the stochastic process are presented in Table 5.2. In practice, the autocorrelation function can be obtained from monitored pressure records and time lag data using appropriate curve fitting techniques. The EOLE method is a series expansion method with an infinite number of terms arranged in descending order. However, it is essential to determine the appropriate truncation terms (N_{xx}) in the discretization process to capture the non-zero eigenvalues (Eq. (5.20)). A truncation term of N_{xx} =115, as shown in Figure 5.4, captures the non-zero eigenvalues of the fluid pressure expansion series.

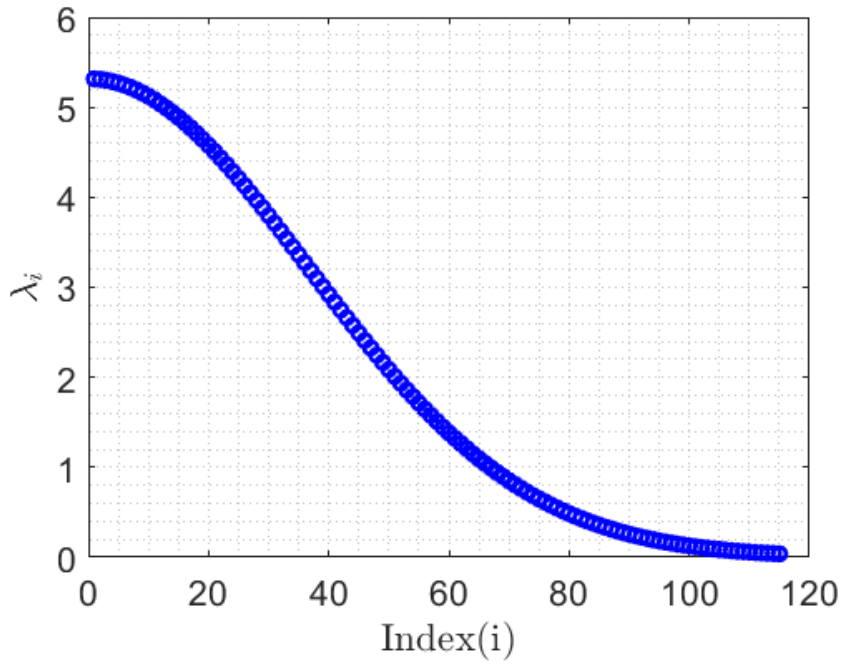

Figure 5.4. EOLE random process discretization eigenvalues for $\boldsymbol{P_p}(t)$.

The random variables (pressure) from the fluid pressure discretization are essential in the time-dependent reliability assessment of the pipeline segment.

5.4.2.4. Pipeline time-dependent reliability assessment

The time-dependent reliability of the natural gas pipeline is an integral part of its resilience quantification. Using the LSF approach, failures occur when there is a violation of the LSF (when the LSF is zero or a negative value). Eqs. (5.30) to (5.32) present the pipeline's leak, burst, and rupture failure condition. For the probability of leak failure, as shown in Eq. (5.30), a violation of the leak LSF ($g_i^l(t)$) in at least one of the defect locations occurs with no possible violation of the burst LSF ($g_i^b(t)$). Similarly, for the probability of burst failure (Eq. (5.31)), a violation of the burst LSF ($g_i^b(t)$) in at least one of the defect locations occurs with no possible violation of the leak LSF ($g_i^l(t)$).

$$P_{fc}{}^{leak}(0,t) = P_r\left[\bigcup_{i=1}^{n_d}\left(g_i^l(t) \le 0\right) \cap \left(g_i^b(t) > 0\right)\right] \quad (5.30)$$

$$P_{fc}{}^{burst}(0,t) = P_r\left[\bigcup_{i=1}^{n_d}\left(g_i^l(t) > 0\right) \cap \left(g_i^b(t) \le 0\right)\right] \quad (5.31)$$

$$P_{fc}{}^{rupture}(0,t) = P_r\left[\bigcup_{i=1}^{n_d}\left(g_i^l(t) > 0\right) \cap \left(g_i^b(t) \le 0\right) \cap \left(g_i^r(t) \le 0\right)\right] \quad (5.32)$$

In addition, for a pipeline rupture failure (Eq. (5.32)), a violation of the burst and rupture LSF, as expressed in Eqs. (5.22) and (5.23) will occur in at least one of the defect locations with no possible violation of the leak condition (Eq. (5.21)). The time-dependent IS approach described in Section 5.2.3 is utilized to obtain the pipeline cumulative failure probability for failure conditions [$P_{fc}{}^{leak}(0,t)$, $P_{fc}{}^{burst}(0,t)$ and $P_{fc}{}^{rupture}(0,t)$] considering the pipeline input variables and all corrosion defects. In this study, $N_{IS} = 10^6$ sample points are utilized in the time-varying reliability analysis.

The corresponding IS reliability index (β^{IS}) is obtained from $P_{fc}{}^{IS}(0,t)$ using Eq. (5.33), and this is shown in Figure 5.5 for the leak, burst, and rupture conditions.

$$\beta^{IS} = -\Phi^{-1}\left(P_{fc}{}^{IS}(0,t)\right) \quad (5.33)$$

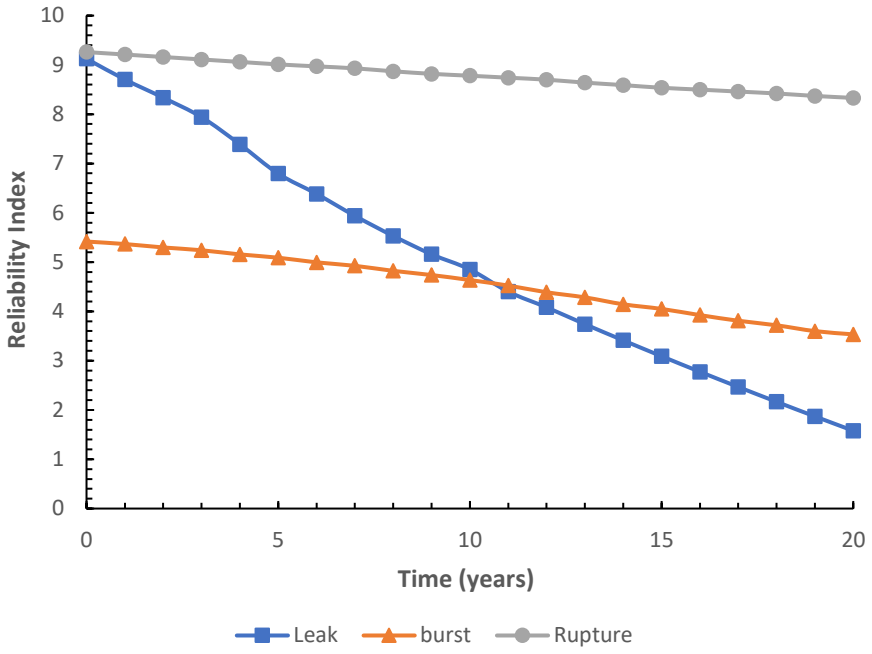

Figure 5.5. Pipeline reliability index for the leak, burst, and rupture failure condition.

From Figure 5.5, the pipeline is least likely to fail from a rupture condition. The $CoV_{P_{fc}}{}^{IS}$ (Eq. (5.17)) for the different pipeline failure modes is presented in Figure 5.6. with a high $CoV_{P_{fc}}{}^{IS}$ observed for the leak and rupture conditions using the IS approach and specified sample points ($N_{IS} = 10^6$).

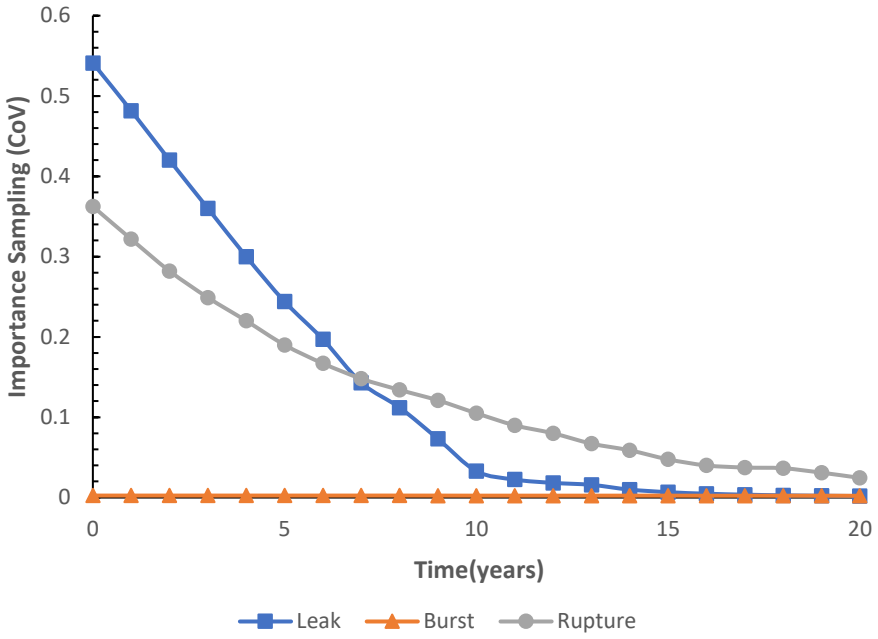

Figure 5.6. Pipeline Importance Sampling $CoV_{P_{fc}}{}^{IS}$ *plot* ($N_{IS} = 10^6$).

The failure probability for the different pipeline failure modes is essential in resilience quantification since it represents the term $F_{pi}(0,t)$ in Eq. (5.12). A leak, burst, or rupture condition of the pipeline segment leads to system failure. Consequently, the pipeline segment failure conditions are evaluated in series to obtain the time-dependent probability of failure of the system (Eq. (5.34)), and R(0, t).

$$P_{fc(sys)}(0,t) = 1 - \left[\left(1 - P_{fc}{}^{leak}(0,t)\right).\left(1 - P_{fc}{}^{burst}(0,t)\right).\left(1 - P_{fc}{}^{rupture}(0,t)\right)\right] \qquad (5.34)$$

5.4.2.5. Pipeline recovery analysis

Recovery analysis of a structural system is a critical aspect of resilience assessment. This study adopts the concept of maintainability in recovery modeling. As discussed in Section 5.3, repair information is obtained from historical data, then the distribution is determined, and the maintainability function is developed. A gamma repair distribution is fitted to the pipeline repair

data for demonstration purposes. The gamma distribution is an excellent choice to characterize repair times because of its flexibility, ability to model wait times, and represent various maintenance data (Dhillion,2006). The probability of repair at a given time is obtained using the gamma maintainability function shown in Eq. (5.35).

$$M(t_g) = \frac{C^m}{\Gamma(m)} \int_0^{t_g} {t_g}^{m-1}\, e^{-ct_g} dt_g \tag{5.35}$$

The maintainability parameters C and m in Eq. (5.35) are obtained from the mean repair time ($\frac{m}{c}$) and standard deviation ($\frac{\sqrt{m}}{c}$) of the gamma-fitted repair data. The target repair time, otherwise called the repair goal, is represented by t_g. Table 5.6 shows the statistical parameters of the assumed repair data and the values of $M(t_g)$ for specified t_g obtained using Eq. (5.35). The repair time for the offshore natural gas pipeline depends on the water depth, failure type, repair crew competence, logistics, repair method, and equipment availability. The repair methods include clamps and sleeves installation, repair robots, hyperbaric welding, and a complete pipe section replacement (Eidaninezhad et al., 2019). Leak repairs can typically involve the introduction of sleeves and clamps, while burst and rupture repairs can result in a total replacement of the pipe section.

Table 5.6. Offshore natural gas pipeline repair and maintainability data.

	Leak Repair	Burst Repair	Rupture Repair
Mean repair time(weeks)	8	11	13
CoV	0.4	0.7	0.3
t_g (weeks)	10	15	15
C, m	(6.25,0.78)	(2.04,0.19)	(11.11,0.85)
$M(t_g)$	0.79	0.76	0.73

The repair time described includes time to locate the damaged section, pipeline preparation and repair planning, actual repair, installation, and pressure testing on completion of repairs. Due to data unavailability for actual pipeline repair, the data presented in Table 5.6 is obtained from experience gathered by the researchers. The repair data describes the recovery from a single failure condition at a time.

5.4.2.6. Pipeline resilience quantification

The evaluation of the time-dependent reliability of the pipeline, the likelihood of recovery when faced with disruptive events, and the performance ratios (Table 5.7) are essential parameters in quantifying its resilience. The adaptability of the structure in the disruptive phase is defined by $A_d = q_e$ and the ratio q_{avg} (Table 5.7) describes the performance loss ratio for the period of the pipeline recovery. For simplicity of analysis, this study assumes the same performance ratio for all failure modes of the offshore pipeline.

Table 5.7. Performance ratio of the natural gas pipeline (recovery and loss).

Performance ratio	Distribution type	Mean	CoV
q_r	Lognormal	0.8	0.2

q_e	Lognormal	0.3	0.05
q_{avg}	Lognormal	0.2	0.01

With the resilience expression (Eq. (5.12)), $\eta(t)$ is determined considering the pipeline segment. Figure 5.7 shows the pipeline resilience plot for the design life (20 years).

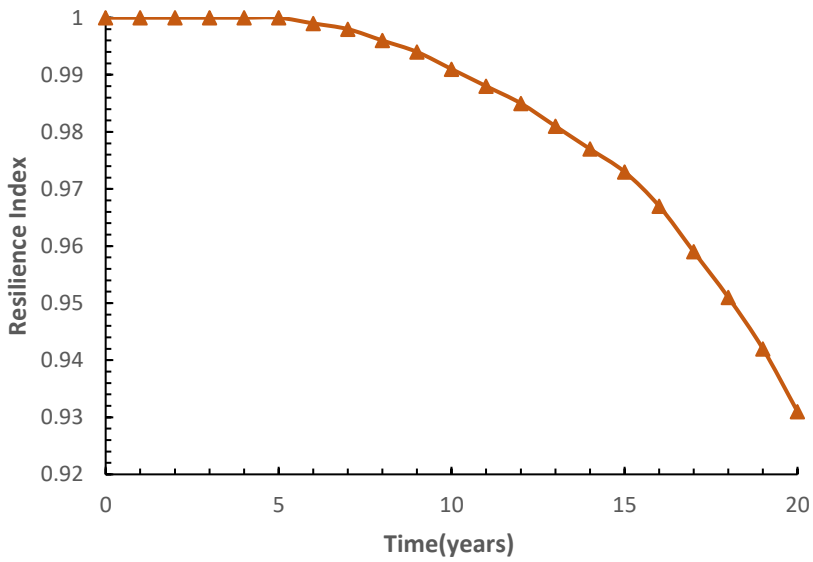

Figure 5.7. Resilience index ($\boldsymbol{\eta(t)}$) for the offshore natural gas pipeline.

5.4.2.7. Pipeline Resilience Sensitivity Analysis

It is essential to analyze the influence of input parameters on the resilience index through its design lifecycle. The Borgonovo index, a global sensitivity analysis method, is utilized in the pipeline's sensitivity analysis (Borgonovo, 2007). The advantages of using the Borgonovo index are that it is moment independent, utilizes the entire input and output response, and evaluates correlated and uncorrelated variables. Eq. (5.36) shows the expression of the Borgonovo index (δ_B).

$$\delta_{B_i} = \frac{1}{2}\int_{D_{X_i}} f_{X_i}(x_i) \int_{D_y} \left| f_Y(y) - f_{Y|X_i}(y) \right| d_y d_{X_i} \tag{5.36}$$

Where $f_Y(y)$ is the PDF of the model output, $f_{Y|X_i}(y)$ is the conditional distribution on X_i and $f_{X_i}(x_i)$ is the PDF of the input variable X_i. For the sensitivity index, when the given input variable is independent of the output $\delta_{B_i} = 0$. Also, when all input variables contribute to the output response, the sum of $\delta_{B_i} = 1$ for $i = 1,2..n$ where n is the number of input variables.

From the resilience expression (Eq. (5.12)), the sensitivity analysis of the pipeline is evaluated using δ_B to determine the sensitivity of the resilient input variables for its design life. Figure 5.8 shows the sensitivity analysis outcome for the gas pipeline.

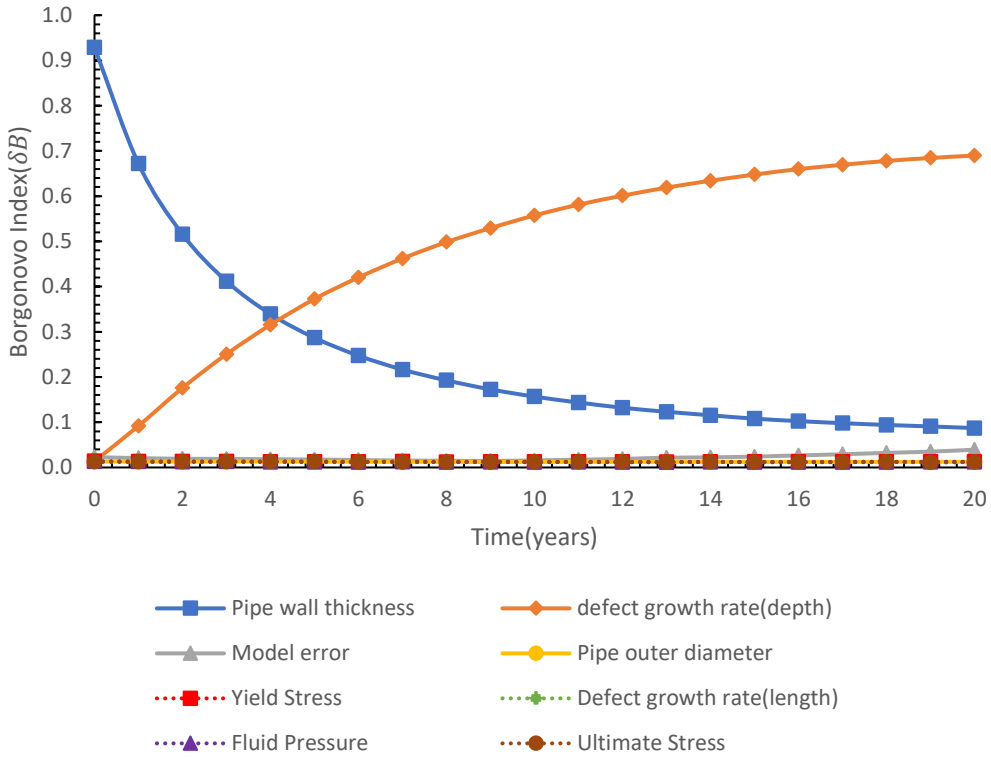

Figure 5.8. Pipeline resilience sensitivity plot of the using Borgonovo Index.

From Figure 5.8, the segmented pipeline resilience was highly sensitive to the pipe wall thickness and the defect growth rate (depth) parameters, while other parameters had less impact on resilience.

5.4.3. Discussion of results

For the offshore natural gas pipeline segment considered, the outcome, as shown in Figure 5.7, reveals an approximately constant resilience index ($\eta(t)$) for the first five years with the index equals 1; this is followed by a gradual decline from the fifth year through its design life ($(\eta(20)) = 0.931$). Although there was no known target resilience value to compare the evaluated resilience index in this study, the resilience evaluation outcome indicates a high safety level and ability to recover under the given conditions and disruptive events (leak, burst, or rupture) considered. A significant aspect of structural resilience is modeling the recovery process; a change in repair goals (t_g) affects $M(t_g)$ and the resilience index of the structural system using the framework presented. Hence, it is essential to effectively model the recovery process and set realistic repair goals. Furthermore, Figure 5.5 reveals that the pipeline segment is more likely to fail due to burst conditions than other failure modes in the early operating years and a leak in subsequent years. This information could be helpful for pipeline asset operating parameter monitoring and maintenance planning during its service life.

The influence of pipeline parameters on the system's resilience is critical during the asset life cycle. In this study, the result of the resilience sensitivity analysis (Figure 5.8) indicates that the pipeline wall thickness (t_w) has a significant impact on its resilience, especially in the early years of its design life. Consequently, this emphasizes the importance of appropriate material selection and determination of pipe wall thickness for strength and toughness during the pipeline design, particularly for short service life pipelines. The pipe joint thrust resistance, appropriate corrosion

management strategy (to improve pipeline durability), adaptability of pipeline materials with appurtenances to the offshore operating environment, and effective management during operations against cyber and physical attacks are additional measures to improve pipeline resilience. Another noticeable trend from the sensitivity analysis (Figure 5.8) is the gradual increase in the influence of corrosion depth growth rate (g_d); this parameter becomes the most sensitive factor affecting the pipeline's resilience from the fifth year. Consequently, an increase in g_d indicates the importance of corrosion on the pipeline integrity, which could trigger a failure (leak, burst, or rupture). Hence, the need to consider corrosion prevention and maintenance planning strategies through the pipeline lifecycle and for asset life extension purposes (operating beyond the design life).

The unavailability of actual pipeline repair data and offshore industry pipeline resilience standards to help set appropriate resilience targets is a limitation of this study. A realistic implementation of the proposed framework can be achieved with data availability.

5.5. Conclusions

A framework for offshore pipeline resilience quantification is presented based on the system's time-dependent reliability, adaptability, and maintainability. The approach considers disruptive events characterized by their LSF. The framework is demonstrated using an internally corroded offshore natural gas pipeline segment considering leak, burst, and rupture failure conditions over its design life. From the description presented in subsequent sections, the study arrives at the following conclusions.

1. The framework provides the possibility to quantify the ability of a structural system to bounce back if faced with disruptive events over the design life, as demonstrated by the

case study of the natural gas pipeline segment detailed in this study ($\eta(0) \approx 1$, $\eta(20)) \approx 0.931$).

2. It provides a means to identify critical parameters that affect the structural system's resilience during its life cycle; this is essential for informed decision-making in structural design and maintenance planning during the asset's operational life. For the case study presented, the sensitivity analysis showed that the pipe wall thickness (t_w) and the corrosion depth growth rate (g_d) are important parameters that affect the resilience of the pipeline under stated conditions.
3. With the LSF approach presented in this framework, the resilience of a structural system faced with multiple disruptive events can be easily determined.

Although this study focuses on the resilience quantification of an offshore natural gas pipeline segment, the approach can be extended and applied to other oil and gas support structures. Finally, areas for further research include the resilience assessment of complex marine structural systems using metamodels and assessing pipeline resilience utilizing the framework presented and considering the following factors: external disruptive events, the effect of interacting defects, and variable dependency.

Acknowledgment

The authors thankfully acknowledge the financial support provided by the Natural Sciences and Engineering Research Council of Canada (NSERC) through Discovery Grant and the Canada Research Chair (Tier I) Program in Offshore Safety and Risk Engineering.

Appendix 5A

Resilience Metric:

Community Earthquake Resilience describes resilience as a function of the quality of the structural system and recovery time (Bruneau et al., 2003).

$$\eta(t) = \int_{t_e'}^{t_r'} \big(100 - Q(t)\big)dt \qquad (5A.1)$$

Q(t) is the structural functionality, t_e' : loss of quality start time, t_r': recovery time to steady-state.

Resilience Expression (multiple failure path and component) Derivation of Eq. (5.12)

$$\eta(t) = R_s(0,t) + \big(1 - R_s(0,t)\big)\sum_{i=1}^{N_c}[P_r\{Recovery|{C_f}^i, S_f\}.P_r\{{C_f}^i, S_f\}\omega_i] \qquad (5A.2)$$

Determine cumulative failure probability and maintainability for different failure mode

$$F_{pi}(0,t) = \big(1 - R_s(0,t)\big).P_r\{{C_f}^i, S_f\} \qquad (5A.3)$$

$$P_r\{Recovery|{C_f}^i, S_f\} = \prod_{j=1}^{n^i} \mathrm{M}\big(t_g\big)^i(j) \qquad (5A.4)$$

Obtain component performance ratio

$$\omega_i = \frac{q_{r_i} - q_{e_i} - q_{avg}t_{reci}}{1 - q_{e_i}} \qquad (5A.5)$$

$$q_{e_i} = 1 - \sum_{j=1}^{n^i} 1 - {q_e}^i(j)\ ,\ q_{r_i} = 1 - \sum_{j=1}^{n^i} 1 - {q_r}^i(j),\ t_{reci} = \sum_{j=1}^{n^i} {t_{rec}}^i(j)$$

$$\omega_i = \frac{[1 - \sum_{j=1}^{n^i} 1 - {q_r}^i(j)] - [1 - \sum_{j=1}^{n^i} 1 - {q_e}^i(j)] - q_{avg}\sum_{j=1}^{n^i} {t_{rec}}^i(j)}{1 - [1 - \sum_{j=1}^{n^i} 1 - {q_e}^i(j)]} \qquad (5A.6)$$

$$\omega_i = \frac{\sum_{j=1}^{n^i} {q_r}^i(j) - \sum_{j=1}^{n^i} {q_e}^i(j) - q_{avg} \sum_{j=1}^{n^i} {t_{rec}}^i(j)}{n^i - \sum_{j=1}^{n^i} {q_e}^i(j)} \quad (5A.7)$$

ω_i : Performance ratio for a given failure mode

n^i : Number of failure components in a failure path

${C_f}^i$: Component failure event

Folias Factor

$M_f(t)$ (Folias Factor): dependent on the pipeline ratio $\frac{l_i(t)^2}{Dt_w}$.

$$M_f(t) = (1 + 0.6275\left(\frac{l_i(t)^2}{Dt_w}\right) - 0.003375(\frac{l_i(t)^2}{Dt_w})^2)^{0.5} \quad (5A.8)$$

$$M_f(t) = 3.3 + 0.032\left(\frac{l_i(t)^2}{Dt_w}\right) \quad (5A.9)$$

For $\frac{l_i(t)^2}{Dt_w} \leq 50$, Eq.5A.1 is utilized to determine $M_f(t)$. Conversely, for $\frac{l_i(t)^2}{Dt_w} \geq 50$, $M_f(t)$ is determined using Eq.5A.2.

References

Adger, W. N., Hughes, T. P., Folke, C., Carpenter, S. R., & Rockström, J. (2018). Social-ecological resilience to coastal disasters. In:Hamin Infield , E.M., Abunnasr, Y., Rayn, R.L.(Eds.), *Planning for Climate Change: A Reader in Green Infrastructure and Sustainable Design for Resilient Cities*, *309*, Routledge, New York, 151–159. https://doi.org/10.4324/9781351201117-18

Andrieu-Renaud, C., Sudret, B., & Lemaire, M. (2004). The PHI2 method: A way to compute time-variant reliability. *Reliability Engineering and System Safety*, *84*(1), 75–86.

https://doi.org/10.1016/j.ress.2003.10.005

Asadzadeh, S. M., Maleki, H., & Tanhaeean, M. (2020). A resilience engineering-based approach to improving service reliability in maintenance organizations. *International Journal of Systems Assurance Engineering and Management*, *11*(5), 909–922. https://doi.org/10.1007/s13198-020-01015-5

ASME. (2009). *Manual for determining the remaining strength of corroded pipelines—a supplement to ASME B31G code for pressure piping. New York: American Society for Mechanical Engineers.*

Ayyub, B. M. (2015). Practical Resilience Metrics for Planning, Design, and Decision Making. *ASCE-ASME Journal of Risk and Uncertainty in Engineering Systems, Part A: Civil Engineering*, *1*(3), 04015008. https://doi.org/10.1061/ajrua6.0000826

Bao, J., & Zhou, W. (2021). Journal of Pipeline Science and Engineering Influence of depth thresholds and interaction rules on the burst capacity evaluation of naturally corroded pipelines. *Journal of Pipeline Science and Engineering*, *1*(1), 148–165. https://doi.org/10.1016/j.jpse.2021.01.001

Barker, K., Ramirez-Marquez, J. E., & Rocco, C. M. (2013). Resilience-based network component importance measures. *Reliability Engineering and System Safety*, *117*, 89–97. https://doi.org/10.1016/j.ress.2013.03.012

Bie, Z., Lin, Y., Li, G., & Li, F. (2017). *Battling the Extreme : A Study on the Power System Resilience*. *Proceedings of the IEEE. 105*(7), 1253–1266. https://doi.org/10.1109/JPROC.2017.2679040

Borgonovo, E. (2007). A new uncertainty importance measure. *Reliability Engineering and System Safety*, *92*(6), 771–784. https://doi.org/10.1016/j.ress.2006.04.015

Bruneau, M., Eeri, M., Chang, S. E., Eeri, M., Ronald, T., Eeri, M., Lee, G. C., Eeri, M., Rourke, T. D. O., Eeri, M., Reinhorn, A. M., Eeri, M., Shinozuka, M., Eeri, M., Wallace, W. A., & Winterfeldt, D. V. (2003). A Framework to Quantitatively Assess and Enhance the Seismic Resilience of Communities. *Earthquake Spectra*, *19*(4), 733–752. https://doi.org/10.1193/1.1623497

Cai, B., Xie, M., Liu, Y., Liu, Y., & Feng, Q. (2018). Availability-based engineering resilience metric and its corresponding evaluation methodology. *Reliability Engineering and System Safety*, *172*, 216–224. https://doi.org/10.1016/j.ress.2017.12.021

Cai, B., Zhang, Y., Wang, H., Liu, Y., Ji, R., Gao, C., Kong, X., & Liu, J. (2021). Resilience evaluation methodology of engineering systems with dynamic-Bayesian-network-based degradation and maintenance. *Reliability Engineering and System Safety*, *209*, 107464. https://doi.org/10.1016/j.ress.2021.107464

Cai, B., Zhang, Y., Yuan, X., Gao, C., Liu, Y., Guo-ming, C., Liu, Z., & Ji, R. (2020). A Dynamic-Bayesian-Networks-Based Resilience Assessment Approach of Structure Systems : Subsea Oil and Gas Pipelines as A Case Study. *China Ocean Engineering*, *34*(5), 597–607.

Choi, S.K, Grandhi, R.V, & Canfield, RA. (2007). Reliability-based structural design. Springer, pp 1–7

Cimellaro, G P, Villa, O., & Kim, H. U. (2013). Resilience-Based design of Natural Gas Pipelines. *World Environment*, *4*(3), 345–354.

Cimellaro, G. P., Dueñas-Osorio, L., & Reinhorn, A. M. (2016). Special Issue on Resilience-Based Analysis and Design of Structures and Infrastructure Systems. *Journal of Structural Engineering* , *142*(8), 1–3. https://doi.org/10.1061/(ASCE)ST.1943-541X.0001592

Denyer, D. (2017). *Organizational Resilience: A summary of academic evidence, business insights and new thinking.* BSI and Cranfield School of Management.

Dhillon, B.S. (2006). Maintainability, Maintenance, and Reliability for Engineers, CRC Press. ISBN 0-8493-7243-7, ISBN 978-0-8493-7243-8

Eidaninezhad, A., Ziyaei, P., & Zare, A. (2019). An overview of marine pipeline repair methods. *8th International Offshore Industries Conference*, *June 2019*, Sharif University of Technology, Tehran, Iran.

Eldosouky, A. R., Saad, W., & Mandayam, N. (2021). Resilient critical infrastructure: Bayesian network analysis and contract-Based optimization. *Reliability Engineering and System Safety*, *205*, 107243. https://doi.org/10.1016/j.ress.2020.107243

Feng, Q., Zhao, X., Fan, D., Cai, B., Liu, Y., & Ren, Y. (2019). Resilience design method based on meta-structure: A case study of offshore wind farm. *Reliability Engineering and System Safety*, *186*, 232–244. https://doi.org/10.1016/j.ress.2019.02.024

Feofilovs, M., & Romagnoli, F. (2017). Resilience of critical infrastructures: Probabilistic case study of a district heating pipeline network in municipality of Latvia. *Energy Procedia*, *128*, 17–23. https://doi.org/10.1016/j.egypro.2017.09.007

Francis, R., & Bekera, B. (2014). A metric and frameworks for resilience analysis of engineered and infrastructure systems. *Reliability Engineering and System Safety*, *121*, 90–103. https://doi.org/10.1016/j.ress.2013.07.004

Ghanem, R.-G., & Spanos, P.-D. (1991). *Stochastic Finite Elements—A Spectral Approach*. Springer Berlin Heidelberg.

Gong, C., & Zhou, W. (2017). First-order reliability method-based system reliability analyses of corroding pipelines considering multiple defects and failure modes. *Structure and Infrastructure Engineering*, *13*(11), 1451–1461. https://doi.org/10.1080/15732479.2017.1285330

Han, L., Zhao, X., Chen, Z., Wu, Y., Su, X., & Zhang, N. (2021). Optimal allocation of defensive resources to defend urban power networks against different types of attackers. *International Journal of Critical Infrastructure Protection*, *35*, 100467. https://doi.org/10.1016/j.ijcip.2021.100467

Holling, C. S. (1973). Resilience and stability of ecological systems. *Annual Review of Ecology and Systematics*, *4*, 1–23.

Hosseini, S., Barker, K., & Ramirez-Marquez, J. E. (2016). A review of definitions and measures of system resilience. *Reliability Engineering and System Safety*, *145*, 47–61. https://doi.org/10.1016/j.ress.2015.08.006

Hu, Z., & Du, X. (2013a). A Sampling Approach to Extreme Value Distribution for Time-Dependent Reliability Analysis. *Journal of Mechanical Design*, *135*(7). https://doi.org/10.1115/1.4023925

Hu, Z., & Du, X. (2013b). Time-dependent reliability analysis with joint upcrossing rates. *Structural and Multidisciplinary Optimization*, *48*(5), 893–907. https://doi.org/10.1007/s00158-013-0937-2

Hu, J., Khan, F., & Zhang, L. (2021). Dynamic resilience assessment of the Marine LNG offloading system. *Reliability Engineering and System Safety*, *208*. https://doi.org/10.1016/j.ress.2020.107368

Hu, Z., & Mahadevan, S. (2016). A Single-Loop Kriging Surrogate Modeling for Time-Dependent Reliability Analysis. *Journal of Mechanical Design, Transactions of the ASME*, *138*(6), 1–10. https://doi.org/10.1115/1.4033428

Iannacone, L., Sharma, N., Tabandeh, A., & Gardoni, P. (2022). Modeling time-varying reliability and resilience of deteriorating infrastructure. *Reliability Engineering and System Safety*, *217*, 108074. https://doi.org/10.1016/j.ress.2021.108074

Imani, M., & Hajializadeh, D. (2020). A resilience assessment framework for critical infrastructure networks' interdependencies. *Water Science and Technology*, *81*(7), 1420–1431. https://doi.org/10.2166/wst.2019.367

JCSS. (2008). Risk Assessment in Engineering—Principles, System Representation & Risk Criteria; The Joint Committee on Structural Safety (JCSS): Zurich, Switzerland.

Kale, A., Thacker, B. H., Sridhar, N., & Waldhart, C. J. (2004). A probabilistic model for internal corrosion of gas pipeline. *International Pipeline Conference, Alberta,Canada*, *IPC 2004-483*, 1–9.

Kammouh, O., Gardoni, P., & Cimellaro, G. P. (2019). Resilience assessment of dynamic engineering systems. *MATEC Web of Conferences*, *281*, 01008. https://doi.org/10.1051/matecconf/201928101008

Li, C.-C. & Der-Kiureghian, A. (1993). "Optimal discretization of random fields", ASCE, J. Eng. Mech., 119 (6), 1136-1154.

Minaie, E., & Moon, F. (2017). Practical and Simplified Approach for Quantifying Bridge Resilience. *Journal of Infrastructure Systems*, *23*(4). https://doi.org/10.1061/(ASCE)IS.1943-555X.0000374.

National Infrastructure Advisory Council (NIAC). (2009). Critical Infrastructure Resilience: Final Report and Recommendations. National Infrastructure Advisory Council.

Nocera, F., Gardoni, P., & Cimellaro, G. P. (2019). Time-Dependent Probability of Exceeding a Target Level of Recovery. *ASCE-ASME Journal of Risk and Uncertainty in Engineering Systems, Part A: Civil Engineering*, *5*(4), 04019013. https://doi.org/10.1061/ajrua6.0001019

Noortwijk, J. M. V. (2009). A survey of the application of gamma processes in maintenance. *Reliability Engineering and System Safety*, *94*, 2–21. https://doi.org/10.1016/j.ress.2007.03.019

Nyborg, R. (2002). Overview of CO2 Corrosion Models for Wells and Pipelines. *Corrosion 2002*. *02233*, 1–16.

Ossai, C. I., Boswell, B., & Davies, I. J. (2016). Application of Markov modelling and Monte Carlo simulation technique in failure probability estimation - A consideration of corrosion defects of internally corroded pipelines. *Engineering Failure Analysis*, *68*, 159–171. https://doi.org/10.1016/j.engfailanal.2016.06.004

Pandey, M. D. (1998). Probabilistic models for condition assessment of oil and gas pipelines. *NDT&E International*, *31*(5), 349–358.

Pant, R., Barker, K., Ramirez-Marquez, J. E., & Rocco, C. M. (2014). Stochastic measures of resilience and their application to container terminals. *Computers and Industrial Engineering*, *70*(1), 183–194. https://doi.org/10.1016/j.cie.2014.01.017

Quiel, S. E., Marjanishvili, S. M., & Katz, B. P. (2016). Performance-Based Framework for Quantifying Structural Resilience to Blast-Induced Damage. *Journal of Structural Engineering*, *142*(8). https://doi.org/10.1061/(ASCE)ST.1943-541X.0001310

Reddy, R. S., Payal, G., Karkulali, P., Himanshu, M., Ukil, A., & Dauwels, J. (2016). Pressure and flow variation in gas distribution pipeline for leak detection. *Proceedings of the IEEE International Conference on Industrial Technology*, *2016*, 679–683. https://doi.org/10.1109/ICIT.2016.7474831

Reed, D. A., Powell, M. D., & Westerman, J. M. (2010). Energy Supply System Performance for Hurricane Katrina. *Journal of Energy Engineering*, *136*(4), 95–102. https://doi.org/10.1061/(asce)ey.1943-7897.0000028

Rose, A., & Liao, S. Y. (2005). Modeling regional economic resilience to disasters: A computable general equilibrium analysis of water service disruptions. *Journal of Regional Science*, *45*(1), 75–112. https://doi.org/10.1111/j.0022-4146.2005.00365.x

Sarwar, A., Khan, F., Abimbola, M., & James, L. (2018b). Resilience Analysis of a Remote Offshore Oil and Gas Facility for a Potential Hydrocarbon Release. *Risk Analysis*, *38*(8), 1601–1617. https://doi.org/10.1111/risa.12974

Sarwar, A., Khan, F., James, L., & Abimbola, M. (2018a). Integrated offshore power operation resilience assessment using Object Oriented Bayesian network. *Ocean Engineering*, *167*, 257–266. https://doi.org/10.1016/j.oceaneng.2018.08.052

Shafieezadeh, A., & Ivey Burden, L. (2014). Scenario-based resilience assessment framework for critical infrastructure systems: Case study for seismic resilience of seaports. *Reliability Engineering and System Safety*, *132*, 207–219. https://doi.org/10.1016/j.ress.2014.07.021

Shang, Q., Wang, T., & Li, J. (2022). A Quantitative Framework to Evaluate the Seismic Resilience of Hospital Systems. *Journal of Earthquake Engineering*, *26*(7), 3364–3388. https://doi.org/10.1080/13632469.2020.1802371

Sharma, N., Tabandeh, A., & Gardoni, P. (2018). Resilience analysis: a mathematical formulation to model resilience of engineering systems. *Sustainable and Resilient Infrastructure*, *3*(2), 49–67. https://doi.org/10.1080/23789689.2017.1345257

Stevens, M., & Tuchscherer, R. (2020). Quantifying a Bridge's Structural Resilience. *Practice Periodical on Structural Design and Construction*, *25*(4). https://doi.org/10.1061/(ASCE)SC.1943-5576.0000517

Sudret, B., & Der Kiureghian, A. (2000). *Stochastic finite element methods and reliability-a state-of-the-art report." Report No. UCB/SEMM-2000/08,* Department of Civil and Environmental Engineering, University of California, Berkeley.

Taleb-berrouane, M., & Khan, F. (2019). Dynamic Resilience Modelling of Process Systems. *Chemical Engineering Transactions*, *77*, 313–318. https://doi.org/10.3303/CET1977053

Tang, L.C., Shen, L., Cassottana, B., Shen, L., & Tang, L.C. (2019). Modeling the recovery process: a key dimension of resilience. *Reliability Engineering and System Safety* 190, 106528.1–106528.10. doi: 10.1016/j.ress.2019.106528.

Todman, L. C., Fraser, F. C., Corstanje, R., Deeks, L. K., Harris, J. A., Pawlett, M., Ritz, K., & Whitmore, A. P. (2016). Defining and quantifying the resilience of responses to disturbance: A conceptual and modelling approach from soil science. *Scientific Reports*, *6*, 1–12. https://doi.org/10.1038/srep28426

Toroghi, S. S. H., & Thomas, V. M. (2020). A framework for the resilience analysis of electric infrastructure systems including temporary generation systems. *Reliability Engineering and System Safety*, *202*, 107013. https://doi.org/10.1016/j.ress.2020.107013

Wang, J., Cao, R., & Sun, Z. (2021). Importance Sampling for Time-Variant Reliability Analysis. *IEEE Access*, *9*, 20933–20941. https://doi.org/10.1109/ACCESS.2021.3054470

Wang, Z., Mourelatos, Z. P., Li, J., Baseski, I., & Singh, A. (2014). Time-dependent reliability of dynamic systems using subset simulation with splitting over a series of correlated time intervals. *Journal of Mechanical Design, Transactions of the ASME*, *136*(6). https://doi.org/10.1115/1.4027162

Wu, Y., Chen, Z., Gong, H., Feng, Q., Chen, Y., & Tang, H. (2021). Defender–attacker–operator: Tri-level game-theoretic interdiction analysis of urban water distribution networks. *Reliability Engineering and System Safety*, *214*, 107703. https://doi.org/10.1016/j.ress.2021.107703

Yodo, N., Wang, P., & Zhou, Z. (2017). Predictive resilience analysis of complex systems using dynamic bayesian networks. *IEEE Transactions on Reliability*, *66*(3), 761–770.

Youn, B. D., Hu, C., & Wang, P. (2011). Resilience-driven system design of complex engineered systems. *Journal of Mechanical Design, Transactions of the ASME*, *133*(10). https://doi.org/10.1115/1.4004981

Yousef, Y. A., Imtiaz, S., & Khan, F. (2021). Subsea Pipelines Leak-Modeling Using Computational Fluid Dynamics Approach. *Journal of Pipeline Systems Engineering and Practice*, *12*(1), 04020056. https://doi.org/10.1061/(asce)ps.1949-1204.0000500

Zeng, Z., Fang, Y. P., Zhai, Q., & Du, S. (2021). A Markov reward process-based framework for resilience analysis of multistate energy systems under the threat of extreme events. *Reliability Engineering and System Safety*, *209*, 107443. https://doi.org/10.1016/j.ress.2021.107443

Zhang, J., & Ellingwood, B. (1994). Orthogonal series expansion of random fields in reliability analysis. *J. Eng. Mech., ASCE*, vol. 120, no 12, p. 2660-2677.

Zhao, S., Liu, X., & Zhuo, Y. (2017). *Hybrid Hidden Markov Models for resilience metrics in a dynamic infrastructure system*. *164*, 84–97.

Zhou, Y., Wang, J., & Yang, H. (2019). Resilience of Transportation Systems : Concepts and Comprehensive Review. *IEEE Transactions on Intelligent Transportation Systems*, *20*(12), 4262–4276.

Zinetullina, A., Yang, M., Khakzad, N., & Golman, B. (2020). Dynamic resilience assessment for process units operating in Arctic environments. *Safety in Extreme Environments*, *2*(1), 113–125. https://doi.org/10.1007/s42797-019-00008-3

Zinetullina, A., Yang, M., Khakzad, N., Golman, B., & Li, X. (2021). Quantitative resilience assessment of chemical process systems using functional resonance analysis method and Dynamic Bayesian network. *Reliability Engineering and System Safety*, *205*, 107232. https://doi.org/10.1016/j.ress.2020.107232

Chapter 6

Reliability-Based Design Optimization of Complex Offshore Structure

Preface

A version of this chapter is under review in ***Reliability Engineering and System Safety Journal****. I am the primary author that produced this work, along with Co-authors Faisal Khan and Salim Ahmed. I reviewed the relevant literature and developed a framework for variable dependency in the reliability-based optimization of offshore structures. I prepared the original manuscript, carried out formal analysis and software implementation, reviewed and revised the manuscript following the co-authors' feedback. Co-author Faisal Khan assisted in the concept development and methodology refinement, supervision, funding for the work, reviewing, and editing of the manuscript. Co-author Salim Ahmed assisted in concept development and methodology, research supervision, reviewing, and manuscript editing.*

Abstract

A trade-off between cost and safety is essential in the reliability-based design of offshore support structures operating in uncertain harsh environments. This study proposes a dependence-based double-loop optimization framework for complex structural systems under such environmental conditions. It considers the dependency of the environmental variables using a D-vine copula. The reliability (inner loop of the design cycle) is modeled using the adaptive PCK approach as a metamodel. The study employs a hybrid optimization approach that combines Genetic Algorithm (GA) and Sequential Quadratic Programming (SQP) in the outer loop optimization phase. The dependency effect is demonstrated on a steel column and a deepwater segmented SCR at various hang angles to the offshore structure. The study shows the importance of multivariate dependence modeling in the RBDO process. It also highlights the significance of : i) optimal copula selection,

ii) the impact of variable order in the D-vine copula's dependence tree, and iii) the efficiency provided by the PCK metamodel. The method described in this study provides a road map for a dependency-based optimal design of complex ocean structures. Also, it allows for strategic design decision-making under uncertainty, considering cost and safety.

Keywords: Steel Catenary Riser, Reliability-Based Design Optimization, Copula Functions, Polynomial Chaos Kriging, Reliability.

6.1. Introduction

In traditional structural optimization problems, uncertainty is considered using partial safety factors. However, partial safety factors present an implicit and conservative approach to accounting for uncertainty in optimization. This approach can lead to increased cost and raises questions about the safety of the structural design (Ditlevsen and Madsen, 1996). Uncertainty exists in structural systems, and its explicit consideration during optimization cannot be over-emphasized. The main aim of every design is to achieve the desired safety while minimizing the cost as much as practicable. Hence, a trade-off between the safety and cost of a structure considering uncertainty during the service life is essential. Reliability-Based Design Optimization (RBDO) extends the concept of Deterministic Design Optimization (DDO) by considering the uncertainties in the structural system, such as those related to loading, material, and the model.

RBDO is an active area of research with a growing number of contributions to the field. The RBDO concept considers the best trade-off between a given structural system's safety and economic cost. The approach allows designers to incorporate uncertainty while achieving the desired performance at a minimal cost.

For RBDO problems, the double-loop, mono-level, and decoupled approaches are the three commonly used methods for optimization under uncertainty(Yi et al., 2016). A vast amount of research contribution using the double-loop (Dutta, 2020; Slowik et al.,2021; Qi et al., 2022; Chaudhuri et al.,2020), mono-level (Yang et al.,2021b; Yang et al., 2020), and decoupled techniques (Zhang et al.,2021; Sohouli et al., 2018; Li et al.,2019) are available in the literature. The double-loop RBDO is a nested approach that comprises an inner loop reliability phase and an outer loop optimization phase. The mono-level method, also called the Single Loop Approach (SLA), utilizes the Karush-Kuhn-Tucker (KKT) condition (Kuschel & Rackwitz, 1997) to solve optimization problems. Furthermore, the decoupled approach solves a deterministic optimization and reliability problem sequentially. The SORA method is a typical decoupled method (Du & Chen, 2004). SORA involves converting probabilistic constraints to deterministic ones using a shifting vector. Other decoupling RBDO methods include the B-Spline approach (Dizangian & Ghasemi, 2016), the threshold shift method (Goswami et al., 2019), and the evidence-based decoupling approach (Huang & Jiang, 2017).

These methods of RBDO have their drawbacks in implementation. Among the significant challenges with the mono-level and decoupled approach is the difficulty in dealing with multiple failure domains and convergence issues, especially with nonlinear LSF (Dubourg et al., 2011). The double-loop approach provides high accuracy and ease of implementation; this is not without its problem of high computational cost. The use of metamodels and a simulation-based reliability approach in the inner loop for an RBDO problem further improves the computational cost and efficiency of the double-loop method (Moustapha & Sudret, 2019).

The application of the concept of RBDO to structures spreads across various engineering disciplines as the quest remains to obtain an optimally safe design at a minimal cost. RBDO has

gained tremendous research acceptance and application in diverse engineering design fields, including civil engineering (Ni et al.,2021; Peng et al.,2021) and manufacturing (Liu et al., 2018; Yang et al.,2021a). Other areas with significant research application of the RBDO technique include automobile systems (Wang et al.,2020**),** marine structural design (Eamon & Rais-Rohani, 2009; Karadeniz et al.,2009; Gholinezhad & Hosein, 2021; Debiao et al.,2020; Yan et al.,2017), and aerospace (Song et al., 2021; Nguyen et al., 2022; Tekaslan et al., 2021). The research contribution to RBDO includes renewable energy structures (Lee et al.,2014; Leimeister & Kolios,2021**;** Yang et al.,2018) and systems for nuclear power plants (Velayudhan et al., 2021).

With the presented drawback of the double-loop approach, the use of metamodels which provides a computationally cheap option to evaluate LSF, is viable for computational cost reduction in RBDO analysis, especially for complex engineering systems such as oil and gas support structures (Moustapha & Sudret, 2019). The use of metamodel for complex, difficult-to-evaluate systems has been a typical approach for reliability-based problems. Metamodels replace the time-consuming use of the FEA for RBDO and improve the computational cost.

Different metamodels have been utilized for RBDO analysis in recent times. Amongst these are the Kriging metamodel (Kim & Song, 2021; Ni et al., 2020; Lacaze & Missoum, 2013; Cui et al., 2020; Zhang et al., 2021; Fathima Sana et al., 2022; Li et al., 2022; Jung et al., 2022; Jiang et al., 2021; Xiao et al.,2020), the response surface method, also called polynomial regression (Li, 2013; Youn & Choi, 2004; Shi & Lin, 2016; Lee,2019), PCE (Dutta & Putcha, 2020; Lopez et al., 2017) and the SVR approach (Strömberg, 2018). For a complex engineering system with no closed-form LSF, a combination of metamodel types to improve the accuracy of the constructed LSF is essential (Stromberg, 2019). This study uses the combined advantage of the interpolation approach

(Kriging) and the regression PCE method to develop a metamodel for the probability constraints (hard constraints) of the double-loop RBDO optimization problem.

The accuracy of optimizing complex structures with no closed-form LSF is essential. Copulas play a vital role and help capture the nonlinear correlation and tail dependence between variables where such a relationship exists. A few attempts have been made to consider copula in structural optimization under uncertainty. Wang et al. (2020) studied the influence of individual copulas on vehicle body crashworthiness optimization. Although unable to capture nonlinear and tail dependence (Lebrun & Dutfoy, 2009), the Gaussian copulas have been utilized to model dependency in structural optimization cases (Choi et al., 2007; Noh et al., 2009; Shuai et al., 2019). Also, the concept of copula has been implemented in a two-dimensional evidence-based design optimization problem (Huang et al., 2019) and bivariate RBDO problems using Clayton and Frank copula (Kuczera et al., 2010). For ocean structures, the environment in which they operate is uncertain, and the interaction with the ocean environment poses a risk to the ability of these structures to perform their intended function. The need to capture and better understand interactions between ocean variables (linear, nonlinear, and possible tail dependence) is essential to account for uncertainties and make efficient optimal design decisions related to the tradeoff between the engineering design costs and the safety of these structures.

Dependence-based RBDO has not been well explored in the literature, especially for multivariate systems. Typically, variables (environmental and design) are assumed to be independent. However, with the ocean environment's complexity and the operating structures' safety-sensitive nature, the dependency between environmental variables needs to be considered in an RBDO design context. This study attempts to fill this gap by developing an approach that considers the multivariate dependence between environmental variables during structural optimization.

In the light of considering dependency and ensuring improved computational efficiency in nested RBDO problems, this study aims to:

1. Provide an efficient design framework for RBDO using the D-vine copula and capture the dependence between the environmental variables affecting the offshore structural system.
2. Develop an optimization case that considers a hybrid metamodel to improve the inner loop's computational accuracy, cost, and time in a nested RBDO approach.

The remainder of this study is organized as follows: Section 6.2 describes the preliminaries of RBDO, vine copulas, metamodels, and optimization. Section 6.3 details the methodology for the RBDO concept. Section 6.4 presents an illustrative example (Steel Column Function) and a case study of optimizing a segmented SCR under uncertain harsh operating conditions. Section 6.5 discusses the results related to the Steel Column Function and SCR. Section 6.6 concludes the study.

6.2. RBDO Formulation and Preliminaries

This section describes the essential elements for implementing the dependency-based RBDO problem ranging from problem formulation and dependency modeling to the integral constituent of the double-loop process (inner loop reliability and outer loop optimization).

6.2.1. RBDO problem formulation

Optimization problems comprise an objective function herein referred to as a cost function $c(d)$ and a set of constraints to be satisfied. From a structural perspective, the cost function in the optimization case mainly refers to minimizing dimensions such as weight, mass, and volume, which can have a financial implication on the design. Eq. (6.1) shows the general formulation of an RBDO problem.

$$d^* = \min_{d \in D} c(d)$$

$$\text{subject to } \begin{cases} m_j(d) \leq 0 \\ P_r(g_h(X(d), Z) \leq 0) \leq \hat{P}_{fh} \end{cases} \quad (6.1)$$

Where $j = 1,2,3 \ldots . s$ and $h = 1,2,3 \ldots n$ from Eq. (6.1).

d^* represents the optimal values, and the term $m_j(d)$ represents the soft constraints, which are simple functions that bound the design space. The probabilistic constraints ((Eq. (6.1)), otherwise called the hard constraints, are represented by the LSF $g_h(.)$ which is a function of the design $X(d)$ and environmental (Z) variables. For the design variables, the designer can exercise control over them and, consequently, be optimized. The desired safety levels of the structure are essential in the RBDO implementation; and expressed using the target failure probability $(\hat{P}_{fh})$ as shown in Eq. (6.1).

Eqs. (6.2) and (6.3) show the relationships between the target and system reliability indices $(\hat{\beta}_h, \beta_h)$ and the corresponding failure probabilities $(\hat{P}_{fh}, P_{fh})$. The symbol Φ represents the standard normal cumulative Gaussian distribution.

$$\hat{P}_{fh} = \Phi(-\hat{\beta}_h) \quad (6.2)$$

$$P_{fh} = \Phi(-\beta_h) \quad (6.3)$$

Consequently, the optimization problem described in Eq. (6.1) can be formulated in terms of β_h as shown in Eq. (6.4)

$$d^* = \min_{d \in D} c(d)$$

$$\text{subject to } \begin{cases} m_j(d) \leq 0 \\ \hat{\beta}_h - \beta_h(X(d), Z) \leq 0) \end{cases} \quad (6.4)$$

Where $j = 1,2,3 \ldots\ldots s$ and $h = 1,2,3 \ldots n$

In fulfilling the constraint requirement of the optimization problem, then $P_{fh} \leq \hat{P}_{fh}$ and $\beta_h > \hat{\beta}_h$

6.2.2. Copula Functions (D-vine Copula)

The Pearson correlation coefficient between variables only measures linear dependence and cannot capture nonlinearity and tail dependence. Copulas are flexible with uniform marginals and link the marginals of random variables with the joint CDF; they provide a means to handle nonlinearity and tail dependence relationships effectively between variables. The concept of copulas was initially used in financial mathematics but has recently gained wide application in modeling dependency between variables in other fields. The joint PDF decomposition results in the marginal distribution and associated copula functions. The approximation of the CDF using copulas is adequately described by Sklar's theorem (Nelsen.,2006), as shown in Eqs. (6.5) and (6.6).

$$F(z_1, z_2, \ldots\ldots z_n) = C\big(F_1(z_1), F_2(z_2) \ldots\ldots F_n(z_n)\big) \tag{6.5}$$

$$f(z_1, z_2, \ldots\ldots z_n) = c\big(F_1(z_1), F_2(z_2) \ldots\ldots F_n(z_n)\big) \prod_{i=1}^{n} f_i\,(z_i) \tag{6.6}$$

Where $z_1, z_2, \ldots\ldots z_n$ represent *n* random variables. $F(.)$the joint probability distribution function, $f(.)$ the joint PDF. Also, $C(.)$ is the copula function, and $c(.)$ copula density function.

A copula that can capture multivariate and conditional dependence between variables using pair-copula decomposition is the vine copula (Bedford & Cooke, 2002). A vine copula is a graphical object which comprises nodes, edges, and trees. Also, using different bivariate copula functions, the vine copula approach can decompose a multivariate function. The D-vine and C-vine are the most common vines applied to multidimensional dependence problems. The C-vine is utilized for dependence modeling when there is a leading variable; otherwise, the D-vine configuration is

selected (Aas et al., 2009). The expression for the D-vine and C-vine are shown in Eqs. (6.7) and (6.8), respectively.

$$f(z_1 \dots . z_n)$$

$$= \prod_{k=1}^{n} f(z_k) \prod_{j=1}^{n-1} \prod_{i=1}^{n-j} c_{i,i+j|i+1\dots i+j-1} \left\{F\left(z_i \middle| z_{i+1} \dots \dots, z_{i+j-1}\right), F\left(z_{i+j} \middle| z_{i+1} \dots \dots, z_{i+j-1}\right)\right\} \quad (6.7)$$

$$f(z_1 \dots . z_n)$$

$$= \prod_{k=1}^{n} f(z_k) \prod_{j=1}^{n-1} \prod_{i=1}^{n-j} c_{j,j+i|1\dots j-1} \left\{F\left(z_j \middle| z_1 \dots \dots, z_{j-1}\right), F\left(z_{j+i} \middle| z_1 \dots \dots, z_{j-1}\right)\right\} \quad (6.8)$$

The notations i and j (Eqs. (6.7) and (6.8)) represent the edges and trees of the vine copula expression. Also, $F_1(z_1) = u_1 \dots . F_n(z_n) = u_n$ for n variables described in Eqs. (6.5) to (6.8). For subsequent trees beyond the first tree of the D-vine copula, the conditional distribution for the pair-copula construction is given by Eq. (6.9).

$$F(z|\mathbb{v}) = \frac{\partial C_{z,\mathbb{v}_j|\mathbb{v}_{-j}}\{F\left(z\middle|\mathbb{v}_{-j}\right), F\left(\mathbb{v}_j\middle|\mathbb{v}_{-j}\right)\}}{\partial F(\mathbb{v}_j|\mathbb{v}_{-j})} \quad (6.9)$$

Where $\mathbb{v}$ is the vector of random variables, $\mathbb{v}_j$ represents an arbitrarily chosen component of the vector $\mathbb{v}$ and $\mathbb{v}_{-j}$ is the vector $\mathbb{v}$, which excludes component $\mathbb{v}_j$. Appendix 6A (Table 6A.1) presents the h function required in conditional copula determination.

The different copula functions with varying properties create flexibility in determining dependence between variables. This study utilizes commonly used elliptical (Gaussian, Student t) and Archimedean copulas (Gumbel, Clayton, Frank) in the determination of optimal copula for the environmental variables in the RBDO analysis (Appendix 6A, Table 6A.1 and 6A.2). The MLE

method determines the copula parameter (θ). The AIC defines the information loss generated while obtaining θ (Eqs. (6.10) to (6.12)). Consequently, a minimum AIC value determines the best-fit copula type for the random variables considered.

$$InL(\theta) = \prod_{i=1}^{n} c(u_1 \dots u_n; \theta) = \sum_{i=1}^{n} Inc(u_1 \dots u_n; \theta) \tag{6.10}$$

$$\frac{\partial InL(\theta)}{\partial \theta} = 0 \tag{6.11}$$

$$AIC = -2InL(\theta) + 2K \tag{6.12}$$

where $L(\theta)$ is the loglikelihood function, K is the number of model parameters, $u_1 \dots u_n \in [0,1]$ (standard uniform input variables).

In copula determination, the Kendall Tau Coefficient (τ_k), which is a measure of dependence is adopted. The coefficient τ_k is non-parametric, independent of the marginal distribution, and measures the strength of association based on the concordance and discordance between paired variables (Joe, 2014). An expression for τ_k is shown in Eq. (6.13).

$$\tau_k = 4 \int_{-1}^{1} \int_{-1}^{1} C(u_1, u_2|\theta) dC(u_1.u_2) - 1 \tag{6.13}$$

The non-parametric coefficient τ_k determines the independence test between variables as shown in Eq. (6.14), with n being the number of observations.

$$\sqrt{\frac{9n(n-1)}{2(2n+5)}} |\tau_k| < 1.96 \tag{6.14}$$

The null hypothesis of independence is accepted if Eq.(6.14) is satisfied at a 5% confidence interval (Genest & Favre, 2007).

This study utilizes the D-vine copula for the dependence modeling of the variables, and the order of the first tree is such that the strongest variable dependence is created. The first tree variable order is achieved by determining the shortest Hamiltonian Path using the weighted absolute $1 - |\tau_k|$ and solving a traveling salesman's problem (Brechmann,2010).

6.2.3. Metamodel construction and reliability for RBDO

Metamodels reduce the computational burden and complexity of analysis obtained from numerical models. Although several metamodels have been utilized in the reliability studies of complex systems, the two commonly used methods are Kriging (interpolation) and PCE (regression). Kriging interpolates the local variability of the output as a function of the input variables, and PCE determines the global response behavior using a set of orthogonal polynomials (Schöbi et al., 2015). The PCK (Eq. (6.15)) approach takes advantage of the unique properties of Kriging and PCE to construct a metamodel with improved performance and computational efficiency. PCK is a hybrid metamodel developed from ordinary Kriging and PCE metamodels. Okoro et al.(2021) demonstrated improved PCK metamodel outcomes compared to Kriging and PCE for structural reliability assessment and provided further details on both methods individually. A Kriging metamodel comprises two parts which are the trend and stochastic process terms. For PCK, the trend term is a weighted sum of multivariate orthogonal polynomials, as shown in the first part of Eq. (6.15). and the stochastic component is given by ($\sigma_g^2 T(z)$). The symbol $\Psi_\alpha(z)$ represents the multivariate orthogonal polynomial function with coefficient y_α. For the trend term, a tensor product of univariate polynomial results in the orthogonal function $\Psi_\alpha(z)$ (Eq. (6.16)).

$$y \approx M^{PC-K}(z) = \sum_{\alpha=A} y_\alpha \Psi_\alpha(z) + \sigma_g^2 T(z) \qquad (6.15)$$

$$\Psi_{\alpha}(Z) = \prod_{i=1}^{M} \Psi_{\alpha}^{(i)}(Z_i) \tag{6.16}$$

Where σ_g^2 is the variance of the Gaussian process and $T(z)$ represents the stationary Gaussian process. The stochastic term (Eq.(6.15)) is determined from a range of autocorrelation functions, including linear, Gaussian, exponential, and the Materń function (Schöbi et al., 2015). This study utilizes the Materń autocorrelation function which is more generic than others described (Santner et al.,2003). The orthogonal polynomial for the trend term (Eq.(6.15)) can be attributed to specific probability distribution (Xiu & Karniadakis, 2002); they grow with increased input variable dimension, and truncation of terms is achieved using the LARS method with consideration of only the non-zero terms (Blatman & Sudret, 2011). The computational efficiency of the PCK approach can be improved by an adaptive process that approximates the metamodel close to the limit state surface. The adaptive approach of the metamodel is implemented by enriching the ED and selecting the next best point in an iterative pattern from a candidate sample pool until the required stopping criterion is achieved. Learning functions that drive the adaptive process include EGO (Jones et al.,1998), EFF (Bichon et al.,2008), H function (Lv et al.,2015), LIF (Sun et al.,2017), and U function (Echard et al., 2011). This study adopts the U learning function due to its fast convergence and simplicity in implementation. The U learning function enriches the ED based on the probability of misclassification of samples. The expression for the U learning function with the predicted mean $\mu_{\hat{g}}(z,x)$ and standard deviation ($\sigma_{\hat{g}}(z,x)$) using the PCK model is presented in Eq. (6.17). Also, Eq. (6.18) shows the next best point (z_{next}, x_{next}) selected from the candidate MCS pool (*S*) for the enrichment of the ED.

$$U(z,x(d)) = \frac{\left|\mu_{\hat{g}_h}(z,x(d))\right|}{\sigma_{\hat{g}_h}(z,x(d))} \tag{6.17}$$

$$(z_{next}, x(d)_{next}) = arg \min_{z^i \epsilon S} \left(U\left(z^i\right) \right) \tag{6.18}$$

In this study, the stopping criterion for ED enrichment using the U learning function is achieved when $U(z_{next}, x(d)_{next}) > 2$. The PCK metamodel is constructed in the so-called augmented space of the environmental and design variables (Kharmanda et al., 2002; Moustapha et al., 2016; Taflanidis & Beck, 2008; Zhang et al., 2017). The augmented space prevents the cumbersome nature of building a new model at every iteration step by constructing a global metamodel in the input space of both the design and environmental variables. The metamodels in this space are reusable during the RBDO iteration phase and reduce likely model construction inefficiency during iteration. For the constructed PCK metamodel, the quality of the metamodel can be determined using the leave one out cross-validation error (ε_{LOO}) as shown in Eq. (6.19).

$$\varepsilon_{LOO} = \frac{1}{n}\left[\frac{\sum_{i=1}^{n}\left(M\left(x_i(d), z_j\right) - M_{\hat{Y},(-i)}\left(x_i(d), z_j\right)\right)^2}{Var(y)}\right] \tag{6.19}$$

n is the number of sample points, $Var(y)$ is the response data variance, $M_{\hat{Y},(-i)}(.)$ is the model response with the exclusion of a data point from ED. $M(.)$ represents the model response considering all input variables in the ED. The input design and environmental variables of the ED are denoted by $x_i(d)\ and\ z_j$, respectively.

In this study, the reliability of the adaptive process (inner loop of the RBDO problem) described in this section is computed using the MCS in the input space. The CoV from the MCS serves as a convergence criterion that can adaptively increase the sample pool (*S*) during the active learning reliability process (Eq. (6.20)). The failure probability using the MCS simulation approach (P_{fMC}) is obtained from the number of samples (N_f) that violates the constructed LSF where the total

sample population is N_{mcs} (Eq. (6.21)). A violation of the LSF occurs when $g_h(X(d), Z) \leq 0$ (Eq. (6.1)).

$$CoV = \sqrt{\frac{1 - P_{fMC}}{(N_{mcs} - 1)P_{fMC}}} \tag{6.20}$$

$$P_{fMC} = \frac{N_f}{N_{mcs}} \tag{6.21}$$

In this paper, a CoV $\leq$ 5% is utilized as the convergence criterion for the MCS in the inner RBDO loop.

6.2.4. RBDO Outer Loop Optimization

To determine the optimal values of $C(d)$ (Eq. (6.1)) subject to the specified constraints, the outer loop of the RBDO is evaluated as an optimization problem. The gradient-free and gradient-based methods are typical approaches utilized for optimization. Gradient-free optimization methods such as (Genetic Algorithms (GA), evolutionary strategies, and PSO can determine optimal global solutions. In contrast, gradient-based methods such as (Sequential Quadratic Programming (SQP) and Interior Point Method) are effective strategies for obtaining local optimal solutions (Meng et al., 2021). This paper adopts a hybrid approach using a combination of GA and SQP in the optimization phase of the double-loop RBDO. The optimization phase is implemented using *fmincon* (minimizing constrained, nonlinear, and multivariate functions), a MATLAB built-in function. First, a global optimal is obtained using GA and refined using SQP. The GA approach is gradient-free, biologically inspired, and can deal with complex optimization problems. GA optimization starts with an initial random population where good strings are selected for the mating pool (reproduction), the crossover process creates new generations, and the mutation operators

alter the offspring. The GA process undergoes successive iterations (generations) until convergence is attained. Katoch et al.(2021) provide further details on the concepts and terminologies of GA. Also, the SQP approach is efficient and offers fast convergence; it can handle constrained, differentiable, nonlinear, and convex optimization problems. In the SQP optimization phase, the gradient of the cost function is obtained using a finite difference approach. The Lagrangian function whose gradient satisfies the KKT necessary optimality condition at the optimal values of the objective function and applicable lagrangian multipliers is developed, leading to a quadratic subproblem formulation solved at every iteration. The corresponding positive definite Hessian matrix of the Lagrange function is updated at every iteration stage using Newton's approach until convergence is achieved. Further details can be found in (Rao,2019).

6.3. The Methodology (RBDO with dependence)

This section describes the steps for structural optimization under uncertainty using the double-loop RBDO approach and considering the dependency of the environmental variables. Figure 6.1 shows a flowchart of the process.

Step 1: *Determine input parameters, optimization function, and associated data*

Identify the RBDO input variables (environmental and design), the corresponding probability distributions with design bounds, and collect associated variable data that describe the structure's performance for the optimization process. Also, determine the RBDO cost function that requires optimization considering possible constraints, including the target failure probability or reliability index to be satisfied. The RBDO formulation in (Section 6.2, Eqs. (6.1) to (6.4)) clearly describes these essential design elements.

Step 2: *Dependence modeling of environmental variables*

For the environmental variables described in Step 1, model their dependency using vine copula as described in (Section 6.2, Eqs. (6.5) to (6.8)). This study assumes the non-existence of a leading variable and utilizes the D-vine copula (Eq. (6.7)) for dependence modeling. The D-vine copula is flexible and can capture possible multivariate dependence (linear, nonlinear, or tail dependence) between variables, as described in Section 6.2. For the D-vine structure, the order of variables in the first tree of the D-vine is determined using the shortest Hamiltonian path, as described in Section 6.2. The selection of optimal copula for the vine tree is made from Gaussian, Student t, Clayton, Gumbel, and Frank (bivariate) copulas. Copula parameters evaluation and optimal copula selection (including the test for independence) for the vine tree is determined using the MLE and AIC criteria described in (Section 6.2, Eqs. (6.9) to (6.14)). Furthermore, with the marginals of environmental variables defined by their statistical distributions and associated parameters (obtained by fitting distribution to data) in the input space (Step 1), and the vine structure with optimally selected copula and parameters, the joint PDF is estimated.

Step 3: *Development of sampling strategy for metamodel construction*

Following the joint PDF estimated in Step 2, develop initial sampling points of input variables (initial ED) in the space of the environmental and design variables using a space-filling Latin Hypercube Sampling (LHS) method (Forrester, 2008). The associated structural response for the initial sampling points is determined using a defined LSF or the FEA approach for complex structural systems. The nested RBDO process is utilized in this study and comprises an inner loop reliability phase with an outer loop optimization. The inner loop stage is carried out by first adaptively constructing a metamodel within an augmented space. A metamodel is computationally cost-effective and approximates the LSF of the complex system. The developed metamodel is

required for the inner loop reliability assessment (failure probability evaluation). Also, the metamodel serves as the probabilistic performance constraint in the optimization phase. The PCK approach is adopted for the inner loop metamodel construction and reliability evaluation in this paper due to its high efficiency and ability to integrate the merits of the global predictive capability of PCE and the local interpolation potential of Kriging, as described in (Section 6.2, Eqs. (6.15) to (6.16)) of this study.

Step 4: *Metamodel construction and inner-loop reliability assessment*

The adaptive PCK metamodel construction starts with the initial ED described in Step 3 and is continually enriched until the stopping criterion is attained, as described in (Eqs. (6.17) to (6.18)). The error from the adaptive PCK metamodel construction is also determined (Eq. (6.19)). In this study, the enrichment process for the adaptive PCK metamodel construction is obtained from an MCS pool of 10^8 sample points. The U learning function is adopted in this paper with its stopping criterion described by U (z, x(d)) $>$ 2. A global adaptive PCK metamodel is developed, which does not change during the RBDO iteration process, making it easy to employ the simulation approach for reliability assessment. Reliability assessment of the constructed metamodel is carried out using the MCS approach described in (Eqs. (6.20) to (6.21)). Reliability is implemented in Uqlab, a MATLAB-based framework for uncertainty quantification and reliability analysis (Marelli & Sudret, 2014). The metamodel developed from this process represents the probabilistic constraint of the RBDO problem.

Step 5: *Outer-loop structural cost optimization*

Further to the inner loop reliability described in Step 4, evaluate the outer loop optimization (minimization) of the cost function of the structure described in Step 1, given the constraints in the

RBDO problem. As presented in Section 6.2, a hybrid approach that combines GA and SQP is utilized for optimization. First, the GA iteratively explores the entire design space until convergence is achieved and obtains a global solution to the cost function using the principle of survival of the fittest. Consequently, an SQP (a gradient-based approach) is utilized to refine the global optimization's outcome (starting point for optimization using SQP). This study uses the forward finite difference approach to obtain gradients with a step size of 0.001. The SQP optimization iteration continues until a minimal cost is attained and the constraints of the cost function, as presented in Eqs. (6.1) to (6.4) are satisfied. The maximum iteration for the SQP approach is set as 10^3. Also, due to the stochasticity and inherent noise of the failure probability obtained using the MCS approach described in Step 4, the common random number strategy is adopted to eliminate this effect in the gradient-based optimization phase. The *common random number* approach involves using the same random seed used in generating the MCS samples for the different iterations stages (Spall, 2003). Furthermore, the large sample size eliminates the introduced error bias. For the first stage optimization using GA, the number of generations and stall generations for iteration are set at 100 and 50, respectively. Also, the initial population size of 20 is utilized for the GA.

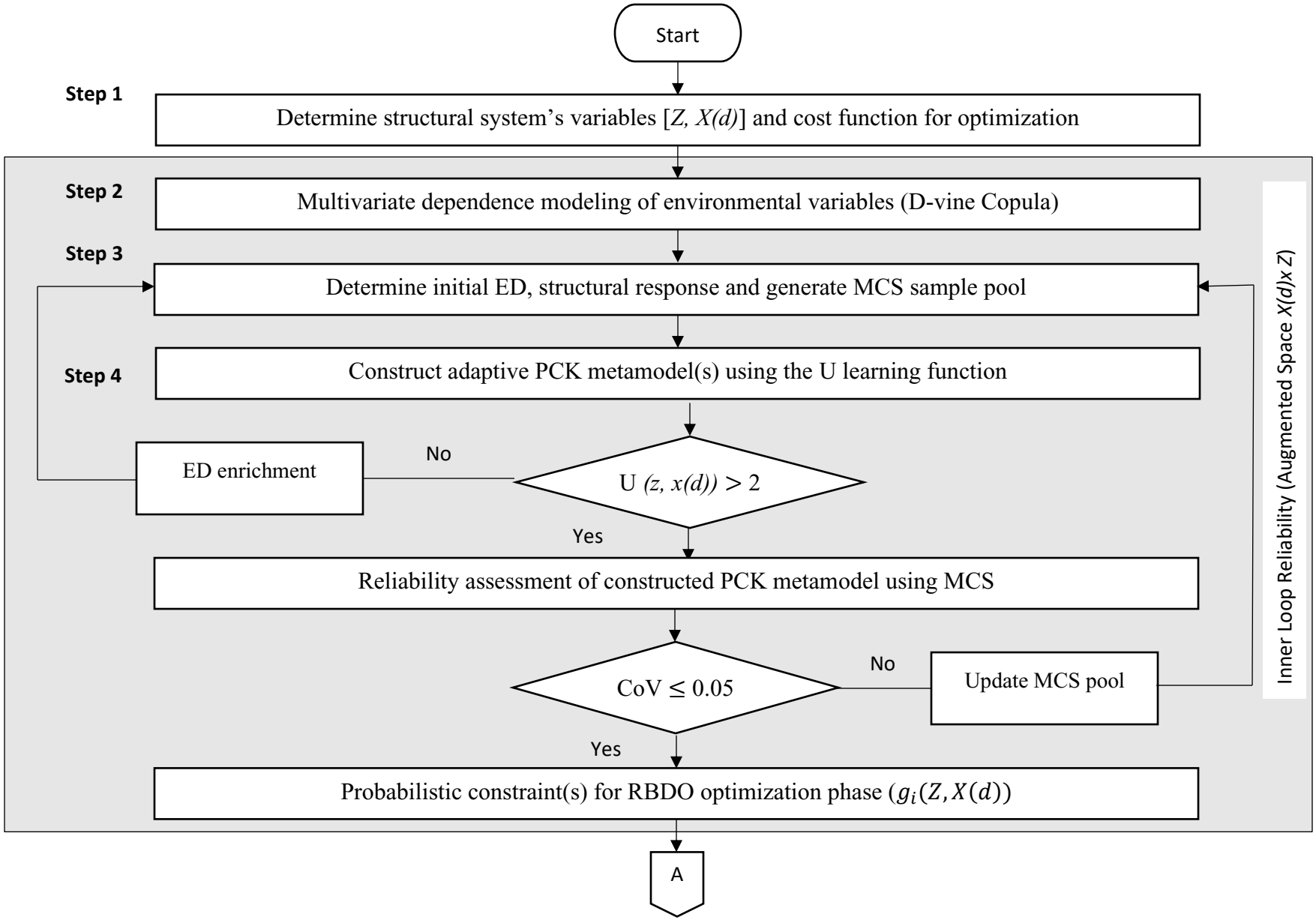
Start
Step 1
Determine structural system's variables [Z, X(d)] and cost function for optimization
Step 2
Multivariate dependence modeling of environmental variables (D-vine Copula)
Step 3
Determine initial ED, structural response and generate MCS sample pool
Step 4
Construct adaptive PCK metamodel(s) using the U learning function
No
ED enrichment
U (z, x(d)) > 2
Yes
Reliability assessment of constructed PCK metamodel using MCS
No
CoV ≤ 0.05
Update MCS pool
Yes
Probabilistic constraint(s) for RBDO optimization phase ($g_i(Z, X(d))$
A
Inner Loop Reliability (Augmented Space X(d)x Z)

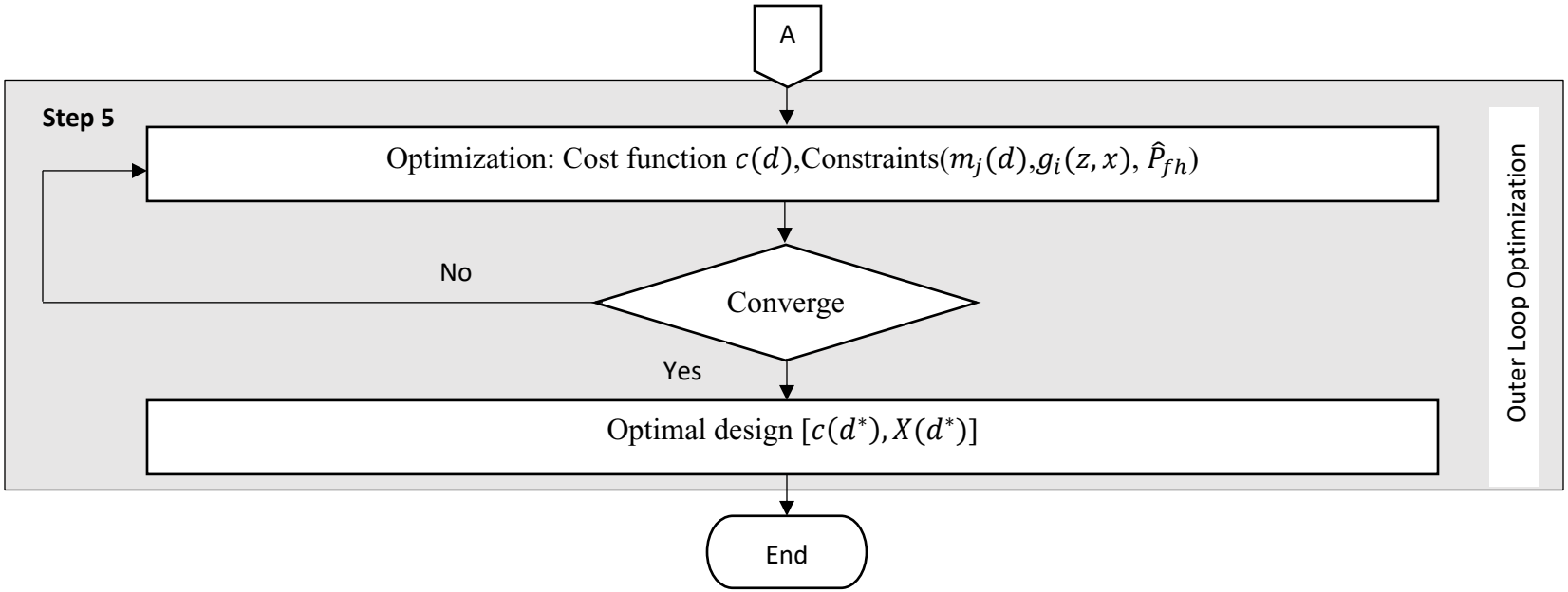

Figure 6.1. Double-loop RBDO flowchart considering variable dependency.

6.4. Application of the RBDO with dependence

This section investigates the effect of dependence modeling on structural optimization under uncertainty using the framework described in Section 6.3. The method is demonstrated using a mathematical example (steel column function) and a practical case study of a deepwater segmented SCR.

6.4.1. Steel Column Function [modified from(Eldred et al., 2008)]

The steel column function is a nine-dimensional RBDO problem and comprises six environmental variables and three design variables. This example investigates the effect of dependency and various copula types in optimizing the steel column under uncertainty. In addition, the impact of the order of load variables in the D-vine first tree on the optimization process is examined.

The problem aims to determine the optimal design variables (b, t, and h) at which C_{sc} is minimized (Eq. (6.22)) subject to the constraint shown in Eq. (6.23). The bounds (upper and lower) of the design variables (b, t, and h) are b= [250 450], t= [5 40], and h = [150 600]; all units are in mm. The target reliability for the steel column is $\hat{\beta}_h$=3

$$C_{sc} = (b * t) + 8 * h \tag{6.22}$$

The adaptive PCK metamodel, which serves as a constraint for the RBDO process, is constructed from Eq. (6.23).

$$g_h(X_d, Z_d) = F_s - F\left(\frac{1}{2bt} + \left(\frac{F_o}{bth} \cdot \left(\frac{\xi_b}{\xi_b - F}\right)\right)\right) \tag{6.23}$$

where ξ_b and F represents the Euler buckling load and the steel column's combined load, respectively. Also, $F = Z_1 + Z_2 + Z_3$ and $\xi_b = \frac{\pi^2 Ebth^2}{2L^2}$.

Table 6.1 shows details of the design and environmental variables of the steel column function. The length of the steel column is given by (L=8000mm).

Table 6.1. Statistical summary of the steel column function variables [modified from(Eldred et al., 2008)].

Variables	Symbol	Distribution	Mean	CoV	Unit
Flange Breath	b	Uniform	μ_b	0.2	mm
Flange Thickness	t	Uniform	μ_t	0.1	mm
Height of Steel Profile	h	Uniform	μ_h	0.3	mm
Yield Stress	F_s	Uniform	400	0.15	MPa
Young's Modulus	E	Uniform	21000	0.1	MPa
Initial Deflection	F_o	Uniform	30	0.1	mm
Dead Weight Load	Z_1	Uniform	600000	0.15	N
Variable Load	Z_2	Uniform	700000	0.1	N
Variable Load	Z_3	Uniform	500000	0.2	N

An independent relationship is assumed between other variables, except the load of the steel column. This study uses a D-vine copula to capture the dependency between the deadweight and variable loads of the function. Dependence modeling of the steel column load is limited to commonly used elliptical and Archimedean pair copulas (Gaussian, Student t, Clayton, Gumbel, and Frank). Also, this study assumes a non-parametric dependence measure (τ_k) between the load variables of the steel column (Table 6.2).

Table 6.2. Non-parametric relationship of steel column loads.

	Z_1Z_2	Z_2Z_3	Z_1Z_3
τ_k	0.85	0.92	0.61

The copula parameters (θ), rotation (θ_R), and possible tail dependence [upper (λ_u) and lower (λ_L)] are determined using expressions described in Appendix 6A (Table 6A.1 and Table 6A.2). In addition, all possible D-vine structures (Figure 6.2) are considered to investigate the impact of the load variable order (first tree) on the steel column optimization.

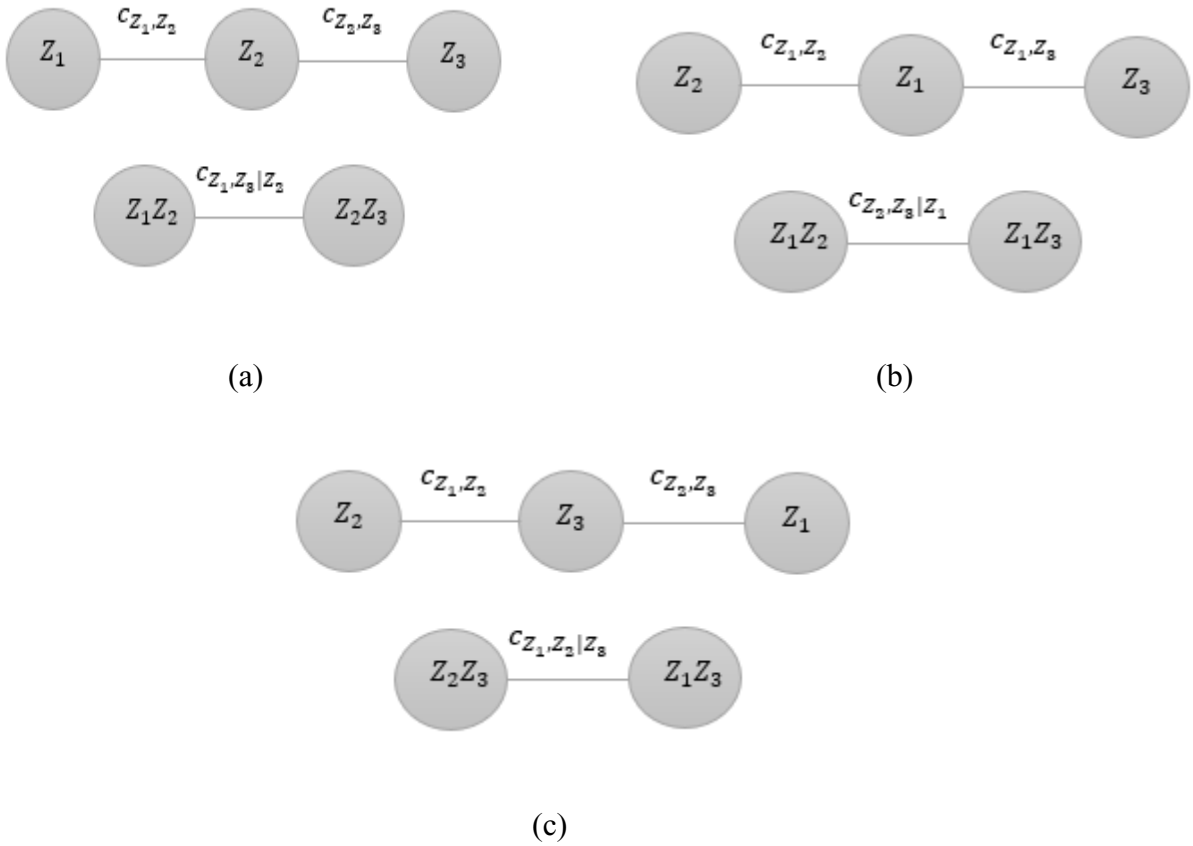

Figure 6.2. D-vine copula configuration for steel column function loads.

In Figure 6.2, the notation c_{Z_1,Z_2}, c_{Z_2,Z_3} and c_{Z_1,Z_3} represents the copula density for the steel column loads in the first tree of the structure. Also, $c_{Z_1,Z_2|Z_3}$, $c_{Z_1,Z_3|Z_2}$ and $c_{Z_2,Z_3|Z_1}$ represent the conditional copula density of the second tree. The evaluated θ and corresponding θ_R for the three D-vine structural configurations using the various copula types considered in this study are presented in Table 6.3.

Table 6.3. D-vine copula parameters and rotations for steel column loads.

D-vine Structure	Copula Type	θ_{Z_1,Z_2}	θ_{Z_2,Z_3}	θ_{Z_1,Z_3}	$\theta_{Z_1,Z_3\|Z_2}$	$\theta_{Z_2,Z_3\|Z_1}$	$\theta_{Z_1,Z_2\|Z_3}$	θ_R (Deg)
$Z_1Z_2Z_3$	Gaussian	0.98	0.89	-	0.91	-	-	(0,0,0)
	Student t	(0.98,4.73)	(0.89,5.64)	-	(0.92,4.64)	-	-	(0,0,0)
	Clayton	10.33	3.77	-	1.66	-	-	(180,180,0)
	Gumbel	7.96	3.39	-	4.10	-	-	(0,0,180)
	Frank	29.39	11.44	-	14.54	-	-	(0,0,0)
$Z_2Z_1Z_3$	Gaussian	0.98	-	0.95	-	-0.78	-	(0,0,0)
	Student t	(0.98,4.73)	-	(0.96,5.09)	-	(-0.8,5.35)	-	(0,0,0)
	Clayton	10.33	-	6.88	-	0.56	-	(180,0,90)
	Gumbel	7.96	-	5.45	-	2.64	-	(0,0,270)
	Frank	29.40	-	19.61	-	6.85	-	(0,0,0)
$Z_2Z_3Z_1$	Gaussian	-	0.89	0.95	-	-	0.96	(0,0,0)
	Student t	-	(0.89,5.64)	(0.96,5.09)	-	-	(0.96,5.61)	(0,0,0)
	Clayton	-	3.77	6.88	-	-	3.89	(0,0,180)
	Gumbel	-	3.39	5.45	-	-	6.45	(0,0,0)
	Frank	-	11.44	19.61	-	-	22.89	(0,0,0)

The pair copula in the D-vine structure can capture non-linear dependence and the degree of tail dependence between steel column load variables, as shown by the scatter plot in Figure 6.3.

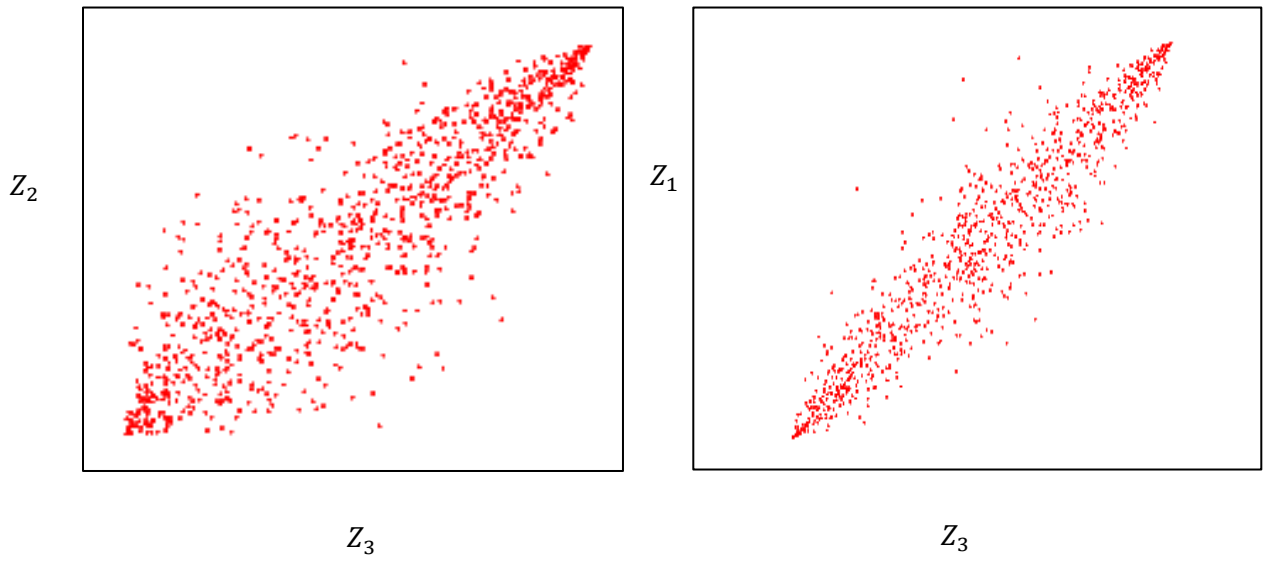

Gumbel (λ_u = 0.77)

Student t (λ_u=λ_L=0.72)

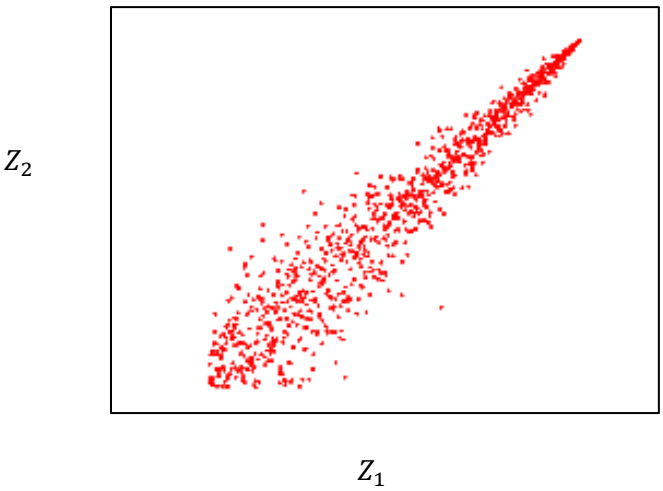

Clayton (λ_u=0.94, θ_R=180^o)

Figure 6.3. Steel column function scatter plots of bivariate copulas.

The scatter plot (Figure 6.3) shows the nonlinearity between the environmental variables and also captures upper and lower tail dependence between variables Z_1 and Z_3 using the Student t copula, upper tail dependence between variables Z_2 and Z_3 using the Gumbel copula. The rotated Clayton copula also captures the tail dependence between variables Z_2 and Z_1.

This study utilizes the double-loop RBDO approach comprising a reliability analysis in the inner loop with an outer loop optimization. With the LSF (Eq. (6.23)), an adaptive PCK metamodel is developed using the approach described in Section 6.2. First, an initial ED sample of random input variables using 20 LHS sample points in the input space is created. The learning (U function) and enrichment of ED are carried out until convergence is attained based on the stopping criteria (Figure 6.1). The initial ED is enriched with 270 sample points for the steel column function to develop the global PCK metamodel for the random input variables comprising different dependent structures and pair copula functions. The inner nested loop reliability is evaluated using the MCS approach, considering the target value $\hat{\beta}_h$=3. The outer loop optimization is implemented using a hybrid approach (GA and SQP) described in Section 6.2. For the optimization phase, a starting point [*b*=300mm, *t*=12mm, *h*=250mm] and the upper and lower bounds for the design variables are utilized. Table 6.4 shows the optimization outcome from the double-loop RBDO approach for the various steel column load dependency considered and the errors (ε_{LOO}) in constructing the metamodel using the adaptive PCK method.

Table 6.4. RBDO outcome considering steel column loads dependency.

Dependence Structure	Copula	$C_{sc}(\text{mm}^2)$	*b*(mm)	*t*(mm)	*h*(mm)	N_{itr}	ε_{LOO}
$Z_1Z_2Z_3$	Gaussian	6.56E+3	264.31	19.74	167.50	224	1.602E-5
	Student t	6.59E+3	276.43	18.89	170.99	345	8.431E-6

	Clayton	6.57E+3	282.23	18.68	162.20	323	2.659E-5
	Gumbel	6.80E+3	258.96	20.56	183.42	314	8.463E-6
	Frank	6.22E+3	372.15	13.23	162.20	319	1.630E-5
$Z_2Z_1Z_3$	Gaussian	6.70E+3	446.25	12.10	162.45	253	1.667E-4
	Student t	6.88E+3	394.15	13.57	191.26	334	5.919E-4
	Clayton	6.59E+3	287.81	18.50	158.17	328	6.346E-4
	Gumbel	6.81E+3	387.53	13.79	182.67	323	6.124E-4
	Frank	6.50E+3	356.80	13.59	206.83	324	4.175E-4
$Z_2Z_3Z_1$	Gaussian	6.82E+3	388.05	13.53	196.75	334	1.100E-3
	Student t	6.67E+3	338.29	15.96	158.92	345	3.759E-4
	Clayton	6.73E+3	309.43	17.12	179.87	307	1.400E-3
	Gumbel	6.99E+3	414.01	12.97	202.19	251	3.332E-4
	Frank	6.77E+3	390.22	13.64	180.77	332	5.766E-4
Independent	-	6.36E+3	291.97	17.22	166.96	363	3.826E-6

For comparison, the steel column cost function is optimized while considering the uncertainty of variables as implicit (DDO) using safety factors (assumed safety factor = 1.8). The resulting DDO problem is evaluated using fmincon in MATLAB. Table 6.5 and Figure 6.4 present the DDO results for the steel column cost minimization, the associated optimal design variables, and the iteration steps in its evaluation.

Table 6.5. DDO outcome for steel column function.

Optimization Method	$C_{sc}(\text{mm}^2)$	b(mm)	t(mm)	h(mm)
DDO	2473.5	256.2	5.0	150.0

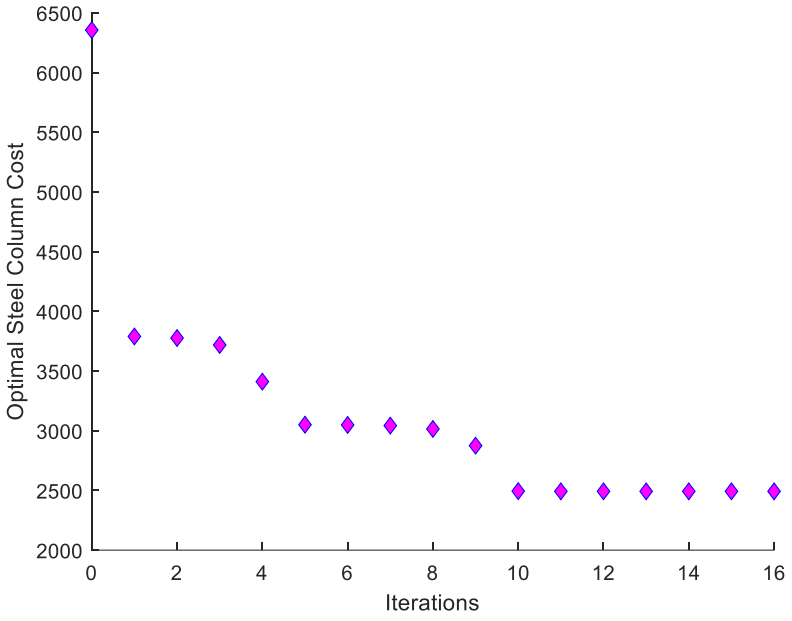

Figure 6.4. DDO iteration steps for steel column function.

For the DDO convergence plot (Figure 6.4), the optimal steel column cost function gradually declined from 6500mm^2 until a convergence value of 2473.5mm^2 was attained from the tenth iteration cycle.

For the RBDO case of the steel function, all three D-vine configurations satisfied the target reliability index (Figure 6.5) at the optimal point.

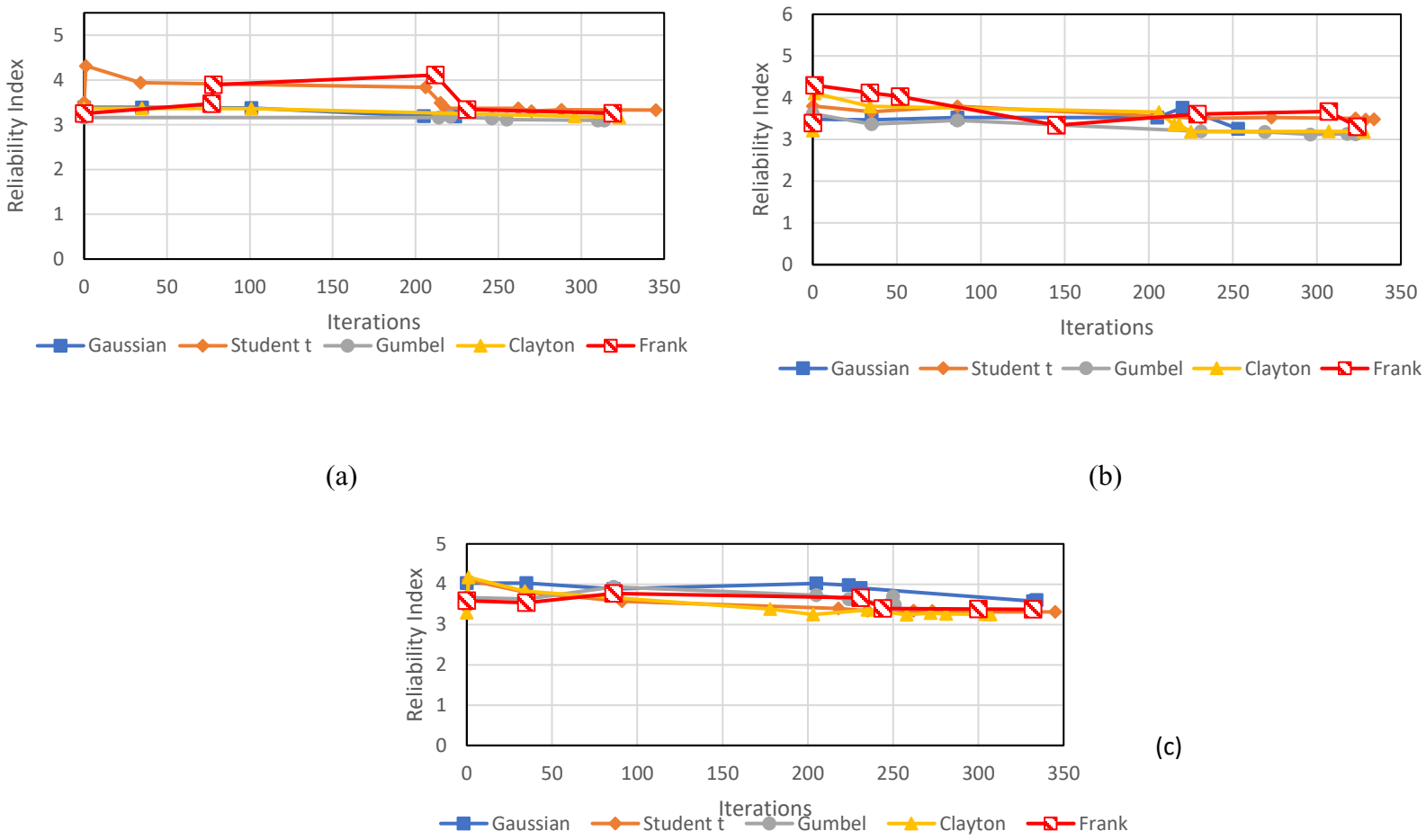

Figure 6.5. Convergence plot for D-vine structure (a) Z_1-Z_2-Z_3 (b) Z_2-Z_1-Z_3 (c) Z_2-Z_3-Z_1 .

6.4.2. Practical Application: Segmented SCR Optimization

6.4.2.1. Background and SCR dimensions

SCR has served as a preferred solution in deepwater hydrocarbon transport for oil and gas production, export, and gas injection activities (Bai & Bai,2005). This study investigates the effect of environmental load dependence in optimizing a free-hanging segmented SCR under operating load conditions. The sea load condition in the Bay du Nord area of the Flemish Pass is considered for demonstration purposes. The Flemish Pass is a basin about 400km off the coast of Newfoundland with significant oil discoveries and a potential area for offshore oil and gas production in Canada. This area is an essential point of concern as it is hoped to be the future of deepwater activities in the region. The location has a water depth of about 1000m to 1200m (C-CORE, 2017). Due to the water depth described, a typical offshore production asset for SCR dynamic analysis for this location is the FPSO platform. For this analysis, the SCR internal transport fluid is crude oil. Table 6.6 shows the SCR and FPSO properties considered in this study.

Table 6.6. Segmented SCR parameters and FPSO dimensions.

SCR and Vessel Particulars	Dimensions
SCR Length (L_R)	1955m
Internal Diameter (D_I)	0.22m
Riser Material	Steel X_{65} (API 5L)
Internal Fluid	Crude Oil (mass density:900kg/m^3)
SCR Yield Stress (σ_y)	450MPa
FPSO	Length=300m, Height = 40m, Width=50m
Inertia Coefficient (C_I)	2.0
Drag Coefficient (C_d)	1.2

6.4.2.2. Statistical Parameters of Environmental Load

The Flemish Pass Basin's prevailing wave and current conditions are the environmental operating load considered in optimizing the segmented SCR. Typically, the Significant Wave Height (H_s) and the Zero-Crossing Period (T_z) are the random wave variables for analysis.

The available statistical summary and data for the environmental load (H_s , T_z and ocean current (V_c)) for the Flemish Pass (C-CORE, 2017; Okoro et al.,2021) are utilized for the RBDO analysis. The marginals for the environmental variables are selected from six probability distribution types using the minimum AIC (Appendix 6A, Table 6A.3). Table 6.7 shows the statistical data summary and dominant direction of H_s, T_z and V_c.

Table 6.7. Statistical summary of environmental variables (operating condition) (C-CORE, 2017).

Variables	Distribution	Mean	CoV	Direction (Deg)
H_s (m)	Weibull	3.19	0.53	225^o
T_z (s)	Lognormal	10.21	0.18	225^o
V_c (m/s)	Weibull	0.284	0.56	225^o

In this study, V_c is assumed to be a random variable at a depth of 2m below the ocean surface during normal operations and deterministic at other depths for simplicity of analysis (Table 6.8). The ocean current decreases with ocean depth.

Table 6.8. Flemish Pass Ocean Current profile at 1200m water depth (C-CORE,2017).

Depth from Ocean Surface (m)	Mean Ocean Current (m/s)	Distribution
2	0.284 (CoV:0.56)	Weibull
250	0.14	Deterministic
500	0.12	Deterministic
1000	0.07	Deterministic
1200	0.05	Deterministic

6.4.2.3 Environmental data dependence analysis

With the possibility of nonlinear and tail dependence between ocean environment variables, the multivariate dependency between the random variables associated with waves and current in the Flemish Pass basin is determined using a D-vine copula. The D-vine configuration of the first tree is obtained by solving a traveling salesman's problem described in Section 6.2, and the optimal selection of pair copula is made, as explained in Step 2 (Section 6.3). Table 6.9 and Figure 6.6 show the optimal copula selected and scatter copula plot for the operating environmental load case.

Table 6.9. Copula Selection (operating load case).

Tree	Copula Density	Type	τ_k	θ	θ_R (Deg)
1	$C_{H_s T_z}$	Clayton	0.0196	0.04	0
1	$C_{V_c T_z}$	Clayton	0.0240	0.05	270
2	$C_{V_c H_s \mid T_z}$	Independent	-	-	0

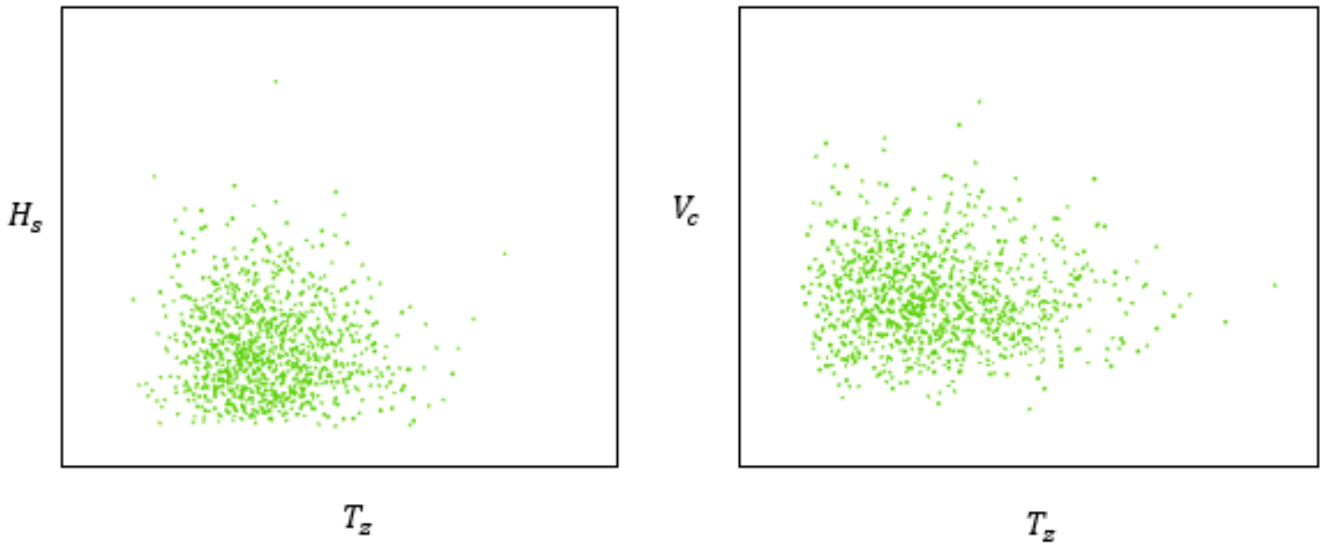

Clayton Copula τ_k=0.0196 Clayton Copula τ_k=0.024

Figure 6.6. Copula scatter plot for SCR environmental data.

6.4.2.4. RBDO formulation for segmented SCR.

The SCR considered in this study has three segments to be optimized. The original dimensions of the segments are (seabed section: L_{o1}=675m**,** t_{o1}=0.055m**)**, (mid-section: L_{o2}=475m, t_{o2}=0.035m) and (section connected to FPSO: L_{o3}=805m, t_{o3}=0.021m). Where L_{oi} and t_{oi} represents the original length and thickness of the SCR sections, respectively. The SCR parameters to be optimized (design parameters) are shown in Table 6.10, with all design tolerance assumed to be normally distributed.

Table 6.10. Statistical parameters of the segmented SCR design variables

Segment Description	Symbol	Distribution	CoV
Seabed section length	L_1	Gaussian	0.5
Mid-section length	L_2	Gaussian	0.5

Section connected to the vessel (length)	L_3	Gaussian	0.5
Seabed section thickness	t_1	Gaussian	0.5
Mid-section thickness	t_2	Gaussian	0.5
Section connected to the vessel (thickness)	t_3	Gaussian	0.5

The total dry weight (W^d) of the segmented SCR (Eq. (6.24)) is the optimized cost function while satisfying the optimization problem's hard and soft constraints.

$$W^d = \int (D_I, L_1, L_2, t_1, t_2, t_3) \quad (6.24)$$

As described in Section 6.2 of this chapter, $m_j(d)$ represents the soft constraints for optimization, which are simple functions that bound the design space. Also, the probabilistic constraints (hard) describe the segmented riser's LSF and are characterized by the environmental variables. In this study, the target $\hat{P}_{fh}$ of the segmented riser is based on known safety cases described by regulatory standards (DNV,2001). This study considers the DNV high safety class for serviceability conditions ($\hat{P}_{fh} = 10^{-3}$) as target value (Table 6A.4, Appendix 6A). As the standard describes, the high safety case considers a design that reduces the risk of human injury and significant environmental pollution from SCR failure. Eqs. (6.25) to (6.27) show the soft constraints for the segmented riser; the design variable L_3 is described in terms of L_1 and L_2 (Eq. (6.27)). The goal is to have a highly reliable SCR at increased water depth and optimal (minimal) cost.

$$L_2 \leq L_1 \quad (6.25)$$

$$L_3 \leq L_2 \quad (6.26)$$

$$L_3 = L_R - L_1 - L_2 \quad (6.27)$$

The probabilistic constraints (inner loop RBDO) are obtained using adaptive PCK and consider tension (maximum and minimum), maximum von Mises stress, and the bending moment of the segmented SCR. Eqs. (6.28) to (6.31) show the formulated probabilistic constraints for the segmented SCR considering the operational case where T_{min}, T_{max} denotes the minimum and maximum effective tension, respectively. Also, S_{vms} and M_B represents the maximum equivalent stress and bending moment on the segmented riser.

$$g_1(H_s, T_z, V_c) = T_{min} \qquad T_{min} \geq 0 \tag{6.28}$$

$$g_2(H_s, T_z, V_c) = T_a - T_{max} \tag{6.29}$$

$$g_3(H_s, T_z, V_c) = S_a - S_{vms} \tag{6.30}$$

$$g_4(H_s, T_z, V_c) = M_a - M_B \tag{6.31}$$

For this demonstration, T_a=3500 kN, S_a=0.67σ_y (API,2013) and M_a=1200kN.m. These values represent the allowable tension (T_a), stress (S_a) and bending moment (M_a) of the segmented SCR. For the DDO case considered in this study for comparison, a safety factor of 1.5 is adopted for the SCR.

6.4.2.5. SCR Numerical Modeling and Response Determination

The SCR is considered free hanging and connected to an FPSO using a flex joint. The modeling and response analysis of the segmented riser is evaluated using an FEA tool called Flexcom (Wood,2019). The analysis comprises static and dynamic evaluation of the SCR, with the coupled effect of the FPSO in random seas considered in the dynamic phase. The ocean wave is modeled as a random sea using the Pierson- Moskowitz spectrum, which assumes a deep and fully developed sea (Bai and Jin, 2016). Figure 6.7 shows the FEA model, including the TDP of the

segmented SCR in 1200m water depth. The SCR geometry, seabed properties, internal fluid, hydrodynamics, and vessel (FPSO) characteristics are modeled for the static phase. The seabed stiffness is assumed linear elastic with longitudinal and transverse stiffness considered (longitudinal friction coefficient: 0.2, transverse friction coefficient: 0.4).

Ocean structures are complex and mostly do not have explicit LSF, which describes their performance. Consequently, the need to construct a reasonably accurate metamodel, cheap to evaluate, reduces the computational burden of numerical models and reflects the system's reality. With the determination of optimal copula for the environmental variables, an ED of 20 LHS sample points of the random input variables (H_s, T_z, V_c) is set up in the input space.

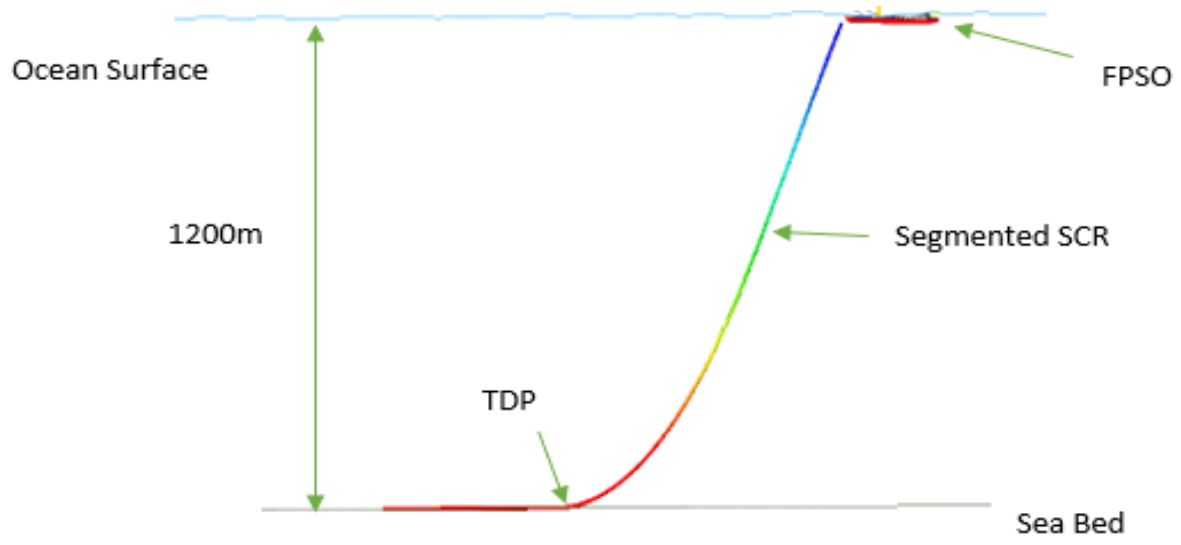

Figure 6.7. Segmented SCR FEA model using Flexcom (Wood,2019).

The responses related to tension, stress, and bending moments are determined for various selected hang angles ($14.5^o, 16.5^o, 18^o$ and 18.5^o) of the segmented SCR using FEA. Figure 6.8 shows a

typical response plot of the segmented riser for the input sample (H_s=0.89m, T_z=7.9s, V_c=0.43m/s) at a hang angle of 16.5^o. Similar responses are obtained for all sample points and hang angles considered. The effective tension plot (Figure 6.8) shows both the maximum and minimum values at various sections of the SCR length. From Figure 6.8, SCR maximum tension occurs near the connecting vessel (FPSO) with the maximum bending moment and von Mises stress near the TDP.

The PCK metamodels describing the tension, stress, and bending moment of the segmented SCR are built by an adaptive process by enriching the initial ED using the U learning function until convergence is achieved (Figure 6.1). The responses from constructed PCK metamodels for the RBDO problem and all SCR hang angles considered were close to those obtained using FEA, as shown by the validation plots using 30 MCS input sample points (Figure 6.9).

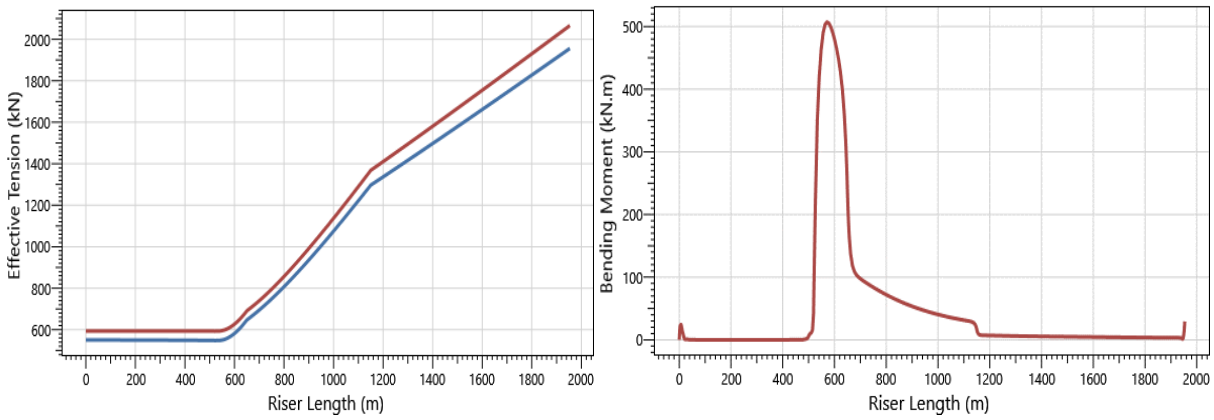

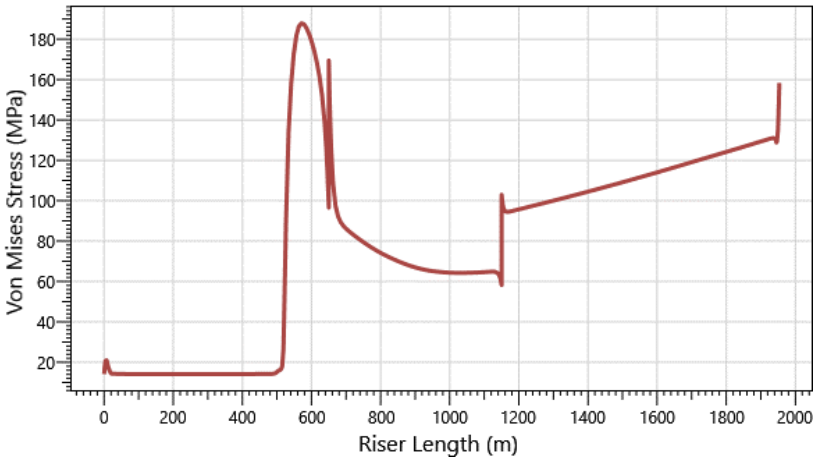

Figure 6.8. Response plot of segmented SCR at hang angle (16.5^{o}).

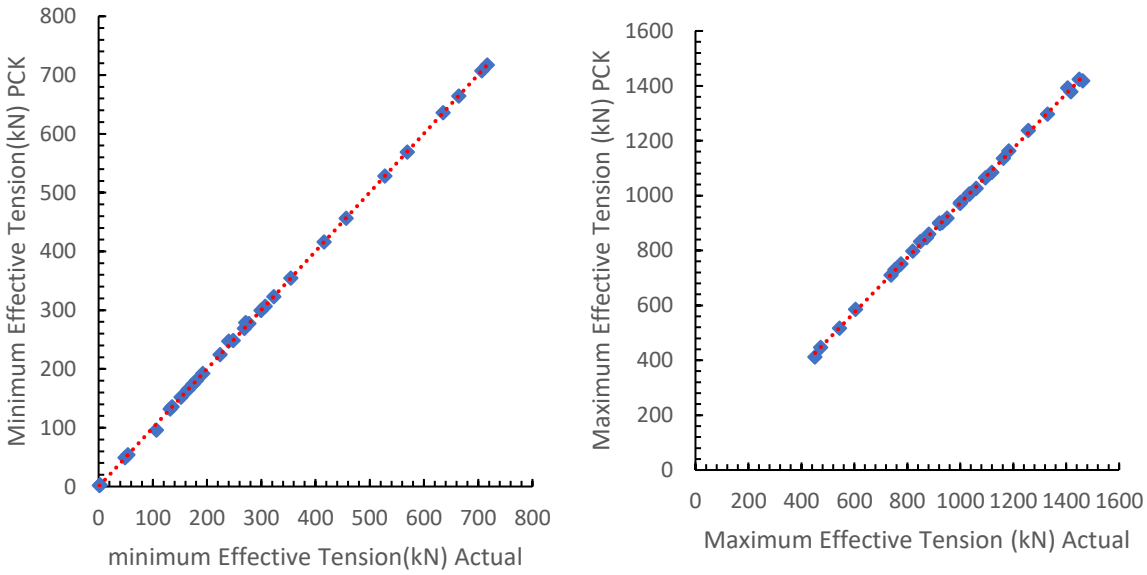

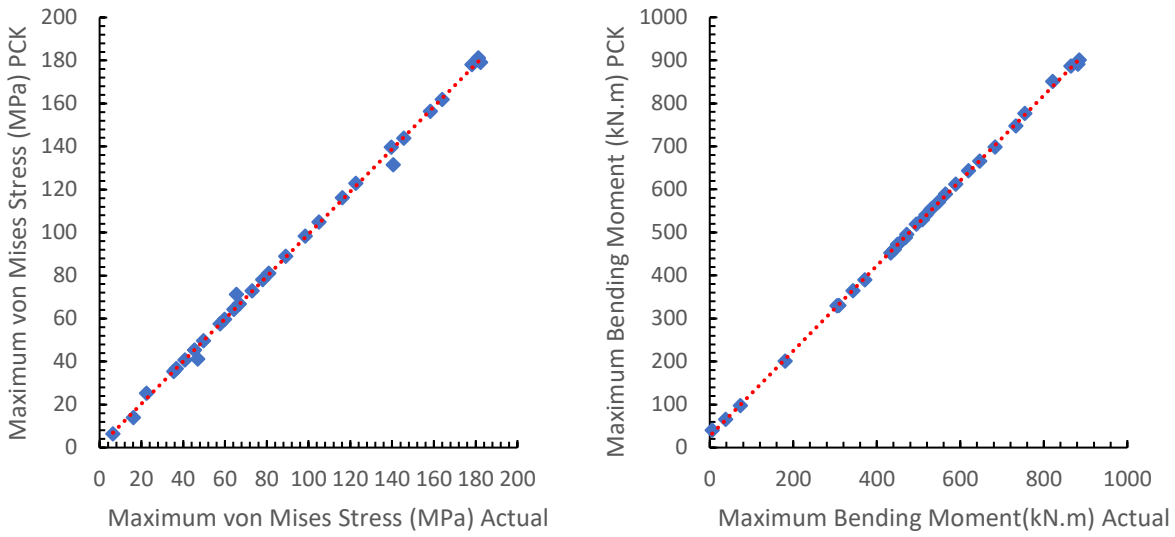

Figure 6.9. Response validation plots using adaptive PCK for SCR at hang angle (18.5^{O}).

Appendix 6A (Table 6A.5) of this study provides further details about the error from the PCK construction for the segmented SCR and its comparison with Kriging and PCE. Also, the RBDO inner loop reliability is implemented using the MCS described in Section 3. Table 11 shows the optimization outcome from the double-loop RBDO approach for the SCR using adaptive PCK and hybrid optimization methods. Also, Figure 6.10 shows the optimization plots at various hang angles.

Table 6.11. RBDO optimal weight and design variables for segmented SCR.

Dependence	Hang Angle (Deg)	W^d (kN)	t_1 (mm)	t_2 (mm)	t_3 (mm)	L_1 (m)	L_2 (m)	L_3(m)	β_h
D-vine copula	14.5^o	2042	41.6	25.8	22.2	674.5	640.4	640.12	3.35
	16.5^o	2892	53.3	41.7	18.7	755.6	612.7	586.7	3.50
	18^o	2391	41.8	31.2	19.2	871.7	830.2	253.1	3.52
	18.5^o	3414	64.4	28.2	25.1	897.3	691.9	365.8	3.42
Independent	14.5^o	2914	47.5	41.4	25.7	819.3	670.0	465.8	3.26
	16.5^o	4202	63.2	49.5	20.1	896.3	882.8	176.0	3.22
	18^o	4136	62.2	57.8	26.7	889.1	589.2	476.8	3.34
	18.5^o	4414	60.3	58.7	41.2	828.9	708.1	417.9	3.40
DDO	-	1142	20.3	18.0	15.0	846.0	844.8	264.2	

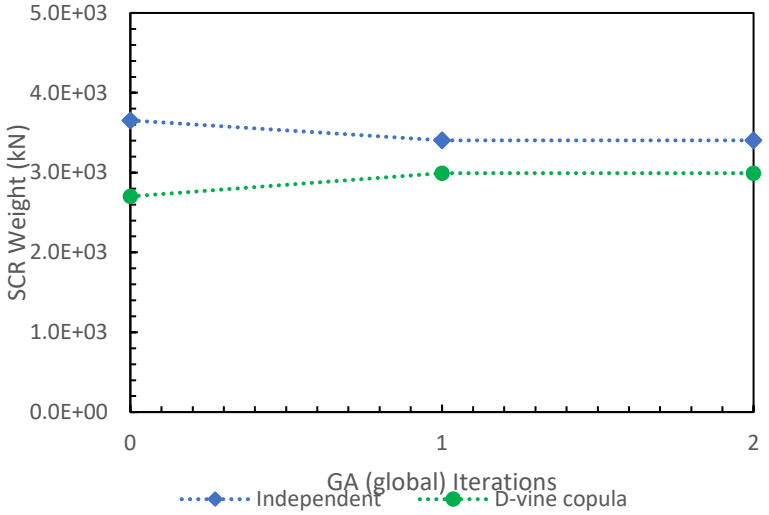

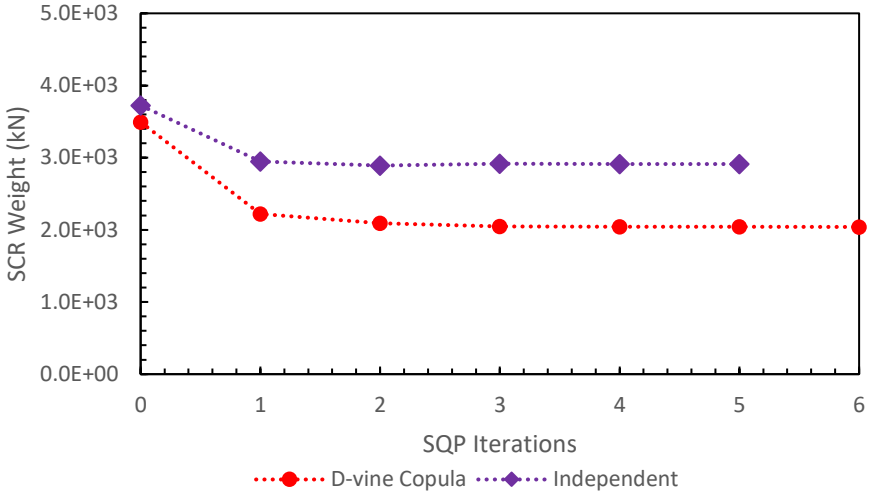

(a) Hang Angle 14.5^o

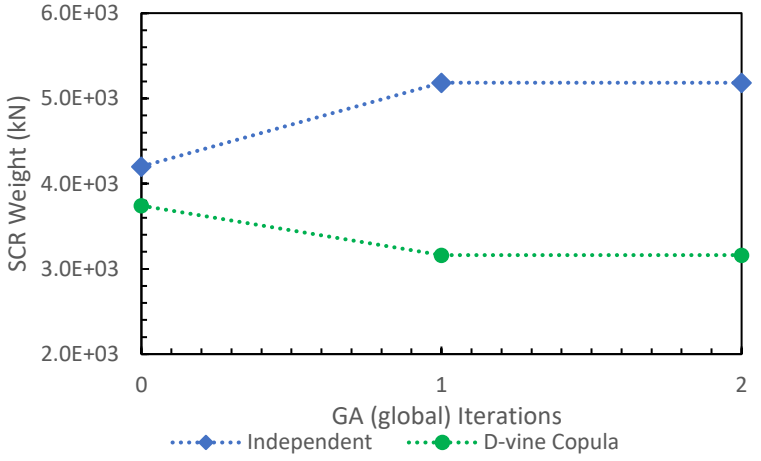

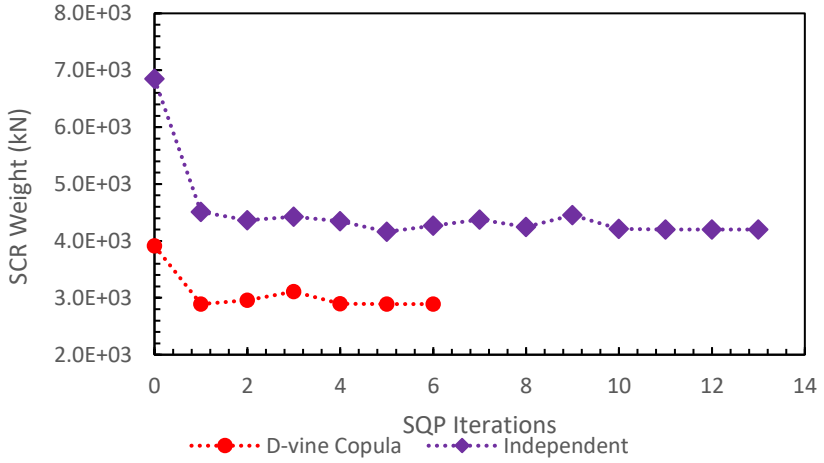

(b) Hang Angle 16.5^o

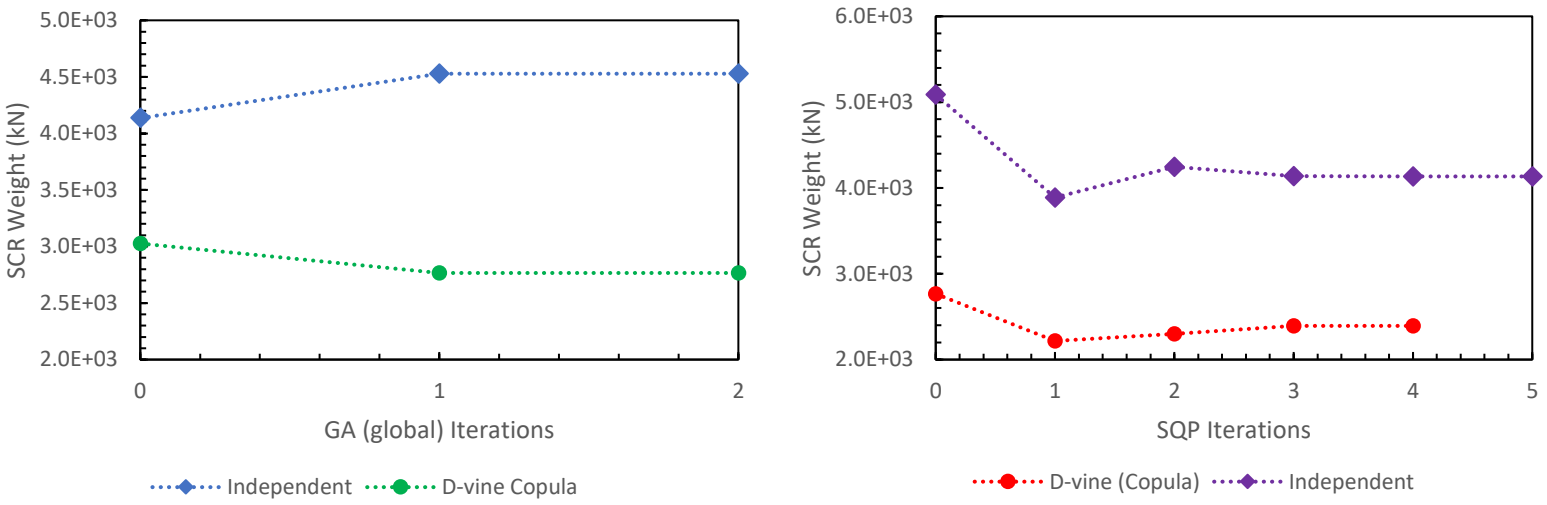

(c) Hang Angle 18^o

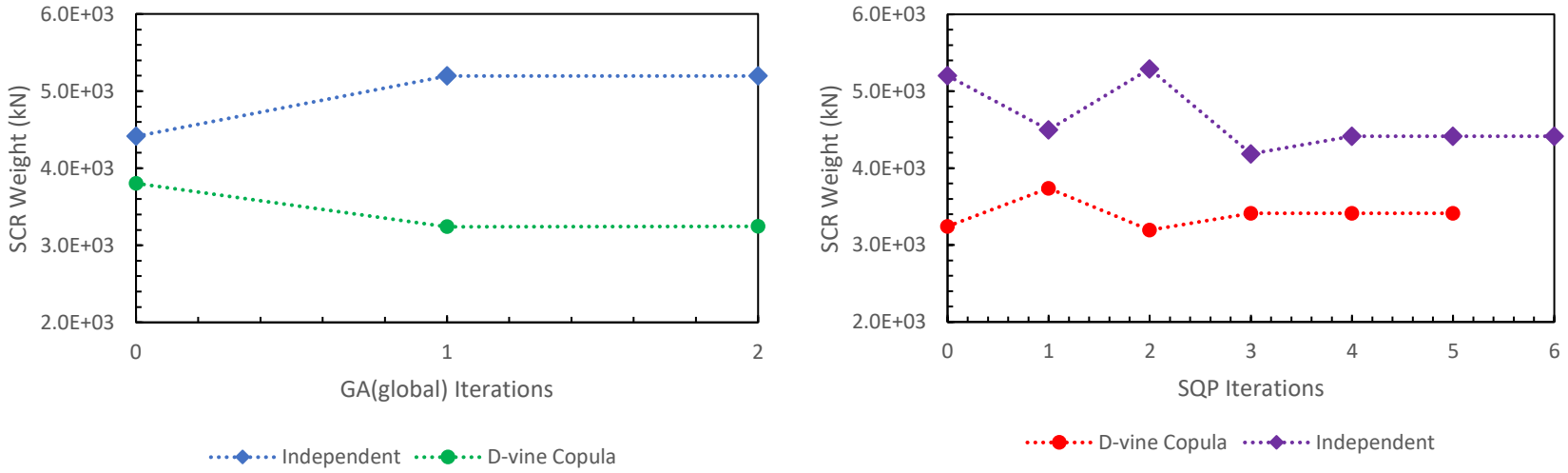

(d) Hang Angle 18.5^o

Figure 6.10. SCR optimization plots at different hang angles.

6.5. Discussion

This section describes the outcomes from the RBDO study of the presented example of a steel column function and a deepwater segmented SCR case study.

For the steel column function described in Section 6.4.1, this paper examines the effect of the environmental variable configurations in the first tree of the D-vine structure for various copula types (Gaussian, Student t, Clayton, Gumbel, and Frank). As seen in Table 6.4, for different D-vine orders with consideration of Gaussian Copula (linear dependence) between variables, the optimal steel column cost is (3.14%, 5.34%, and 7.23%) higher than the cost when variables are considered independent. Consequently, a non-consideration of possible dependence between variables could affect the accuracy level of the RBDO optimal cost; this can impact structural safety and ultimately affect the decision made regarding design variables during optimization. Also, Table 6.4 shows a difference in the RBDO outcome (optimal cost (C_{sc}) and dimensions of design variables $(b, t \text{ and } h))$ for the various dependence modeling conditions considered (independent variables and dependent variables modeled with different bivariate copulas). In addition, the order of variables in the first tree of the vine configuration also contributes to the difference in the optimization results. This variance indicates that the choice of copula for dependence modeling between variables and variable order significantly impacts the design decision in selecting optimal variable parameters, cost, and the overall safety of the structure. Consequently, the result of the steel column provides a learning outcome on D-vine variable configuration, which is critical in the RBDO of offshore structures where there exists probable nonlinear and tail dependence between ocean variables that interact with these structures with

various levels of dependency among themselves. Therefore, choosing an appropriate copula for multivariate dependence modeling and its variable order using vine copula raises the confidence level in the optimal design of offshore structures while meeting the required safety targets.

Also, for the DDO outcome (Tables 6.5 and 6.11), uncertainties are only captured implicitly using safety factors during the optimization process. The choice of safety factor primarily depends on engineering experience and related design codes for a given optimization case. Consequently, this could result in wide variability in the optimal cost (sub-optimal or superoptimal) of the structure, as noticed in the relatively low DDO optimal cost outcome in Table 6.5 (C_{sc}=2473.5mm^2) and Table 6.11 (W^d=1142kN), resulting in cost values that might not be reliable and affect the design variables' decision accuracy. Therefore, using safety factors may not provide reliable and robust optimization results concerning uncertainty.

The consideration of dependence using D-vine copula for the segmented SCR at various hang angles resulted in a lower optimal cost value than when variables were considered independent [29.9%(14.5^o), 31.2%(16.5^o), 42.2%(18^o), 22.7%(18.5^o)]; this further reveals that the SCR hang angle to the FPSO affects the cost and design variable outcomes during dependence-based RBDO analysis (Figure 6.10), which invariably impacts the design decision during optimization studies. Appropriate determination of the SCR hang angle to the fixed offshore installation is necessary for optimal design purposes.

Furthermore, the adaptive PCK metamodel in the inner loop of the RBDO problem shows a high prediction ability of the computational model, as seen in the validation plot of segmented SCR (Figure 6.9) and a relatively smaller ε_{LOO} compared to outcomes from ordinary Kriging and PCE, as shown in (Appendix 6A , Table 6A.5) for the segmented SCR, this shows its suitability for

metamodel-assisted RBDO. Also, Table 6.4 for the steel column function shows low error values using adaptive PCK for the RBDO inner loop (1.1E-3 to 3.826E-6).

The ability of copula functions to capture possible nonlinearity and tail dependence, as seen in (Figures 6.3 and 6.6), shows their suitability in obtaining a high level of accuracy in RBDO analysis, especially for offshore structures.

A limitation of this study is that only commonly used copulas have been considered; this could be extended to other copula types for a more robust dependence effect investigation.

6.6. Conclusions

This study presents a framework for optimization under uncertainty for an offshore structure considering the effect of complex multivariate dependency modeling between environmental ocean variables using a D-vine copula. The optimization of a steel column function (example) and a segmented SCR (practical application) were used to demonstrate the implementation of the framework.

The following can be inferred from the outcomes of the study:

1. Considering uncertainty and dependence between environmental variables significantly affects offshore structural reliability evaluation and the design decision related to the optimal structural cost and choice of design variables from optimization studies.
2. The steel column function and segmented SCR study reveal that if dependency between the variables of offshore structures is ignored during RBDO analysis, a possible suboptimal or superoptimal structural cost is obtained. Conversely, capturing multivariate dependence

raises confidence in the design and produces a reliable and safe structure for offshore operations.

3. From the steel column example, determining the correct variable order of the D-vine copula structure in the first tree is essential in ensuring appropriate modeling of multivariate dependence between variables and obtaining reliable optimization outcomes (cost and design variables).
4. The uncertainty in the ocean environment requires that existing nonlinearity and tail dependence between ocean variables are captured to ensure an appropriate tradeoff between structural safety and design cost. The steel column function and segmented SCR examples show that the D-vine copula is a flexible and efficient method to capture this vital information between ocean variables.
5. Using adaptive PCK for the inner loop of the RBDO problem improves the accuracy of the two-level RBDO approach, produces a relatively minimal error, and provides a level of confidence in the overall optimization process.

Future research areas include vine copula-based RBDO problems with mixed uncertainty (epistemic and aleatory), a study that considers fatigue, and extreme load effect on the structural optimization of deepwater SCR. Also, further investigation into the impact of design variables' dependency on the RBDO problem is necessary. Finally, implementing the dependence-based framework to other complex offshore structures to investigate further the effect of multivariate dependence modeling in the optimal design of offshore structures is essential.

Acknowledgment

The authors thankfully acknowledge the financial support provided by the Natural Sciences and Engineering Research Council of Canada (NSERC) through Discovery Grant and the Canada Research Chair (Tier I) Program in Offshore Safety and Risk Engineering.

Appendix 6A

Table 6A.1. Expression for selected copula functions (Elliptical and Archimedean).

Copula	$C(u_1, u_2\|\theta)$	h function	h^{-1}function	θ range
Gaussian	$\Phi(\Phi^{-1}(u_1), \Phi^{-1}(u_2)\|\theta)$	$\Phi(\frac{\Phi^{-1}(u_1)-\theta\Phi^{-1}(u_2)}{\sqrt{1-\theta^2}})$	$\Phi(\Phi^{-1}(u_1)\sqrt{1-\theta^2}+\theta\Phi^{-1}(u_2))$	[-1,1]
Student t	$t_{\theta,\nu}(t_\nu{}^{-1}(u_1), t_\nu{}^{-1}(u_2)\|\theta)$	$t_{\nu+1}(\frac{t_\nu{}^{-1}(u_1)-\theta t_\nu{}^{-1}(u_2)}{\sqrt{\frac{\left(\nu+\left(t_\nu{}^{-1}(u_2)\right)^2\right)(1-\theta^2)}{\nu+1}}})$	$t_\nu(t_{\nu+1}{}^{-1}(u_1)\sqrt{\frac{\nu+\left(t_\nu{}^{-1}(u_2)\right)^2)(1-\theta^2)}{\nu+1}}+\theta t_\nu{}^{-1}(u_2)$	[-1,1]
Clayton	$((u_1)^{-\theta}+(u_2)^{-\theta}-1)^{-\frac{1}{\theta}}$	$(u_2)^{-\theta-1}((u_1)^{-\theta}+(u_2)^{-\theta}-1)^{-1-\frac{1}{\theta}}$	$((u_1u_2)^{\theta+1})^{-\frac{\theta}{\theta+1}}+1-(u_2)^{-\theta})^{-\frac{1}{\theta}}$	[0 ∞]
Gumbel	$\exp(-((-lnu_1)^\theta+(-lnu_2)^\theta)^{\frac{1}{\theta}})$	$C(u_1,u_2\|\theta)\frac{1}{u_2}(-logu_2)^{\theta-1}.((-logu_1))^\theta+(-logu_2))^\theta)^{\frac{1}{\theta-1}}$	-	[1,+∞]
Frank	$-\frac{1}{\theta}\ln(1+\frac{(e^{-\theta u_1}-1)(e^{-\theta u_2}-1)}{e^{-\theta}-1})$	$\frac{e^{-\theta u_2}}{\frac{1-e^{-\theta}}{1-e^{-\theta u_1}}+e^{-\theta u_2}-1}$	$-\log(1-\frac{1-e^{-\theta}}{((u_1)^{-1}-1)e^{-\theta u_2}+1})/\theta$	$[-\infty,+\infty]$

ν : degree of freedom of the t copula.

Table 6A.2. Tail dependence expression for selected copulas

Tail Dependence	Gaussian	Student t	Clayton	Gumbel	Frank
Upper Tail Dependence (λ_U)	0	$2t_{\nu+1}(-\sqrt{(\nu+1)}\sqrt{\frac{1-\theta}{1+\theta}})$	0	$2-2^{-\frac{1}{\theta}}$	0
Lower Tail Dependence (λ_L)	0	$t_{\nu+1}(-\sqrt{\nu+1})\sqrt{\frac{1-\theta}{1+\theta}})$	$2^{-\frac{1}{\theta}}$	0	0

Table 6A.3. Minimum AIC values for variables H_s , T_z and V_c

Probability Distribution	H_s(m)	T_z(s)	V_c(m/s)
	AIC	AIC	AIC
Gaussian	11300.08	11714.27	-2405.40
Lognormal	11495.82	11610.45	-2354.80
Exponential	12616.08	19386.39	-1569.61
Logistic	11330.69	11742.88	-2409.65
Weibull	10975.31	12013.79	-2855.03
Gamma	11063.35	11615.62	-2783.35

Table 6A.4. Target failure probability (DNV,2001)

Limit State	Safety Class		
	Low	Normal	High
Serviceability	10^{-1}	$10^{-1} - 10^{-2}$	$10^{-2} - 10^{-3}$
Ultimate	10^{-3}	10^{-4}	10^{-5}
Fatigue	10^{-3}	10^{-4}	10^{-5}

Table 6A.5. Metamodel error for the segmented SCR

Metamodel	14.5^o	16.5^o	18^o	18.5^o
ε_{LOO}	SCR Hang Angles			
Adaptive PCK	1.242E-9	1.85E-9	4.68E-9	1.48E-9
Adaptive Kriging	6.43E-7	7.11E-5	8.31E-6	2.22E-6
PCE	2.13E-3	5.73E-4	6.22E-5	3.62E-4

References

Aas, K., Czado, C., Frigessi, A., & Bakken, H. (2009). Pair-copula constructions of multiple dependence. *Insurance: Mathematics and Economics*, *44*(2), 182–198. https://doi.org/10.1016/j.insmatheco.2007.02.001

American Petroleum Institution [API]. (2013). "*Dynamic Risers for Floating Production Systems. API Standard 2RD*". Second Ed. API Publishing Services, Washington, DC.

Bai, Y., & Bai, Q. (2005). "Subsea Pipelines and Risers, Elsevier Ocean Engineering Book Series," Elsevier, Amsterdam, pp. 751-785. doi:10.1016/B978-008044566-3/50042-7.

Bai, Y., & Jin, WL. (2016). Marine Structural Design. Second edition, Elsevier Butterworth Heinemann, United Kingdom.

Bedford, T., & Cooke, R. M. (2002). Vines - a new graphical model for dependent random variables. *The Annals of Statistics*, *30*(4), 1031–1068.

Bichon, B. J., Eldred M.S., Swiler L.P., Mahadevan S., & McFarland J.M. (2008). Efficient Global Reliability Analysis for Nonlinear Implicit Performance Functions. *AIAA Journal*,46(10),2459-2468.

Blatman, G., & Sudret, B. (2011). Adaptive sparse polynomial chaos expansion based on least angle regression. *Journal of Computational Physics*, *230*, 2345–2367. https://doi.org/10.1016/j.jcp.2010.12.021

Brechmann, E. C. (2010). Truncated and simplified regular vines and their applications. Diploma thesis, Technische Universitaet Muenchen.

C-CORE. (2017). Metocean Climate Study Phase II – Offshore Newfoundland & Labrador. Study Main Report; Volume 1: Full Data Summary Report. Report prepared for Nalcor Energy Oil and Gas. https://exploration.nalcorenergy.com/wp -content/uploads/2017/07/Metocean-Study-Report-Vol.-I-Final-29-06-2017.pdf.

Chaudhuri, A., Kramer, B., & Willcox, K. E. (2020). Information Reuse for Importance Sampling in Reliability-Based Design Optimization. *Reliability Engineering and System Safety*, *201*, 106853. https://doi.org/10.1016/j.ress.2020.106853

Choi, K. K., Noh, Y., & Du, L. (2007). Reliability based design optimization with correlated input variables. *SAE Technical Papers*, *2007*(724). https://doi.org/10.4271/2007-01-0551

Cui, D., Wang, G., Lu, Y., & Sun, K. (2020). Reliability design and optimization of the planetary gear by a GA based on the DEM and Kriging model. *Reliability Engineering and System Safety*, *203*, 107074. https://doi.org/10.1016/j.ress.2020.107074

Debiao, M., Hu, Z., Wu, P., Zhu, S.-P., Correia, J. A. F. O., & Jesus, A. M. P. De. (2020). Reliability-based optimisation for offshore structures using saddlepoint approximation. *Proceedings of the Institution of Civil Engineers - Maritime Engineering*. https://doi.org/10.1680/jmaen.2020.2

Ditlevsen, O., & Madsen, H. O. (1996). Structural reliability methods, Wiley, Chichester, United Kingdom.

Dizangian, B., & Ghasemi, M. R. (2016). A fast decoupled reliability-based design optimization of structures using B-spline interpolation curves. *Journal of the Brazilian Society of Mechanical Sciences and Engineering*, *38*(6), 1817–1829. https://doi.org/10.1007/s40430-015-0423-4

DNV. (2001). Offshore Standard DNV-OS-F201 Dynamic Risers. Det Norske Veritas.

Du, X., & Chen, W. (2004). Sequential Optimization and Reliability Assessment Method. *Journal of Mechanical Design*, *126*, 225–233. https://doi.org/10.1115/1.1649968

Dubourg, V., Sudret, B., & Bourinet, J. M. (2011). Reliability-based design optimization using kriging surrogates and subset simulation. *Structural and Multidisciplinary Optimization*, *44*(5), 673–690. https://doi.org/10.1007/s00158-011-0653-8

Dutta, S. (2020). A sequential metamodel-based method for structural optimization under uncertainty. *Structures*, *26*, 54–65. https://doi.org/10.1016/j.istruc.2020.04.009

Dutta, S., & Putcha, C. (2020). Reliability-Based Design Optimization of a Large-Scale Truss Structure Using Polynomial Chaos Expansion Metamodel. *Lecture Notes in Mechanical Engineering*, 481–488. https://doi.org/10.1007/978-981-13-9008-1_39

Eamon, C. D., & Rais-Rohani, M. (2009). Integrated reliability and sizing optimization of a large composite structure. *Marine Structures*, *22*(2), 315–334. https://doi.org/10.1016/j.marstruc.2008.03.001

Echard, B., Gayton, N., & Lemaire, M. (2011). AK-MCS: An active learning reliability method combining Kriging and Monte Carlo Simulation. *Structural Safety*, *33*(2), 145–154. https://doi.org/10.1016/j.strusafe.2011.01.002

Eldred, M., Webster, C., & Constantine, P. (2008). Evaluation of Non-Intrusive Approaches for Wiener-Askey Generalized Polynomial Chaos. *49th AIAA/ASME/ASCE/AHS/ASC Structures, Structural Dynamics, and Materials Conference*. https://doi.org/10.2514/6.2008-1892

Fathima Sana, V. K., Nazeeh, K. M., Dilip, D. M., & Sivakumar Babu, G. L. (2022). Reliability-Based Design Optimization of Shallow Foundation on Cohesionless Soil Based on Surrogate-Based Numerical Modeling. *International Journal of Geomechanics*, *22*(2), 1–8. https://doi.org/10.1061/(asce)gm.1943-5622.0002274

Forrester, A., Sobester, A., & Keane, A. (2008). Engineering Design via Surrogate Modelling: a Practical Guide. Wiley.

Genest, C., & Favre, A. (2007). Everything You Always Wanted to Know about Copula Modeling but Were Afraid to Ask. *Journal of Hydrologic Engineering*, *12*, 347–368. https://doi.org/10.1061/(ASCE)1084-0699

Gholinezhad, H., & Hosein, S. (2021). Reliability-based multidisciplinary design optimization of an underwater vehicle including cost analysis. *Journal of Marine Science and Technology*, *0123456789*. https://doi.org/10.1007/s00773-021-00804-2

Goswami, S., Chakraborty, S., Chowdhury, R., & Rabczuk, T. (2019). Threshold shift method for reliability-based design optimization. *Structural and Multidisciplinary Optimization*, *60*, 2053–2072.

Huang, Z. L., & Jiang, C. (2017). A decoupling approach for evidence-theory-based reliability design optimization. *Structural and Multidisciplinary Optimization*, 647–661. https://doi.org/10.1007/s00158-017-1680-x

Huang, Z. L., Jiang, C., Zhang, Z., Zhang, W., & Yang, T. G. (2019). Evidence-theory-based reliability design optimization with parametric correlations. *Structural and Multidisciplinary Optimization*, *60*, 565–580.

Jiang, C., Yan, Y., Wang, D., Qiu, H., & Gao, L. (2021). Global and local Kriging limit state approximation for time-dependent reliability-based design optimization through wrong-classification probability. *Reliability Engineering and System Safety*, *208*, 107431. https://doi.org/10.1016/j.ress.2021.107431

Joe, H. (2014). Dependence modeling with copulas. In *Dependence Modeling with Copulas*. Chapman & Hall /CRC. https://doi.org/10.1201/b17116

Jones D.R., Schonlau M., & Welch W.J. (1998). Efficient global optimization of expensive black-box functions. *Journal of Global Optimization*, 13(4), 455-492.

Jung, Y., Jo, H., Choo, J., & Lee, I. (2022). Statistical model calibration and design optimization under aleatory and epistemic uncertainty. *Reliability Engineering and System Safety*, *222*, 108428. https://doi.org/10.1016/j.ress.2022.108428

Karadeniz, H., Toğan, V., & Vrouwenvelder, T. (2009). An integrated reliability-based design optimization of offshore towers. *Reliability Engineering and System Safety*, *94*(10), 1510–1516. https://doi.org/10.1016/j.ress.2009.02.008

Katoch, S., Chauhan, S. S., & Kumar, V. (2021). A review on genetic algorithm: past, present, and future. *Multimedia Tools and Applications*, *80*(5), 8091–8126. https://doi.org/10.1007/s11042-020-10139-6

Kharmanda, G., Mohamed, A., & Lemaire, M. (2002). Efficient reliability-based design optimization using a hybrid space with application to finite element analysis. *Structural and Multidisciplinary Optimization*, *24*(3), 233–245. https://doi.org/10.1007/s00158-002-0233-z

Kim, J., & Song, J. (2021). Quantile surrogates and sensitivity by adaptive Gaussian process for efficient reliability-based design optimization. *Mechanical Systems and Signal Processing*, *161*, 107962. https://doi.org/10.1016/j.ymssp.2021.107962

Kuczera, R. C., Mourelatos, Z. P., & Nikolaidis, E. (2010). System RBDO with correlated variables using probabilistic re-analysis and local metamodels. *Proceedings of the ASME 2010 International Design Engineering Technical Conferences & Computers and Information in Engineering Conference IDETC/CIE 2010*.

Kuschel, N., & Rackwitz, R. (1997). Two basic problems in reliability-based structural optimization. *Mathematical Methods of Operations Research*, *46*(3), 309–333. https://doi.org/10.1007/BF01194859

Lacaze, S., & Missoum, S. (2013). Reliability-based design optimization using Kriging and support vector machines. *Safety, Reliability, Risk and Life-Cycle Performance of Structures and Infrastructures - Proceedings of the 11th International Conference on Structural Safety and Reliability, ICOSSAR 2013*, *June 2013*, 3305–3312. https://doi.org/10.1201/b16387-477

Lebrun, R., & Dutfoy, A. (2009). An innovating analysis of the Nataf transformation from the copula viewpoint. *Probabilistic Engineering Mechanics*, *24*(3), 312–320. https://doi.org/10.1016/j.probengmech.2008.08.001

Lee, S. (2019). Reliability based design optimization using response surface augmented moment method. *Journal of Mechanical Science and Technology*, *33*(4), 1751–1759. https://doi.org/10.1007/s12206-019-0327-9

Lee, Y. S., Choi, B. L., Lee, J. H., Kim, S. Y., & Han, S. (2014). Reliability-based design optimization of monopile transition piece for offshore wind turbine system. *Renewable Energy*, *71*, 729–741. https://doi.org/10.1016/j.renene.2014.06.017

Leimeister, M., & Kolios, A. (2021). Reliability-based design optimization of a spar-type floating offshore wind turbine support structure. *Reliability Engineering and System Safety*, *213*, 107666. https://doi.org/10.1016/j.ress.2021.107666

Li, H. S. (2013). Reliability-based design optimization via high order response surface method. *Journal of Mechanical Science and Technology*, *27*(4), 1021–1029. https://doi.org/10.1007/s12206-013-0227-3

Li, X., Gong, C., Gu, L., Jing, Z., Fang, H., & Gao, R. (2019). A reliability-based optimization method using sequential surrogate model and Monte Carlo simulation. *Structural and Multidisciplinary Optimization*, *59*, 439–460.

Li, X., Zhu, H., Chen, Z., Ming, W., Cao, Y., He, W., & Ma, J. (2022). Limit state Kriging modeling for reliability-based design optimization through classification uncertainty quantification. *Reliability Engineering and System Safety*, *224*, 108539. https://doi.org/10.1016/j.ress.2022.108539

Liu, Y., Liu, Z., Qin, H., Zhong, H., & Lv, C. (2018). An efficient structural optimization approach for the modular automotive body conceptual design. *Structural and Multidisciplinary Optimization*, *58*, 1275–1289.

Lopez, C., Bacarreza, O., Baldomar, A., Hernandez, S., & Aliabadi, F. M. H. (2017). Reliability-based design optimization of composite stiffened panels in post-buckling regime. *Structural and Multidisciplinary Optimization*, *55*, 1121–1141. https://doi.org/10.1007/s00158-016-1568-1

Lv, Z., Lu, Z., & Wang, P. (2015). A new learning function for Kriging and its applications to solve reliability problems in engineering. *Computers and Mathematics with Applications*, *70*(5), 1182–1197. https://doi.org/10.1016/j.camwa.2015.07.004

Marelli, S., & Sudret, B. (2014). UQLAB: a framework for Uncertainty Quantification in MATLAB. *Second International Conference on Vulnerability and Risk Analysis and Management (ICVRAM 2014)*, 2554–2563. https://doi.org/10.1061/9780784413609.257

Meng, Z., Li, G., Wang, X., Sait, S. M., & Yıldız, A. R. (2021). A Comparative Study of Metaheuristic Algorithms for Reliability-Based Design Optimization Problems. *Archives of Computational Methods in Engineering*, *28*(3), 1853–1869. https://doi.org/10.1007/s11831-020-09443-z

Moustapha, M., & Sudret, B. (2019). Surrogate-assisted reliability-based design optimization : a survey and a unified modular framework. *Structural and Multidisciplinary Optimization*, *60*, 2157–2176.

Moustapha, M., Sudret, B., Bourinet, J. M., & Guillaume, B. (2016). Quantile-based optimization under uncertainties using adaptive Kriging surrogate models. *Structural and Multidisciplinary Optimization*, *54*(6), 1403–1421. https://doi.org/10.1007/s00158-016-1504-4

Nelsen, R. B. (2006). *An Introduction to Copulas: Lecture Note in Statistics*. Springer US. https://doi.org/https://doi.org/10.1007/0-387-28678-0_1

Nguyen, V. L., Kuo, C.-H., & Lin, P. T. (2022). Reliability-Based Analysis and Optimization of the Gravity Balancing Performance of Spring-Articulated Serial Robots With Uncertainties. *Journal of Mechanisms and Robotics*, *14*(3), 1–12. https://doi.org/10.1115/1.4053048

Ni, P., Li, J., Hao, H., Yan, W., Du, X., & Zhou, H. (2020). Reliability analysis and design optimization of nonlinear structures. *Reliability Engineering and System Safety*, *198*, 106860. https://doi.org/10.1016/j.ress.2020.106860

Ni, P., Li, J., Hao, H., & Zhou, H. (2021). Reliability based design optimization of bridges considering bridge-vehicle interaction by Kriging surrogate model. *Engineering Structures*, *246*, 112989. https://doi.org/10.1016/j.engstruct.2021.112989

Noh, Y., Choi, K. K., & Du, L. (2009). Reliability-based design optimization of problems with correlated input variables using a Gaussian Copula. *Structural and Multidisciplinary Optimization*, *38*(1), 1–16. https://doi.org/10.1007/s00158-008-0277-9

Okoro, A., Khan, F., & Ahmed, S. (2021). An Active Learning Polynomial Chaos Kriging metamodel for reliability assessment of marine structures. *Ocean Engineering*, *235*, 109399. https://doi.org/10.1016/j.oceaneng.2021.109399

Peng, Y., Ma, Y., Huang, T., & De Domenico, D. (2021). Reliability-based design optimization of adaptive sliding base isolation system for improving seismic performance of structures. *Reliability Engineering and System Safety*, *205*, 107167. https://doi.org/10.1016/j.ress.2020.107167

Qi, Y., Jin, P., Cai, G., & Li, R. (2022). A Bi-stage Multi-objective Reliability-based Design Optimization Using Surrogate Model for Reusable Thrust Chambers. *Reliability Engineering and System Safety*, *221*(9), 108362. https://doi.org/10.1016/j.ress.2022.108362

Rao, S. S. (2019). "Engineering Optimization: Theory and Practice," John Wiley & Sons, New Jersey. https://doi.org/10.1002/9781119454816

Santner, T., Williams, B., & Notz, W. (2003). The Design and Analysis of Computer Experiments. Springer Series in Statistics. Springer.

Schöbi, R., Sudret, B., & Wiart, J. (2015). Polynomial-Chaos-Based Kriging. *International Journal for Uncertainty Quantification*, *5*(2), 171–193.

Shi, L., & Lin, S. P. (2016). A new RBDO method using adaptive response surface and first-order score function for crashworthiness design. *Reliability Engineering and System Safety*, *156*, 125–133. https://doi.org/10.1016/j.ress.2016.07.007

Shuai, L., Zhencai, Z., Hao, L., & Gang, S. (2019). A system reliability-based design optimization for the scraper chain of scraper conveyors with dependent failure modes. *Eksploatacja i Niezawodnosc*, *21*(3), 392–402. https://dx.doi.org/10.17531/ein.2019.3.5.

Slowik, O., Lehký, David., & Novak, D. (2021). Reliability-based optimization of a prestressed concrete roof girder using a surrogate model and the double-loop approach. *Structural Concrete*, 1–18. https://doi.org/10.1002/suco.202000455

Sohouli, A., Yildiz, M., & Suleman, A. (2018). Efficient strategies for reliability-based design optimization of variable stiffness composite structures. *Structural and Multidisciplinary Optimization*, *57*, 689–704. https://doi.org/10.1007/s00158-017-1771-8

Song, L. K., Bai, G. C., Li, X. Q., & Wen, J. (2021). A unified fatigue reliability-based design optimization framework for aircraft turbine disk. *International Journal of Fatigue*, *152*, 106422. https://doi.org/10.1016/j.ijfatigue.2021.106422

Spall, J. C. (2003). *Introduction to stochastic search and optimization: estimation, simulation, and control* (First). John Wiley & Sons.

Stromberg, N. (2019). Reliability-based design optimization by using ensembles of metamodels. *Uncertainty Quantification in Computational Sciences and Engineering*, 701–712. https://doi.org/10.7712/120219.6372.18496

Strömberg, N. (2018). Reliability-based design optimization by using support vector machines. *Safety and Reliability – Safe Societies in a Changing World*, *2012*, 2169–2176. https://doi.org/10.1201/9781351174664-272

Sun, Z., Wang, J., Li, R., & Tong, C. (2017). LIF: A new Kriging based learning function and its application to structural reliability analysis. *Reliability Engineering and System Safety*, *157*, 152–165. https://doi.org/10.1016/j.ress.2016.09.003

Taflanidis, A. A., & Beck, J. L. (2008). Stochastic Subset Optimization for optimal reliability problems. *Probabilistic Engineering Mechanics*, *23*(2–3), 324–338. https://doi.org/10.1016/j.probengmech.2007.12.011

Tekaslan, H. E., Imrak, R., & Nikbay, M. (2021). Reliability Based Design Optimization of a Supersonic Engine Inlet. *AIAA Propulsion and Energy Forum, 2021*, *August*. https://doi.org/10.2514/6.2021-3541

Velayudhan, G., Venugopal, P. R., Thankareathenam, E. S. G., Selvakumar, M., & Ramaswamy, T. P. (2021). Reliability-based design optimization of pump penetration shell accounting for material and geometric nonlinearity. *Strojniski Vestnik/Journal of Mechanical Engineering*, *67*(6), 331–340. https://doi.org/10.5545/sv-jme.2021.7104A

Wang, Q., Huang, Z., & Dong, J. (2020). Reliability-based design optimization for vehicle body crashworthiness based on copula functions. *Engineering Optimization*, *52*(8), 1362–1381. https://doi.org/10.1080/0305215X.2019.1657112

Wood. (2019). Flexcom 8.10.4 [Computer Software]. Wood Group Kenny Ireland Limited, Technology Park, Parkmore, Galway, Ireland.

Xiao, M., Zhang, J., & Gao, L. (2020). A system active learning Kriging method for system reliability-based design optimization with a multiple response model. *Reliability Engineering and System Safety*, *199*, 106935. https://doi.org/10.1016/j.ress.2020.106935

Xiu, D., & Karniadakis, G. E. (2002). The Wiener-Askey Polynomial Chaos for Stochastic Differential Equations. *SIAM Journal on Scientific Computing*, *24*(2), 619–644.

Yan, J., Yang, Z., Zhao, P., Lu, Q., Wu, W., & Yue, Q. (2017). Reliability Optimization Design of the steel tube umbilical cross section based on Paricule Swarm Algorithm. *Proceedings of the ASME 2017 36th International Conference on Ocean, Offshore and Arctic Engineering OMAE2017*, 1–9.

Yang, M., Zhang, D., Cheng, C., & Han, X. (2021a). Reliability-based design optimization for RV reducer with experimental constraint. *Structural and Multidisciplinary Optimization*, *63*, 2047–2064. https://doi.org/https://doi.org/10.1007/s00158-020-02781-3

Yang, M., Zhang, D., & Han, X. (2020). Enriched single-loop approach for reliability-based design optimization of complex nonlinear problems. *Engineering with Computers*, *1*. https://doi.org/10.1007/s00366-020-01198-2

Yang, M., Zhang, D., Jiang, C., Han, X., & Li, Q. (2021b). A Hybrid Adaptive Kriging-based Single Loop Approach for Complex Reliability-based Design Optimization Problems. *Reliability Engineering and System Safety*, 107736. https://doi.org/10.1016/j.ress.2021.107736

Yang, H., Zhang, X., & Xiao, F. (2018). Dynamic Reliability based Design Optimization of Offshore Wind Turbines Considering Uncertainties. *Proceedings of the Thirteenth (2018) Pacific-Asia Offshore Mechanics Symposium*, 325–331.

Yi, P., Zhu, Z., & Gong, J. (2016). An approximate sequential optimization and reliability assessment method for reliability-based design optimization. *Structural and Multidisciplinary Optimization*. https://doi.org/10.1007/s00158-016-1478-2

Youn, B. D., & Choi, K. K. (2004). A new response surface methodology for reliability-based design optimization. *Computers and Structures*, *82*(2–3), 241–256. https://doi.org/10.1016/j.compstruc.2003.09.002

Zhang, J., Taflanidis, A. A., & Medina, J. C. (2017). Sequential approximate optimization for design under uncertainty problems utilizing Kriging metamodeling in augmented input space. *Computer Methods in Applied Mechanics and Engineering*, *315*, 369–395. https://doi.org/10.1016/j.cma.2016.10.042

Zhang, X., Lu, Z., & Cheng, K. (2021). Reliability index function approximation based on adaptive double-loop Kriging for reliability-based design optimization. *Reliability Engineering and System Safety*, *216*, 108020. https://doi.org/10.1016/j.ress.2021.108020

Chapter 7

Contributions, Conclusions and Recommendations for Future Research

An improved reliability prediction method for offshore structures is necessary to ensure the safety of life, asset, and the environment. This research demonstrates the effect of appropriate modeling of the complex interaction between multivariate ocean variables and their impact on the reliability assessment and optimization of offshore structures under uncertainty. In addition, the study investigates the use of a hybrid metamodel to reduce the computational burden of the numerical technique (FEA) for complex offshore structures and develops a framework for its resilience. The technical activities of this research aimed at developing a reliability-based design approach for oil and gas structures are detailed in four chapters of this work (Chapters 3-6). These activities constitute a version of manuscripts accepted and published by journals or are currently under review. The contributions, conclusions, and recommendations for future research are presented in the sections of this chapter.

7.1. Novelty and Contributions

This doctoral research's major novelty and contribution relate to dependency modeling, metamodel construction, resilience assessment, and structural optimization under uncertainty. Details of contributions are highlighted below.

1. Development of a multivariate dependence-based modeling approach for reliability evaluation of complex offshore structures using the D-vine copula. The method can capture ocean variables' complex interaction and possible linearity, nonlinearity, and tail dependence between variables.

2. A hybrid metamodel developed from Kriging and PCE through an adaptive technique and multiple-enrichment strategy. This hybrid approach can improve the computational cost and efficiency for response determination in the reliability-based assessment of offshore structures.
3. A novel framework for offshore structural resilience quantification is developed. It utilizes the concept of reliability, adaptability, and maintainability. The framework created can handle multiple disruptive events and adopts a probabilistic approach to address the recovery phase of the resilient assessment.
4. A methodology for offshore structures optimization under uncertainty that considers the multivariate dependency of the environmental variables (ocean) is developed.
5. Develops an approach that utilizes a hybrid metamodel (adaptive PCK) for inner loop reliability in dependence-based structural optimization under uncertainty.

7.2. Conclusions

The research outcomes indicate that multivariate dependence modeling captures the complex interaction in ocean variables for the reliability assessment of offshore structures and their optimal design. Also, a combination of metamodels can improve their computational efficiency, and offshore structural resilience can be adequately quantified for its design life. In addition, nonlinear functions, modeled jacket structure, offshore pipeline segment, and deepwater SCR were used to demonstrate the developed frameworks. The data for demonstration purposes for this research was from met ocean data for Newfoundland and Labrador's offshore areas (Jeanne D' Arc and Flemish Pass basins), related research journal articles, international standards, and reasonable data assumptions made where necessary (due to data unavailability).

7.2.1. A Multivariate Dependence Modeling Approach for Offshore Structures

The appropriate modeling of the complex interaction (linear, nonlinear, and tail dependence) for multivariate ocean variables using the powerful and flexible D-vine copula tool as detailed in this study (Chapter 3) provides confidence in the outcomes from the reliability assessment of offshore structures under a specified limit state condition or a combination of conditions, especially for complex offshore systems with no closed form LSF. This approach prevents the simplification and assumption of independence or Pearson correlation (linear dependence) between ocean variables in reliability-based studies.

7.2.2. A Hybrid Metamodel for Reliability Assessment of Offshore Structures

Metamodel alleviates the computational complexities of response determination from time-consuming numerical methods for large and complex offshore structures. However, constructing a metamodel whose output reflects the offshore structure's actual response under stated conditions is essential for appropriate reliability evaluation. This technical activity (Chapter 4) investigates the performance of a hybrid active learning metamodeling approach using Kriging and PCE, with multiple enrichment of ED (APCKKm-MCS). The research proves that combining metamodels can provide the needed computational efficiency (with minimal error), produce fast convergence, reduce model evaluation, decrease computing time in response determination, and reflect the actual offshore structure's response under stated conditions.

7.2.3. Structural Resilience Quantification for Offshore Structures

The research outcome from the technical activity in Chapter 5 demonstrates that the resilience of offshore structures can be quantified using a probabilistic approach. The developed framework quantified resilience based on its time-dependent reliability, adaptability, and maintainability.

Furthermore, the framework builds on the limit state approach and can evaluate the resilience of multiple disruptive events on an offshore structure. In addition, the framework helps ascertain critical factors affecting the structure's resilience for a specified disruptive event.

7.2.4. Dependence-based Structural Optimization under Uncertainty

The research activity (Chapter 6) presents a dependence-based double-loop RBDO approach for the optimal design of offshore structures. The method assesses the impact of modeling the complex interaction of ocean variables (using a D-vine copula) and utilizing a hybrid metamodel (adaptive PCK) in the inner loop of the nested RBDO problem. The results revealed that design variable optimal decisions could vary significantly if dependence between the environmental variables in the optimization case is ignored, which invariably affects the structure's optimal cost. The adaptive PCK method also revealed its high performance in the inner loop of the nested RBDO case presented.

7.3. Future Research Activities

The research aspects considered in this thesis can be expanded to improve further the reliability-based design approach to offshore structures required for oil and gas activities. Some areas for future research and consideration include:

1. For the fixed offshore structure case study in Chapter 3, the multivariate dependence modeling was limited to wave and current related load variables with no consideration of the dependence of offshore soil parameters due to the unavailability of data. Further research on high dimensional dependence modeling is desired considering other ocean variables such as ice, wind, tidal effect, and soil parameter dependency related to variables

such as shear strength, stress, weight, friction angle, and cohesion. In addition, the research task in Chapter 3 focused on ULS conditions only; the dependence-based approach could be expanded to include SLS, fatigue, and possible damage limit state of offshore structure.

2. The active learning hybrid metamodel (APCKKm-MCS) developed in Chapter 4 for offshore structural response determination and reliability studies focused on the use of specific functions and sampling strategies such as the U learning function for ED enrichment, Matérn autocorrelation function for metamodel construction, and LHS sampling strategy for ED. However, with the quest to constantly develop efficient metamodels for complex offshore structures, a comparative study that investigates the possibility of improving the hybrid metamodel through a combination of different learning functions, sampling strategies, and various autocorrelation functions might be necessary. Also, the application of APCKKm-MCS can be expanded to more complex offshore structures beyond SCR.

3. The resilience quantification framework presented in Chapter 5 described the multiple disruptive events of the offshore pipeline segment with explicit LSF; it does not consider dependency between input variables and focuses on internal disruptive events only. Consequently, further research into a metamodel-assisted, dependence-based offshore structural resilience quantification framework in terms of the system's reliability, adaptability, and maintainability is desired. Also, a combination of internal and external disruptive events could be considered in offshore structural resilience quantification.

4. The concept of structural optimization under uncertainty presented in Chapter 6 considers the dependence of environmental variables and time-independent reliability in the inner loop of the RBDO problem. Further research into dependence modeling of both environmental and design variables using vine copula and considering a time-dependent reliability assessment in the nested RBDO problem for offshore structures could provide an improved and more realistic approach for an effective reliability-based design. Also, the present study considers a single cost function for optimization, with the possibility of multiple optimization cost options for offshore structural design, a methodology for dependence-based structural multiobjective optimization of offshore structures could be investigated.